Spatial and Temporal Variability of Preferential Flow in a Subsurface-Drained Landscape in North-Central Iowa

A DISSERTATION
SUBMITTED TO THE FACULTY OF THE GRADUATE SCHOOL
OF THE UNIVERSITY OF MINNESOTA
BY

Erik Allen Smith

IN PARTIAL FULFILLMENT OF THE REQUIREMENTS
FOR THE DEGREE OF
DOCTOR OF PHILOSOPHY

Dr. Paul D. Capel, Adviser

March 2012

© Erik Allen Smith, 2012

Acknowledgments

I would first like to thank Paul Capel for his valuable insight and support in completing this dissertation. Paul has been my mentor now for over six years, since the beginning of my field work experience in 2005 before I was a PhD candidate up until the present. His patience and long-term vision for this project kept me going. Funding for this study was part of the USGS National Water Quality Assessment Program.

In the field, there were many people who contributed to my efforts. Current and former students from the Capel lab, including Jonathon Thornburg, Scott Kronholm, Jamie Velkoverh, and Rose Tusa provided valuable field and laboratory assistance. Jay Roth was an invaluable sounding board for ideas and provided critical assistance by completing the DRAIN-Pro model. Hydrologists from the Iowa Water Science Center, including Jessica Garrett, Stephen Kalkhoff, James Caldwell, Kate Segreto, and Laura Hubbard provided critical review of this dissertation and also helped collect much of the data included in this study. I also want to thank other students from the Department of Civil Engineering, specifically Tucker Burch, Patrick McNamara, and Mark Krzmarzick.

My committee of Bruce Wilson, Gary Sands, Melinda Erickson, Satish Gupta, and Rick Johnson all provided support and helpful advice at critical periods during my time at the University of Minnesota. In the case of Rick Johnson, he acted as a second mentor during our many field work stints throughout the course of this study.

My parents (Dick and Lynda Hachmann, Craig Smith), friends and family have always been a source of love and encouragement. Finally, I would like to thank the most important person in my life: my wife and best friend, Jessica Eichmiller.

Abstract

Preferential flow can have a direct impact on agricultural chemical transport, especially where preferential flow allows a significant fraction of the total rainfall to quickly move to underlying subsurface drains. The spatial and temporal variability of preferential flow was studied from 2006-2008 in a 38.8 hectare row-cropped (corn, soybeans) agricultural field with two topographically-located subsurface drains (north-central Iowa). Continuous measurements of water levels, soil moisture, stream and drain discharge, stream and drain specific conductance (SC) and precipitation were obtained. Persistent, but variable preferential flow was found to exist at the study site throughout the growing season. Four independent mathematical approaches were used to explore the spatial and temporal variability of preferential flow. A specific conductance end-member mixing analysis (EMMA) was performed based on the temporally varying SC in the subsurface drain water for two separate events, with 54 events classified solely on decreases in SC without accounting for drain flow (full calculations in supplementary file: SCanalysis.xlsm) . These 54 events were utilized to calculate the mean onset time of preferential flow and the mean time to maximum preferential flow. The maximum water velocity (v_{max}) was calculated based on the initial rise of the observed water level relative to rainfall (full calculations in supplementary file: MaxTransportVelocity.xlsx). The highest v_{max} values occurred in the early spring and mid-to-late summer (i.e., higher number of preferential flow pathways), and the slowest v_{max} in the fall and early summer (i.e., lower number of preferential flow pathways). Spatial and temporal variability of preferential flow was best assessed with v_{max}. A simple unsaturated zone, one-dimensional, dual domain model (source-responsive) was conducted based on the timing

and magnitude of the change in ground water levels relative to precipitation events (full calculations in supplementary file: S-Rmodel.xlsm). The source-responsive model described the size of the preferential flow space necessary to accommodate preferential flow. Finally, a simple theoretical model of soil infiltration and flow to subsurface drains (DRAIN-Pro), based on the Green-Ampt and Hooghoudt equations, accounted for preferential flow by estimating the effective vertical and horizontal hydraulic conductivities.

Table of Contents

List of Tables

List of Figures

Chapter 1: Introduction

1. Introduction

Various models and approaches exist to calculate water movement for subsurface drained landscapes and quantify the relative importance of various hydrologic flowpaths, such as surface runoff, unsaturated zone flow, and groundwater discharge. However, many of these models neglect the variable nature of preferential flowpaths as part of unsaturated zone flow (Jarvis, 1991). As opposed to matrix flow, preferential flow results in water moving faster in certain parts of the soil profile and causing the irregular wetting of the soil profile (Šimůnek et al., 2003). Preferential flow also varies both spatially and temporally because it is influenced by soil characteristics, biological activity, climatological effects, and tillage management (Andreini and Steenhuis, 1990; Haria et al., 1994). Artificial subsurface drainage quickly delivers water and agricultural chemicals via preferential flow after rainfall or snowmelt events, via the subsurface drains, into nearby surface water bodies. Without adequately accounting for the interplay between matrix and preferential flow, models are unable to accurately predict water transport. In order to quantify the role of preferential flow, this study focused on a 31 km^2 rural agricultural watershed encompassing the headwaters of the South Fork of the Iowa River (SFIR). This watershed is located in north central Iowa on the Des Moines lobe, a region characterized by prairie potholes, ground moraine, and till plains (Prior, 1981). Additionally, a 38.8 hectare rectangular field located in the northeastern corner of the watershed was selected for more intensive study on preferential flow dynamics, which included two monitored subsurface tile drains, two well nests with more than 30 piezometers, and several vadose zone soil moisture probes. Both subsurface tile drains

were monitored for discharge, and several of the piezometers had continuous pressure transducers for water levels.

2. Research Objectives

Preferential flow is important for subsurface drainage because it can have a direct impact on agrichemical transport. Water bypassing matrix flow has a shorter contact time with soils, thereby lessening the degree of natural attenuation of agrichemicals (Pilgrim et al., 1979). A major observation from the two-year record for both the subsurface drain from the 38.8 hectare agricultural field and the stream draining the entire 31 km^2 watershed was the fast response of their discharges to large rainfall events. In **Chapter 2**, end-member mixing analysis (EMMA), utilizing specific conductance as a tracer, clearly showed this large increase in subsurface-drain flow during storm events due to fast-flow preferential flow (Schilling and Helmers, 2008; Kobayashi, 1986).

However, EMMA alone cannot fully explain the preferential flow dynamics. Given this limitation and the need for further quantification of preferential flow, a second technique was explored in **Chapter 3** to calculate the maximum water velocity (v_{max}) of preferential flow through the unsaturated zone to the water table (Nimmo, 2007). Maximum water velocity and drainable porosity, based on the timing and amount of precipitation, respectively, were calculated for 51 events, totaling 188 individual observations. Variability in maximum water velocities due to seasonality, proximity to the subsurface drain, and land cover was investigated. Variability in the field-saturated hydraulic conductivities was also compared for the same factors, as well as the connection with the maximum transport velocity.

In **Chapter 4**, a one-dimensional, dual domain model (source-responsive model) was used to reproduce a series of water table rises from an array of shallow water table monitors. The premise of the source-responsive model is that water flows quickly through the unsaturated zone along preferential flow pathways, responding more to the infiltrating water at the surface rather than the local potential gradients that control matrix flow (Nimmo, 2010; Ebel and Nimmo, 2009). Matrix flow is continuous, but can be suspended (or becomes unimportant) in cases of rapid water accretion. The hallmark feature of the source-responsive model is the small number of parameters necessary to run the model. The model was calibrated against data from a field array of piezometers with continuous water levels, varying in depth and distance from a subsurface drain. Differences between water table rises at various piezometer locations provided estimates of preferential flow pathways in the soil.

Finally, in **Chapter 5**, three approaches were utilized to describe two rainfall events that led to both water table rises and increased subsurface drainage that were attributed to preferential flow. These approaches include a specific conductance end-member mixing analysis (EMMA) (**Chapter 2**), a source-responsive preferential flow model (**Chapter 4**), and a one-dimensional, non-steady state unsaturated zone model (DRAIN-Pro). DRAIN-Pro was found to be better suited for the larger of the two rainfall events with already saturated antecedent moisture conditions, whereas EMMA worked better for the small and short-duration rainfall event and the source-responsive model worked equally well for both rainfall events. With the usage of DRAIN-Pro, the effect of lateral drain spacing distance (10 to 100 m) between adjacent subsurface drains was assessed. The hypothetical drain spacing scenarios found little difference between the expected

drainage efficiency (percentage of total subsurface drain outflow to cumulative precipitation) of any of the K_v and K_h combinations when the drain spacing distance was >60 m. At and below 20 m between adjacent drain spacings, the drainage efficiency quickly increased with a transitional zone between >20 and 60 m. Finally, a preferential flow contributing area between 2.7 to 4.8 m wide was calculated from four preferential flow events. This preferential flow contributing area helped contextualize the hypothetical drain spacing scenarios by illustrating that nearly 40% of the subsurface drain contributing area would be connected by preferential flow pathways at a lateral drain spacing of 40 feet (12 m).

References

Andreini, M.S. and T.S. Steenhuis. 1990. Preferential paths of flow under conventional and conservation tillage. Geoderma 46: 85–102.

Ebel, B.A., and J.R. Nimmo. 2009. Estimation of unsaturated zone traveltimes for Rainier Mesa and Shoshone Mountain, Nevada Test Site, Nevada, using a source-responsive preferential-flow model. Open-File Rep. 2009-1175. USGS, Menlo Park, CA.

Haria, A.H., A.C. Johnson, J.P. Bell, and C.H. Batchelor. 1994. Water movement and isoproturon behaviour in a drained heavy clay soil: 1. Preferential flow processes.J. Hydrol. 163: 203–216.

Jarvis, N., P-E. Jansson, P.E. Dik, and I. Messing. 1991. Modeling water and solute transport in macroporous soil. I. Model description and sensitivity analysis. J. Soil Sci. 42: 59-70.

Kobayashi, D. 1986. Separation of a snowmelt hydrograph by stream conductance. J. Hydrol. 84: 157–165.

Nimmo, J.R. 2007. Simple predictions of maximum transport rate in unsaturated soil and rock. Water Resour. Res. 43: 1-11.

Nimmo, J.R. 2010. Theory for source-responsive and free-surface film modeling of unsaturated flow. Vadose Zone Journal 9: 295–306.

Pilgrim, D.H., D.D. Huff, and T.D. Steele. 1979. Use of specific conductance and contact time relations for separating flow components in storm runoff. Water Resour. Res. 15: 329–339.

Schilling, K.E. and M. Helmers. 2008. Tile drainage as karst: Conduit flow and diffuse flow in a tile-drained watershed. J. Hydrol. 349: 291–301.

Šimůnek, J., N.J. Jarvis, M. Th. van Genuchten, and A. Gärdenäs. 2003. Review and comparison of models for describing non-equilibrium and preferential flow and transport in the vadose zone. J. Hydrol. 272: 14-35.

Chapter 2: Using specific conductance as a tracer of water infiltration in macropore soils

Abstract

The sources of water to natural streams include direct precipitation, overland flow, and groundwater inflow. In agricultural areas that were recently glaciated, the presence of artificial surface and subsurface drainage networks, a common practice for removing excess water from fields, provides additional pathways of water movement to the stream. The artificial drainage of agricultural fields allows rainfall to move quickly through the landscape to the stream, with implications for increased transport of dissolved chemicals. A largely agricultural (92%), 31-km^2 subcatchment of the South Fork of the Iowa River in north-central Iowa was studied for two years. Stream discharge and subsurface drain specific conductance (SC) were measured continuously, with discrete SC measurements made for the unsaturated zone, precipitation, groundwater, a temporary field pond, and an overland flow site. The end-members of SC were precipitation and groundwater, with mean values of 12 μS/cm and 863 μS/cm, respectively. Within a few hours after a measurable rain or large snowmelt event, the subsurface drain SC decreased (at times less than 200 μS/cm). The subsurface drain SC generally returned to the typical base-flow values over the following hours (generally within 8 hr), demonstrating a short travel distance and relatively fast hydrologic flow path. This strong relation between rainfall and SC was used to calculate the relative contribution and time scale of the short hydrologic pathways to the subsurface drain, mainly soil macropores and surface cracks (i.e. preferential flow paths). In particular, utilizing a mass-balance mixing model for the subsurface drain, preferential flow was quantified as up to 78% of the water in the

subsurface drain during two storm events. Antecedent moisture conditions, storm rainfall intensity, evapotranspiration, and crop growth all influence the unsaturated zone, and each factor was explored to explain the temporal variability in preferential flow. Finally, given the similarity in behavior between the subsurface drain SC and the stream SC, precipitation via preferential flow paths must be a major water source to the study stream shortly after any substantial rainfall or snowmelt event.

1. Introduction

Throughout the upper Midwestern United States, covering a vast region from eastern North Dakota to Ohio, the last glacial advances left a large province of poorly drained soils, characterized by isolated wetland basins (Blann et al., 2009). The installation of artificial surface and subsurface drainage networks, a common practice for removing excess water from agricultural fields, has allowed these poorly drained soils to become productive agricultural land. Artificial drainage allows rainfall to move quickly through the catchment to the stream, transporting nutrients, pesticides and other agriculture-related constituents (Schilling and Helmers, 2008; Tomer et al., 2008).

Many agricultural fields throughout this region are characterized by subsurface drainage (Madramootoo et al., 2007). The inclusion of extensive subsurface drainage networks has two major effects. First, previously unconnected and isolated watersheds, formerly dominated by high evapotranspiration (ET) rates, have become linked watersheds with characteristically lower ET rates (Woo and Rowsell, 1993; Blann et al., 2009). Second, hydrologic flow paths quickly transport water and dissolved constituents to surface ditches, which are connected to natural streams, rivers and lakes. As a

consequence of the fast hydrologic flow paths indicative of subsurface-drained landscapes, agricultural drainage has been indirectly connected to issues such as downstream flood damage from increased overall discharge (Burkhart and James, 1999) and excessive nutrient transport (Alexander et al., 2008). These altered watersheds, some of the most productive agricultural lands in the world, have also become the focus of a large body of research because of the unintended consequences from agrichemical runoff (Jaynes et al., 1999; Kladivko et al., 2004; Kanwar et al., 2005).

One outcome from this research has been the recognition of preferential flow as an important contributor to subsurface drainage (Chikhaoui et al., 2008; Heppell et al., 2002). Preferential flow is important for subsurface drainage because it has a direct effect on chemical transport. Matrix flow, in contrast, is water that drains slowly through much smaller pores between soil particles. Water bypassing matrix flow has a shorter contact time with soils, thereby lessening the degree of natural attenuation. Following the convention of Jury and Horton (2004), preferential flow can be subdivided into three components: macropore flow, funnel flow, and unstable flow. The bulk of this study focused on preferential flow via macropores. Macropores form from plant root channels and the burrowing activity of earthworms and other animals. Macropore characteristics also depend on soil types (Bouma, 1981), climate (Bergstrom et al., 2001), tillage management (Andreini and Steenhuis, 1990), and vegetation (Beven and Germann, 1982). Soil desiccation can produce cracks, fissures, and soil aggregates, especially in clay soils (Haria et al., 1994), and can vary seasonally because of soil drying variations (Øygarden et al., 1997).

Edwards et al. (1993) illustrated that rainfall intensity and soil antecedent moisture conditions greatly affect the amount of preferential flow, with highest flow rates occurring after high intensity storms on relatively dry soils. Additionally, Shipitalo and Edwards (1996) found the highest relative contribution to preferential flow (via macropores) when the soil antecedent moisture conditions were dry. On the other hand, Watson and Luxmoore (1986) found the largest macropore flow contributions occurred under ponded conditions when the entire pore space is fully saturated (high soil antecedent moisture conditions). Despite these seemingly conflicting results, soil moisture conditions have been shown to have a strong effect on the resulting hydrologic framework in relation to subsurface flows. As antecedent soil moisture increases, previously unconnected preferential flow pathways can become connected with only moderate increases in soil moisture. Differences found in the published literature between the amount of preferential flow under variable soil antecedent moisture conditions are likely influenced by the macropore characteristics, soil wetness, local topography, and soil organic matter (Sidle et al., 2000), as well as differing preferential flow behavior under lab versus field conditions.

Hydrologic flow paths to natural streams include direct precipitation, overland flow, and groundwater inflow. In glaciated areas, the presence of artificial surface and subsurface drainage networks provide additional pathways of water movement to the stream. Water moving through each of these pathways has different characteristic time scales and different degrees of interactions with the soil yielding different ionic contents, thus, different specific conductance (SC). The SC of water can be a characteristic signature for the different water sources and flow paths.

SC works as a tracer because water increases in dissolved ionic concentrations with a longer contact time and a higher degree of interaction with the soil (Pilgrim et al., 1979). Because SC measures the ability of a water solution to conduct an electrical current, the SC value will increase with more dissolved ionic species in the water solution. Water traveling through longer flow paths, given more contact time with the soil, will develop a higher SC value. Water moving through preferential flow paths in the soil will have a characteristically low SC in comparison to groundwater because of the shorter contact time and less interaction with the surrounding soil matrix. Using SC as a tracer of water contact time, the relative contribution of water via macropores can be calculated for specific storm events. In previous studies, continuous specific conductance records have been shown to be useful watershed-scale tools to delineate relative source contributions on both short- and long-term time scales, noted as hours to a few days and several days to weeks, respectively (e.g., Schilling and Helmers, 2008; Heppell and Chapman, 2006).

This paper describes the use of a continuous subsurface drain outlet specific conductance record, in combination with a precipitation record, to exemplify the importance of macropores in glacial till soils throughout the entire year. Soil moisture content and subsurface drain discharge were measured during the two-year study to verify substantial macropore flow. Results of the specific conductance tracer study were used to understand the temporal variability associated with preferential flow contributing to subsurface drainage into streams. Temporal variability is examined utilizing SC in relation to several different factors that contribute to the degree of macroporosity, such as antecedent moisture conditions, storm rainfall intensity, evapotranspiration, and crop

growth. The temporal variability in macropore soils is also discussed for future modeling implications.

2. Site Description

The South Fork Iowa River (SFIR) watershed is located in north central Iowa on the glacial margin of the Des Moines lobe (Fig. 2.1). The South Fork watershed is composed of two sections. The lower section is a natural, meandering stream with alluvial valleys, connected above the Des Moines lobe glacial margin to the upper section, which is highlighted by knob-and-kettle topography, prairie potholes, ground moraine, and till plains (Prior, 1981). This study focuses on a sub-watershed of the upper section, located in Hamilton County, Iowa. The surface water sub-watershed is approximately 31 km^2, and is largely dominated by corn and soybean rotations. Fig. 2.1 shows light to dark green areas that are dominated by row crops (corn, soybeans) and gray (often circular) areas that denote poorly drained land inundated in 2008. The red outline shows the estimated extent of the sub-watershed, based on elevation differences. Groundwater drainage may extend beyond the surficial watershed due to subsurface drains.

The channel of the SFIR in the subwatershed is a drainage ditch that was excavated around 1900 to drain prairie potholes, allowing the land to be used for agricultural production. Additional subsurface drainage networks were installed to help drain the relatively shallow water table (Tomer et al., 2008). Along the first 7.6 km of the SFIR upstream from the USGS stream gage near the agricultural field site, 114 overland and subsurface drain outlets discharge into the channel (Thornburg, 2009).

The 38.8-hectare field-scale study site is located near the northeastern corner of the sub-watershed. The soils, mainly of silt loam and silty clay loam textures, are developed on glacigenic diamicton deposits (Quade et al., 2000). Along upland slopes, soils are predominantly the well-drained Clarion loam. The poorly drained lowland soils are dominated by Nicollet and Canisteo loams (USDA National Resource Conservation Service, 2009). Minor component soils also include the Harps, Webster, and Okoboji loams. Generally, the upper soil layer is 2 m in depth, with subsurface drainage generally lying approximately 1–1.5 m below the ground surface. Below the upper layer of soils, surficial deposits of the Des Moines Lobe, typically 15–20 m thick, are subdivided into the Alden and Morgan members of the Dows Formation (Bettis et al., 1996). Both members are distinguished by their distinctive clay mineralogy and act as a confining layer. This agricultural field would normally have a persistently high water table without subsurface drainage, making productive agriculture difficult or impossible.

The study site was drained by two active subsurface drains, with outlets located just downstream from the stream gage (Fig. 2.2). The exact installation date for either of the subsurface drains is unknown. The study's primary subsurface drain, terminating with a 21-cm (inner diameter, ID) subsurface drain outlet, was located approximately 150 m SE of the stream gage and a second subsurface drain, terminating with a 60-cm ID subsurface drain outlet, was located another 75 m further downstream. The study focused on the subsurface drain with the 21-cm subsurface drain outlet. Additionally, one vertical inlet was connected to this subsurface drain approximately 650 m from the drain outlet; however, based on multiple attempts to trace water from this inlet, this surface inlet is probably only active during large precipitation events.

3. Methods

3.1 Continuous data and discrete water samples

The subsurface drain outlet was outfitted with a conductivity and temperature probe (Campbell Scientific CS547A) attached to a datalogger that recorded data every 15 min (USGS 423232093351801; U.S. Geological Survey National Water Information System). Continuous drainage discharge measurements were calculated using an area velocity module (Teledyne ISCO 2150) for portions of the two-year record, converted to $m^3 s^{-1}$ based on Manning's flow equation.

Three additional sites had continuous SC and discharge measurements during the 2007–2008 field seasons. Two stream gages were located at either end of the sub-watershed, both measuring instantaneous discharge every 30 min. The upstream gage was located at the SFIR-Origin, a culvert with three inflowing subsurface drains (USGS 05451070; U.S. Geological Survey National Water Information System) outfitted with the same conductivity and temperature probe as the subsurface drains, and is referred to as the "origin" throughout the rest of this paper. The downstream gage, SFIR-Blairsburg (USGS 05451080; U.S. Geological Survey National Water Information System), had continuous (30-minute increment) stream conductance (SC) and temperature measurements during the non-winter seasons utilizing a multi-parameter water-quality monitor (YSI 6600 sonde), and is referred to as the "stream" throughout the rest of this paper. The water-quality monitor was cleaned and calibrated on a biweekly basis during the field season. Precipitation was measured with a 20.3-cm diameter tipping bucket rain gage (Texas Electronics TE525WS). The overland flow site, draining a total of 2.28 km^2,

had continuous SC and discharge (USGS 423135093373301; U.S. Geological Survey National Water Information System), collected in the same manner as the two subsurface drains, with the probes installed inside of an outlet culvert that integrated all the surface runoff directly into the stream.

Groundwater SC measurements were made from piezometers, located less than 200 m from the stream gage site in the SFIR agricultural field site. The 2.54-cm diameter piezometers were divided into two categories: <2.8 m and >2.8 m below land surface. The data are categorized by depth based on 2.8 m being the estimated maximum depth of surficial soils. All of the piezometers were bottom screened for 0.3 m. Piezometer samples were collected in July and October 2007, and April, June, and October 2008, with SC measurements made in conjunction with the collection of nutrient, alkalinity, and major ion samples. Due to the low hydraulic conductivities for the deep piezometers at this site (>2.8 m), deep piezometers were purged two weeks prior to sampling and sampled without further purging at the sampling time. Samples were collected into 1-L baked glass bottles utilizing a peristaltic pump. The SC was measured in the field, utilizing a YSI 6600 sonde.

Unsaturated zone SC values were obtained from suction lysimeters installed at either 0.6 or 0.9 m below ground surface of the drained agricultural field. The suction lysimeters were ceramic, porous cup collection devices with a sampling chamber capacity of 400 mL (Soil Moisture Corp. Model 1920F1). To collect the samples, a 70-centibar suction was applied with a hand vacuum pump (Soil Moisture Corp. Model 2006G2), setting the sampling chamber at vacuum and allowing water from the unsaturated zone to flow into the chamber for approximately 24 hours. After 24 hours, water was withdrawn

by using the hand vacuum pump and filling a 1-L baked glass bottle. The SC was then measured using the same procedure as groundwater samples.

Unsaturated zone volumetric water content (VWC), cubic meters of water per cubic meter of soil, was obtained from four soil moisture probes (Decagon EC-5) installed beneath the tilled agricultural field, close to the edge of the grassy buffer strip, and adjacent to the suction lysimeters. Four separate probes were located either at 0.6 or 0.9 m below land surface. BT-1.0A and BT-1.0B represent two probes located 1 m from the buried 21-cm subsurface drain. BT-1.0A and BT-1.0B were at depths of 0.6 and 0.9 m, respectively. The other probes, BT-7.5A/B, were located 7.5 m from the buried 21-cm subsurface drain, with the A suffix denoting a 0.6 m depth and B suffix denoting a 0.9 m depth. All of the equipment and locations for the field site, such as the piezometers, subsurface drain outlets, and soil moisture probes (suction lysimeters are located adjacent to these probes), are shown on Fig. 2.2.

Other environmental data for this study included weekly precipitation SC measurements, SC measurements from a temporary pond in the agricultural field, and continuous air temperature measurements from the field site. Precipitation SC data were obtained (via the website) from the National Atmospheric Deposition Program site at the Big Springs Fish Hatchery, located about 200 km northeast of the study area (National Atmospheric Deposition Program, 2011). SC measurements from the ponded water, surrounding a vertical inlet in a surface depression connected to the 60-cm subsurface drain, were obtained from a series of temporary ponds over a three-month period between May–August 2008 (Roth, 2010).

As part of the quality assurance for the continuous SC data, the subsurface drain SC data were censored under the following conditions: (1) Stream gage height above 1.92 m, to avoid periods when the SFIR submerged the subsurface drain outlet; (2) SC probe in the subsurface drain not completely submerged; (3) random, short duration SC spikes >100 μS/cm over the previous 2-hr SC moving average (60–210 min of the record censored due to residual spike effects); and (4) random, single, short duration SC spikes >50 μS/cm (no residual spike effects). For the origin gage, all negative SC values and measurements below a gage height of 0.39 m (SC probe not submerged) were removed. For the overland flow site, only SC data associated with measurable discharge were used.

3.2 Soil volumetric water content

Soil volumetric water content (VWC) can help characterize the soil antecedent moisture conditions and the overall distribution of water within the soil profile prior to a rainfall event. Soil VWC was determined indirectly by using soil moisture probes that measure the water dielectric content versus the surrounding soil media. The overall soil bulk permittivity (Ka_b), or dielectric constant, is governed mainly by the presence of water since the dielectric content of water is 81 (Ka_w) versus 2–5 (Ka_s) for soil minerals and 1 for air (Muñoz-Carpena, 2004). At the field site, Decagon EC-5 probes were used (excited at 2500 mV). For more accurate results, a soil-specific calibration equation for the field site was established with a cored soil subsection (D. Cobos, Decagon Devices, Inc., personal communication, 28 May 2011; Appendix C), converting the probe's output (P, in millivolts) to VWC (in percent):

$$\mathrm{VWC} = 1.34 \times 10^{-3} * \mathrm{P} + 0.442 \qquad [1]$$

3.3 Subsurface drain flow events, identification methodology

Subsurface drain flow events were classified for the entire duration of the two-year subsurface drain SC record from December 11, 2006, to November 5, 2008. An SC event was classified as any SC decrease >10% of the previous two-hr SC average with either a minimum total precipitation of 0.05 in. (1.27 mm) or following a snowmelt with one hour or greater of temperatures >3°C. Also, an event was required to have at least a two-hour period of stable SC values prior to the initial decrease in SC, in order to establish the pre-event mean SC value. Each precipitation event was paired with a corresponding SC event. The end of an SC event was determined when the SC of the drain water returned to 90% of the SC value preceding the event. As a precondition for analysis, no event was considered if the stream gage height was greater than 1.92 m, which is the relative height of the 21-cm subsurface drain outlet above the stream gage height. Above this height the stream could cause potential interference with the subsurface drain discharge and SC. Although this eliminated inclusion of some of the largest events, 54 events were classified, including eight snow melt events.

Several new parameters were derived from this analysis, including the following parameters for time, in minutes:

- τ_S: event start time of the first rainfall recorded at the tipping bucket for SC events, equal to 0 min (second hr after sustained >3°C for snowmelt to account for melting delay);
- τ_{EO}: event onset time from τ_S to the initial decrease in the SC measurement;
- τ_{EM}: event minimum time from τ_S to the lowest SC measurement;

- τ_{50}: time from τ_S to 50% SC recovery, also known as 50% recovery;
- τ_{90}: time from τ_S to 90% SC recovery, also known as 90% recovery.

Both τ_{EO} and τ_{EM} are in 15-min increments, as this is the resolution of the SC record. Analogous SC parameters to the time parameters were also derived for each event, in μS/cm:

- SC_{EO}: mean SC value over a two-hour period preceding τ_{EO};
- SC_{EM}: SC value at τ_{EM};
- SC_{50}: SC value at τ_{50};
- SC_{90}: SC value at τ_{90};

SC_{50} and SC_{90} were calculated with the following formulas, given that the time to 50% or 90% recovery often fell between two 15-min measurements. In turn, τ_{EO} and τ_{EM} were calculated based on the time between two consecutive SC measurements:

$$SC_{50} = SC_{EM} + \left((SC_{EO} - SC_{EM}) * 0.50\right) \quad [2]$$

$$SC_{90} = SC_{EM} + \left((SC_{EO} - SC_{EM}) * 0.90\right) \quad [3]$$

$$\tau_{50} = \tau_{i-1} + \left(15 * \left(\frac{SC_{50} - SC_{i-1}}{SC_{i-1} - SC_i}\right)\right) \quad [4]$$

$$\tau_{90} = \tau_{i-1} + \left(15 * \left(\frac{SC_{90} - SC_{i-1}}{SC_{i-1} - SC_i}\right)\right) \quad [5]$$

Fig. 2.3 shows a sample event (July 18, 2007) with the time and SC parameters illustrated. Of these new parameters, the τ_s influences the timing and resultant SC values

for the other parameters. Other criteria for τ_s were attempted, such as a minimum threshold of 1-mm; however, to remain consistent, the initial rainfall criteria for τ_s was the least arbitrary and easiest to select across all events.

3.4 Evapotranspiration and above-ground biomass

Daily evapotranspiration and above-ground live biomass were estimated using the Water Erosion Prediction Project (WEPP) model. The WEPP model is a continuous-process-based hill slope hydrology and erosion prediction tool (Flanagan et al., 1995). To more accurately represent the field conditions, several site-specific data were acquired and configured for use in the model. Daily minimum/maximum temperature and total precipitation values were from Webster City, Iowa, for 2006–2008 (NCDC, 2010). Other necessary climate parameters not available were augmented using CliGen, a stochastic climate generator included with the WEPP model (Nicks, 1985). The hill slope elevation profile input used in this effort was obtained using a digital elevation model (DEM) of the field site. The representative soil type, Canisteo clay loam, was determined through inspection of SSURGO data (USDA National Resource Conservation Service, 2009). Agricultural management regimes were configured to reflect the occurrence and timing of actual field activities for the duration of the modeled scenarios: i.e., crop type, planting and harvest dates. Preconfigured corn and soybean plant growth and tillage input files, part of the WEPP model, were used in the simulation.

3.5 End-member mixing analysis (EMMA) model

A mass-balance mixing model for the 21-cm subsurface drain uses two sources with direct input into the subsurface drain: fast flow and slow flow. Fast flow consists of

ponded water runoff, via vertical inlets into the subsurface drain, and preferential flow (mainly macropores). Slow flow considers soil matrix flow and groundwater inputs where the subsurface drain is below the water table. Subsurface drain discharge, fast flow, and slow flow are represented by Q_{DF}, Q_{FF}, and Q_{SF}, respectively. Subsurface drain SC, fast flow SC, and slow flow SC are represented by SC_{DF}, SC_{FF}, and SC_{SF}, respectively. For the mass balance, the SC_{SF} value is equal to SC_{EO}, assuming that prior to an event all the flow is derived from slow flow sources rather than preferential flow sources. The basic mass balance is shown as:

$$Q_{DF}SC_{DF} = Q_{FF}SC_{FF} + Q_{SF}SC_{SF} \quad [6]$$

$$Q_{DF} = Q_{FF} + Q_{SF} \quad [7]$$

The relative amount of slow and fast flow can be calculated during periods of known subsurface drain SC and discharge by combining equations 6 and 7:

$$Q_{FF} = \frac{Q_{DF}SC_{DF} - Q_{DF}SC_{SF}}{SC_{FF} - SC_{SF}} \quad [8]$$

$$Q_{SF} = \frac{Q_{DF}SC_{DF} - Q_{DF}SC_{FF}}{SC_{SF} - SC_{FF}} \quad [9]$$

A value of 12 μS/cm, based on the average rainfall SC at the Big Springs Fish Hatchery, was used for the low SC water (SC_{FF}). In combination with a substitution of SC_{EO} for SC_{SF}, assuming all subsurface drain discharge (Q_{TD}) prior to the event was from slow flow sources (Q_{SF}), the amount of fast flow (Q_{FF}, low SC water) can be calculated. An additional sensitivity analysis was conducted with a shifting SC_{FF} in a 24 hr period, changing from the average rainfall value (12 μS/cm) up to the >12 hr overland flow value (264 μS/cm).

A end-member mixing analysis (EMMA) based on two end-members (Q_{FF} and Q_{SF}) is used to determine how much water infiltrating through soil macropores (fast flow water) needs to be combined with the subsurface drain flow to result in decreased SC (SC_{EM}) in subsurface drain water SC_{DF} during rain and snowmelt. In order to develop the EMMA relation in equations 8 and 9, two assumptions were necessary. The first assumption was the average SC value for precipitation was used for fast flow sources, based on the average from the two-year record (Table 2.1). As discussed further in the discussion section, the sensitivity analysis was completed to address the more likely scenario of a shifting SC_{FF}, as longer contact times with the surrounding soil matrix even for the fast flow would lead to higher SC values. The second assumption was that the fast flow was due to preferential flow. During large rainfall and snowmelt events, the largest SC events were already censored because of the precondition of non-inundation of the subsurface drain outlet, making drainage from a vertical subsurface drain inlet non-viable.

4. Results

4.1 Precipitation, continuous discharge, and continuous SC

Fig. 2.4 shows precipitation, in addition to the discharge and SC for the origin and stream gages, from December 11, 2006, to November 5, 2008. Weather during the two-year study period was extremely wet for north-central Iowa. The final five months of 2007 included the wettest August on record, followed by the abnormally wet months of October and December; 2008 was the fourth wettest year for Iowa in 136 years of climate records (Hillaker, 2008).

A strong relation existed throughout the two-year record between precipitation and discharge. Whenever a rain or snowmelt event occurred, stream discharge in the South Fork of the Iowa River generally increased rapidly, often within one hour after rainfall. The same pattern existed for the origin. The origin is sourced by three inflowing subsurface drains, so the similarity in patterns between the origin and stream suggests that a significant percentage of the stream discharge is an integration of the numerous subsurface drains along the channel course. In fact, this assumption was examined by measuring the flow rates of all flowing subsurface drains during two separate synoptic trips in 2006 and 2007 (during late summer base-flow conditions). Adding up all the flows, the difference between the subsurface drains and the measured stream discharge was <10% (Thornburg, 2009). However, an important distinction of the origin discharge is that it decreased faster (steeper slope) than the stream discharge. This suggested that the faster flow paths, close to subsurface drains, provided water to the origin subsurface drains shortly after a rainfall or snowmelt event. Shortly thereafter, the primary water source dissipated to stable, longer flow paths from a wider portion of the watershed area. It is important to note that the minimum threshold for accurate origin discharge measurements after September 2007 occurred around 0.057 m^3/s (due to a weir removal); therefore, for periods when the origin discharge seemingly flattens out after September 2007, the true discharge is likely below the minimum threshold. However, the relation of a faster decrease (steeper slope) after substantial rainfall and snowmelt events still holds true.

SC also exhibited a strong relation with precipitation, decreasing rapidly after rainfall or snowmelt event before recovering back to the previous level. Taken together

with the discharge patterns, this signified a rapid change in the overall water source after a rainstorm. Based on the principle of increased SC with more interaction time, low SC water indicates rainfall travelling short distances, such as preferential flow paths directly to the subsurface drains, and higher SC water indicates longer flow paths. For dry periods, the stream SC suggested water sources indicative of longer flow paths, such as groundwater (Table 2.1). After rainfall and snowmelt events, the sources were dominated by overland flow and preferential flow. During the recovery period after an event, the stream was a mixture of different water sources via shorter flow paths and longer flow paths, although this relation was complicated in regards to specific conductivity since the longer the water contact time, the characteristic SC signature would be closer to groundwater values.

An analysis of the two-year record shows a complicated relation between stream SC and stream discharge, suggesting that the sources of water to the stream vary from season to season (Fig. 2.4). For 2007, periods of higher stream discharge and lower stream SC generally occurred shortly after a rain event or snowmelt event. After the event subsided and stream discharge returned to pre-event flows, the SC would return to values >700 μS/cm. Taken on a seasonal basis, the baseline SC between events increased from 720 μS/cm to 770 μS/cm between April and November, indicating progressively more influence from longer flow path sources. Whereas this same inverse relationship between stream SC and stream discharge held through 2008, an overall drop seemed to occur in the baseline stream SC after mid-July 2008 despite similar patterns in stream discharge to the previous year. Prior to this period, the typical baseline SC would recover to >700 μS/cm, but during the period between mid-July 2008 and early October 2008, the stream

SC remained <600 μS/cm. This signified the primary water source during this particular low-flow period had a characteristically lower SC, denoting a shorter contact time.

Fig. 2.5 depicts precipitation and the SC records for the 21-cm subsurface drain. Specific conductance data from the subsurface drain shows the close connection between rainfall, or large snowmelt events in winter, and the quick appearance of low SC water in the subsurface drain. Throughout the year, the subsurface drain water discharges low SC water after any substantial rainfall or snowmelt event, indicative of water that must have relatively little contact with soil and fast movement via macropores. Generally, SC events returned to background levels quickly after a rainfall or snowmelt event without sustained periods of depressed SC values. Once a rainfall (snowmelt) event occurred, SC decreased within a few hours and reached an event minimum shortly thereafter, indicating a substantial water source not equilibrated with the surrounding soil matrix, characteristic of new rain water infiltrating from the land surface via macropores (preferential flow). Therefore, the fast arrival of low SC water into subsurface drains was due to a prevalence of a substantial macropore network. Similar to the trend for the stream SC, the subsurface drain SC baseline generally increased through the course of the growing season, likely caused by inflows from a larger area of influence integrating longer flow paths. Through the summer and fall season leading up to October, the base line SC values increased from 600 μS/cm to >800 μS/cm.

Also depicted in Fig. 2.5, shown as an inset, is the 2008 overland flow SC. In contrast to flow in the subsurface drain, the overland flow only occurs after a few of the largest rainfall or snowmelt events; therefore, overland flow SC was collected only during these active periods. For example, during the period the overland flow site was

outfitted, 10 overland flow events occurred, whereas 23 subsurface drain events occurred. Finally, SC increases throughout the course of individual overland flow events, indicating that water has been in contact with the soil and/or suspended particles for a longer period of time, leading to increased dissolution of soluble minerals and resulting in greater SC.

4.2 Soil moisture conditions

Individual soil VWC profiles were measured from December 11, 2006, to November 5, 2008, in the agricultural field site adjacent to the subsurface drain (Fig. 2.6). The measured VWC profiles are plotted in Fig. 2.6, for the 0.6- and 0.9-m depths buried 1.0 and 7.5 m from the subsurface drain. VWC responded in less than 60 min after many rainfall events, although a measurable response was not recorded during all rainfall events. Even though these probes were <10 m apart, not all VWC profiles respond in the same manner or to all of the same events, demonstrating the importance of spatial and temporal variability in the unsaturated zone antecedent moisture conditions.

For reference, the average effective porosity for silty clay loam soils, 43.2% (0.432), has been added to give an approximate value to determine fully saturated conditions (Rawls et al., 1983). It is important to note that 43.2% represents a mean value of the average effective porosity, gathered from a compilation of published soil- water data characteristic for silty clay loams. Although values above 43.2% are not necessarily fully saturated soils, as total porosity is higher (47.1%), this gives a good basis for comparison when the soil was near total saturation. Values above the effective porosity likely indicate either a water table rise above the probes or that the entire pore space, including the macropores, was temporarily filled with water moving through the soil. In order to highlight the difference between these temporary rises and the baseline soil-moisture

conditions, Fig. 2.7 represents the weekly minimum baseline VWC value for each of the profiles, thereby removing the flashy, temporary changes.

The differences between 2007 and 2008 were striking in the soil moisture record. In 2007, the baseline soil moisture conditions steadily increased (Fig. 2.7), overlaid by spikes (Fig. 2.6) above saturation when either the water table rose above the soil moisture probes or all the pore spaces were temporarily saturated from the rainfall moving downward. Although a steady VWC decline going into the winter of 2007–2008 occurred before soils froze, the baseline soil moisture values were substantially higher in spring 2008 than the previous winter. Combined with high amounts of rainfall in the preceding months, June 2008 had sustained saturated soil conditions. Finally, another substantial difference between 2007 and 2008 occurred after July. After a winter with record snowfall and an extremely wet spring period, summer 2008 was dry compared to the same period of 2007. Soil-moisture conditions decreased more rapidly from August through October 2008 compared to the same period in 2007.

4.3 Characteristic SC signatures of water sources to the stream

Table 2.1 summarizes the mean values for all the characteristic SC of the various sources of water to the stream, plus the overall mean for the stream. The sources of water to the South Fork Iowa River can be grouped into three distinct categories: low SC water, intermediate SC water, and high SC water. Low SC water includes precipitation, overland flow, and the water in the temporary ponds. All these sources are indicative of short contact time with the soil. Overland flow SC values were subdivided into two categories, <12 hours and >12 hours after the beginning of the precipitation event, to divide samples with low contact time from those with a longer period of contact. Samples

from the first 12 hours had a mean value of 91 μS/cm, whereas the samples collected after the first 12 hours from the overland flow site had a mean value of 264 μS/cm. The intermediate SC categories include water from the soil lysimeters (unsaturated zone), the subsurface drain, stream origin, and groundwater <2.8 m in depth. The high SC category includes groundwater >2.8 m in depth. Stream SC is closest to the value of the subsurface drain and the stream origin, another indication of the primary source to the South Fork of the Iowa River.

4.4 Subsurface drain flow events

A typical SC event (Fig. 2.3) at the field site is characterized by the quick and precipitous decrease in SC after a modest rain. For this particular event on July 18th, 2007, 17.7 mm of rain fell in three hours. Within 165 min (τ_{EO}), the initial SC decrease occurred and reached the event minimum, τ_{EM}, in 180 min. Recovery to SC_{50} and SC_{90} occurred at τ_{50} = 259 min and τ_{90} = 425 min, respectively. In order to account for this SC response, nearly 65% of the water in the drain must have been from extremely low SC water originating at land surface that moved to the drain in a matter of three hours. Such a modest event would not likely have caused ponding with subsequent drainage into a vertical surface inlet, so surface inflow is not an important cause of the decrease in subsurface drain SC. While the time for low SC water to reach the subsurface drain was small, the time to return to pre-event SC values was also short.

Table 2.2 summarizes the calculated time and SC parameters for 54 rainfall and snowmelt events (expanded summary, Appendix A). The difference between the average SC_{EO} and SC_{EM} (271 μS/cm) (Table 2.2) represented a 40% decrease in SC. To explain

such a precipitous decrease, a substantial portion of the subsurface drain outlet water was coming from extremely low SC water. The mean time for the average event onset τ_{EO} was 139 min, and the mean time to the average event minimum τ_{EM} as 197 min. This implies that, on average, the time required for the first evidence of low SC water (precipitation via preferential flow) was about two hours, and a substantial portion of the rain water made it to the subsurface drain in a little over three hours. The event minimums, both τ_{EM} and SC_{EM}, had high degrees of variability (Table 2.2).

5. Discussion

5.1 Factors governing spatial and temporal variability

Preferential flow is important for agrichemical transport because it moves water directly into subsurface drainage. The water bypassing matrix flow has a shorter contact time with soils, thereby lessening the degree of natural chemical attenuation (Thomas and Phillips, 1979). A major observation from the two-year study in the 38.8-hectare agricultural field was the fast decrease in SC after rainfall or snowmelt events. Given a lack of vertical inlet inputs into the 21-cm subsurface drain, the fast arrival of low SC water into subsurface drains must be due to a presence of a substantial preferential flow network.

A number of mechanisms will affect the preferential flow regime over time, including antecedent moisture conditions, storm rainfall intensity, evapotranspiration, crop growth, tillage practices (constant for this study), surface sealing, and the swelling of saturated, clay-rich soils (Leeds-Harrison et al., 1986). This discussion will be limited to the following factors that can be distinguished by using SC: antecedent moisture

conditions, storm rainfall intensity, evapotranspiration, and crop growth. For discussion, these factors are presented separately, but in reality these factors are not meant to be mutually exclusive but contribute to the overall effect.

5.2 Antecedent moisture conditions

With elevated antecedent moisture conditions, the likelihood of preferential flow events is greater because the smaller pores are saturated, diverting water into larger pores (Jury and Horton, 2004). On the other hand, if the antecedent moisture conditions are drier, the suction from smaller pores absorbs available water, and little or no water will be available to move through the larger pores. The changes in antecedent moisture conditions can be due to the seasonal buildup of soil moisture from rainfall or the removal of water by evapotranspiration. Rapid increases occur after rainfall and snowmelt events or large decreases occur under drought conditions. In turn, rapid increases in antecedent moisture conditions for several different locations at the same time can help confirm a widespread infiltration event.

Volumetric water content (VWC) over time, presented as the fraction of a given soil volume filled by water, in comparison to subsurface drain specific conductance, yielded insights into specific events where sudden increases in soil moisture levels led directly to a SC event. In the study field, an event caused by a large spike in VWC was preceded by rainfall or snowmelt during the preceding hours or days.

Fig. 2.8 presents two separate time periods; one period is a result of snowmelt (2.8A) and the other period is a result from rainfall (2.8B). In the case of these particular events, even a small-to-modest rain event or snowmelt event was found to cause rapid water

movement through the subsurface environment, as shown by the SC events which occurred prior to any shift in the VWC on the preceding days. These findings are in line with the findings of Shipitalo and Edwards (1996) that found some of the highest macropore flow occurred under drier soil conditions. It is important to note that this goes against the conventional understanding of unsaturated zone flow and the framework for certain models such as RZWQM (Ahuja et al., 1993), with macropore flow only starting after all of the smaller pores are saturated and surface ponding begins to occur (Watson and Luxmoore, 1986). However, as noted by Nimmo (2010), the unsaturated zone is often not in equilibrium between the smaller and larger pores, leading to infiltration through larger pores (i.e., macropores) even under dry conditions.

For Fig. 2.8A, the study area was covered with snow, and air temperatures the two days preceding February 21, 2007, were well above 3°C. During each of the two previous days, an SC event occurred without a discernible increase in the VWC. For these first two events, the likely explanation was that the thawing, previously frozen water in the larger pores (i.e., macropores) quickly moved towards the subsurface drain. Another possibility for these earlier events was infiltration in other parts of the drainage network where the soil thawed earlier. A high likelihood of large preferential flow paths exists given the known complexity of freeze–thaw cycles in northern climates augmenting soil characteristics, such as frost action modifying the surface and subsurface soil structure (Benoit et al., 1986). With a fast rise in soil temperatures after much of the overlying snowpack had melted, a large release of low SC (short contact time) water through preferential flow paths to the subsurface drain would lead to an SC event in the subsurface drain water. Finally, with the flush of water on the third day, the open

macropores conducted the water directly to the subsurface drain and caused the soil moisture content to increase. SC decreased steadily over the course of several hours and took 540 min (9 hr) before reaching the event low (τ_{EM}), and the SC dropped about 120 μS/cm from SC_{EO} (701 μS/cm) to SC_{EM} (580 μS/cm). A similar phenomenon was shown by Meadows et al. (2009) in response to spring snowmelt in the southern Sierra Nevada Mountains (California), where a rapid increase in VWC was attributed to macropore flow.

In the case of Fig. 2.8B, a series of rains preceding the ensuing SC event on April 22, 2007, caused the synchronized rise in soil VWC. With soil already dampened from the previous rains, a modest rainfall (<10 mm) resulted in water moving through the pathways of least resistance (macropores). The event low (τ_{EM}) was attained within 90 min and had a much wider range from the SC_{EO} (620 μS/cm) to SC_{EM} (325 μS/cm) compared to Fig. 2.8A. In all likelihood, a small rainfall event like that which occurred on April 22, 2007, would not normally cause a substantial portion of low SC water to move through the soil, via preferential flow paths, if the antecedent moisture conditions were not already close to saturated levels.

Overall, both events illustrate that antecedent moisture conditions can influence whether or not water moves through the preferential flow paths. However, as illustrated with back-to-back SC events under seemingly different antecedent moisture conditions, a straightforward relation between the antecedent moisture conditions and the timing of preferential flow does not exist. Instead, utilizing VWC as a way to track variable antecedent moisture conditions can lend insight into the timing of preferential flow.

5.3 Storm rainfall intensity

Short, high intensity rainfall events generally led to larger drops in SC. With large events, subsurface drain discharge rapidly increased with a nearly simultaneous decrease in subsurface drain SC (Fig. 2.9). In another study on the same soil type as this study's field site, Kumar et al. (1997) found for some rain storms greater than >25.4 mm (1 in.) that preferential flow was found to be up to 60% of the total subsurface drain discharge.

Fig. 2.9 highlights two, mid-summer high intensity storms that resulted in large drops in SC. Both occurred during periods when negligible amounts of rain occurred in the preceding seven days (<5 mm), before substantial rainfalls of 47.2 mm and 38.1 mm, respectively. The onset time for both events (τ_{EO}) was very short, 15 min and 90 min for the July and August events, respectively. In fact, the July event was almost concurrent with the rainfall (given the data-collection resolution of the tipping bucket was 30 min versus 15 min for the SC record). The event minimum (τ_{EM}) during the August event was 210 min after the onset of rain and τ_{EM} was 90 min after onset of the July event. Part of the difference between the two events was the rainfall for the July event came in a large, sudden burst, whereas rain during the August event had steady rainfall over several hours. Storm rainfall intensity as the major cause to a preferential flow event was not constrained to these two events, and was found to be one of the leading causes of substantial preferential flow.

5.4 Evapotranspiration and crop growth

Evapotranspiration is the combined effect of water evaporating from the soil and transpiration of water through plant leaves. As annual crops grow, such as corn and

soybeans, more water is diverted towards the plant and away from infiltration into the subsurface. For north-central Iowa, evapotranspiration becomes pronounced through the summer and reaches a maximum in mid-July. Part of the reason for the elevated evapotranspiration levels is due to the higher air temperatures this time of year, in addition to the high throughput of water to the plant.

To illustrate the effect of evapotranspiration over the course of the crop growth cycle, the onset time (τ_{EO}) was plotted against the Julian date for all classified SC events (Fig. 2.10) between Julian date 151 (June 1st) to Julian date 305 (November 1st). Two different curves are plotted behind the onset times, evapotranspiration (mm) in 2007 (soybean crop) and live above-ground biomass (kg m^{-2}) for 2008 (corn crop). Evapotranspiration steadily increased from crop emergence and during initial crop development with a peak during the mid-season (Allen et al., 1998). After the evapotranspiration began to decrease, the 2008 onset times continued to exhibit an upward trend (longer time period). At this time, the live above-ground biomass (kg m^{-2}) plotted for the 2008 season with corn, continued to increase in tandem with the onset time (τ_{EO}).

The onset time for a typical event in 2008 was delayed, indicating preferential flow arriving to the subsurface drain was delayed. Despite an expectation during the mid-summer for enhanced earthworm activity and shrinkage cracking, leading to more preferential flow paths, the combined effect of evapotranspiration and dry conditions buffered the more pronounced preferential flow events. The soil at the height of evapotranspiration was at a moisture deficit from the plant roots drawing out water, so the infiltrating water was likely absorbed by the soil matrix, due to capillary flow, until

the high matric potential gradients were low enough for surface ponding to occur (Jury and Horton, 2004). On a physical basis, the increase in biomass caused more water to be deflected by the plant leaves, leading to a delay in water reaching the ground. Overall, the longer it took water to move to the subsurface drain, the more likely the water would equilibrate more with the surrounding soil matrix and show an increase in SC. Eventually, the water will not be as distinguishable from water with longer contact times such as groundwater. In contrast to these trends, the circled events in Fig. 2.10 showed a fast preferential flow response, either due to the size of the event (rainfall intensity effect) or previous rainfall had dampened the soil (higher antecedent moisture conditions).

5.5 End-member mixing analysis (EMMA)

Several authors have used SC as a means to conduct an EMMA of stream discharge, including Laudon and Slaymaker (1997) and Kobayashi (1986). Schilling and Helmers (2008) used SC of subsurface drain discharge to separate conduit and diffuse flow, analogous to preferential and matrix flow. Using data from this study, EMMA was conducted for two storm events with measured subsurface drain discharge and SC for the subsurface drain.

For the May 7, 2007, event (Fig. 2.11A; Appendix B1), 26.2 mm of rainfall occurred over a seven-hour period with the event onset (τ_{EO}) occurring after 195 minutes. Using an SC_{EO} value of 593 μS/cm, the absolute Q_{ff} was calculated over the duration of the event. The Q_{ff} percentage peaked at 41% after only 90 min from the τ_{EO}, or 285 min from τ_S. After 4.5 hours from the beginning of the event, only <10% of the flow can still be attributed to Q_{FF}, based on equation 8. In other words, the subsurface drain flow increased over three-fold with >40% of the flow attributed to low SC water sources (i.e.,

precipitation moving through the soil as fast flow). Being a modest sized rainfall event, the only major source that can be attributed to the sudden increase in subsurface drainage was precipitation via preferential flow.

For the October 14–15, 2008 event (Fig. 2.11B; Appendix B2), 21.1 mm of rainfall occurred over a 13- period with the event onset (τ_{EO}) occurring after only 330 min. The rainfall pattern was largely spread out throughout the entire period, likely causing some of the earlier rainfall to flow into smaller pores as this later season event occurred on drier soils. Using an SC_{EO} value of 712 μS/cm, the Q_{ff} percentage peaked at 78% after only 150 min from the τ_{EO}. With a modest pulse of water, preferential flow still occurred as a higher percentage of the overall discharge than the May 7, 2007, event and showed discharge increases with each new small pulse of rainwater after the macropore flow was able to flow unimpeded.

Both events begin to recover to pre-event SC values only hours after the events occur, although the discharge remains elevated for a much longer period. The source of water for both events continues to be from the rainfall event, because the discharge does not dissipate. The subsurface drain discharge could still have a substantial portion from preferential flow paths, but the water must travel a farther distance horizontally. Additionally, the water is equilibrating more with the soil as the contact time for the water increases. This phenomenon is also shown in Fig. 2.5 in the observations of the overland flow SC, as shown in the inset. There was a rapid increase in SC over the course of each overland flow event. Despite only contacting surficial soils before discharging to the stream via the outlet culvert, the overland flow site SC increased from values close to

precipitation up to values >400 μS/cm (Table 2.1, Fig. 2.5). The subsurface drain water temperature (Fig. 2.11) also indicates that a new water source has entered into the subsurface drain. At approximately the same time that the SC decreased in the subsurface drain, the water temperature increased signifying that a new source of water was responsible for the increased discharge, rather than matrix flow.

As a sensitivity analysis, both events were also analyzed with a shifting SC_{FF} to investigate the influence of dynamically increasing SC_{FF} on the calculated fast flow discharge. Instead of the static SC_{FF} of 12 μS/cm, the value increased over a24-hr period up to the long-term average for the >12 hr overland flow (264 μS/cm). Although this seemingly arbitrary end-member is not necessarily the end-member for the real values, it represents the potential influence of longer contact times on the resultant SC_{FF}. For the May 7, 2007, the Q_{ff} percentage for the sensitivity analysis peaked at 46% after only 90 min from the τ_{EO}, rather than 41% for the static SC_{FF} calculation. After 4.5 hours from the beginning of the event, 12.4% of the flow rather than 10% can still be attributed to Q_{FF}. Similar small shifts occurred for the October 14-15, 2008 event. Given the fast hydrologic response of the preferential flowpaths, even more dynamic SC shifts in a short duration of time would be necessary to strongly influence the calculated fast flow discharge. Also, higher assumed SC_{FF} would lead to even higher Q_{FF}.

Overall, this EMMA shows that a significant portion of the subsurface drain discharge can be attributed to preferential flow, as indicated by the low SC water. As a cautionary note, SC can be used as a tracer of preferential flow only during the early stages after a rainfall or snowmelt event, given the original source of low SC water,

precipitation, will begin to equilibrate with the surrounding soil matrix. As a consequence of this equilibration, this method of distinguishing preferential flow from matrix flow would actually underestimate the amount of preferential flow in the later stages of an SC event.

5.6 Implication of subsurface drain and macropore soils

The hydrologic responses of subsurface-drained watersheds, specifically in glaciated areas such as north-central Iowa, are different from that of groundwater-dominated watersheds. Rather than being governed by matrix (piston) flow, the subsurface drains short-circuit the typical groundwater flow paths. Furthermore, the presence of subsurface drainage networks seems to reinforce existing preferential flow paths, allowing such pathways to persist throughout the year contrary to the commonly held position that field tillage cuts off macropores at the surface (Ehlers, 1976; Heard et al., 1988). The amount of preferential flow can be affected by soil antecedent moisture conditions, storm rainfall intensity, evapotranspiration, crop growth, tillage practices, surface sealing, and soil swelling.

Within a few hours after a measurable rain or large snowmelt event, both the subsurface drain SC and stream SC decrease. On a watershed scale, the artificial drainage of agricultural fields allows rainfall to move quickly through the landscape to the stream, transporting dissolved agrichemicals.

6. Conclusions

In agricultural areas with soils developed on glacial deposits, the presence of artificial surface and subsurface drainage networks provides additional pathways of water

movement to the stream. In this study, preferential flow was shown to be an important pathway of water from the land surface to the subsurface drain, connecting the land surface directly into the stream via the subsurface drain. Specific conductance has been used in the past to demonstrate preferential flow (Schilling and Helmers, 2008; Chikhaoui et al., 2008; Werellagama et al., 1997); however, previous studies have not thoroughly examined this relation from subsurface drains for longer periods of time or shown strong evidence of preferential flow throughout the year.

Within a few hours after a measurable rain or large snowmelt event, the subsurface drain SC decreased rapidly (at times <200 μS/cm). The subsurface drain SC generally returned to the typical base-flow values over the following hours, demonstrating a short travel distance and relatively fast hydrologic flow path, compared to the higher SC groundwater flow path. This is evidence of a substantial macropore network, leading to rapid preferential flow under various conditions throughout the year. Even during relatively dry periods, the SC illustrated a substantial drop shortly after the rainfall or snowmelt event contrary to the conventional idea that macropore flow only starts after all of the smaller pores are saturated and surface ponding begins to occur. Other publications have found this result of preferential flow under drier conditions, though, such as Villholth et al. (1998) and Shipitalo and Edwards (1996).

This strong relation between rainfall and SC was used to calculate the relative contribution and time scale of the short hydrologic pathways, mainly macropores and surface cracks. Using SC as a tracer illustrated the important role of macropores for water movement. Antecedent moisture conditions, storm rainfall intensity, evapotranspiration, and crop growth were all shown to influence the amount of preferential flow.

References

Ahuja, L.R., D.G. Decoursey, B.B. Barnes, and K.W. Rojas. 1993. Characteristics of macropore transport studied with the ARS Root-Zone Water-Quality Model. Trans. ASAE 36:369–380.

Alexander, R.B., R.A. Smith, G.E. Schwarz, E.W. Boyer, J.V. Nolan, and J.W. Brakebill. 2008. Differences in phosphorus and nitrogen delivery to the Gulf of Mexico from the Mississippi River basin. Environ. Sci. Technol. 42: 822–830.

Allen, R.G., L.S. Pereira, D. Raes, and M. Smith. 1998. Crop evapotranspiration: guidelines for computing crop water requirements. Food and Agriculture Organization Irrigation and Drainage Paper No. 56.

Andreini, M.S. and T.S. Steenhuis. 1990. Preferential paths of flow under conventional and conservation tillage. Geoderma 46: 85–102.

Benoit, G.R., S. Mostaghimi, R.A. Young, and M.J. Lindstrom. 1986. Tillage-residue effects on snow cover, soil-water, temperature and frost. Trans. ASAE 29: 473–479.

Bergström, L., N. Jarvis, M. Larsson, F. Djodjic, and A. Shirmohammadi. 2001. Factors affecting the significance of macropore flow for leaching of agrochemicals. Preferential Flow Water: Movement and Chemical Transport in the Environment, Proc. 2nd Intl. Symp. (3–5 January 2001). Am. Soc. Agric. Biol. Eng., St. Joseph, MI.

Bettis III, E.A., D.J. Quade, and T.J. Kemmis. 1996. Hogs, Bogs, and Logs: Quaternary Deposits and Environmental Geology of the Des Moines Lobe. Geological Survey Bureau Guidebook Series No. 18. Ames, Iowa: Iowa Department of Natural Resources.

Beven, K. and P. Germann. 1982. Macropores and water flow in soils. Water Resour. Res. 18: 1311–1325.

Blann, K.L., J.L. Anderson, G.R. Sands, and B. Vondracek. 2009. Effects of agricultural drainage on aquatic ecosystems: a review. Crit. Rev. Environ. Sci. Technol. 39: 909–1001.

Bouma, J. 1981. Soil morphology and preferential flow along macropores. Ag. Water Manage. 3: 235–250.

Burkhart, M. and D. James. 1999. Agricultural-nitrogen contributions to hypoxia in the Gulf of Mexico. J. Environ. Qual. 28: 850–859.

Chikhaoui, M., C. Madramootoo, M. Eastman, and A. Michaud. 2008. Estimating preferential flow to agricultural tile drains, Proc. 2008 ASABE Ann. Intl. Meet. (29 June–2 July 2008). Am. Soc. Agric. Biol. Eng., St. Joseph, MI.

Edwards, W.M., M.J. Shipitalo, L.B. Owens, and W.A. Dick. 1993. Factors affecting preferential flow of water and atrazine through earthworm burrows under continuous no-till corn. J. Environ. Qual. 22: 453–457.

Ehlers, W. 1976. Rapid determination of undisturbed hydraulic conductivity in tilled and untilled loess soil. Soil Sci. Soc. Am. J. 40: 837–840.

Flanagan, D. C., and M. A. Nearing, eds. 1995. USDA Water Erosion Prediction Project hillslope and watershed model documentation. NSERL Report No. 10. West Lafayette, Ind.: USDA-ARS National Soil Erosion Research Laboratory.

Haria, A.H., A.C. Johnson, J.P. Bell, and C.H. Batchelor. 1994. Water movement and isoproturon behaviour in a drained heavy clay soil: 1. Preferential flow processes.J. Hydrol. 163: 203–216.

Heard, J.R., E.J. Kladivko, and J.V. Mannering. 1988. Soil macroporosity, hydraulic conductivity and air permeability of silty soils under long-term conservation tillage in Indiana. Soil Tillage Res. 11: 1–18.

Heppell, C.M. and A.S. Chapman. 2006. Analysis of a two-component hydrograph separation model to predict herbicide runoff in drained soils. Ag. Water Manage. 79: 177–207.

Heppell, C.M., F. Worrall, T.P. Burt, and R.J. Williams. 2002. A classification of drainage and macropore flow in an agricultural catchment. Hydrol. Processes 16: 27–46.

Hillaker, H.J. 2008. Iowa annual weather summary – 2008. Des Moines, IA: Iowa Dept. of Ag. and Land Stewardship. Available at http://www.iowaagriculture.gov/climatology/weatherSummaries/2008/fas2008.pdf (verified 21 March 2011).

Iowa DNR. 2008. 2008 National Agriculture Imagery Program (NAIP) Aerial Photography Mosaic of Hamilton County, Iowa. Iowa Geological Survey, DNR, GIS Section. Iowa City, Iowa.

Jaynes, D.B., J.L. Hatfield, and D.W. Meek. 1999. Water quality in Walnut Creek Watershed: Herbicides and nitrate in surface waters. J. Environ. Qual. 28: 45–59.

Jury, W. and R. Horton. 2004. Soil Physics (6th edition). Hoboken, NJ: John Wiley and Sons, Inc.

Kanwar, R.S., R.M. Cruse, M. Ghaffarzadeh, A. Bakhsh, D.L. Karlen, and T.B. Bailey. 2005. Corn–soybean and alternative cropping systems effects on NO_3-N leaching losses in subsurface drainage water. Appl. Eng. Agric. 21: 181–188.

Kladivko, E.J., J.R. Frankenberger, D.B. Jaynes, D.W. Meek, B.J. Jenkinson, and N.R. Fausey. 2004. Nitrate leaching to subsurface drains as affected by drain spacing and changes in crop production system. J. Environ. Qual. 33: 1803–1813.

Kobayashi, D. 1986. Separation of a snowmelt hydrograph by stream conductance. J. Hydrol. 84: 157–165.

Kumar, A., R.S. Kanwar, and G.R. Hallberg. 1997. Separating preferential and matrix flows using subsurface tile flow data. J. of Environ. Sci. and Health, Part A: Toxic/Hazardous Substances and Environ. Engineering 32: 1711–1729.

Laudon, H. and O. Slaymaker. 1997. Hydrograph separation using stable isotopes, silica and electrical conductivity: an alpine example. J. Hydrol. 201: 82–101.

Leeds–Harrison, P.B., C.J.P. Shipway, N.J. Jarvis, and E.G. Youngs. 1986. The influence of soil macroporosity on water retention, transmission and drainage in a clay soil. Soil Use and Manage. 2: 47–50.

Madramootoo, C.A., W.R. Johnston, J.E. Ayars, R.O. Evans, and N.R. Fausey. 2007. Agricultural drainage management, quality and disposal issues in North America. Irr. Drain. 56: S35–S45.

Meadows, M., R. Bales, J. Hopmans, P. Hartsough, T. O'Geen, and P. Kirchner. 2009. Soil moisture response to snowmelt and rainfall across elevation, aspect and canopy cover in the Southern Sierra Nevada. Eos Trans. AGU 90, Fall Meet. Suppl.: Abstract H33A–0856.

Muñoz-Carpena, R. 2004. Field devices for monitoring soil water content. Homestead, FL, Department of Agricultural and Biological Engineering, Florida Cooperative

Extension Service, Institute of Food and Agricultural Sciences, University of Florida**:** 17.

National Atmospheric Deposition Program. 2011. National Atmospheric Deposition Program Office. Champaign, IL: Illinois State Water Survey. Available at http://nadp.sws.uiuc.edu/sites/siteinfo.asp?net=NTN&id=IA08 (verified 10 February 2011).

NCDC. 2010. Climate Record for Webster City, IA, United States. Webster City, IA: National Climatic Data Center. Available at http://www4.ncdc.noaa.gov/cgi-win/wwcgi.dll?wwDI~StnSrch~StnID~12001856 (verified 17 December 2010).

Nicks, A.D. 1985.Generation of climate data. Proceedings of the Natural Resources Modeling Symposium. USDA–ASA ARS, 30:297–300.

Nimmo, J.R. 2010. Theory for source-responsive and free-surface film modeling of unsaturated flow. Vadose Zone Journal 9: 295–306.

Øygarden, L., J. Kværner, and P.D. Jenssen. 1997. Soil erosion via preferential flow to drainage systems in clay soils. Geoderma 76: 65–86.

Pilgrim, D.H., D.D. Huff, and T.D. Steele. 1979. Use of specific conductance and contact time relations for separating flow components in storm runoff. Water Resour. Res. 15: 329–339.

Prior, J.C. 1991. Landforms of Iowa (1st edition). Iowa City, IA: University of Iowa Press.

Quade, J., J.D. Giglierano, E.A. Bettis, and R.J. Wisner. 2000. Surficial geologic map of the Des Moines Lobe of Iowa: Hamilton and Webster Counties. Geological Survey Bureau Open File Map 2000–1.

Rawls, W.J., D.L. Brakensiek, and N. Miller. 1983. Green-Ampt infiltration parameters from soils data. J. Hydr. Eng. 109: 62–70.

Roth, J. 2010. The hydrology of a drained topographical depression within an agricultural field in north central Iowa. MS Thesis. Minneapolis, MN: University of Minnesota, Dept. of Civil Engineering.

Schilling, K.E. and M. Helmers. 2008. Tile drainage as karst: Conduit flow and diffuse flow in a tile-drained watershed. J. Hydrol. 349: 291–301.

Shipitalo, M.J. and W.M. Edwards. 1996. Effects of initial water content on macropore/matrix flow and transport of surface-applied chemicals. J. Environ. Qual. 25: 662–670.

Sidle, R.C., Y. Tsuboyama, S. Noguchi, I. Hosoda, M. Fujieda, and T. Shimizu. 2000. Stormflow generation in steep forested headwaters: a linked hydrogeomorphic paradigm. Hydrol. Processes 14: 369–385.

Thomas, G.W. and R.E. Phillips. 1979. Consequences of water-movement in macropores. J. Environ. Qual. 8: 149–152.

Thornburg, J. 2009. Temporal and spatial variability in nitrate and water quality parameters of subsurface drains in an agricultural stream. MS Thesis. St. Paul, MN: University of Minnesota, Water Resources Science.

Tomer, M.D., T.B. Moorman, and C.G. Rossi. 2008. Assessment of the Iowa River's South Fork watershed: Part 1. Water Quality. J. Soil Water Conserv. 63: 360–370.

USDA National Resource Conservation Service. 2009. Soil Survey Geographic (SSURGO) database for Hamilton County, Iowa. Fort Worth, Texas. Available at http://datagateway.nrcs.usda.gov/ (verified 10 February 2011).

Villholth, K.G., K.H. Jensen, and J. Fredericia. 1998. Flow and transport processes in a macroporous subsurface-drained glacial till soil I: Field investigations. J. Hydrol. 207: 98–120.

Watson, K.W. and R.J. Luxmoore. 1986. Estimating macroporosity in a forest watershed by use of a tension infiltrometer. Soil Sci. Soc. Am. J. 50: 578–582.

Werellagama, D.R.I.B., U. Matsubayahsi, and F. Takagi. 1997. Hysteresis observed in SC vs. Q relationships and its implications on flowpath identification. Ann. J. Hydr. Eng. 41: 197–202.

Woo, M. K. and R.D. Rowsell. 1993. Hydrology of a Prairie Slough. J. Hydrol. 146: 175–207.

Table 2.1: Summary of the characteristic specific conductance of the various sources of water to the stream. The different environmental compartments are sorted from lowest to highest mean SC value.

Environmental Compartments	Number of Stations	Mean	Median	Standard Deviation	5th Percentile	95th Percentile	Number of observations
Precipitation[1]	1	12	11	6	4	23	86
Overland flow, <12 hr	1	91	90	48	23	183	330
Temporary pond[2]	1	129	136	64	43	254	15
Overland flow, >12 hr	1	264	248	99	118	416	872
Unsaturated zone	6	456	461	173	63	702	10
Subsurface drain	1	654	690	122	387	795	49330
Origin	1	666	700	141	408	879	30284
Groundwater, <2.8 m	10	675	654	120	512	894	27
Stream	1	681	715	105	470	809	37856
Groundwater, >2.8 m	24	863	829	156	636	1118	98

1: Weekly integrated samples from Big Springs Fish Hatchery (NADP IA08) (NADP, 2011).
2: Grab samples from a series of temporary ponds over a three-month period between May- and August 2008 (Roth, 2010).

Table 2.2: Summary of the calculated time (minutes) and SC (μS/cm) parameters for the 54 classified SC events. All the parameters are relative to the beginning time of an event (τ_S). Values in parentheses under the Maximum Time Value denote one anomalous event in April, 2007.

Time Parameter (in min)	**Mean (in min)**	**Median (in min)**	**Standard Deviation (in min)**	**Minimum Time Value (in min)**	**Maximum Time Value (in min)**
τ_{EO}	139	120	82	15	330 (1035)
τ_{EM}	197	195	120	30	540 (1155)
τ_{50}	310	248	198	85	980 (1339)
τ_{90}	457	423	288	115	1365 (1655)

SC Parameter (μS/cm)	**Mean (μS/cm)**	**Median (μS/cm)**	**Standard Deviation (μS/cm)**	**Minimum SC Value (μS/cm)**	**Maximum SC Value (μS/cm)**
SC_{EO}	681	668	62	518	853
SC_{EM}	410	439	154	46	622
SC_{50}	546	562	77	361	665
SC_{90}	654	651	55	509	780

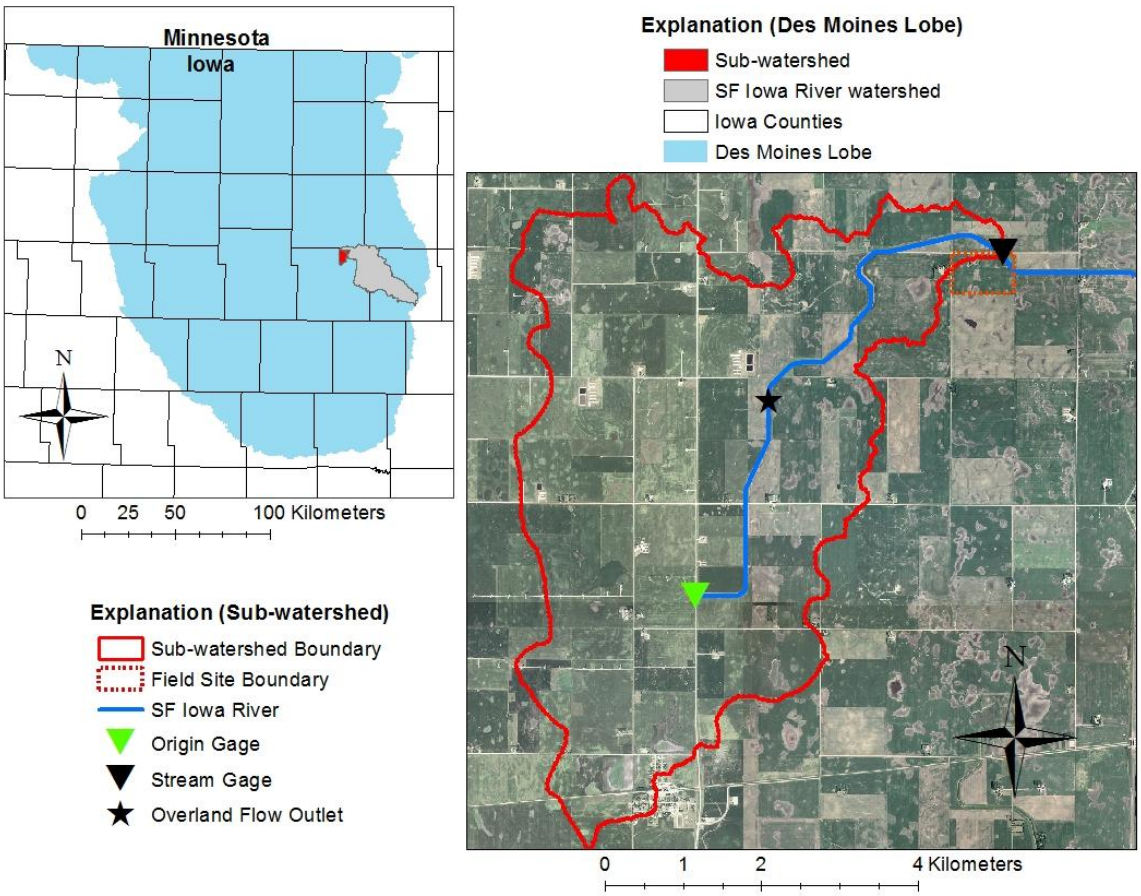

Fig. 2.1: South Fork Iowa River (SFIR) watershed upstream from stream gage (USGS 05451080), the origin stream gage (USGS 05451070), the overland flow site (USGS 423135093373301), and the field site boundary (dashed red line). The watershed land cover photo is from 2008 (Iowa DNR, 2008). Also shown is the extent of the Des Moines Lobe, with the subwatershed and overall SFIR watershed highlighted.

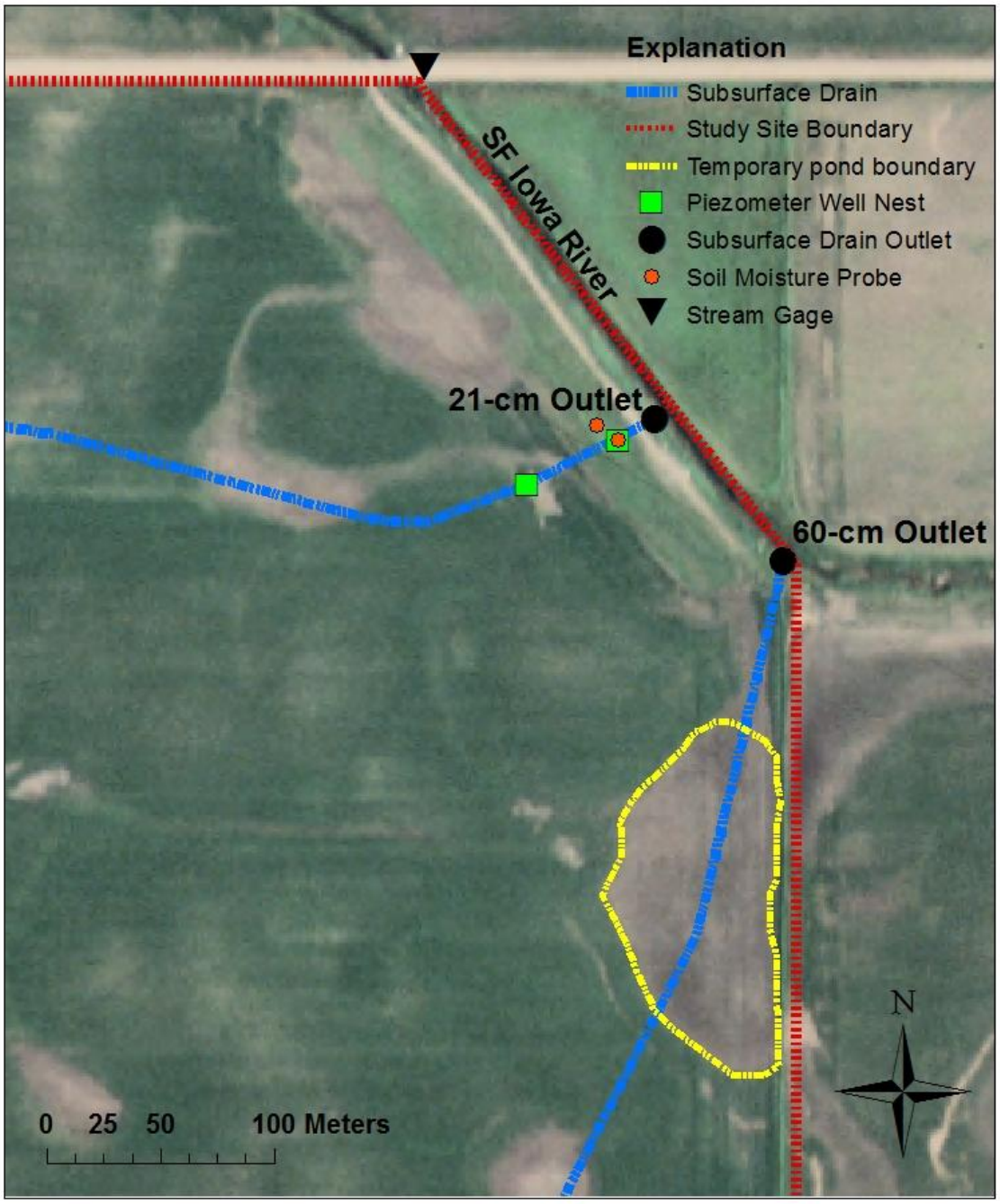

Fig. 2.2: Major site locations in the northeast part of the field site, including the piezometer well nests, soil moisture probes, and subsurface drain locations. The South Fork of the Iowa River flows to the southeast within this figure.

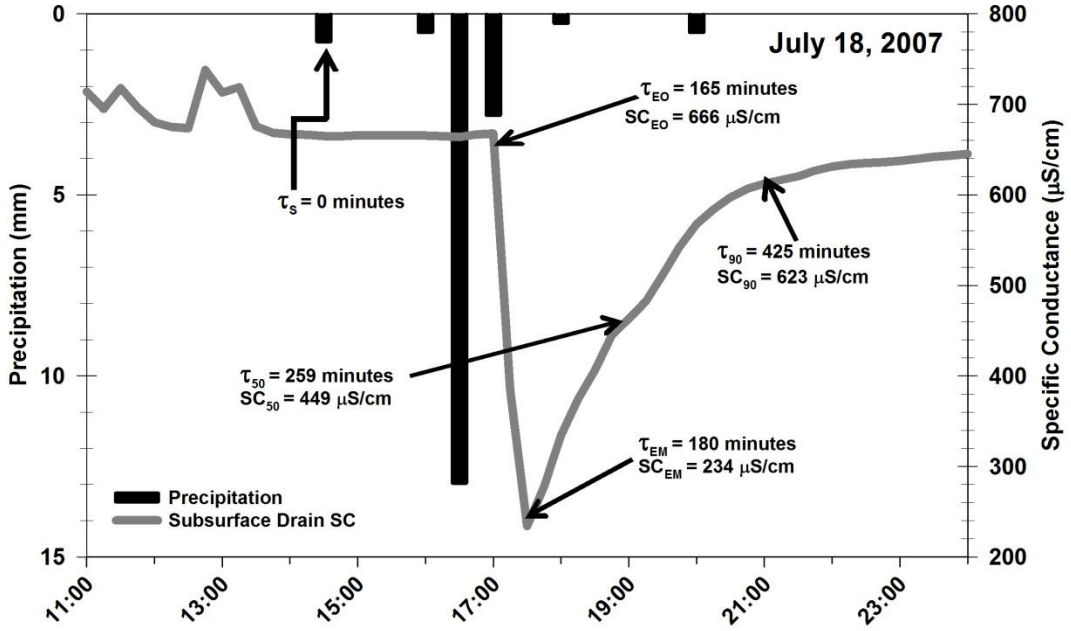

Fig. 2.3: An example event illustrating the various time and SC parameters. Arrows point to the significant points in the subsurface drain SC curve with the time and SC parameter labeled.

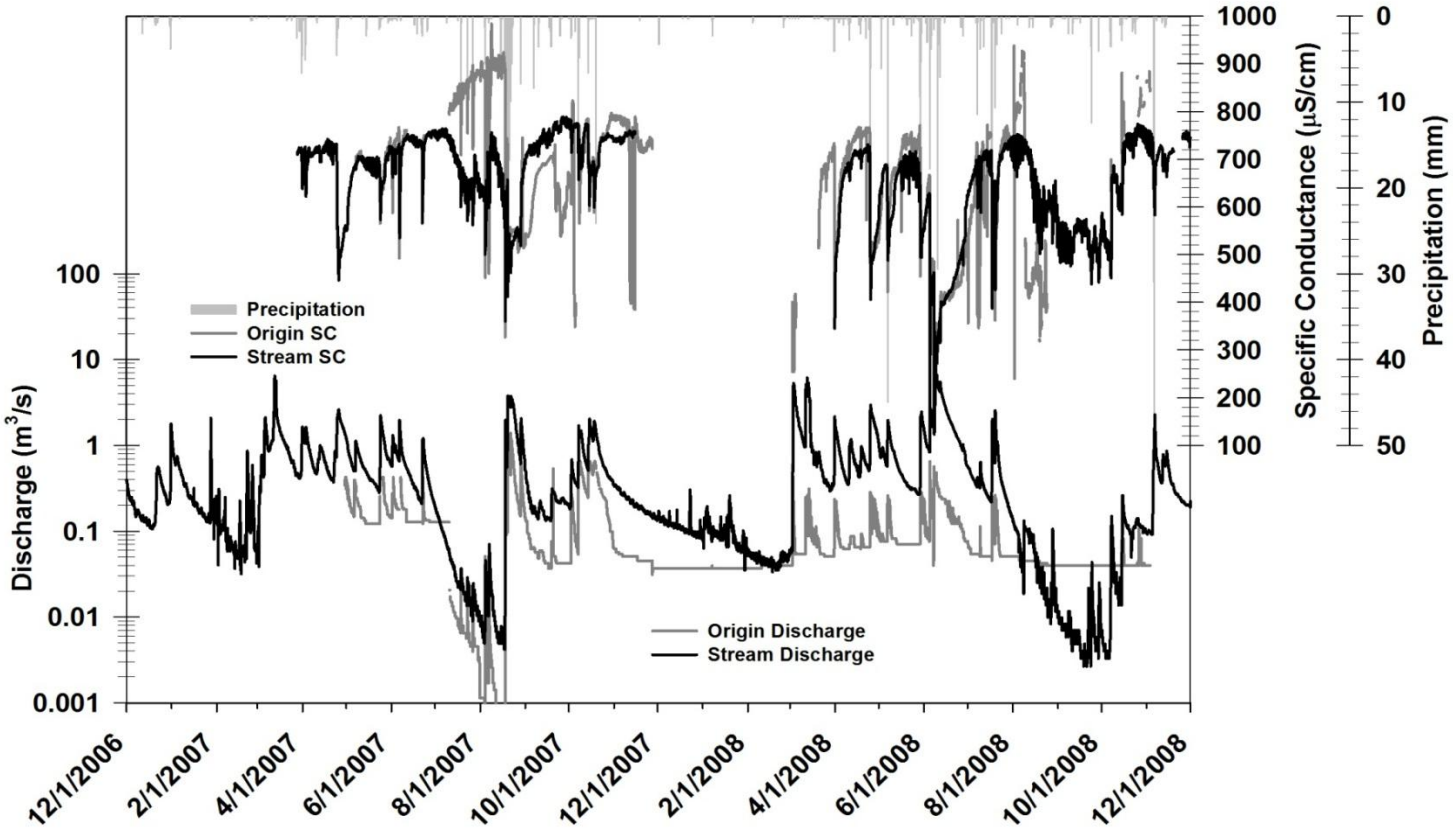

Fig. 2.4: Precipitation (mm), discharge (m^3/s) and specific conductance (µS/cm), from 12/5/2006 to 11/4/2008, for the stream (USGS 05451080). Also shown is the discharge (m^3/s) and specific conductance (µS/cm) for the origin (USGS 05451070). The minimum threshold for accurate origin discharge measurements after September 2007 occurred at ~0.057 m^3/s (due to a weir removal); therefore, for periods when the origin discharge seemingly flattens out after September 2007, the true discharge is likely below the minimum threshold.

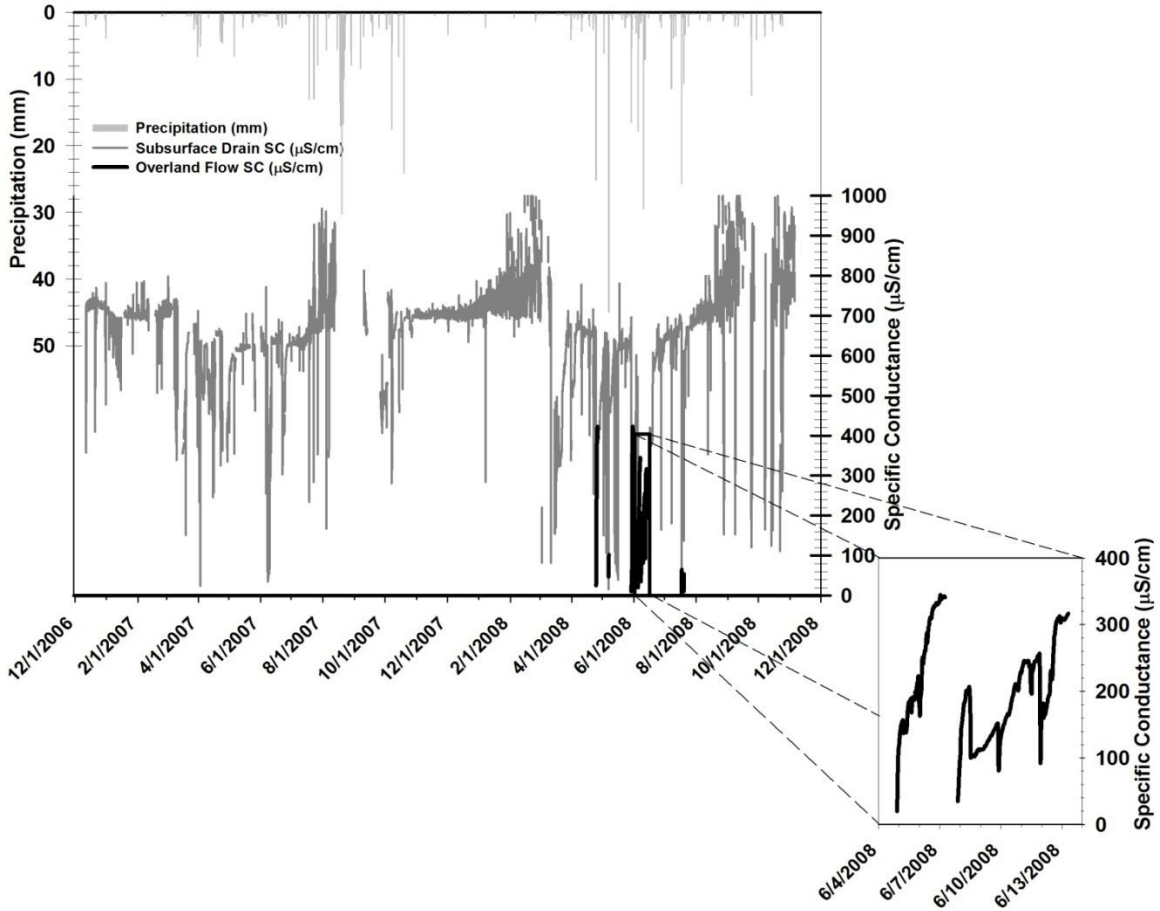

Fig. 2.5: Precipitation (mm) and specific conductance (µS/cm) for the 21-cm subsurface drain (USGS 423232093351801) and the overland flow site (USGS 423135093373301).

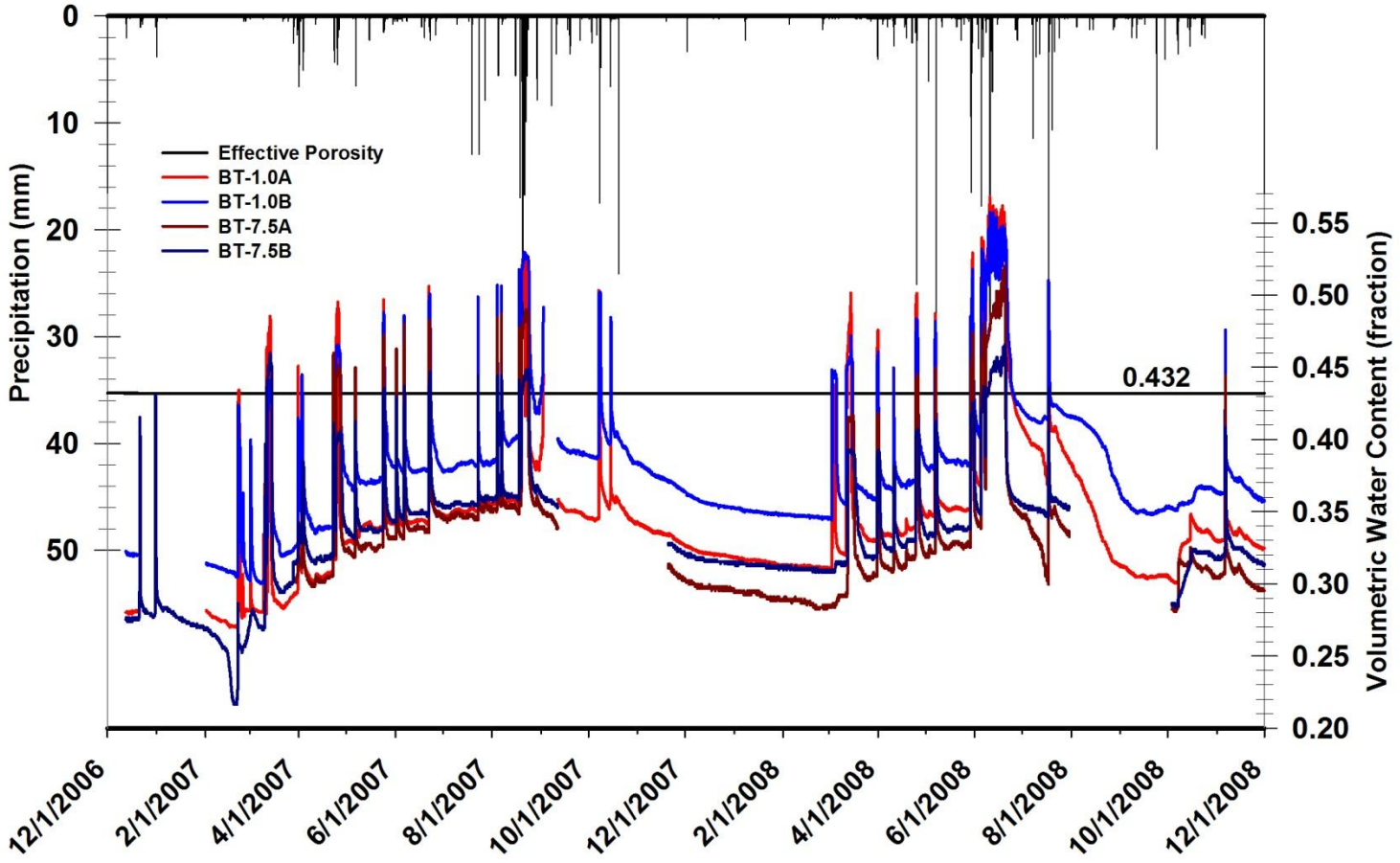

Fig. 2.6: Precipitation and volumetric water content for four soil moisture probes at the field site. The probes were located at two distances from the subsurface drain: 1-m (BT-1.0A, BT-1.0B) and 7.5-m (BT-7.5A, BT-7.5B). The suffix denotes depth (A=0.6 m, B=0.9 m). The average effective porosity for the soil type at the site (0.432 for silt clay loams, Rawls et al., 1983) is shown for comparison.

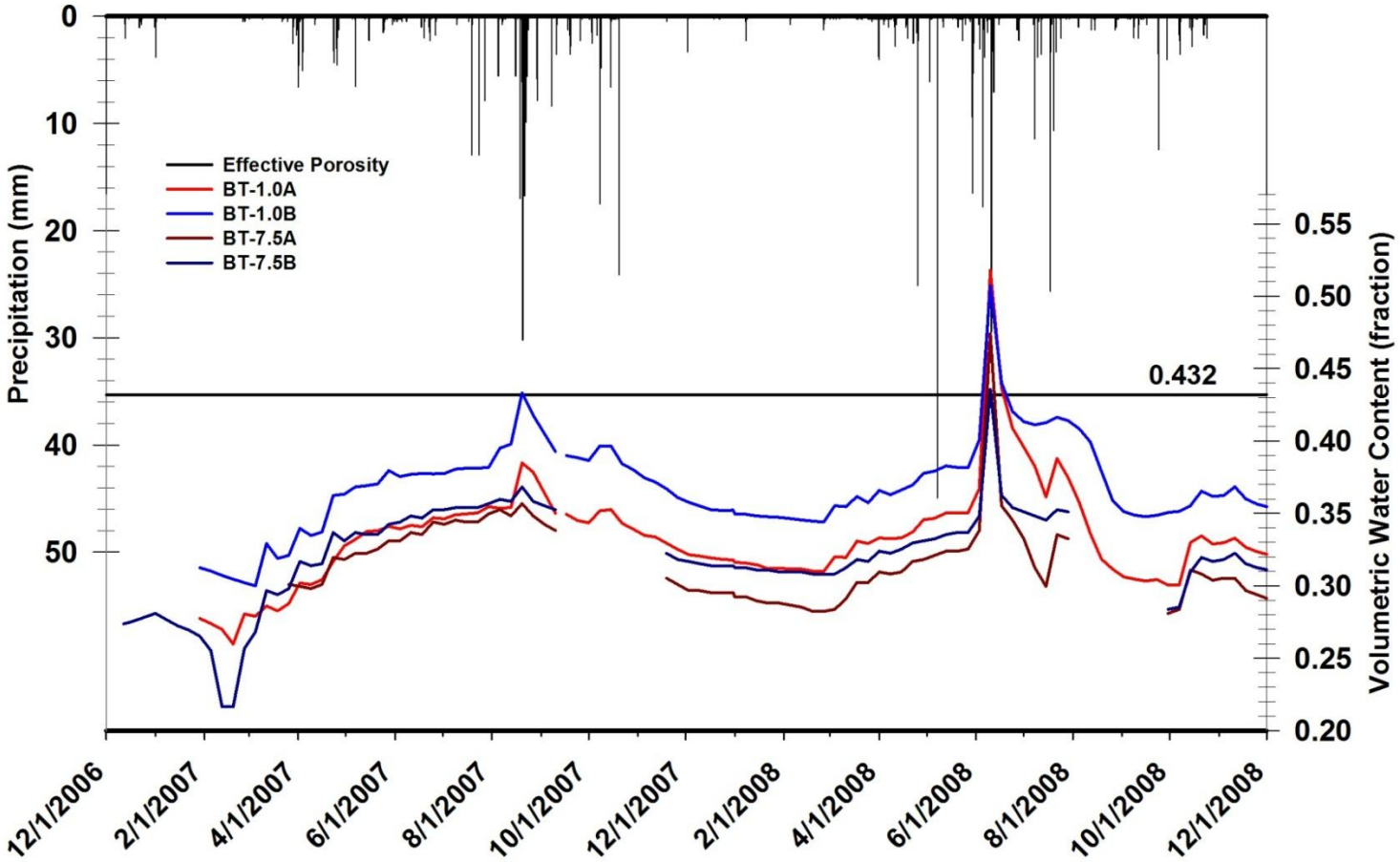

Fig. 2.7: Precipitation and weekly minimum baseline volumetric water content for four soil moisture probes at the field site. The probes were located at two distances from the subsurface drain: 1-m (BT-1.0A, BT-1.0B) and 7.5-m (BT-7.5A, BT-7.5B). The suffix denotes depth (A=0.6 m, B=0.9 m). The average effective porosity for the soil type at the site (0.432 for silt clay loams, Rawls et al., 1983) is shown for comparison.

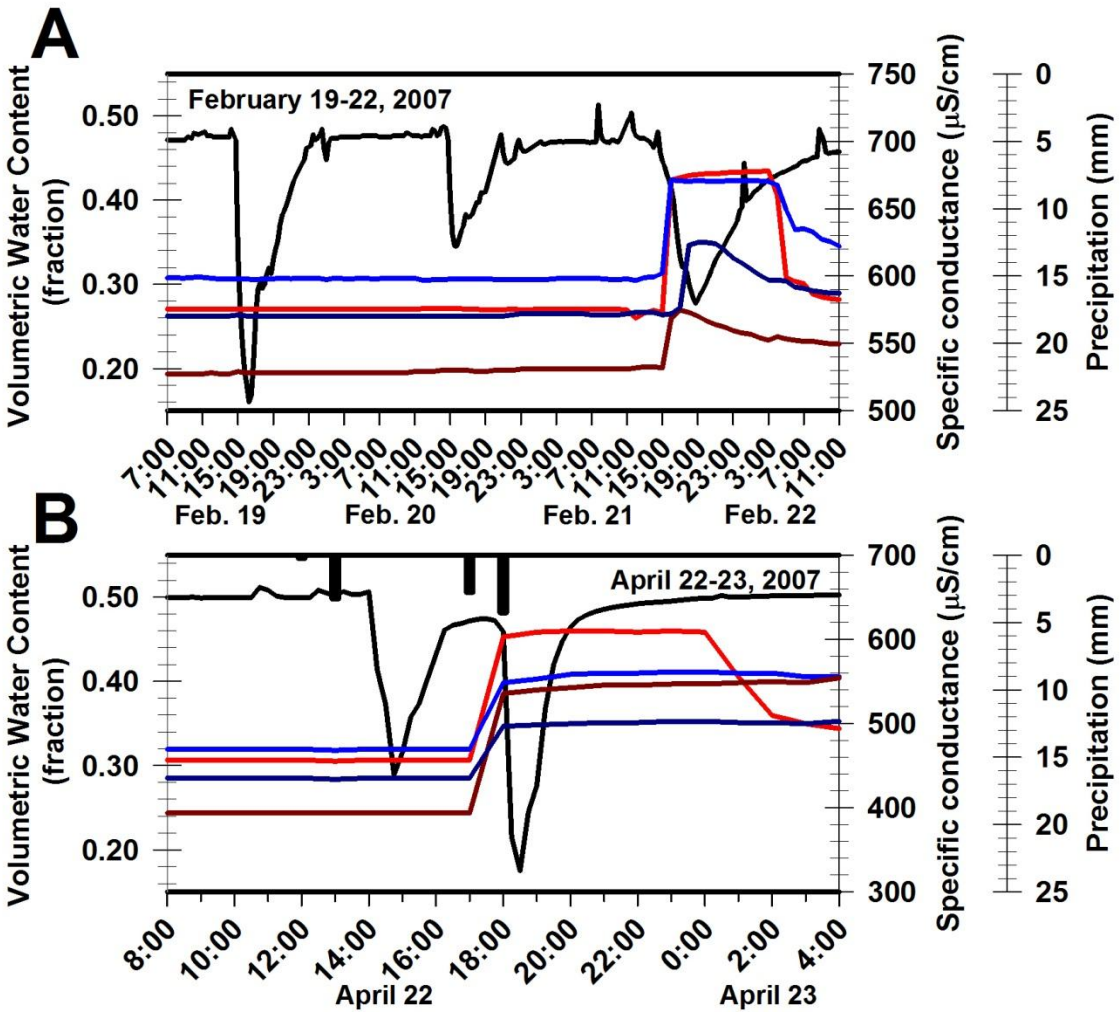

Fig. 2.8A-B: Subsurface drain SC (black), precipitation (black bars), BT-1.0A VWC (red), and BT-1.0B VWC (blue) for two dates. These data highlight the fast increase in soil VWC at 0.6 m (BT-1.0A) and 0.9 m (BT-1.0B) and the simultaneous drop in SC.

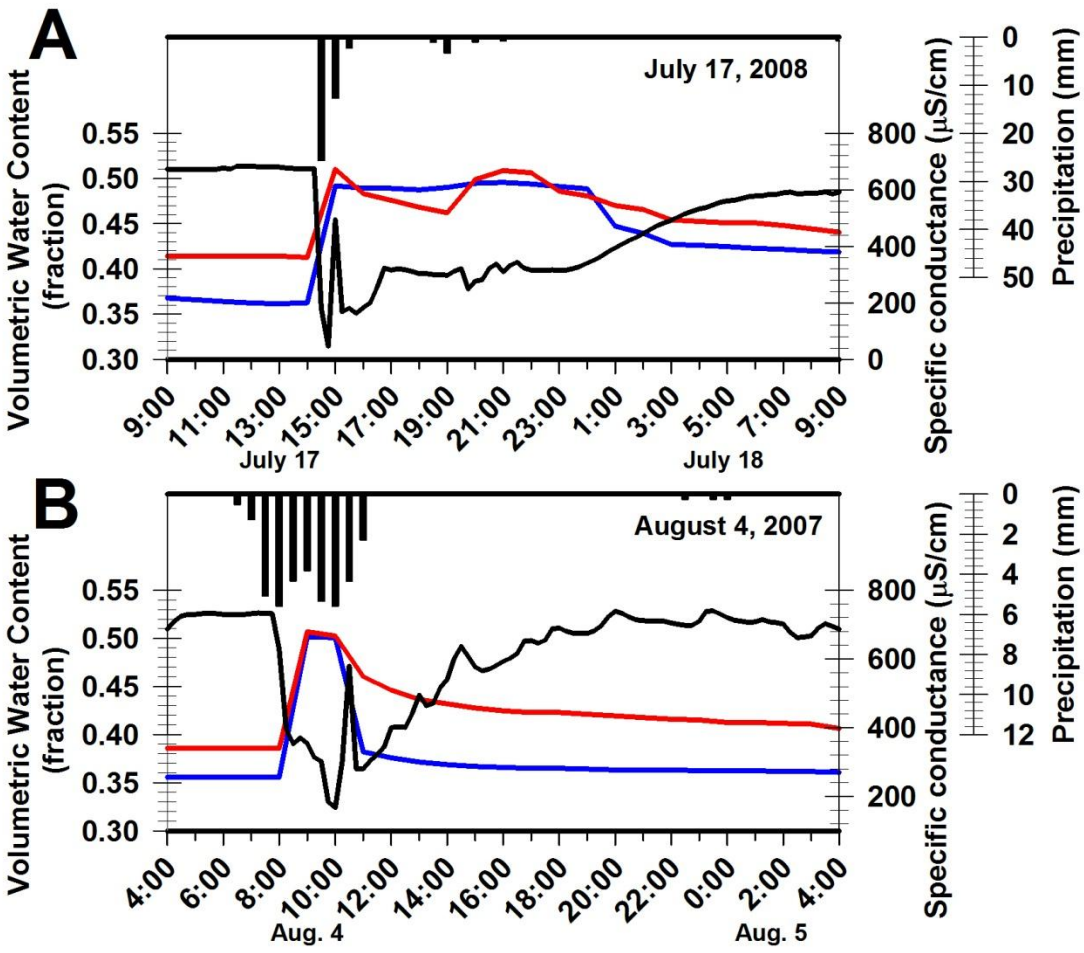

Fig. 2.9A-B: Subsurface drain SC (black), precipitation (black bars), BT-1.0A VWC (red), and BT-1.0B VWC (blue) for two different dates. These data highlight the fast increase in soil VWC at 0.6 m (BT-1.0A) and 0.9 m (BT-1.0B) and the simultaneous drop in SC in response to rainfall greater than 1.5 in. (38 mm) in a short period of time.

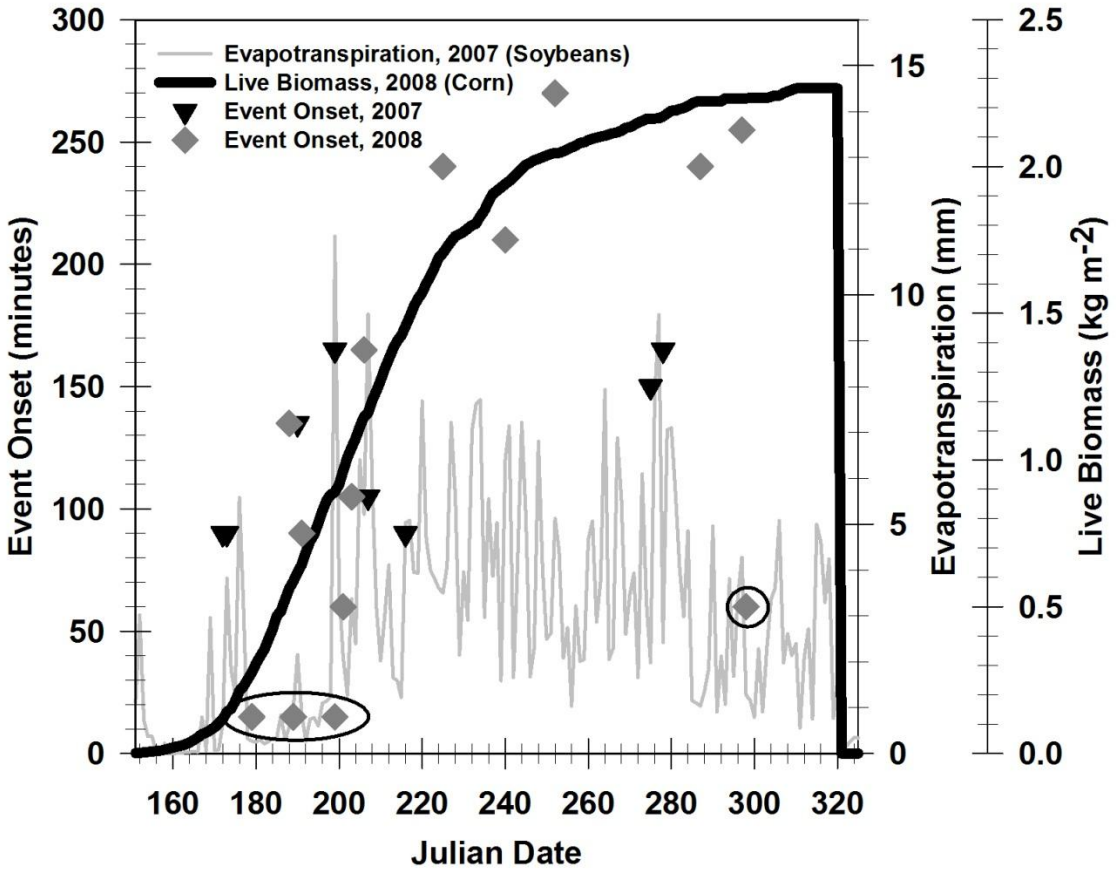

Fig. 2.10: Onset time (τ_{EO}) plotted against the Julian date for all classified SC events between Julian date 151 (June 1st) to Julian date 305 (November 1st). Two different curves are plotted behind the onset time data: evapotranspiration (mm) and live, above-ground biomass (kg m^{-2}) for 2007. The output for these two parameters was produced using the Water Erosion Prediction Project (WEPP) model (Flanagan et al., 1995) for the field site (Webster City, IA daily climate record (2005-2008), Canisteo soil, corn as crop (2006, 2008), soybeans as crop (2005, 2007), and spring chisel plow tillage). The circled areas denote anomalies for four points in 2008. The short onset times for these four points were caused by either intense rainfall events or smaller rainfall events on already dampened soils.

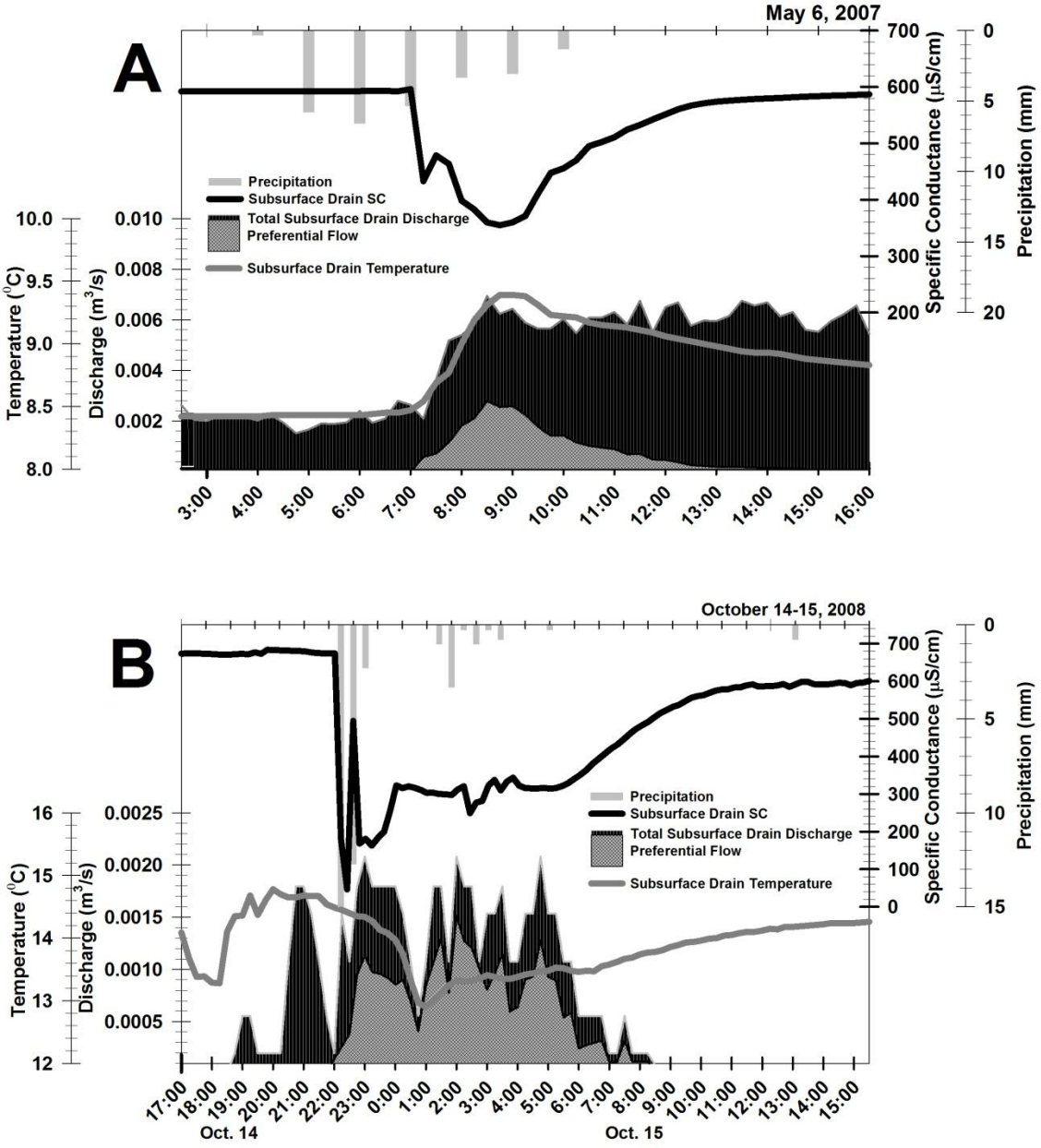

Fig. 2.11A-B: Precipitation (mm), subsurface drain SC (µS/cm), total subsurface drain discharge (m^3/s), calculated preferential flow (m^3/s), and subsurface drain water temperature (°C) for 21-cm subsurface drain for (A) May 6, 2007 and (B) October 14–15, 2008.

Chapter 3: Rapid water infiltration velocities as an indicator of preferential flow

Abstract

Water table fluctuations during and after precipitation events can give insight into unsaturated zone flow processes that contribute to groundwater recharge. Persistent preferential flow pathways through the unsaturated zone allow for rapid water infiltration from the land surface to the water table and then to artificial subsurface drains, which are common in north-central Iowa to remove excess water from agricultural fields. Water table rises in proximity to a subsurface drain were monitored continuously to study the immediate capture zone surrounding the subsurface drain. Two separate piezometer arrays were installed within a 38.8 hectare study site; one within the row-cropped field and another within a nearby grassy buffer. Maximum water velocities of infiltration (as opposed to maximum transport speed of water infiltration) were calculated for a total of 51 events by dividing the vertical distance to the water table by the difference in time between the first recorded increment of precipitation and the first water level rise. Additionally, field-saturated hydraulic conductivities (K_{fs}) were measured using simple infiltrometers throughout the growing season at a number of locations throughout the study field. The mean maximum water velocity (v_{max}) was 10.7 m day^{-1} and 10.2 m day^{-1} underneath the agricultural field and the grassy buffer, respectively. Strong seasonal trends in v_{max} occurred, with the fastest v_{max} in early spring and mid-to-late summer, and the slowest v_{max} in the fall and early summer. Higher v_{max} values observed when the water table was closer to land surface was probably caused by more preferential flow. Distance away from the subsurface drain was not shown to influence the v_{max}. K_{fs} values

progressively grew larger throughout the growing season, with the exception of mid-summer which had the lowest K_{fs} values. The influence of above-ground cover (corn, soybeans, grassy buffer, and bare ground) on K_{fs} values was only significant between corn and bare ground; spatial variability of K_{fs} was not statistically significant.

1. Introduction

An improved understanding of water movement and its dissolved solutes (e.g. nitrate, pesticides) through upper Midwest agricultural watersheds has been the focus of considerable research (Randall and Mulla, 1991; Kladivko et al., 1991; Fenelon and Moore, 1998; Kladivko et al., 2001; Kalkhoff et al., 2003). Critical to this understanding is how quickly water moves through the various pathways in the unsaturated zone towards the water table. As a rough approximation, water flow through the unsaturated zone is commonly divided into two separate components: matrix flow and preferential flow (Jury and Horton, 2004). Matrix flow is the slow and even water movement through the soil micropores due to gravitational, adhesive, and capillary forces, as described by the application of Darcy-Buckingham law for unsaturated flow (Narasimhan, 1998). Preferential flow is highlighted by rapid and uneven water movement, which bypasses a significant fraction of the porous matrix via structural voids, biopores (i.e. roots, burrowing animals), and a limited spectrum of the pore space (i.e. macropores) (Beven and Germann, 1982; Jury and Horton, 2004).

The potential velocity water can travel through preferential flow pathways ranges from 1 to 100 m/d, at least in cases of continuously supplied water (Nimmo, 2003). Mohanty et al. (1994) utilized various methods to measure the saturated hydraulic

conductivity for Iowa soils. By dividing the calculated hydraulic conductivity by the measured porosity, values up to 12.5 m day^{-1} were found. This calculation assumes flow through the entire soil matrix, whereas the likely explanation for the faster flows is preferred flow through a much smaller percentage of the soil volume. Flury et al. (1994) showed water flow through structured soils often would bypass the soil matrix, moving through cracks, fissures and larger pores in unpredictable patterns. Also, given the observation that many identified macropores do not necessarily participate in preferential flow, it is difficult to assess an exact value of how much of the entire soil column is occupied by functionally effective macropores (Ogden et al., 1999).

There have been a number of studies of preferential flow in subsurface drain systems. Kumar et al. (1997) and Stone and Wilson (2006) found nearly instantaneous increases in drain flow after large rain events, noting preferential flow as the main mechanism for transferring such a large quantity of water. Surface-applied solute arrived in subsurface drain discharge after only 3-4 hours in a northern New York study, translating to vertical transport velocities of 4.8-6.4 m day^{-1} (Richard and Steenhuis, 1988). Schilling and Helmers (2008) found increases in subsurface drain discharge after only 2 h. Performing tracer experiments in Iowa on the same soil association as this study, Jaynes et al. (2001) found transport velocities ranging from 2.0×10^{-3} m s^{-1} (173 m day^{-1}) for bromide to 1.3×10^{-3} m s^{-1} (112 m day^{-1}) for difluorobenzoate.

This rapid transport and heterogeneous movement of water through the unsaturated zone makes preferential flow a difficult process to describe in a predictable and uniform manner (Šimůnek et al., 2003). Under controlled laboratory condition, explicit physical models have been constructed that can ascertain the flow of unsaturated zone water flow

and the mechanisms by which water moves through preferential flow pathways (Beven and Clarke, 1986; Heard et al., 1988). For the heterogeneous conditions typical under field conditions, the validity of the uniform-flow assumptions of the Green-Ampt or the Richards' equations can be difficult to apply (Gowdish and Munoz-Carpenter, 2009).

Richard and Steenhuis (1988) cite three categories in which the uniform homogeneous flow assumptions breakdown: (1) preferential flow around inter-aggregates, leading to crack flow; (2) biologically-created macropores; (3) fine-textured soils overlying a more permeable layer, leading to finger flow. As opposed to controlled laboratory conditions, an increasingly large number of field studies have found a wide spatial variability in flow patterns, including preferential flow, where theories of uniform homogeneous flow do not necessarily apply (Williams et al., 2003; Villholth et al., 1998; Kumar et al., 1997; Ogden et al., 1999). These studies also show agreement that preferential flow pathways are difficult to quantify, vary from location to location, and can be very important in terms of water movement.

In the recently glaciated regions of the upper Midwest, the presence of artificial surface and subsurface drainage networks is a common practice for removing excess water from agricultural fields (Blann et al., 2009). The efficiency of water removal from agricultural fields with drainage is further enhanced by preferential flow. This link between preferential flow and subsurface drain outflow has been established by several studies (Chapter 2; Fox et al., 2004; Kladivko et al., 1999; Heppell and Chapman, 2006). A common technique to account for the percentage of storm flow due to preferential flow has been the application of end-member mixing analysis (EMMA) on subsurface drain discharge utilizing conservative tracers (e.g. bromide, chloride) (Richard and Steenhuis,

1988; Stone and Wilson, 2006; Schilling and Helmers, 2008). Increases in subsurface drain discharge within hours after a storm event is often attributed to a large network of preferential flowpaths. In an Indiana subsurface-drained watershed, underlain by poorly drained silty clay loam, Stone and Wilson (2006) found drain flow peaked within two hours of a large rainfall event (45.2 mm) with an estimated 51% of the subsurface drain flow contributed by preferential flowpaths. In Chapter 2, the specific conductance study found similar transport velocities on similar soils in north-central Iowa using continuous measurements of specific conductance.

Monitoring water table height at high-resolution with automated pressure transducers (e.g. 15 minutes), especially during and after storm events, can help give insight into water table fluctuations. For example, several studies have deployed piezometers to evaluate unsaturated zone flowpaths to shallow water tables (Kao et al., 2001; Zhang and Schilling, 2006; Villholth et al., 1998; Heppell et al., 2000). Controlled plot studies, with known amounts of applied irrigation water (Villholth et al., 1998), and longer term rainfall monitoring (James and Fenton, 1993; Heppell et al., 2000) have elucidated insights into the role of preferential flow. Rapid rises in the water table height, during and shortly after rainfall events, are attributed to preferential flow bypassing the soil matrix through the unsaturated zone. Heppell et al. (2000) found that the soil did not have to be completely saturated to initiate preferential flow, at least through inter-aggregate macropores (e.g. structural voids). Measurable water table increases occurred within the period of rainfall events, showing a seemingly instantaneous rise due to the uncertainty of the time series resolution.

As part of a field study attempting to interpret preferential flow patterns, it is important to characterize basic soil parameters (i.e., bulk density, particle density, particle size distribution) and the saturated hydraulic conductivity of the near-surface soils where water infiltration begins. However, saturated hydraulic conductivity (K_s) is difficult to gauge under variable field conditions, especially for soils with a high clay content, as K_s is considered a constant for a rigid, saturated soil and does not take into account air-filled pores (Jury and Horton, 2004). Field-saturated hydraulic conductivity (K_{fs}) measurements, on the other hand, take into account the effect of entrapped air within the downward infiltrating water (Reynolds et al., 2002). For near-surface soils, K_{fs} measurements taken across a broad spectrum of locations at different times during the year can help determine the spatial and temporal variability that can either limit or foster water movement into the subsurface soils (Nimmo et al., 2009).

Subsurface flow processes were investigated as part of a U.S. Geological Survey study to better understand agricultural chemicals transport (Capel et al., 2008). Substantial preferential flow was determined to occur throughout the year, as determined by utilizing specific conductance as a tracer of infiltrating surface water into subsurface drain flow within hours after rainfall or snowmelt events (Chapter 2). Up to 78% of the subsurface drainage flow during two storm events was found to originate from preferential flow. Physical evidence for macropore structures has been documented at the field site, mainly derived from root channels and cracks and fissures between soil aggregates caused by soil desiccation (Fig. 3.1).

This paper describes the use of shallow water-table rises occurring over a period of three years (mainly during the growing season), adjacent to a subsurface drain, to

elucidate the spatial and temporal variability of preferential flow. Additionally, soil moisture contents and field-saturated hydraulic conductivities were measured with single infiltrometers during periods of the three-year study. Maximum water velocity and drainable porosity, based on the timing and amount of precipitation, respectively, were calculated for 51 events, totaling 188 individual observations. Variability in maximum water velocities due to seasonality, proximity to the subsurface drain, and land cover was investigated. Variability in the field-saturated hydraulic conductivities was also compared for the same factors, as well as its connection with the maximum water velocity.

2. **Site Description**

The 38.8 hectare study field (Fig. 3.2) is located in Hamilton County, Iowa, adjacent to a USGS stream gage (USGS 05451080; U.S. Geological Survey National Water Information System). Land use for the study field is mainly row-cropped agriculture, with a 25 m grassy buffer along the northeastern portion of the study site adjacent to the South Fork of the Iowa River (SFIR). The grassy buffer was set aside from row-cropped agriculture (corn, soybeans) in 2006. The field is situated within the SFIR watershed, which is dominated by corn and soybean production covering about 92% of total land area (McCarthy et al., 2011). Planting dates for the field site occurred on May 17, 2007 (soybeans) and May 17, 2008 (corn) with harvest dates occurring in late October for both years (S. Kalkhoff, U.S. Geological Survey, pers. communication, 24 February 2011).

The silty loam and clay loam soils of the study site are part of the Clarion-Nicollet-Webster soil catena, a soil association common in north-central Iowa and south-central Minnesota (Dideriksen, 1986; Swanson, 2003). This soil association is generally flat to

gently sloping (0 to 3 percent) with principally poor drainage except for ridges. Ridges are predominantly the well-drained Clarion loam, lowland flat areas are dominated by the Canisteo, Webster, and Harps loams, shoulder areas are dominated by the Nicollet loam, and the depressions are dominated by Okoboji loam (National Cooperative Soil Survey, 1986). Soils at the field site have a silt to clay loam texture (based on USGS size classes) with an average of 16.0% clay, 27.3% sand, and 56.7% silt. Based on soil cores from the field site, an interbedded layer dominated by medium to coarse sand occurs between 0.6 to 1.2 m, varying in width but averaging approximately 0.3 m. A typical soil profile is 2 m in depth, underlain by glacial deposits of the Des Moines Lobe (Bettis et al., 1996). The Des Moines lobe deposits act as a confining layer, effectively limiting most of the water transport to the upper 2 m.

The study site was drained by two active subsurface drains (21-cm and 60-cm diameter outlets, inner diameter), located just downstream of the stream gage (Fig. 3.2). Known subsurface drain locations throughout the field site, including vertical surface-drain inlets, are also shown. Based on previous work at the site (Roth, 2010; Chapter 2), most of the water inputs to the field site (rainfall, snowmelt) are either lost due to evapotranspiration or removed through subsurface drains via infiltration or vertical surface-drain inlets. The study site is representative of the entire subwatershed, with the subsurface drainage dominating the overall hydrologic budget (Tomer et al., 2008). Subsurface drainage for the entire subwatershed started in the early 1900s to remove excess water from the soil profile, although exact installation dates for the study's two subsurface drains are unknown.

North-central Iowa has a mean annual rainfall of 83 cm, with a strong seasonality in the early spring months (April-June) and occasional heavy mid-summer rainfalls. Two of the three study years, 2007 and 2008, had above average precipitation with 114 cm and 124 cm, respectively (McCarthy et al., 2011). Generally, summer months (July-August) have an annual minimum in rainfall, higher evapotranspiration and lower stream discharge. Annual evapotranspiration is 65 to 75 cm, so the above average precipitation in late 2007 and early 2008 contributed to the record spring floods of 2008 (Krajewski and Mantilla, 2008). Temperatures at the field site range from a mean of -7.7°C in January to a mean of 23.4°C in July.

3. Methods

3.1 Piezometer water levels and soil specific parameters

Two piezometer lines, each containing five piezometers, were installed perpendicular to the drain by a direct push machine (Geoprobe™ Model 540MT) to study the immediate capture zone and flow to the drain (Fig. 3.2). This scheme was duplicated in the cropped portion of the field (referred to as the field array) and in the grassy buffer strip adjacent to the field (referred to as the grassy buffer array). Piezometers were set at approximately 1.2 m below land surface at distances of 0.3 m, 1.0 m, 3.0 m, 7.6 m, and 15.2 m from the subsurface drain. All piezometers were constructed of 2.54-cm (1") diameter polyvinyl chloride. The bottom screen length was 0.3 meters. All piezometers were surveyed and land surface elevations were determined with respect to National Geodetic Vertical Datum 1927 (NGVD).

All of the piezometers were set with encapsulated pressure transducers that calculated the water depth (i.e., depth of water in well) (Solinst Levelogger 3001) every 15 min. All of the water level records were originally recorded to the nearest 0.01 foot (i.e., stated accuracy of pressure transducer), then transformed to meters for the purposes of this publication. Two redundant encapsulated pressure transducers (Solinst Barologger), open to the atmosphere, were installed at the site in order to compensate for changes in air pressure. Monthly site visits included manual steel-tape water level measurements to check against the recorded pressure transducer water level. When the pressure transducer did not match the manual measurement, an adjustment was made to calibrate the recorded level of the pressure transducer to the manual measurement.

Three soil moisture probes (Decagon EC-5) were installed in a parallel line from the buffer array piezometers, set at 0.9 m, 7.6 m, and 15.2 m away from the subsurface drain. Probes were buried 0.6 m below land surface (BLS) underneath the tilled agricultural field (Fig. 3.2). Unsaturated zone volumetric water content (VWC), cubic meters of water per cubic meter of soil, was obtained by converting the output voltage from the soil moisture probe into a VWC percentage. In order to establish more accurate VWC results, a cored soil subsection was used to create a specific calibration equation between excitation voltage and the VWC (D. Cobos, Decagon Devices, Inc., personal communication, 28 May 2011; Appendix C).

The nearby stream gage (USGS 05451080) measured instantaneous discharge and gage height every 30 min. Precipitation was measured with a 20.3 cm diameter tipping bucket rain gage, recorded every 30 min (Texas Electronics TE525WS). Gaps in the precipitation record, as well as all of the 2009 rainfall measurements, were filled with

precipitation data from Webster City, Iowa (28 km from study site) (Iowa Department of Transportation, 2011). Air temperature measurements at the study site were recorded every 15 minutes.

Soil specific parameters were measured by subsampling five 1.7-meter cores, representing the distinct soil types, collected from the field site in 2010 (Appendix F). Measured parameters included soil bulk density, particle density, volumetric water content (VWC), and particle size analysis (PSA) distribution. Bulk density measurements were calculated utilizing the short core method (Grossman and Reinsch, 2002), with an adjustment made for the VWC. Particle density measurements were determined utilizing the pyncometer method (Blake and Hartge, 1986). VWC was determined through the thermogravimetric method using a muffle furnace set at 105°C for 24 h (Topp and Ferre, 2002). PSA was carried out separately at the Menlo Park Unsaturated Zone Flow Laboratory (U.S. Geological Survey), utilizing the Coulter LS-230 Particle Size Analyzer (K. Perkins, U.S. Geological Survey, pers. comm.). PSA measurements were also evaluated from an additional core collected in 2009. Porosity was derived from the bulk and particle densities (Jury and Horton, 2004).

Daily evapotranspiration (ET) was estimated using the Water Erosion Prediction Project (WEPP) model (Flanagan et al., 1995). Daily minimum/maximum temperature and total precipitation values were from Webster City, Iowa (Iowa Department of Transportation. 2011); other necessary climate parameters not available were augmented using a stochastic climate generator included within WEPP. In combination with the WEPP preconfigured plant growth input files, the specific dates for planting, harvesting,

and tillage were utilized to most accurately represent ET along with a digital elevation model (DEM) of the field site.

3.2 Calculation of the maximum water velocity (v_{max})

The piezometer water level records were analyzed for any discernible water level rises, after any rainfall event, to measure the maximum water velocity (Nimmo, 2003). An event was classified as any water level rise greater than 0.02 m, reducing the possibility of artificial rises due to instrument error or other potential interferences. As part of the data analysis, each event required a paired precipitation. For any given precipitation, up to five individual observations (i.e., one from each piezometer in the line) could be observed.

The time to water table rise (t_{WT}, in seconds) was the difference in time between the first recorded increment of precipitation and the first water level rise ≥0.02 m (Fig. 3.3). Water table depth (d_{WT}) was the water table depth BLS at the first instance of a water level rise. In some cases, the water level rise started below the bottom of the piezometer; however, the first water level rise was taken as when the water level was detectable in the piezometer (Fig. 3.3). Dividing the water table depth BLS (d_{WT}) by the t_{WT}, the maximum water velocity (v_{max}) was calculated for each event for every piezometer with a discernible water level rise using Eq. [1]:

$$v_{\max} = \frac{d_{WT}}{t_{WT}} \quad [1]$$

In total, 39 events were classified for 2007-2008 for in the cropped field area, and an additional 12 events in 2009 in the grassy buffer area. A second estimate of maximum water velocity ($v_{max\text{-}1\ mm}$), considered a less conservative estimate, was the difference in

time between a cumulative precipitation of at least 1-mm and the first water level rise ≥0.02 m. This second estimate is based on the concept that a minimum saturation in the uppermost soil layer must occur before preferential flow can occur (Germann et al., 2007). Throughout the rest of the paper, the discussion will characterize the earlier described v_{max}, with specific reference to $v_{max\text{-}1\ mm}$ in order to avoid confusion.

As part of the v_{max} analysis, each event was identified as inundated or non-inundated, dependent on whether the subsurface drain was at least partially inundated by the stream. These events were classified based on the stream gage height, with values greater than 1.92 m classified as inundated given the stream is flush with the bottom of the subsurface drain outlet at this depth.

3.3 Drainable porosity (p_{dp})

Drainable porosity is the available pore space in the unsaturated zone easily filled by infiltrating water, essentially the difference between the field capacity and complete saturation of the soils (Sands, 2001). The ratio of precipitation to water level rise was calculated for every event, following a similar approach used by Fisher and Healy (2008) and Shah and Ross (2009) to calculate specific yield. Total rainfall amount (in mm) falling within a specified period, *R(t)*, was divided by the associated water level rise due to the specific rainfall event (in mm), $\Delta H(t)$, to calculate the drainable porosity ratio, p_{dp}, of water necessary to explain the water level rise.

$$p_{\mathrm{dp}} = \frac{R(t)}{\Delta H(t)} \qquad [2]$$

Eq. [2] is similar to the specific yield (Shah and Ross, 2009), but modeled after the concept of drainable porosity (Skaggs, 1976; Braun and Kruijne, 1994). Eq. [2] assumes

that all of the water infiltrates and assumes zero loss by overland runoff and evapotranspiration.

3.4 Field-saturated hydraulic conductivity (K_{fs})

Field-saturated hydraulic conductivity values (total = 105) were determined in June, July, and August, 2008 and August and October, 2010 across a broad spectrum of study site locations. Based on SSURGO GIS coverage (GIS coverage location), five soils (Clarion, Nicollet, Harps, Canisteo, and Okoboji) were tested under different land covers (corn, soybeans, grassy buffer and bare ground) (USDA National Resource Conservation Service, 2009). A soil core (1.7 m long) was obtained in each of the five soil types and measured for specific parameters previously described to confirm the accuracy of the SSURGO data (Tomer and James, 2004).

The field-saturated hydraulic conductivity (K_{fs}) method was based on the technique from Nimmo et al. (2009) designed for rapid areal characterization of K_{fs} to capture the inherent spatial and temporal variability. A standard plastic, five-gallon bucket with the bottom removed (inner diameter of 26 cm) operated as a single-ring infiltrometer. Each measurement started with driving the bucket into the soil approximately 5 cm after selecting an area free of impediments such as crop residue or large stones. In some cases, the bucket could not be pushed the full distance, so the outside rim of the bucket was packed with bentonite to prevent water leakage. Before starting each test, a plastic mat with an attached string (removed after water added) was placed on the soil surface to prevent disturbance. Water was added to a depth of 7.6 cm (3") at one time. Water infiltration was timed immediately after the start of pouring, and recorded until all the water had infiltrated into the soil surface. In some cases, the test was not taken to

completion due to extremely slow infiltration rates. To document physical evidence for macropore and shrink/swell structures in the soil surface, photographs were taken before and after each test for the August 2010 measurements.

Several simplifying assumptions are built into the K_{fs} derivation (Nimmo et al., 2009), shown in Eq. [3]:

$$K_{fs} = \frac{L_G}{t} \ln\left(\frac{L_G+\lambda+D_0}{L_G+\lambda+D}\right) \quad [3]$$

$$L_G = C_1 d + C_2 b \quad [4]$$

Water depth inside the single-ring infiltrometer is accounted for by an initial depth of water inside the bucket, D_0, and at subsequent water depths during the experiment, D. A series of time-depth measurements are taken throughout the experiment. Time, *t*, is in seconds and for instances where the water has completely run out of the infiltrometer, the final time, t_f, is substituted into Eq. [3]. The λ-value, an index parameter that takes into account the capillary forces that govern water movement, has a given value of 0.08 m based on assumptions given by Elrick et al. (1989). A second parameter, L_G, takes into account the geometry factors of the experiment's setup, including the ring radius, *b*, the ring insertion depth, *d*, and two empirically derived constants from Reynolds and Elrick (1990), C_1 and C_2, as shown in Eq. [4].

For the K_{fs} measurements reported in this study, Eq. [3] is rearranged into Eq. [5] so that the right-hand side of Eq. [5] versus *t* yields a slope of K_{fs}:

$$K_{fs} t = L_G \ln\left(\frac{L_G+\lambda+D_0}{L_G+\lambda+\mathrm{D}}\right) \quad [5]$$

For further elaboration of the field-saturated hydraulic conductivity measurements, the methods and the mathematical theory of the calculated K_{fs} are derived in Nimmo et al., 2009.

4. Results

4.1 Water level rises

Prior to utilizing water level rises to determine maximum water velocity, a connection was established between the between the observed water level rises and the decreases in specific conductance (Chapter 2) values that were shown to illustrate preferential flow events. Fig. 3.4 illustrates an event on June 22, 2007 with synchronous water level rises (t_{WT}) and the SC onset time (τ_{EO}), establishing a linkage between observed increases in water table rises to infiltrating precipitation (low SC).

Gage precipitation (in mm) and water levels (in m) for each of the field array piezometers, from 0.3 to 15.2 m away from the subsurface drain, were collected for 2007 and 2008 (Fig. 3.5). For each piezometer, the land surface, estimated subsurface drain depth, and the maximum piezometer depth are also illustrated for reference. The top of the piezometer screen was within 0.08 m of the top of the subsurface drain except for the 7.6 m piezometer which was 0.16 m below the subsurface drain depth. With this piezometer arrangement, these water levels essentially show the active period of free drainage during which the water table was above the subsurface drain height, assuming the water flows towards the subsurface drain.

A strong association existed between precipitation and piezometer water level rise throughout the two-year study period. After a rain event, the piezometer water level

would generally show a rapid response, often within four hours from the start of a rainfall event. This relation particularly holds true for events earlier in the year, from late March until late June, in both 2007 and 2008. From July until mid-August, the water levels are generally below both the piezometer screen and the subsurface drain depths. Only after large events, such as late August 2007 and mid-October 2007, do the water levels rise above the subsurface drain and again become associated with rainfall events. For 2008, water levels after June rise briefly only in mid-July. None of the late growing season rains in 2008, from mid-August through October, caused measurable water level rises.

Differences in the magnitude of water level rise occurred with increasing distance away from the subsurface drain. Generally, the magnitude of the water level rise was greater for the farther piezometers relative to the closer piezometers (Fig. 3.5). Part of this relationship was due to the slightly increasing land surface elevations (+0.1 m) away from the subsurface drain. Also, the starting water level for the closer piezometers was often unknown as it was below the bottom of the piezometer. However, the overwhelming explanation of this pattern is the drawdown influence of the subsurface drain. Piezometers that are closer drain faster as demonstrated by the steeper slope of the recession of the water levels (Fig. 3.3).

Precipitation (in mm) and water levels (in m) for each of the five grassy buffer array piezometers, from 0.3 m to 15.2 m away from the subsurface drain, were collected for 2009 (Fig. 3.6). For each piezometer, the land surface, estimated subsurface drain depth, and the maximum piezometer depth are also illustrated for reference. An association existed between rainfall and water level rise; however, the association is not as strong as for the field array piezometers. After a rainfall event, fewer events showed a rapid

response and the remainder of the events showed a more subdued response. By looking at the precipitation paired with the various events, the largest events did lead to a substantial water level rise with the smaller rainfall events showing little evidence of causing a water level rise. As in the field array (Fig. 3.5), the height of the water level rise increases with distance away from the subsurface drain.

4.2 Maximum water velocity (v_{max})

The maximum water velocity was calculated for 51 events, including a total of 188 individual observations (Table 3.1; Appendix D). Each year was calculated separately, although there was not a distinct difference for mean v_{max} for the field and grassy buffer arrays based on a t-test (P = 0.874). Within the group of field piezometers, 2007 and 2008 were treated separately and the groups were further subdivided into non-inundated periods and inundated periods. For the buffer array, data was only available for 2009, and the data was also subdivided into non-inundated periods and inundated periods.

The field array did not exhibit a distinct maximum water velocity (v_{max}) from the grassy buffer array (Table 3.1). For 2007, the difference of the means for the non-inundated and inundated events was <3 m day^{-1}. On the other hand, the difference between the means of these two categories for 2008 was >11 m day^{-1}. The large disparity between these two years is discussed below. The v_{max} distributions were skewed and non-normal as shown in a histogram (Fig. 3.7), as small events with lower v_{max} values were more common than the larger v_{max} values that influence the overall larger mean values when compared to the median values. This is also apparent by the large standard deviations for the mean values.

An analysis of v_{max} values over the three-year record presented regular seasonal variations, suggesting that underlying spatial and temporal variations in preferential flow pathways (i.e., macropores, cracks, fissures) affected v_{max} (Fig. 3.8A-C). If the amount of water infiltrating through preferential flow pathways was different by the time of year, distance away from the subsurface drain, the growing season land cover, and/or stream inundation of the subsurface drain, the calculated v_{max} would have been expected to vary systematically.

With respect to time, there were statistically distinct seasonal periods with substantially higher v_{max} values. For 2007 (Fig. 3.8A), v_{max} from April until mid-June was lower relative to mid-summer. By mid-June, the v_{max} values were 10 to 20 m day^{-1}. The event in mid-August led to even higher water velocities (up to 42 m day^{-1}). By October, values returned back to below 15 m day^{-1} and did not begin to increase again until April 2008 when the v_{max} values reached peak values during the early growing season (Fig. 3.8B). Due to the excessive rains from late April until mid-June 2008, the v_{max} values were elevated compared to other time periods (42 m day^{-1} in two observations, and as high as 94 m day^{-1} in one late April event). However, by mid-June, the maximum water velocities decreased. After July 2008 no more events occurred. For 2009 (Fig. 3.8C), the grassy buffer array exhibited the same peak in v_{max} during the growing season, with a maximum v_{max} up to 43.6 m day^{-1}. However, most of the other events exhibited much smaller v_{max} values.

When all the v_{max} data were combined and plotted by Julian date, four distinct periods were distinguished (Fig. 3.9; Table 3.2): Julian date 105 to 135 (April 16th to May 15th), Julian date 136 to 181 (May 16th to June 30th), Julian date 182 to 243 (July 1st to

August 31st), and Julian date 243 to the following Julian date 105 (September 1st to April 15th). Maximum water velocities (v_{max}) were log-transformed for statistical comparison. Using either paired t-tests or Mann-Whitney rank sum tests (Table 3.3), all of these periods were strongly distinct from one another with the exception of the early spring period (Julian date 105 to 135) and the mid-summer period (Julian date 182 to 243). The early spring period was also not statistically significant at the 5% level from the early summer period (Julian date 136 to 181).

With respect to distance away from the subsurface drain, a one-way analysis of variance (ANOVA) test was performed on the v_{max} values to test whether a difference existed. The v_{max} data were log-transformed to perform the one-way ANOVA. The difference in the mean v_{max} values of the different piezometers as a function of distance from the subsurface drain were not statistically significant (P = 0.972).

With respect to growing season land cover, the field array was soybeans for 2007 and corn for 2008. Large v_{max} differences did not exist between the two field array years, as the v_{max} values were only separated by 1.6 m day^{-1} and a t-test of the log-transformed v_{max} values did not show the two years as statistically different (P = 0.969). As previously mentioned, the field array and buffer also did not show a significant difference (P = 0.874) with only a 0.5 m day^{-1} separation between the means.

With respect to stream inundation of the subsurface drain, statistical tests were performed on the log-transformed v_{max} values of the three different years. The two field array years were not significant, although the t-test of the v_{max} values for stream-inundated periods was right at the cutoff of P = 0.050. T-test runs between the 2007 and

2008 field array v_{max} values and the 2009 grassy buffer array v_{max} values were not statistically different, with P values of 0.367 and 0.540, respectively.

The second estimate of maximum water velocity ($v_{max\text{-}1\ mm}$), considered a less conservative estimate, was plotted against the regular v_{max} (Fig. 3.10). For most of the calculations, the new criteria of at least 1-mm of cumulative precipitation did not make a difference as these calculations fell on or close to the 1:1 line; however, there were several calculations that broke away from the 1:1 line. These new averages, $v_{max\text{-}1\ mm}$, are shown in Table 3.1 with higher average values for all the categories. However, despite much higher average v_{max}, these new calculations did not change the overall interpretations but only would have driven the calculated v_{max} to higher values. Instead, these new values only further illustrate the rapid maximum water velocities.

4.3 Drainable porosity (p_{dp})

Drainable porosity (p_{dp}), the percentage (in decimal) of available pore space for water storage, was calculated for 143 individual observations, most <0.20 and only a few from the extremely wet period from April to early June 2008 were greater than 0.20. Mean drainable porosity (p_{dp}) was 0.114 for all the individual field array observations and 0.181 for the grassy buffer array observations; overall, the mean p_{dp} was 0.139. These values are considerably higher than previously published values for similar soils in Indiana (0.045, Fisher and Healy, 2008).

When all the p_{dp} values were combined and plotted by the maximum height of piezometer water level during an event, two distinct patterns were found (Fig. 3.11). All maximum heights <0.55 m were within a small band below a p_{dp} value of 0.10, while a

largely scattered pattern existed above >0.55 m. The likely reason for the scattered pattern is the effect of evapotranspiration and other unaccounted water losses within the upper unsaturated zone. For this reason, the real p_{dp} value for all events was limited to events with a maximum height of piezometer water level <0.55 m.

The overall average p_{dp} for a total of 27 observations with a maximum piezometer height during an event <0.55 m was 0.052. The difference between the mean values of the field and grassy buffer arrays were not statistically significant, based on a t- test (P = 0.060), given the new criteria based on the cutoff at 0.55 m.

4.4 K_{fs} infiltrometers measurements

The field-saturated hydraulic conductivity (K_{fs}) characterizes the hydraulic conductivity of the near surface soils when applying a specific depth of water (3") to the soil surface, replicating the process of large rainfall events (Nimmo et al., 2009). K_{fs} values (total = 105) using the bucket infiltrometers were determined in May-August, 2008, August, 2010 and November, 2010 (Table 3.4; Appendix E). Results are grouped both by sample date and by above-ground cover (i.e., corn, soybeans, grassy buffer, and bare ground). As a note, K_{fs} should also not be confused with the maximum water velocities (v_{max}). K_{fs} is a dynamic parameter that depends on the pores and fractures transmitting the water (Heath, 1983), whereas the v_{max} is a rate that is the product of a hydraulic conductivity divided by an effective porosity.

Starting in June, the infiltrometer measured K_{fs} values grew progressively larger through the summer season to August, where the measurements reached the maximum values of 1.7×10^{-4} m s^{-1} and 1.9×10^{-4} m s^{-1} for 2008 and 2010, respectively (Table 3.4).

The May 2008 infiltrometer measured K_{fs} values were statistically larger than the June 2008 K_{fs} values based on a t-test of the log-transformed values (P = 0.009), but not distinguishable from the July 2008 infiltrometer measured K_{fs} values based on a t-test of the log-transformed values (P = 0.110). At the end of harvest in November, the K_{fs} values were smaller than the August measurements at 1.2×10^{-4} m s^{-1} but still larger than the K_{fs} values of May (3.8×10^{-5} m s^{-1}), June (8.1×10^{-6} m s^{-1}), and July 2008 (2.0×10^{-5} m s^{-1}).

The significance of the effects of above-ground cover on the K_{fs} was tested for four different groups: corn, soybeans, grassy buffer, and bare ground. Using a non-parametric test of significance (Mann-Whitney rank sum test), only the corn and bare ground were significantly different from each other (P = <0.001). All of the other groups were not unique; in fact, the mean and median values for soybeans, grassy buffer, and bare ground were very similar and almost indistinguishable.

The variability of the K_{fs} measurements was tested as a function of soil type (Clarion, Canisteo, Nicollet, Okoboji, and Harps) using the August 2010 measurements. Out of the five different groups, Canisteo had the highest number of measurements (24 out of 46) as this is the most common soil type by area at the study site. No statistical differences were found when performing a one-way ANOVA on the log-transformed K_{fs} values of the five different types of soils (P = 0.119).

4.5 Soil moisture conditions and soil specific parameters

Soil volumetric water content (VWC) was measured in the cropped field portion of the study. The results of the 0.6- and 0.9-m depths from 0.9, 7.6 m, and 15.2 m from the subsurface drain are shown in Fig. 3.5. VWC changed in similar time periods as the water

level rises, with a correspondence of water level rise and an increase in VWC for close to every event. This high association between spikes in the soil VWC and the timing of individual water level rises occurred for events throughout the two-year VWC record in comparison to the field array water levels (Fig. 3.5). Each of the three locations where soil VWC was measured, 0.9 m, 7.6 m, and 15.2 m, behaved in a concerted fashion, such that the timing of VWC rises was similar. However, the magnitudes of the VWC shifts at each location were different, with greater VWCs for locations closer to the subsurface drain. This was likely due to the influence of the subsurface drain on the local antecedent moisture conditions because drainable water from the unsaturated zone was being drawn out faster by proximity to the subsurface drain. Finally, a lack of events during the winter season, from November until early March, suggested that the sub-soils were frozen.

The average total porosity for all five of the soil types at this site was 0.383, based on laboratory measurements of particle and bulk densities (Appendix F). Total porosities ranged from 0.261 and 0.607 for the 5^{th} percentile and 95^{th} percentile, respectively.

5. Discussion

5.1 Seasonal influence on v_{max}

A major observation from the three-year study for both the field and grassy buffer arrays was the fast arrival of rainwater to the water table. Based on the mean v_{max} value for all events (10.5 m day^{-1}) and the average distance to the water table for all events (1.10 m), rainfall on average reaches the water table in 2.5 hours. This is similar to the average of 2.3 hours for a detectable decrease in specific conductance (SC) of the subsurface drain outflow (Smith and Capel, in review). As lower SC water is indicative

of new water, such as rainfall or snow melt, the similarity in these two values suggests a substantial amount of preferential flow exists at the study site.

Fastest water velocities occurred in mid-to-late summer (July 1st to August 31st, period 3) (Fig. 3.8A-C, Fig. 3.9, Table 3.3) when preferential flow pathways would likely be at a maximum. This was supported by the visual observation of surface soil cracks (Fig. 3.1) and the infiltrometer measured K_{fs} values (Table 3.4). Edwards et al. (1993) found maximum preferential flow after high intensity rainfall events on relatively dry no-till soils. While soils at the study site were moldboard plowed in fall 2007, persistent subsurface preferential flowpaths, surface soil cracking and shrinking, and a sustained period of high evapotranspiration would cause high v_{max}. The lack of such large events mid-to-late summer in 2008 and 2009 (Fig. 3.8B, Fig. 3.8C) was likely a combination of less high intensity rainfall events (2008, 2009) and high evapotranspiration from the maturing corn (2008) compared to soybeans (2007).

Due to the rainfall patterns of this region, late summer events occurred less often than the early spring rains (April 15th-May 15th, period 1) which is the second fastest period for v_{max}. Heavy spring rainfall soaked the unsaturated zone, causing a higher amount of preferential flow yielding faster v_{max}. This period also had the highest number of individual water level rises (58 observations). Stone and Wilson (2006) estimated high preferential flow from two May events on similar soils in Indiana. Kumar et al. (1997), studying subsurface drain discharge from the same soil catena as this study's field, found higher amounts of preferential flow in spring and a subsequent seasonal decline in the percentage of subsurface drain discharge attributable to preferential flow. It would be expected that less preferential flow pathways, such as macropores, would exist during

this period; however, preservation of deeper macropores would likely survive the winter season and highly saturated surface soils would overcome the potential lack of continuous macropores directly to the surface. With higher amounts of preferential flow, a higher likelihood of nutrient leaching could occur, as this field often has spring application of fertilizer, particularly before corn planting (S. Kalkhoff, U.S. Geological Survey, pers. communication, 24 February 2011).

Mid-range maximum water velocities occurred from May 16 to June 30 (Table 3.2, period 2), with mean v_{max} of 8.62 m day^{-1}. This period covered the crop emergence, so evapotranspiration became increasingly important both for the field (corn/soybeans) and the grassy buffer. Vertical macropore development directly from the surface also became more important, as shrink/swell cracks form and wormholes became more prevalent (Andreini and Steenhuis, 1990).

The fourth period, from Sept. 1st to April 15th (period 4) had the lowest mean maximum water velocity of 7.05 m day^{-1}. This is partially attributable to the frozen soils during a considerable part of this period and the destruction of surface-connected macropores after fall moldboard plowing that would have occurred in fall 2007. Preferential flow pathways presumably still existed below the plow zone; however, due to the destruction of the surface macropores, the lower v_{max} values indicative of this period were likely caused by the lost junction to the preserved subsurface macropores. Logsdon (1995) found that preferential flow does occur for buried macropores, although not quite as efficiently as continuous macropores. Only after temperatures warmed up in the spring, spring rains started to saturate the surface soils, and biological activity began would the near-surface preferential flowpaths become initiated again.

5.2 Effect of distance to subsurface drain

A range in v_{max} was observed across the field and grassy buffer arrays, but no significant differences in v_{max} existed for the different distances from the subsurface drain ($P = 0.972$). However, considerable variability existed for any given single event. For example, an event on May 6th, 2008, had v_{max} ranging from 5.12 m day^{-1} (0.3 m away) up to 42.4 m day^{-1} (7.6 m away) (*see* box in Fig. 3.8B). Generally though, the v_{max} range for any one event was relatively small for the various distances from the subsurface drain.

The overall magnitude of piezometer water level rise does vary with distance to the subsurface drain. Closer proximity piezometers to the drain declined faster than the piezometers at farther distances. Infiltrating water from the surface, closer to the subsurface drain, had a shorter lateral distance to reach the subsurface drain. Furthermore, this is potentially an indication that the vertical mean transport rate is greater than the horizontal mean transport rate. With increasing distance away from the subsurface drain, the water table took longer to reach an equilibrium static level because water was unable to drain as fast horizontally.

5.3 Spatial and temporal heterogeneity of K_{fs}

The field-saturated hydraulic conductivity (K_{fs}) varied on a seasonal basis; progressively larger infiltrometer measured K_{fs} values were observed as the growing season progresses (Table 3.4). Winter and early spring are expected to have the lowest overall K_{fs}, due to the lack of open surface cracks (Beven and Germann, 1982), frozen surficial soil through much of this period, and low biological activity. The lowest v_{max} occurred during this period (Table 3.3).

The heavy rains of spring began to cause the surface soils to become closer to saturated. Previously unconnected preferential flow pathways opened up; the shrinkage and swelling of the silt clay loam produced open surface cracks (Fig. 3.1). The calculated v_{max} during this period was the second highest (Table 3.3), and the May 2008 K_{fs} values were shown to be in the mid-range of the infiltrometer measured K_{fs} values (Table 3.4).

During the early-to-mid summer, the formation of a surface seal resulting from the spring rains likely impeded vertical infiltration into the subsurface, limiting the infiltration capacity and resulting in lower K_{fs} (Assouline, 2004). K_{fs} values were lower in June and July (8.1×10^{-6} m s^{-1} and 2.0×10^{-5} m s^{-1}, respectively) than in May. This soil surface sealing was caused by fine soil particles, resulting from aggregate destruction, to extensively cover the ground and effectively seal off potential preferential flowpaths. Additionally, the swelling of the highly smectitic clays within these soils can not only cause the formation of large cracks, but also swell other fissures shut.

Open surface cracks and fissures were easily visible in August 2008 and 2010 (Fig. 3.1), and the largest K_{fs} values were measured in August (Table 3.4). As highlighted by Beven and Germann (1982), surface cracks and fissures have been shown to remain open during several wetting and drying cycles. After harvest, tillage destroyed the surface macropores (Ogden et al., 1999; Logsdon, 1995), causing K_{fs} values to once again lower. The K_{fs} values measured in November 2010 were lower than the August 2010 values.

The effects of the above-ground cover on K_{fs} are shown to exist between sites for corn (48 measurements) versus bare ground (38 measurements). This result supports by previous studies, such as Mohanty et al. (1994) and Warner and Young (1991). Corn

roots provide a preferential flow pathway for water infiltration, in addition to the preferential flow pathways formed as the corn roots decay. The other roots, such as soybeans and grasses, also provide superior water infiltration pathways but these values were not statistically different than bare ground.

Spatial variability in K_{fs} was not significant when sub-dividing the August 2010 measurements into five different soil types. The lack of a spatial trend (P = 0.119) was likely caused by the heterogeneous structure of the near-surface soils, despite expected differences in K_{fs} between hillslope soils such as the Clarion versus a depression soil such as the Okoboji (Swanson, 2003). Side-by-side measurements (within three meters) often showed orders of magnitude differences in terms of the K_{fs}. Large differences between nearby measurements demonstrated the heterogeneous structure of the near-surface soils, in agreement with the highly complex spatial variability in preferential flow patterns reported by Andreini and Steenhuis (1990). They suggested that the spatial differences that are important in an area <1 m^2 are not important for larger areas (10's of square meters), as the variability between individual K_{fs} measurements would balance out.

Overall, K_{fs} was shown to vary temporally, but not spatially. These results are consistent with the maximum water velocity (v_{max}) results (Table 3.3), as the four different v_{max} periods were arranged in the same order as the variations in K_{fs}. If surface soils were influencing water velocities and the expected time for water to infiltrate, the changes in K_{fs} over time would also affect the preferential flow flux.

5.4 Inundated periods versus non-inundated periods

Another factor which influences v_{max} was whether or not the subsurface drain outlet was inundated by stream water. In cases where the subsurface drain was partially or fully inundated by the stream, v_{max} tended to have higher magnitudes. For example in 2007, the difference for v_{max} between inundated versus non-inundated periods was 10.6 m day^{-1} and 7.86 m day^{-1}, respectively; however, these results were not statistically different based on a t-test of the log-transformed v_{max} values (P = 0.370). In 2008, the difference for v_{max} between inundated versus non-inundated periods was significantly different (log transformed, P = <0.001), with an inundated mean of 16.0 m day^{-1} versus a non-inundated mean of 4.55 m day^{-1}. In 2009, the difference for v_{max} between inundated versus non-inundated periods was wide again at 14.0 m day^{-1} and 7.90 m day^{-1}, respectively, although these values were not significantly different (log transformed, P = 0.193).

All of the v_{max} data (three years, buffer and field arrays) was divided into two groups, periods of inundation and non-inundation. The following parameters were compared against each other for inundated versus non-inundated periods: rainfall amount, maximum height of stream during an event, pre-event height of piezometer water level, maximum height of piezometer water level during an event, pre-event VWC (for each probe), and maximum VWC during an event (for each probe). Rainfall amount, the pre-event height of piezometer water level, and the maximum height of piezometer water level during an event stood out as significantly different between the two types of periods (Mann-Whitney rank sum test, P = <0.001) and also the most important factors as different between the two periods. For inundated periods (with higher v_{max}), the mean

rainfall amount was 29.2 mm compared to 14.3 mm for non-inundated periods. Mean pre-event height of piezometer water levels were 0.31 m higher for inundated events compared to non-inundated periods, and mean maximum height of piezometer water level during an event were 0.54 m higher for inundated events. For the remaining parameters, all were still significantly different with the exception of the maximum VWC during an event at both 7.6 m (Mann-Whitney rank sum test, P = 0.097) and 15.2 m (Mann-Whitney rank sum test, P = 0.110).

A possible explanation for the different v_{max} for inundated versus non-inundated periods was higher rainfall amounts in general would likely cause more preferential flow and higher v_{max}. With higher pre-event water levels, the water had a shorter distance to travel to reach the water table. As preferential flow pathways have been shown previously to be higher the closer to land surface (Flury et al., 1994; Beven and Germann, 1982), the likelihood of more continuous macropores and cracks to cause water level rises would be increased, leading to higher overall v_{max}. Also, higher rainfall amounts tended to lead to elevated stream flow conditions. This in large part explains why the rainfall amount was correlated with inundated conditions.

5.5 Other factors explaining temporal trends

Temporal variation in the v_{max} can be explained by the degree of formation of preferential flow pathways. Other factors such as antecedent moisture conditions, storm rainfall intensity and amount, climatological effects, and evapotranspiration will have a strong influence on macropore formation, and thereby influence how quickly the water moves to the water table. Factors such as the soil characteristics, biological activity, and tillage have been touched on in previous sections.

Preferential flow events are more likely to occur during periods of elevated soil moisture conditions. As small pores become saturated, water has a higher likelihood to be diverted into larger pores (Jury and Horton, 2004). Soil moisture conditions fluctuate with seasonal conditions, from the increase in soil moisture in the spring to the growing season's removal of water by evapotranspiration. These predictable climatological factors such as heavy spring rains, spring snow melt, increased evapotranspiration in mid-to-late summer, and intense rainfall events in late summer caused predictable patterns over the course of the three-year study period. These predictable factors had an annual effect on preferential flow, and in turn, the maximum water velocity. Atypical climatological factors had an overriding effect on seasonal conditions, such as the above average precipitation that occurred in late 2007 and the first half of 2008.

The maximum water velocities were too fast to be accounted for by matrix flow alone, as most v_{max} values exceeded the matrix flow v_{max} of 2.25 m day^{-1}. During the earlier part of 2007, soil moisture conditions for the locations at 0.9 m and 7.6 m away from the subsurface drain became progressively wetter (Fig. 3.12A). Water level rises corresponded closely with spikes in the VWC record, indicating that even a small-to-modest rain event caused rapid water movement through the subsurface environment. The VWC record tracked the fluctuations caused by the wetting front passing through the unsaturated zone to the water table. This is in line with results from Kung et al. (2000a, 2000b) and Jaynes et al. (2001) that found increasingly faster preferential flow water movement as soils become wetter. Sidle et al. (2000) suggest that soil moisture conditions should have a strong impact on subsurface flows, so the result of rapid increases in soil moisture conditions matching water level rises would be expected.

As the summer began, the VWC continued to slowly rise. With less frequent large rainfall events, there were fewer large fluctuations in VWC (Fig. 3.12B) over the summer. The water level eventually fell below the level of both the subsurface drain and the piezometer. The lack of preferential flow from mid-June to mid-August 2007 was likely caused by a lack of precipitation events, rather than the presence or absence of preferential flow pathways. Finally, starting on August 19th, the next precession of preferential flow events started with some of the fastest v_{max} calculated for the three year period, partly due to the rainfall amount but also attributable to the nearly saturated subsurface soils at 0.6 m leading into the events (Fig. 3.12C).

One of the largest drivers for water movement, aside from precipitation, was evapotranspiration (Winter, 1998). Two different crops, soybeans (2007) and corn (2008), had different evapotranspiration (ET) demands, and, therefore, the timing of maximum ET calculated from the WEPP model was different. To illustrate the effect of evapotranspiration over the course of the crop growth cycle, modeled ET based on nearby climatological data was plotted against the 7.6 m water level and the VWC at 7.6 m. For 2007 (Fig. 3.13A), the ET demand started later in the growing season than in 2008 (Fig. 3.13B). Additionally, total rainfall for the year ended up being above normal only because the rainfall in the latter half of the year made up for the earlier deficits. Faster v_{max} values occurred later in the year in August and October, despite elevated ET due to higher amounts of rainfall.

For 2008 (Fig. 3.13B), the ET increased earlier than 2007 and most of the precipitation arrived in the first half of the year. After July, the combination of elevated ET and low precipitation led to no recorded water level rises and a nearly continuous

water level drop. Gerla et al. (1996) found similar results on North Dakota clayey lacustrine sediments, where a series of water table rises occurred in the spring, only to find rapid depletion in the summer and early fall because of evapotranspiration.

6. Conclusions

In this study, shallow water table rises occurring over a period of three years (mainly during the growing season), adjacent to a subsurface drain, were used to elucidate the spatial and temporal variability of preferential flow. Maximum water velocities (v_{max}) of infiltration, based on the water table rises, were calculated for a total of 51 events (188 observations). Faster v_{max} values implied more preferential transport, as detectable water level rises within a few hours after a precipitation event demonstrated water infiltration that bypassed matrix flow. As v_{max} was shown to be consistently faster than matrix flow alone year-round, a subset of persistent preferential flow pathways were shown to continuously exist and not completely reset after tillage.

Mean maximum water velocity (v_{max}) was 10.7 m day^{-1} and 10.2 m day^{-1} underneath the agricultural field and the grassy buffer, respectively. Strong seasonal trends in v_{max} occurred, with the fastest v_{max} in early spring and mid-to-late summer and slowest v_{max} after fall tillage and early summer after rain-induced soil surface sealing. Proximity of the water table to land surface caused more preferential flow and higher v_{max}. Distance away from the subsurface drain was not shown influence the v_{max}.

Field-saturated hydraulic conductivities (K_{fs}) measured with a simple infiltrometer across a broad spectrum of study site locations were consistent with the seasonal v_{max} trends. K_{fs} values progressively grew larger through the growing season, with the

exception of mid-summer low K_{fs} measurements in late June and July. The influence of above-ground cover (corn, soybeans, grassy buffer, bare ground) on K_{fs} values was only significantly different between corn and bare ground; spatial variability of K_{fs} was not shown to exist.

Temporal trends in preferential flow pathways can be explained by variations in antecedent moisture conditions, storm rainfall intensity and amount, climatological effects, and evapotranspiration. Variations in the soil types must be small enough to not significantly affect the K_{fs}. A decrease after tillage in measured v_{max} and K_{fs} occurred, so tillage must temporarily cutoff surface-connected preferential flow pathways until exchange with the persistent subsurface macropores can be re-established.

References

Andreini, M. S. and T.S. Steenhuis 1990. Preferential paths of flow under conventional and conservation tillage. Geoderma 46: 85-102.

Assouline, S. 2004. Rainfall-induced soil surface sealing: A critical review of observations, conceptual models, and solutions. Vadose Zone J. 3: 570-591.

Bettis III, E.A., D.J. Quade, and T.J. Kemmis. 1996. Hogs, Bogs, and Logs: Quaternary Deposits and Environmental Geology of the Des Moines Lobe. Geological Survey Bureau Guidebook Series No. 18. Ames, Iowa: Iowa Department of Natural Resources.

Beven, K. and P. Germann. 1982. Macropores and water flow in soils. Water Resour. Res. 18: 1311–1325.

Beven, K.J. and R.T. Clarke. 1986. On the variation of Infiltration into a homogeneous soil matrix containing a population of macropores. Water Resour. Res. 22: 383-388.

Blake, G.R., and K.H. Hartge. 1986. Particle density. p. 377-382. *In* A. Klute (ed.) Methods of soil analysis. Part 1. Physical and mineralogical methods. SSSA, Madison, WI.

Blann, K.L., J.L. Anderson, G.R. Sands, and B. Vondracek. 2009. Effects of agricultural drainage on aquatic ecosystems: a review. Crit. Rev. Environ. Sci. Technol. 39: 909–1001.

Braun, H.M.H, and R. Kruijne. 1994. Soil conditions. p. 77-110. *In* H.P. Ritzema (ed.) Drainage principles and applications. International Institute for Land Reclamation and Improvement, Wageningen, The Netherlands.

Capel, P.D., K.A. McCarthy, and J.E. Barbash. 2008. National, holistic, watershed-scale approach to understand the sources, transport, and fate of agricultural chemicals. J. Environ. Qual. 37: 983-993.

Dideriksen, R.O. 1986. Soil survey of Hamilton County, Iowa. United States Department of Agriculture Soil Conservation Service, 157 p.

Edwards, W.M., M.J. Shipitalo, L.B. Owens, and W.A. Dick. 1993. Factors affecting preferential flow of water and atrazine through earthworm burrows under continuous no-till corn. J. Environ. Qual. 22: 453-457.

Elrick, D.E., W.D. Reynolds, and K.A. Tan. 1989. Hydraulic conductivity measurements in the unsaturated zone using improved well analyses. Ground Water Monit. Rev. 9:184–193.

Fenelon, J.M. and R.C. Moore. 1998. Transport of agrichemicals to ground and surface water in a small central Indiana watershed. J. Environ. Qual. 27: 884–894.

Fisher, L.H. and R.W. Healy. 2008. Water movement within the unsaturated zone in four agricultural areas of the United States. J Environ. Qual. 37: 1051-1063.

Flanagan, D. C., and M. A. Nearing, eds. 1995. USDA Water Erosion Prediction Project hillslope and watershed model documentation. NSERL Report No. 10. West Lafayette, Ind.: USDA-ARS National Soil Erosion Research Laboratory.

Flury, M., H. Fluhler, W.A. Jury, and J. Leuenberger. 1994. Susceptibility of soils to preferential flow of water: a field study. Water Resour. Res. 30: 1945-1954.

Fox. G.A., R. Malone, G.J. Sabbagh, and K. Rojas. 2004. Interrelationship of macropores and subsurface drainage for conservative tracer and pesticide transport. J. Environ. Qual. 33: 2281-2289.

Gerla, P.J. and R.K. Matheney. 1996. Seasonal variability and simulation of groundwater flow in a prairie wetland. Hydrological Processes 10: 903-920.

Germann, P., A. Helbling, and T. Vadilonga. 2007. Rivulet approach to rates of preferential infiltration. Vadose Zone J. 6: 207-220.

Gowdish, L. and R. Muñoz-Carpena. 2009. An improved Green-Ampt infiltration and redistribution method for uneven multistorm series. Vadose Zone J. 8: 470-479.

Grossman, W.D., and T.G. Reinsch. 2002. Saturated and field-saturated water flow parameters. p. 201-228. *In* J.H. Dane and G.C. Topp (ed.) Methods of soil analysis. Part 4. Physical methods. SSSA, Madison, WI.

Heard, J.R., E.J. Kladivko, and J.V. Mannering. 1988. Soil macroporosity, hydraulic conductivity and air permeability of silty soils under long-term conservation tillage in Indiana. Soil Tillage Res. 11: 1–18.

Heath, R.C. 1983. Basic ground-water hydrology. USGS Water Supply Paper 2220. USGS, Denver, CO.

Heppell, C.M., T.J. Burt, and R.J. Williams. 2000. Variations in the hydrology of an underdrained clay hillslope. J. Hydrol. 227: 236-256.

Heppell, C.M. and A.S. Chapman. 2006. Analysis of a two-component hydrograph separation model to predict herbicide runoff in drained soils. Ag. Water Manage. 79: 177–207.

Iowa Department of Transportation. 2011. Available at http://mesonet.agron.iastate.edu/AWOS/ (verified 25 July 2011).

James, H.R. and T.E. Fenton. 1993. Water tables in paired artificially drained and undrained soil catenas in Iowa. Soil Sci. Soc. Am. J. 57: 774-781.

Jaynes, D.B., S.I. Ahmed, K.-J.S. Kung, and R.S. Kanwar. 2001. Temporal dynamics of preferential flow to a subsurface drain. Soil Sci. Soc. Am. J. 65: 1368-1376.

Jury, W. and R. Horton. 2004. Soil Physics (6th edition). Hoboken, NJ: John Wiley and Sons, Inc.

Kalkhoff, S.J., K.E. Lee, S.D. Porter, P.J. Terrio, and E.M. Thurman. 2003. Herbicides and herbicide degradation products in upper Midwest agricultural streams during August base-flow conditions. J. Environ. Qual. 32: 1025–1035.

Kao, C., S. Bouarfa, and D. Zimmer. 2001. Steady state analysis of unsaturated flow above a shallow water-table aquifer drained by ditches. J. Hydrol. 250: 122-133.

Kladivko, E.J., G.E. Van Scoyoc, E.J. Monke, K.M. Oates, and W. Pask. 1991. Pesticide and nutrient movement into subsurface tile drains on a silt loam soil in Indiana. J. Environ. Qual. 20: 264–270.

Kladivko, E.J., J. Grochulska, R.F. Turco, G.E. Van Scoyoc, and J.D. Eigel. 1999. Pesticide and nitrate transport into subsurface tile drains of different spacings. J. Environ. Qual. 28: 997-1004.

Kladivko, E.J., L.C. Brown, and J.L. Baker. 2001. Pesticide transport to subsurface tile drains in humid regions of North America. Crit. Rev. Environ. Sci. Technol. 31: 1–62.

Krajewski, W.F. and R. Mantilla. 2010. Why were the 2008 floods so large?. p. 19-30. *In* C.F. Mutel (ed.) A watershed year: Anatomy of the Iowa floods of 2008. University of Iowa Press. Iowa City, IA.

Kumar, A., R.S. Kanwar, and G.R. Hallberg. 1997. Separating preferential and matrix flows using subsurface tile flow data. J. of Environ. Sci. and Health, Part A: Toxic/Hazardous Substances and Environ. Engineering 32: 1711–1729.

Kung, K.-J.S., T.S. Steenhuis, E.J. Kladivko, T.J. Gish, G. Bubenzer, and C.S. Helling. 2000. Impact of preferential flow on the transport of adsorbing and non-adsorbing tracers. Soil Sci. Soc. Am. J. 64: 1290-1296.

Kung, K.-J.S., E.J. Kladivko, T.J. Gish, T.S. Steenhuis, G. Bubenzer, and C.S. Helling. 2000. Quantifying preferential flow by breakthrough of sequentially applied tracers: Silt loam soil. Soil Sci. Soc. Am. J. 64: 1296-1304.

Logsdon, S.D. 1995. Flow mechanisms through continuous and buried macropores. Soil Science 160: 237-242.

McCarthy, K.A., C.E. Rose, and S.J. Kalkhoff. 2012. Environmental Settings of the South Fork Iowa River basin, Iowa, and the Bogue Phalia basin, Mississippi, 2006-10. U.S. Geological Survey Scientific Investigations Report 2012-5021, 30 p.

Mohanty, B.P., M.D. Ankeny, R. Horton, and R.S. Kanwar. 1994. Spatial-analysis of hydraulic conductivity measured using disc infiltrometers. Water Resour. Res. 30: 2489–2498.

Narasimhan, T.N. 1998. Something to think about...Darcy-Buckingham's Law. Ground Water 36: 194-195.

Nimmo, J.R. 2003. How fast does water flow in an unsaturated macropore?: Evidence from field and lab experiments. *In* J. Álvarez-Benedí and P. Marinero (ed.) Estudios de la Zona No Saturada del Suelo, Vol. 6.

Nimmo, J.R., K.M. Schmidt, K.S. Perkins, and J.D. Stock. 2009. Rapid measurement of field-saturated hydraulic conductivity for areal characterization. Vadose Zone J. 8: 142-149.

Ogden, C.B., H.M. van Es, R.J. Wagenet, and T.S. Steenhuis. 1999. Spatial-temporal variability of preferential flow in a clay soil under no-till and plow-till. J. Environ. Qual. 28: 1264-1273.

Randall, G.W. and D.J. Mulla. 2001. Nitrate-nitrogen in surface waters as influenced by climatic conditions and agricultural practices. J. Environ. Qual. 30: 337-344.

Reynolds, W.D., and D.E. Elrick. 1990. Ponded infiltration from a single ring. I. Analysis of steady flow. Soil Sci. Soc. Am. J. 54:1233–1241.

Reynolds, W.D., D.E. Elrick, E.G. Youngs, and A. Amoozegar. 2002. Field methods (vadose and saturated zone techniques). p. 817. In J.H. Dane and G.C. Topp (ed.) Methods of soil analysis. Part 4. Physical methods. SSSA, Madison, WI.

Richard, T.L. and T.S. Steenhuis. 1988. Tile drain sampling of preferential flow on a field scale. J. Contam. Hydrol. 3: 307-325.

Roth , J. 2010. The hydrology of a drained topographical depression within an agricultural field in north central Iowa. MS Thesis. Minneapolis, MN: University of Minnesota, Dept. of Civil Engineering.

Sands, G.R. 2001. Soil water concepts. Agricultural Drainage Publication Series. University of Minnesota. St. Paul, MN.

Schilling, K.E. and M. Helmers. 2008. Tile drainage as karst: Conduit flow and diffuse flow in a tile-drained watershed. J. Hydrol. 349: 291–301.

Shah, N. and M. Ross. 2009. Variability in specific yield under shallow water table conditions. J. Hydrol. Eng. 14: 1290-1298.

Sidle, R.C., Y. Tsuboyama, S. Noguchi, I. Hosoda, M. Fujieda, and T. Shimizu. 2000. Stormflow generation in steep forested headwaters: a linked hydrogeomorphic paradigm. Hydrological Processes 14: 369-385.

Šimůnek, J., N.J. Jarvis, M. Th. van Genuchten, and A. Gärdenäs. 2003. Review and comparison of models for describing non-equilibrium and preferential flow and transport in the vadose zone. J. Hydrol. 272: 14-35.

Skaggs, R.W. 1976. Determination of the hydraulic conductivity—drainable porosity ratio from water table measurements. Trans. ASAE 25: 73-84.

Stone, W.W. and J.T. Wilson. 2006. Preferential flow estimates to an agricultural drain with implications for glyphosate transport. J. Environ. Qual. 35: 1825-1835.

Swanson, H. 2003. Using quantitative landscape modeling and scientific visualization to characterize soil hydrology dynamics. MS Thesis. St. Paul, MN: University of Minnesota.

Tomer, M.D. and D.E. James. 2004. Do soil surveys and terrain analyses identify similar priority sites for conservation? Soil Sci. Soc. Am. J. 68: 1905-1915.

Tomer, M.D., T.B. Moorman, and C.G. Rossi. 2008. Assessment of the Iowa River's South Fork watershed: Part 1. Water Quality. J. Soil Water Conserv. 63: 360–370.

Topp, G.C.and Ferre. 2002. Saturated and field-saturated water flow parameters. p. 422–424. *In* J.H. Dane and G.C. Topp (ed.) Methods of soil analysis. Part 4. Physical methods. SSSA, Madison, WI.

Villholth, K.G., K.H. Jensen, and J. Fredericia. 1998. Flow and transport processes in a macroporous subsurface-drained glacial till soil I: Field investigations. J. Hydrol. 207: 98–120.

USDA National Resource Conservation Service. 2009. Soil Survey Geographic (SSURGO) database for Hamilton County, Iowa. Fort Worth, Texas. Available at http://datagateway.nrcs.usda.gov/ (verified 10 February 2011).

Warner, G.S. and R.A. Young. 1991. Measurement of preferential flow beneath mature corn. *In* T.J. Gish and A. Shirmohammadi (ed.) Proceedings of the National Symposium on Preferential Flow. American Society of Agricultural Engineers. St. Joseph, MI.

Williams, A.G., J.F. Dowd, D. Scholefield, N.M. Holden and L.K. Deeks. 2003. Preferential flow variability in a well-structured soil. Soil Sci. Soc. Am. J. 67: 1272-1281.

Winter, T.C. 1998. Relation of streams, lakes, and wetlands to groundwater flow systems. Hydrogeology Journal 7: 28-45.

Zhang, Y.K. and K.E. Schilling. 2006. Effects of land cover on water table, soil moisture, evapotranspiration, and groundwater recharge: A Field observation and analysis. J. Hydrol. 319: 328-338.

Table 3.1: Summary of maximum water velocity (v_{max}) values for 51 events (188 individual observations) from 2007-2009. {SD = Standard Deviation; N/A = not enough available data}.

	Number of Observations	Mean ± SD (m day^{-1})	Median (m day^{-1})	5th Percentile (m day^{-1})	95th Percentile m day^{-1})	Mean ± SD (m day^{-1}) 1-mm threshold
All events, 2007-2009	188	10.5 ± 11.4	6.61	1.44	32.7	15.3 ± 19.1
Field Array						
All events, 2007-2008	135	10.7 ± 12.1	6.68	1.45	36.8	13.8 ± 13.6
All events, 2007	78	10.0 ± 9.72	6.78	1.44	36.1	12.0 ± 9.30
Non-inundated, 2007	18	7.86 ± 5.68	7.22	N/A	N/A	9.69 ± 6.45
Inundated, 2007	60	10.6 ± 10.6	6.78	1.80	38.9	12.7 ± 9.94
All events, 2008	57	11.6 ± 14.8	6.35	1.42	42.4	16.2 ± 17.6
Non-inundated, 2008	22	4.55 ± 4.57	3.13	1.36	19.4	12.0 ± 15.1
Inundated, 2008	35	16.0 ± 17.2	12.8	1.85	53.0	18.8 ± 18.8
Grassy Buffer Array						
All events, 2009	53	10.2 ± 9.51	6.53	1.22	30.1	19.3 ± 28.4
Non-inundated, 2009	33	7.90 ± 5.80	6.53	1.20	19.0	13.4 ± 20.9
Inundated, 2009	20	14.0 ± 12.9	6.18	2.15	43.2	29.1 ± 36.3

Table 3.2: Summary of the all maximum water velocity (v_{max}) values, separated into four distinct periods (by Julian date). {SD = Standard Deviation}

Seasonal Periods	Julian Dates	Number of Events	Mean ± SD (m day^{-1})	Median (m day^{-1})
(1) Early-to-mid spring	105-135	15	12.0 ± 13.8	8.31
(2) Mid spring-Early summer	136-181	11	8.62 ± 8.00	6.30
(3) Mid-to-late summer	182-243	11	15.2 ± 12.0	12.6
(4) Late summer-Early spring	<105, >243	14	7.05 ± 9.39	3.79

Table 3.3: Summary of t-test results between the different seasonal periods with $P \leq 0.05$ considered significant. {1 = Denotes Mann-Whitney rank sum test in lieu of t-test.}

Seasonal Periods	**(1) 105-135**	**(2) 136-181**	**(3) 182-243**	**(4) <105, >243**
(1) 105-135	----	***0.054***	***0.190***	<0.001
(2) 136-181	----	----	0.004[1]	0.017[1]
(3) 182-243	----	----	----	<0.001[1]
(4) <105, <243	----	----	----	----

Table 3.4: Summary of field-saturated hydraulic conductivity (K_{fs}) from 2008 and 2010. Above-ground cover includes measurements on corn, soybeans, grassy buffer, and bare ground. {SD = Standard Deviation}

K_{fs} infiltrometers measurements					
	Number of Observations[1]	**Mean ± SD (m day^{-1})**	**Median (m day^{-1})**	**25th Percentile (m day^{-1})**	**75th Percentile (m day^{-1})**
All measurements	105	$1.3 \times 10^{-4} \pm 2.3 \times 10^{-4}$	4.1×10^{-5}	1.2×10^{-5}	1.6×10^{-4}
Sampling dates					
May 19, 2008	4	$3.8 \times 10^{-5} \pm 1.7 \times 10^{-5}$	4.1×10^{-5}	--	--
June 2-4, 2008	12	$8.1 \times 10^{-6} \pm 1.5 \times 10^{-5}$	8.3×10^{-7}	--	--
July 28-30, 2008	10	$2.0 \times 10^{-5} \pm 2.7 \times 10^{-5}$	1.1×10^{-5}	--	--
August 20-21, 2008	10	$1.7 \times 10^{-4} \pm 1.8 \times 10^{-4}$	5.7×10^{-5}	--	--
August 23-25, 2010	46	$1.9 \times 10^{-4} \pm 2.6 \times 10^{-4}$	1.3×10^{-4}	4.3×10^{-5}	2.4×10^{-4}
November 9-10, 2010	23	$1.2 \times 10^{-4} \pm 2.6 \times 10^{-4}$	3.9×10^{-5}	1.5×10^{-5}	1.1×10^{-4}
Above-ground cover					
Corn	48	$1.8 \times 10^{-4} \pm 2.6 \times 10^{-4}$	1.2×10^{-4}	3.1×10^{-5}	2.3×10^{-4}
Soybeans	5	$1.3 \times 10^{-4} \pm 1.6 \times 10^{-4}$	7.1×10^{-5}	4.0×10^{-5}	2.0×10^{-4}
Grassy buffer	9	$1.0 \times 10^{-4} \pm 1.5 \times 10^{-4}$	4.3×10^{-5}	3.2×10^{-5}	8.9×10^{-5}
Bare ground	38	$8.4 \times 10^{-5} \pm 2.1 \times 10^{-4}$	1.8×10^{-5}	1.8×10^{-6}	5.5×10^{-5}

1: Total number of observations for all six dates. Total for second portion of table not equal to total observations, as not every trial had the above-ground cover noted.

Fig. 3.1: Evidence of desiccation cracks, common preferential flow pathways at the study field, in April and July 2008.

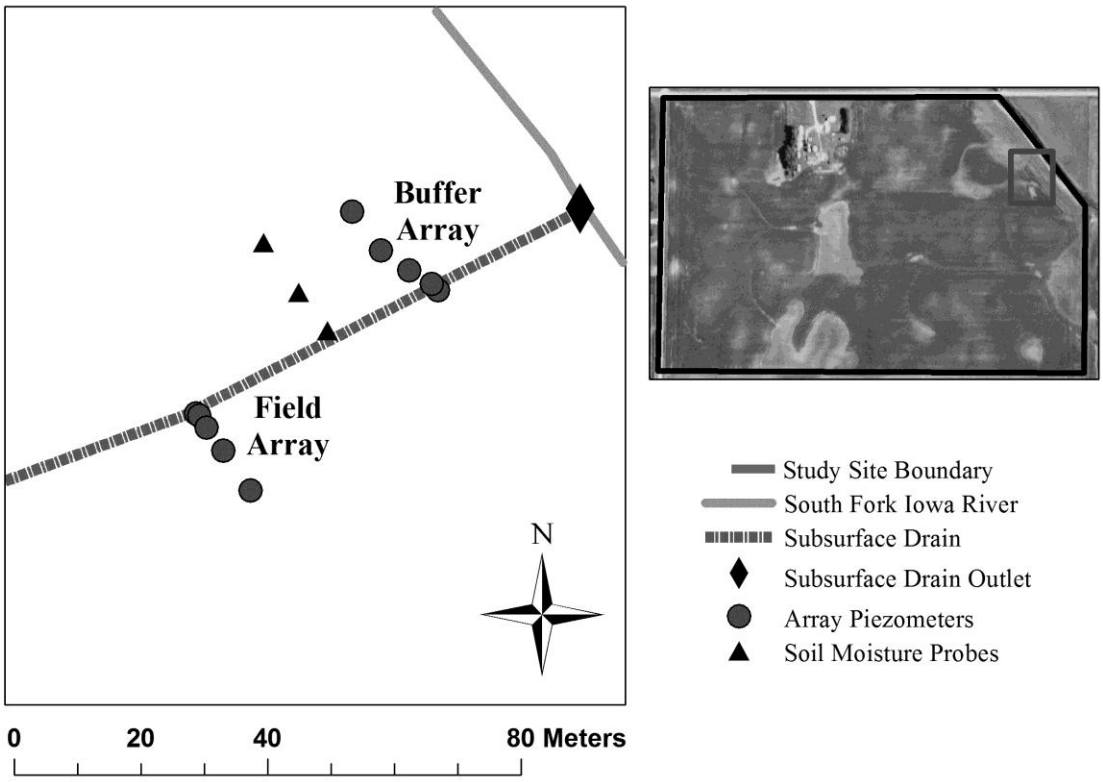

Fig. 3.2: The right-hand map shows the field boundary for the 38.8 hectare field, with a smaller gray box highlighting the inset map on the left. For the left-hand map, major site locations for the field site are shown, including the piezometer well nests, soil moisture probes, subsurface drain location, and subsurface drain outlet.

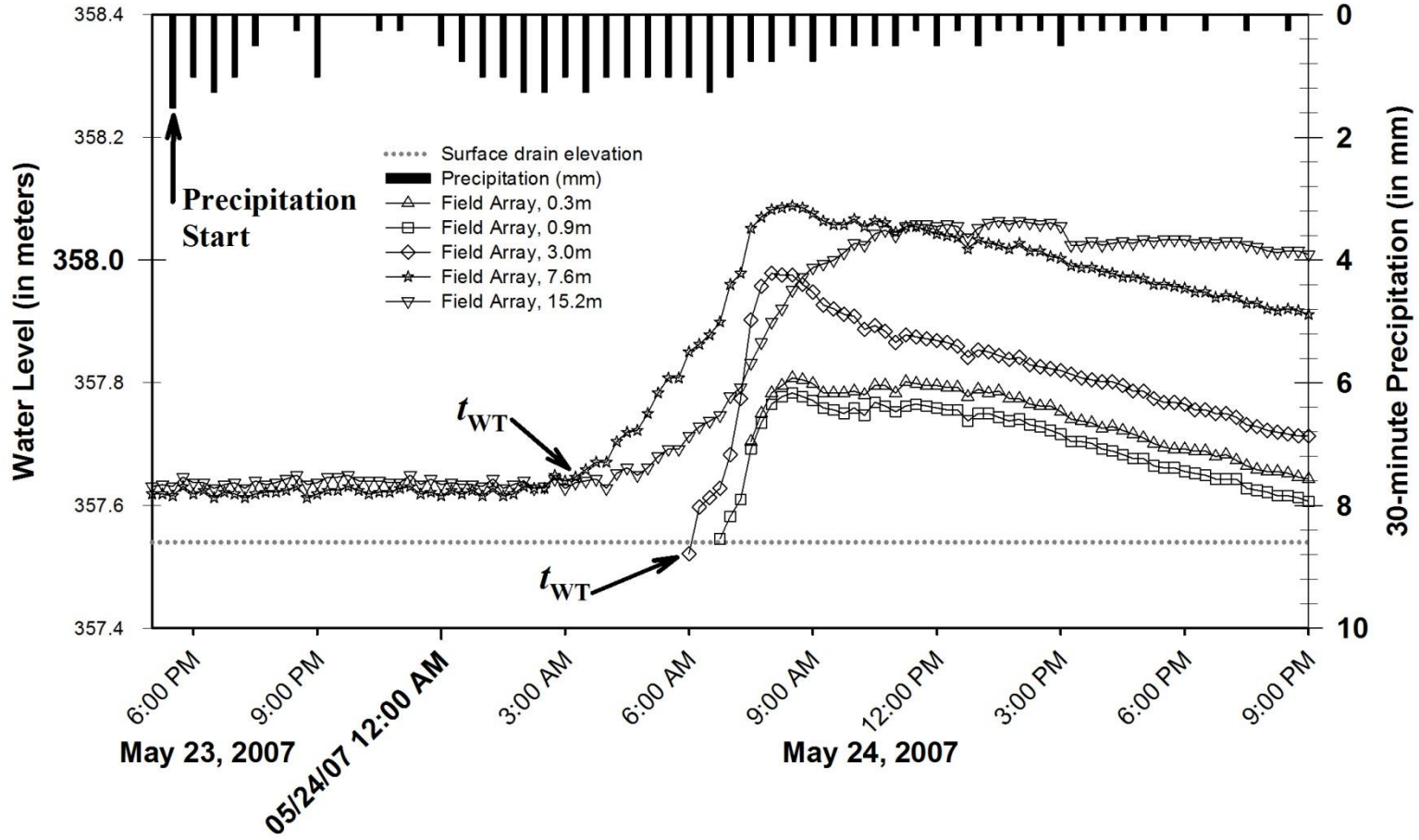

Fig. 3.3: Precipitation (mm) and piezometer water level (m) for the field array on May 23-24, 2007. The starting water level (t_{WT}) for the closer piezometers (0.3 m, 0.9 m) is often unknown as the rise starts below the bottom of the piezometer; in these cases, t_{WT} is the first appearance of water in the piezometer.

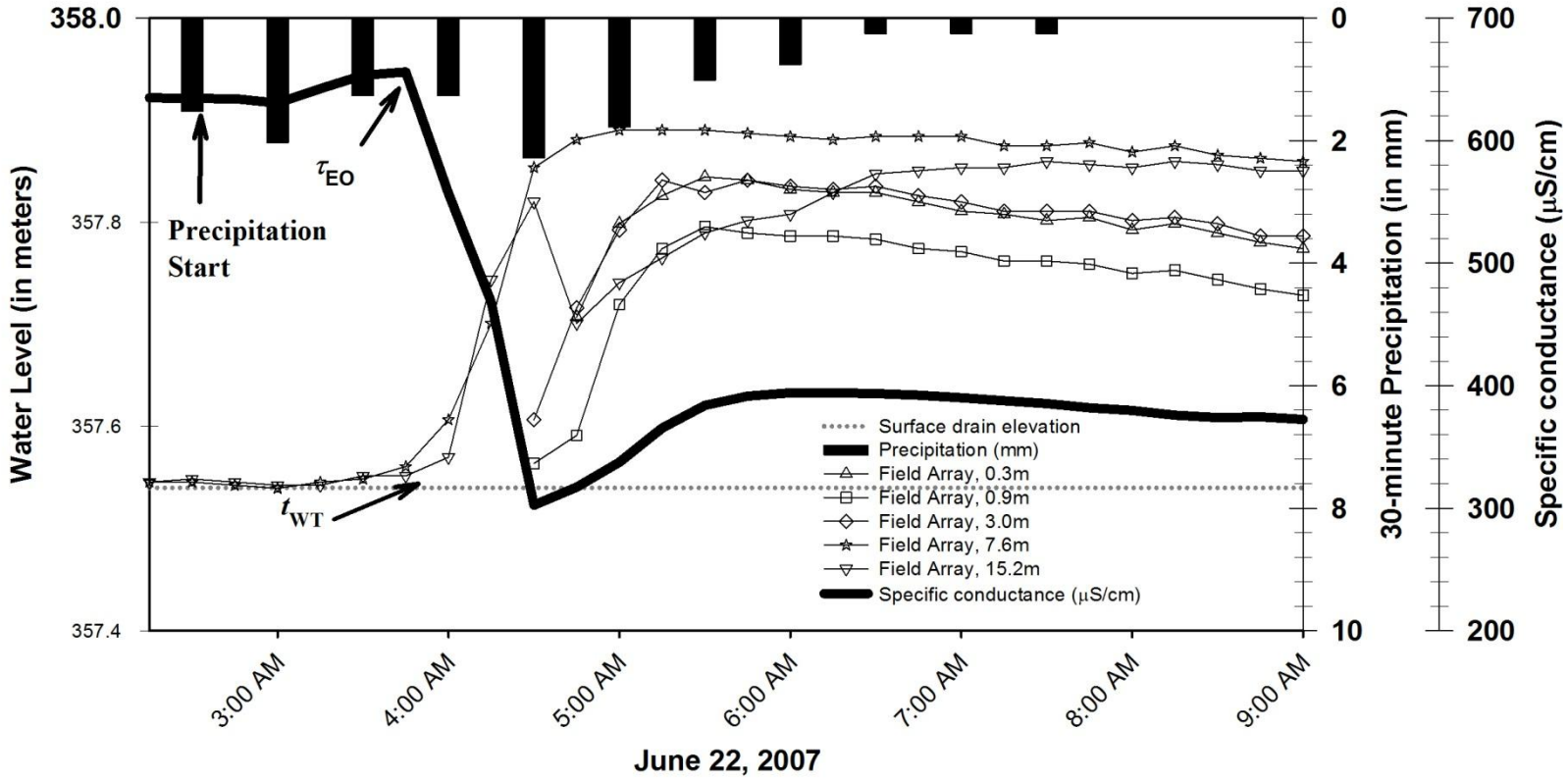

Fig. 3.4: Precipitation (mm), piezometer water level (m) for the field array, and subsurface drain SC on June 22, 2007. The starting water level (t_{WT}) for the piezometers correspond closely in time to the subsurface drain specific conductance (SC) onset time (τ_{EO}), establishing a linkage between the observed water level rises and the decrease in subsurface drain SC.

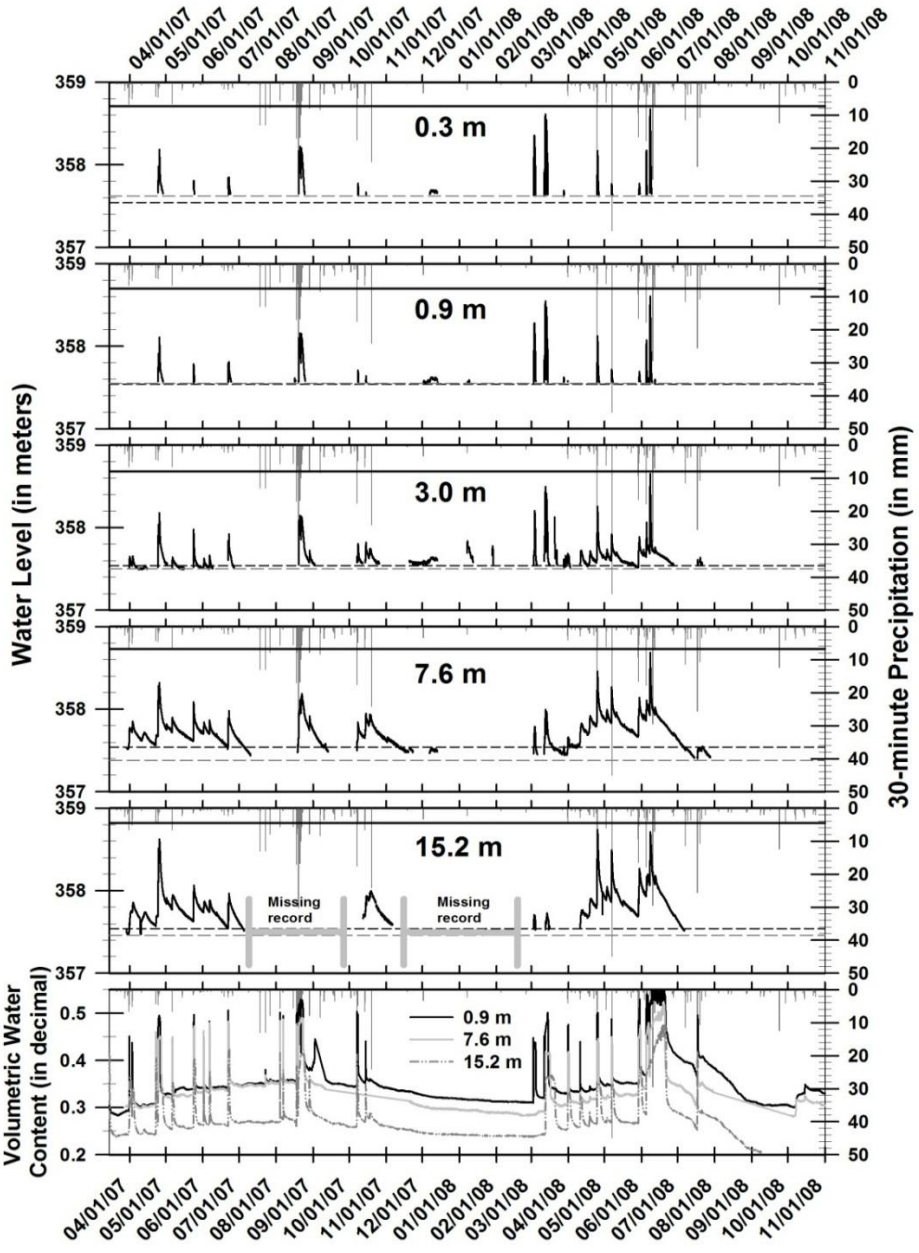

Fig. 3.5: Precipitation (mm), and water level (m) for the field array piezometers, plotted from top to bottom in distance away from the subsurface drain, from 0.3 m to 15.2 m). The black horizontal line on each plot shows the land surface at each piezometer, the dashed gray line on each plot shows the bottom of the piezometer screen and the dashed black line shows the estimated subsurface drain level (357.40 m). Volumetric water content (VWC) and precipitation (mm) for the 0.6 m depth soil moisture probes, at a distance of 0.9 m, 7.6 m, and 15.2 m from the subsurface drain, respectively.

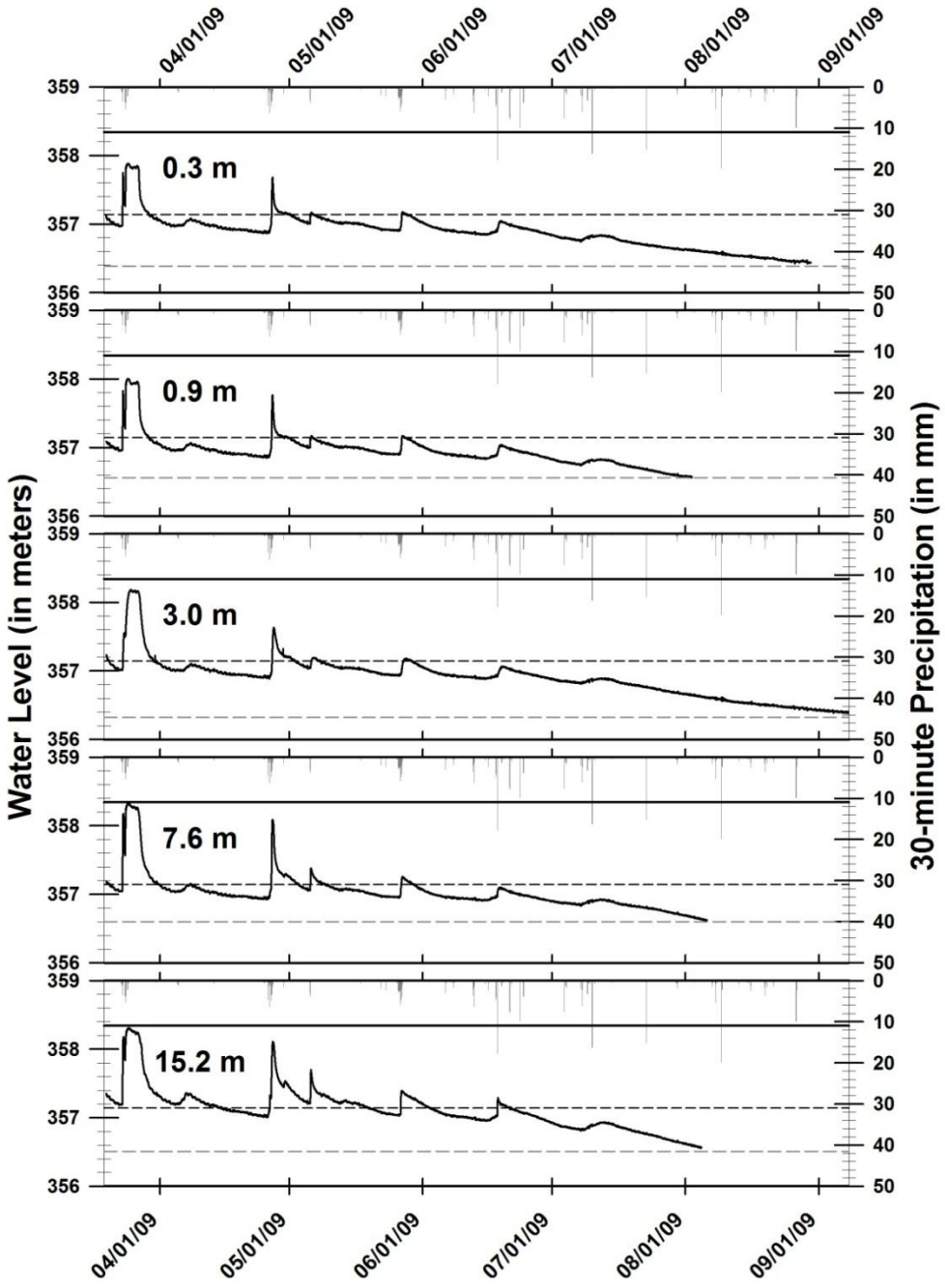

Fig. 3.6: Precipitation (mm), and water level (m) for the grassy buffer array piezometers, plotted from top to bottom in distance away from the subsurface drain, from 0.3 m to 15.2 m). The black horizontal line on each plot shows the land surface at each piezometer, the dashed gray line on each plot shows the bottom of the piezometer screen and the dashed black line shows the estimated subsurface drain level (357.40 m).

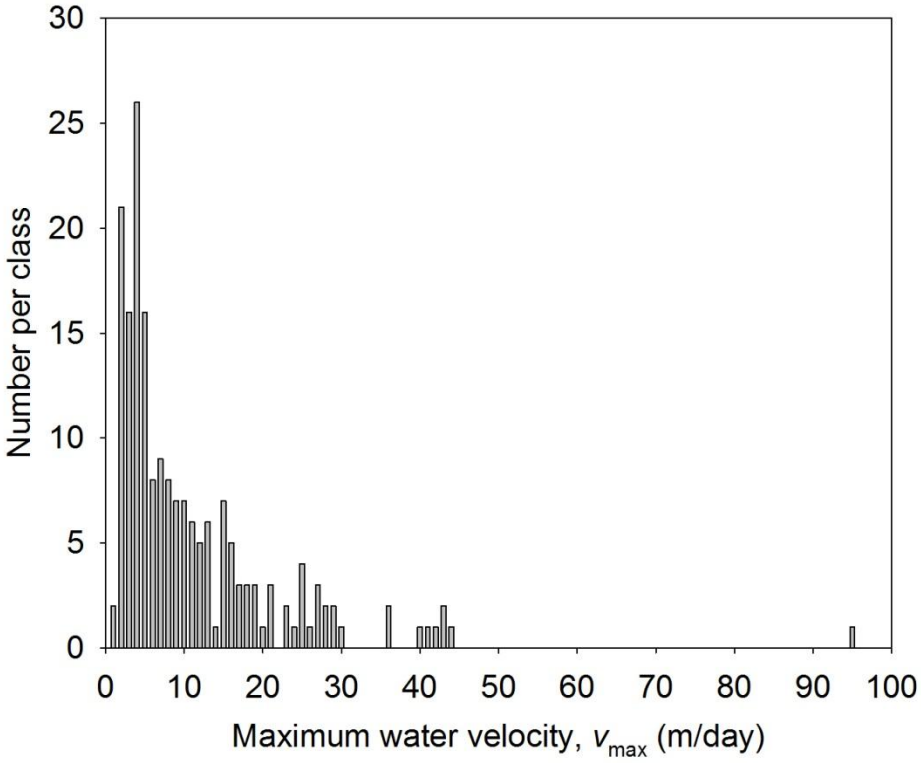

Fig. 3.7: Histogram of the maximum water velocity, v_{max} (m/day).

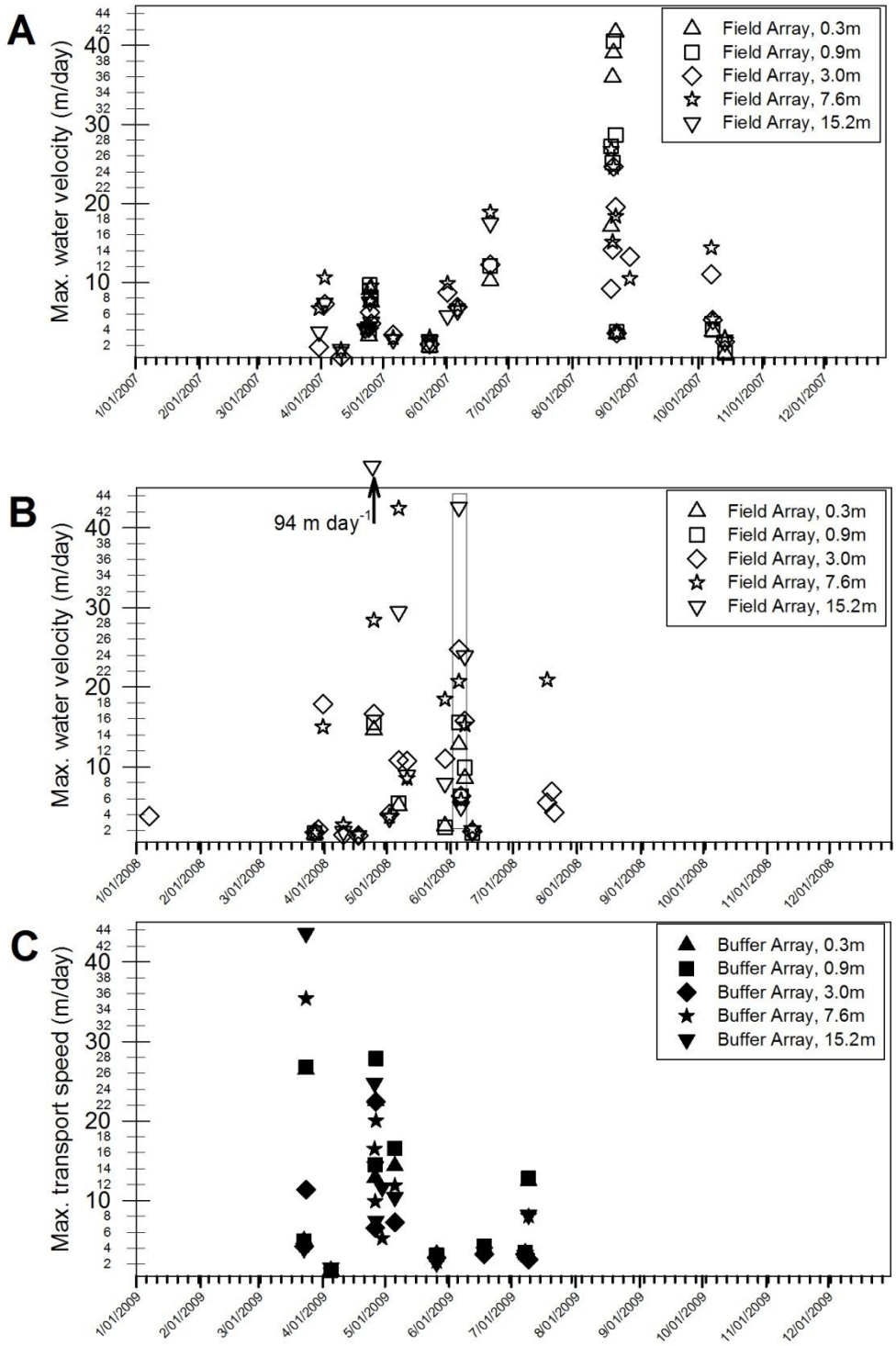

Fig. 3.8: Maximum water velocity (m/day) for all the field array piezometers in (A) 2007 (B) and 2008, and (C) the grassy buffer array piezometers in 2009. The short-hand abbreviation in the respective legends for the buffer array is BT and the field array is FT. This labeling is repeated on subsequent graphs. The box highlights v_{max} ranging from 5.12 m day^{-1} (0.3 m away) up to 42.4 m day^{-1} (7.6 m away) on May 6, 2008.

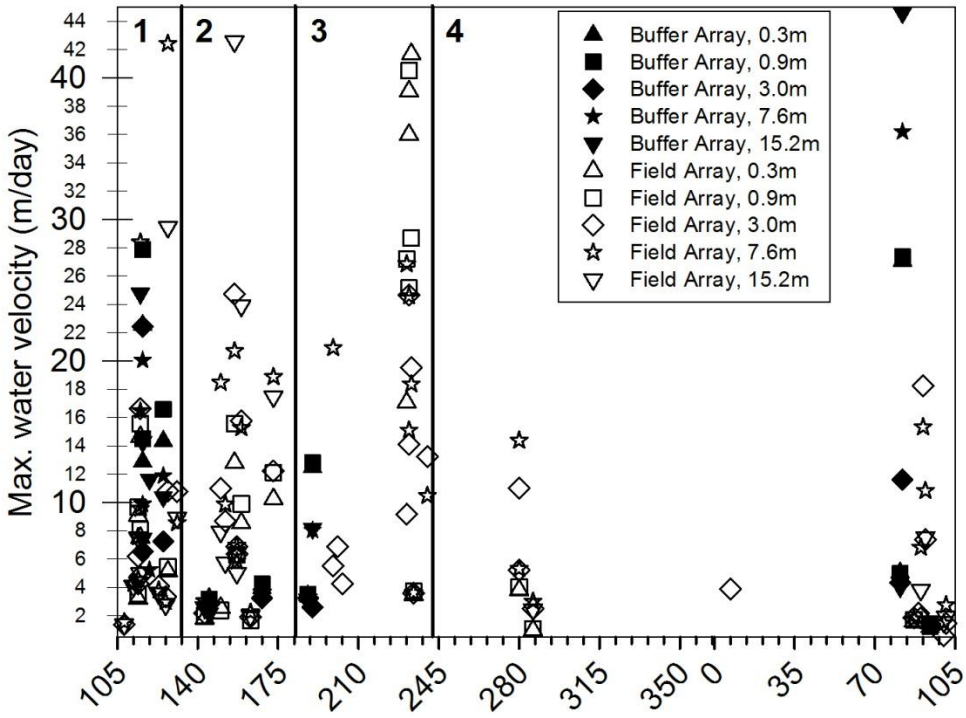

Fig. 3.9: Maximum water velocity (m/day) for all individual observations, including both the field and buffer array piezometers, plotted against the Julian date.

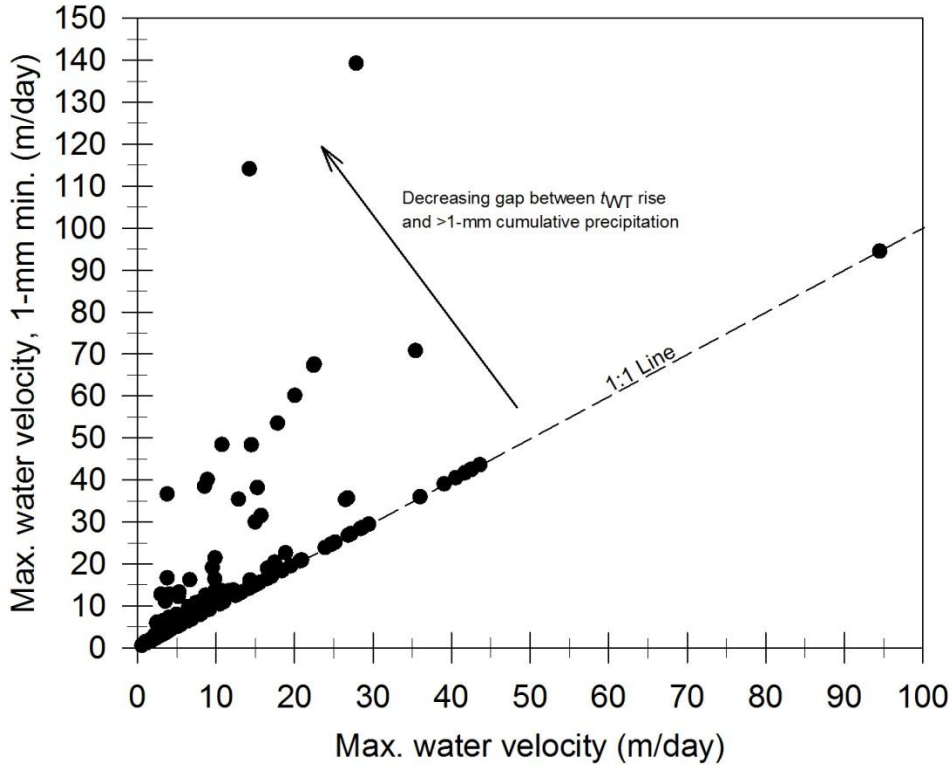

Fig. 3.10: Maximum water velocity, v_{max} (m/day) plotted against the maximum water velocity, $v_{max\text{-}1\ mm}$ (m/day). The 1:1 line shows values that were the same, with the arrow trending towards smaller differences in time between the initial water level rise, t_{WT}, and the >1-mm cumulative precipitation.

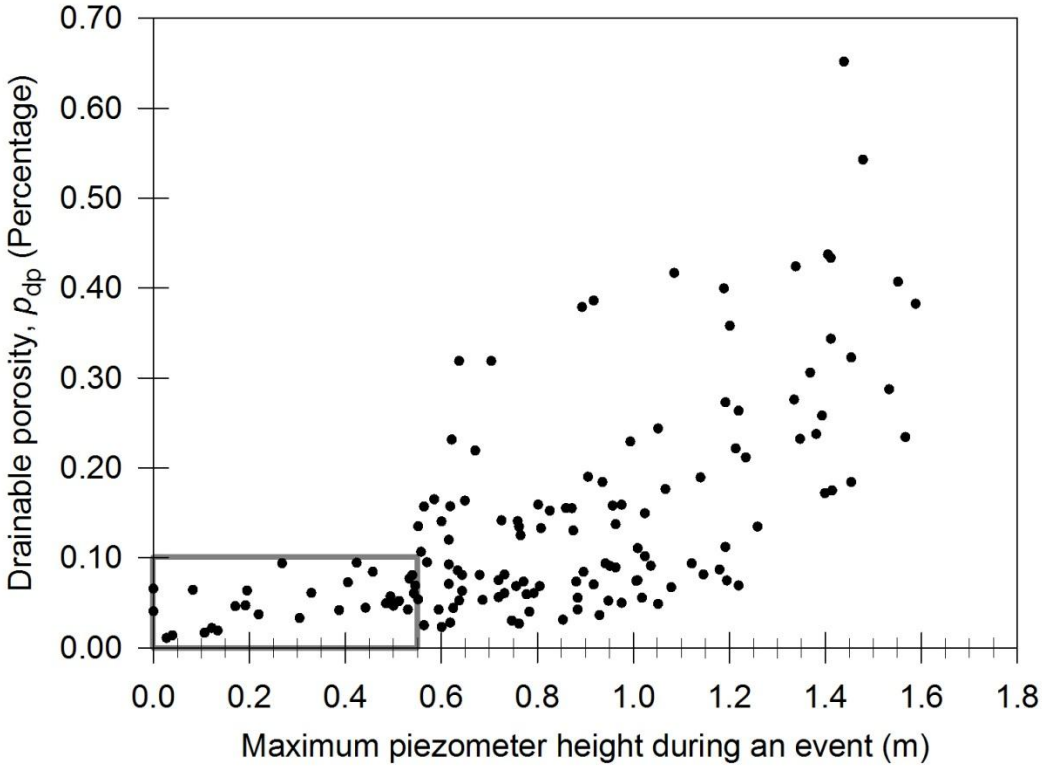

Fig. 3.11: Maximum piezometer height during an event plotted against the calculated drainable porosity, p_{dp}. The gray box highlights the drainable porosity values below a maximum piezometer height of 0.55 m.

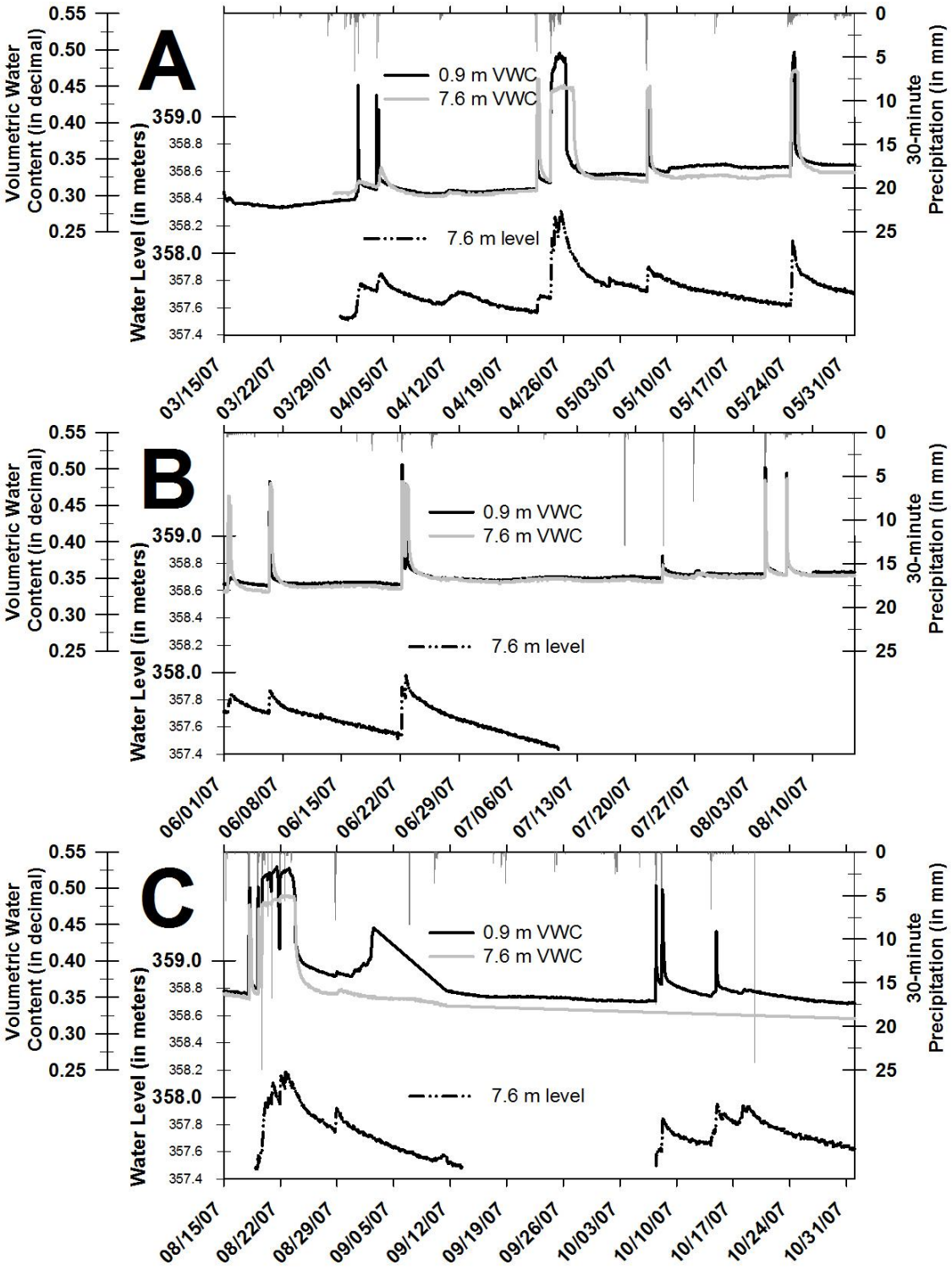

Fig. 3.12: Precipitation (mm), the water level at 7.6 m (m), and the volumetric water content at 0.9 m and 7.6 m, plotted for spring, summer, and fall 2007.

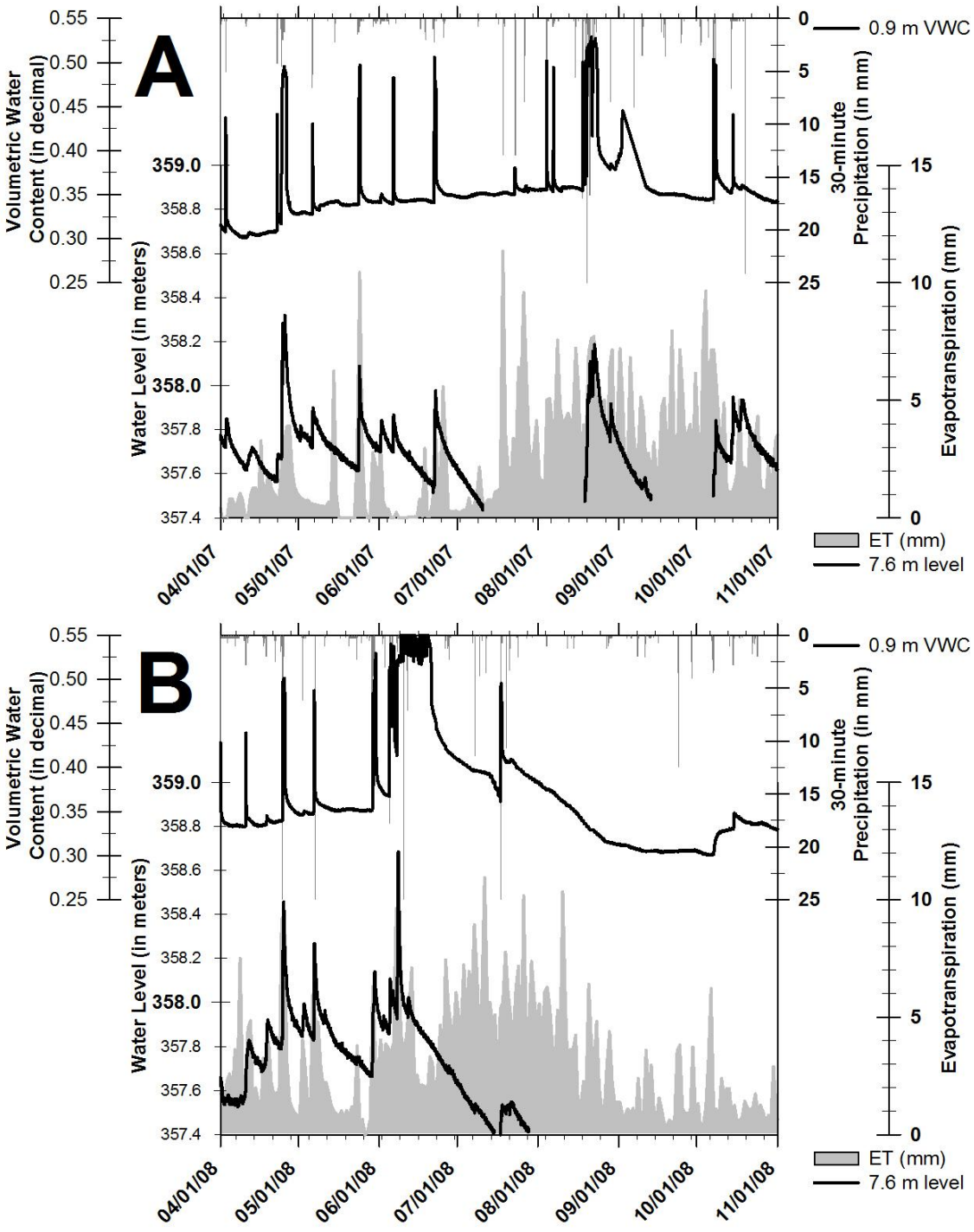

Fig. 3.13: Precipitation (mm), the water level at 7.6 m (m), volumetric water content at 0.9 m, and evapotranspiration (ET) for April to November for 2007 (A) and 2008 (B).

Chapter 4: Using a source-responsive model for preferential flow in a subsurface-drained landscape

Abstract

A one-dimensional, dual domain model (source-responsive model) was used to reproduce a series of water table rises from an array of shallow water table monitors. The water table rises, in close proximity to a subsurface drain, were monitored continuously over a three-year period to study the time interval immediately after a rainfall event to determine the importance of preferential flow. Two shallow (1.2 m) piezometer arrays were installed in order to monitor these water table fluctuations at the approximate depth of a buried subsurface drain. Emphasis was placed on the preferential flow component of the water flux for the source-responsive model output. This focus helped gain an insight into the extent of the preferential flow space and whether the preferential flow space is static or variable through time. Output from the model includes the facial area density (M_{lim}), a property of the medium analogous to other macropore and preferential flow pathway density quantifications. By calibrating to known parameters, an indication of the facial area density both spatially and temporally was determined. Overall, the source-responsive model was run for 12 events (33 individual observations) for three different scenarios to calculate M_{lim}: average v_{max} and two different calculated v_{max} using a fixed drainable porosity. Results show a weak trend towards a more focused preferential flow space during mid-summer. The model results support a continuum approach to preferential flow modeling rather than discretization of the preferential and matrix flow components. Also, the model findings warrant a further exploration of the minimum pore size diameter for source-responsive flow (i.e., preferential flow) currently set at pore

diameter sizes of 30 μm, as back-calculating the M_{lim} solutions to determine the average pore diameter size illustrate a potential for substantial flow at pore diameter sizes <30 μm. Improvements to the model itself included an offset parameter to delay infiltrating water and two goodness-of-fit parameters to match model output to the measured water table height.

1. Introduction

Preferential flow is important for subsurface drainage because it has a direct impact on agrichemical transport, especially in situations where preferential flow is capable of transporting a significant fraction of the total water (Šimůnek et al., 2003). Preferential flow water that bypasses matrix flow has a shorter contact time with soils (Pilgrim et al., 1979), potentially lessening or eliminating the natural attenuation of agrichemicals dissolved within the preferential flow water flux. Although several models exist to simulate water fluxes moving through the unsaturated zone towards the water table, it is often difficult to ascertain how much of the water flow is due to preferential and matrix flow. A common approach to quantify the water flux is to divide the flow into the two separate domains representing preferential flow and matrix flow. The matrix flow domain is dependent on gravitational, adhesive, and capillary forces as described by the Darcy-Buckingham flux law (Jury and Horton, 2004; Narasimhan, 1998), whereas the preferential flow domain describes the often non-equilibrium flow through a smaller spectrum of the total pore space dominated by larger pores and structural voids (Beven and Germann, 1982; Richard and Steenhuis, 1988).

Most of the time, application of the Richards' equation (Richards, 1931) or another water infiltration such as the Green-Ampt infiltration equation (e.g., Mein and Larson, 1973) is appropriate for describing the bulk of water flow, with preferential flow often neglected or treated with minimal regard (Jarvis, 1991). However, for infiltration events that lead to non-equilibrium flow, especially after large rainfall or snowmelt events, characterizing preferential flow is important as these are often critical periods for contaminant transport (Allaire et al., 2009; Cey and Rudolph, 2009; Kung et al., 2000). This is particularly critical for the subsurface-drained systems common in the upper Midwest. As previous research has already shown, the potential magnitude of preferential flow transport in these areas is large (Kumar et al., 1997; Chapter 2; Stone and Wilson, 2006; Schilling and Helmers, 2008). Subsurface drainage allows for preferential flow to quickly deliver water after rainfall or snowmelt events, via the subsurface drain, into nearby surface water bodies.

Several one-dimensional, non-steady state water flow models have been produced in attempt to differentiate preferential flow from matrix flow (Šimůnek et al., 1994; Ahuja et al., 1993; Larsbo and Jarvis, 2007; Gerke and van Genuchten, 1993, Germann and Beven, 1985). Historically, the focus on preferential flow modeling has been conceptualized into four broad categories: dual porosity, dual permeability, multi-porosity and multi-permeability (Šimůnek et al., 2003). Dual porosity divides the soil into the inter-aggregate pores (i.e. preferential flow) and intra-aggregate pores (i.e. matrix flow). Flow only occurs through the inter-aggregate pores, while the soil matrix acts as a reservoir that stores and exchanges water with the inter-aggregate pores. Conversely, dual permeability models allow for movement in both the inter-aggregate pores/macropores

and soil matrix. Examples of available dual permeability models include MACRO (Larsbo and Jarvis, 2007) and RZWQM (Ahuja et al., 1993), both of which have been applied in many environmental settings. Multi-porosity and multi-permeability models are conceptually similar to dual porosity and dual permeability models, respectively, except these models can include more than two domains and require considerably more parameters (Šimůnek et al., 2003).

Despite the widespread usage of models such as RZWQM and MACRO, one distinct disadvantage to these models is the determination of appropriate values for input parameters to run the model. These models often include automated functions such as the Brooks-Corey relationship to define the soil water content-matrix suction curve (Ahuja et al., 1993). However, the requirement to characterize unsaturated hydraulic conductivity properties to characterize the capillarity drive can be difficult to ascertain, especially if considering spatial and temporal variations. Furthermore, as in the case for RZWQM, preferential flow is only initiated after surface ponding begins to occur, despite documented field evidence of preferential flow occurring with even dry soils (Villholth et al., 1998; Shipitalo and Edwards; 1996).

Another approach to differentiating preferential flow from matrix flow is the source-responsive model (Nimmo, 2010). The source-responsive model rests on the principle that non-equilibrium preferential flow often dominates water table fluctuations shortly after a rainfall event, a period in which preferential flow is often not triggered by other models (Nimmo, 2010; Ebel and Nimmo, 2009). Requiring only a small number of input parameters, most of which can be pre-determined through studying water table fluctuations or reasonably approximated from a literature review of similar settings, the

source-responsive model is relatively simple to run. By selecting the source-responsive model, the preferential flow space over short periods, such as immediately following a significant rainfall or snowmelt event, can be characterized for spatial and temporal variability.

The model will be calibrated against data from a field array of piezometers with continuous water levels, varying in depth and distance from a subsurface drain (depth = 1 meter). Differences between separate water table rises will elucidate insights into the model's behavior and whether or not the model properly simulates preferential flow dynamics. The objectives of this study were: (i) alter the source-responsive model to work better in cases of delayed infiltration and add a statistical test for goodness-of-fit; (ii) calibrate the model to measured water level data by utilizing field-measured maximum water velocity and drainable porosity; (iii) characterize an appropriate method for calculating the infiltration water velocity through the unsaturated zone; and, (iv) determine if the source-responsive model has physically meaningful results such as temporal changes in preferential flow space.

2. Methods

2.1 Data for the source-responsive model

Two piezometer arrays, part of a larger 38.8 hectare study site, provided the data to test and calibrate the source-responsive model. The study site was situated along the South Fork of the Iowa River (SFIR) {Hamilton County, Iowa} adjacent to a USGS stream gage (USGS 05451080; U.S. Geological Survey National Water Information

System). Land use for the study site was row-cropped agriculture (corn, soybeans), with a 25 m grassy buffer along the northeastern portion of the study site adjacent to the stream.

The two piezometer arrays were situated perpendicular to a subsurface drain (21-cm inner diameter) in order to study the immediate capture zone and flow to the subsurface drain. Subsurface drainage is necessary to foster agriculture production, as the poorly-drained silty clay loams at the site would naturally be saturated up to land surface for substantial periods of the year. The average soil profile is 1.8-2 m in depth, part of the Clarion-Nicollet-Webster soil catena, and is underlain by a confining layer of Des Moines Lobe glacial deposits of the Des Moines Lobe (Dideriksen, 1986; Bettis et al., 1996).

Based on previous work at the site (Roth, 2010), most of the water inputs to the field site (rainfall, snowmelt) are either lost due to evapotranspiration (65-75 cm, annually) or removed through subsurface drains via infiltration or vertical surface-drain inlets (McCarthy et al., 2011). Mean annual rainfall for this region of Iowa is 83 cm, with a strong seasonality in the early spring months (April-June) and occasional intense mid-summer rain storms (McCarthy et al., 2011), which will prove to be important for temporal differences in the preferential flow domain. Generally, summer months (July-August) have an annual minimum in rainfall, higher evapotranspiration and lower stream discharge. Site precipitation was measured with a 20.3 cm diameter tipping bucket rain gage, recorded every 30 min (Texas Electronics TE525WS), with gaps in the precipitation record filled with precipitation data from Webster City, Iowa (28 km from study site) (Iowa Department of Transportation, 2011).

The two piezometer arrays each contained five piezometers installed by a direct push machine (Geoprobe™ Model 540MT). In order to capture the two major land uses above the subsurface drain, one array was set in the cropped portion of the field (field array) and the other array was set in the grassy buffer (grassy buffer array). The ten piezometers were set at approximately 1.2 m below land surface at the following distances, perpendicular to the subsurface drain: 0.3 m, 1.0 m, 3.0 m, 7.6 m, and 15.2 m. All piezometers were constructed of 2.54-cm (1") diameter polyvinyl chloride. The bottom was screened for 0.3 meters. Each piezometer was set with an encapsulated pressure transducer that calculated water depth (i.e., depth of water in well) and temperature (Solinst Levelogger 3001) every 15 min, with an additional two encapsulated pressure transducers (Solinst Barologger) installed at the site to calculate for barometric pressure adjustments. Regular site visits included manual steel-tape water level measurements to check against the recorded pressure transducer water level. Calibrations were made to the recorded water level data in order to match the manual measurements.

Measured soil moisture was obtained by converting the output voltage from a soil moisture probe (Decagon EC-5) into an unsaturated zone volumetric water content (VWC) percentage. In this particular study, the probe was buried 0.6 m below land surface, located 0.9 m away from the subsurface drain underneath the tilled portion of the field. A specific calibration equation between the probe's excitation voltage and VWC was established (Appendix C).

2.2 Source-responsive model

The premise of the source-responsive model is that water flows quickly through the unsaturated zone along preferential flow pathways, responding more to the infiltrating

water at the surface rather than the local potential gradients that control matrix flow (Nimmo, 2010). Matrix flow, also referred to as diffuse flow, is continuous but can be suspended in cases of rapid water accretion. The hallmark feature of the source-responsive model is the small number of parameters necessary to run the model. As Nimmo (2010) already gave a detailed description of the background and development of the source-responsive model, this discussion will be limited to pertinent details in order to evaluate the current study. As with most dual permeability models, the source-responsive model envisions water to be divided into two fluxes

$$q = q_{\mathrm{D}} + q_{\mathrm{S}} \qquad [1]$$

with the subscript D referring to the diffuse-flow domain (matrix flow) and the subscript S referring to the source-responsive domain (preferential flow). Based on the Darcy-Buckingham law, the diffuse-flow flux density ($m^3\ s^{-1}$) is

$$q_D(\mathrm{z},\mathrm{t}) = -\mathrm{K}(\theta_D)\frac{\partial \Phi}{\partial z} \qquad [2]$$

with z as depth, t as time, K as the unsaturated hydraulic conductivity, θ_D as the diffuse domain volumetric water content, and Φ as total diffuse flow potential.

The source-responsive process is envisioned as a continuum with a water flux q_{Smax} ($m^3\ s^{-1}$) which represents the maximum source-responsive flow that can be accommodated at any particular depth. Flow within the source-responsive domain moves through the unsaturated macropores and fissures as free-surface films that line pore space walls, so the flux will include dimensions of area, volume, film thickness, and speed. However, flow does not occur in all available source-responsive domain space for every

event, so a dimensionless factor f(z,t) (active area fraction) modulates q_{Smax} to adjust for variable source-responsive flow. Combining with the diffuse flow flux , the total flux is

$$q(z,t) = -\mathrm{K}(\theta_D)\frac{\partial \Phi}{\partial z} + f(z,t)q_{S_{\max}}(\mathrm{z}) \quad [3]$$

In order to calculate q_{Smax}, a parameter to define the size of the source-responsive domain is necessary. Since the source-responsive space can be visualized as a complex combination of interconnected cylinders, cracks, and fissures, quantifying the total area per unit volume describes the size of the source-responsive domain. This parameter, the facial area density M(z) [m^2 m^{-3}], will likely vary through time and is geometrically equivalent to common definitions of fracture density (Nimmo, 2010).

Other necessary parameters to determine q_{Smax} include water flux velocity and film thickness. The source-responsive domain is imagined to behave as a free-surface film with laminar flow. This allows relations between the free-surface film speed and film thickness. The maximum velocity (v_{max}) [m s^{-1}] and average laminar-flow (v_{avg}) [m s^{-1}] velocity for the water flux are

$$v_{max} = \frac{1}{2}\frac{g}{v}L^2 \quad [4]$$

$$v_{avg} = \frac{2}{3}v_{max} = \frac{1}{3}\frac{g}{v}L^2 \quad [5]$$

$$L = \sqrt{\frac{2*v*v_{max}}{g}} \quad [6]$$

where g is the gravitational constant, L is the film thickness, and v is the kinematic viscosity of the fluid (Bird et al., 2002). When defining q_{Smax}, the average laminar-flow velocity will be utilized. In the case of L, the free-surface film represented is considered a

maximum, singular value, under the assumption that the true thickness varies in a narrow range around the *L* parameter. Combining these terms together, the flux density for the source-responsive domain is

$$q_{\mathrm{S}_{\max}} = MLv_{\mathrm{avg}} \quad [7]$$

As previously mentioned, q_{Smax} is altered by an active area fraction *f*, so combined with the diffuse-flow domain the flux density is

$$q(z,t) = -\mathrm{K}(\theta_D)\frac{\partial \Phi}{\partial z} + f(z,t)MLv_{\mathrm{avg}} \quad [8]$$

In order to simplify the model, the film thickness *L* is fixed, based on the relationship of developed in eq. 6.

Two competing mechanisms occur in order to describe water table fluctuations within the source-responsive model: recession and accretion. The recession is attributed to the continuous diffuse-flow that would occur in the absence of preferential flow, moving the water table height to a higher level than the water table level would attain without any recharge. This would occur at approximately a linear rate, in hours, designated in the model by the reciprocal of a proportionality constant rate τ. Accretion is the water table height increase and is characterized as the source responsive flux, $q_s(z,t)$, divided by the medium's drainable porosity ratio, p_{dp}. By combining the two mechanisms, the water table fluctuation is depicted by

$$\frac{dH}{dt} = -\frac{H}{\tau} + \frac{q_{\mathrm{S}_{\mathrm{lim}}} f}{p_{\mathrm{dp}}} \quad [9]$$

$$q_{\mathrm{S}_{\mathrm{lim}}} = v_{\mathrm{avg}} L M_{\mathrm{lim}} \quad [10]$$

where H is the rise of the water table and q_{Slim} is the water flux at the critical value of M_{lim}, which is the smallest internal facial area of macropores between land surface and the new water table height, H. In order to solve for H incrementally over the course of a storm event, the solution is

$$H_{\mathrm{i+1}} = H_{\mathrm{i}} \exp\left(\frac{t_{\mathrm{i}} - t_{\mathrm{i+1}}}{\tau}\right) + \frac{q_{\mathrm{Slim}} f_{i+1} \tau}{p_{\mathrm{dp}}} \left[1 - \exp\left(\frac{t_i - t_{i+1}}{\tau}\right)\right] \quad [11]$$

where H_{i} is a starting level. As in eq. 9, the first term describes the water recession, and the second term describes the accretion attributable to source-responsive flow. Eq. 11 is identical to an equation presented in Nimmo (2010), with the exception of the notation for the drainable porosity ratio (p_{dp}) that is modified to be consistent with the nomenclature of Chapter 3. Nimmo (2010) instead used the equivalent term of specific yield (Y).

In practice, the source-responsive model will be utilized only for cases with fast rises (< 8 hours) which cannot be easily explained by matrix flow alone. Fig. 4.1 shows the two domains: water quickly infiltrating towards the water table through macropores, fissures, and around soil aggregates via preferential flow, and the slower percolation of water via matrix flow. Typically these preferential flow pathways are shown to be mostly vertical, but the potential for rapid horizontal movement of water is also a possibility in the presence of a nearby subsurface drain.

As an attempt to isolate the variable dynamics in the preferential flow regime, the diffuse-flow component of eq. 8 will be ignored. With the only water source accounted for by a relationship highlighted in eq. 10, this will offer an opportunity to study

alterations in the available macropore space, as described by the *M* parameter which can be isolated by fixing the other parameters.

2.3 Modifications to the source-responsive model

For the application to the drainage field in Iowa, a key modification to the model has been made in order to yield better model fits with the observed field data. The *f* parameter will be calculated in the same fashion, but a new *f* offset parameter (f_{offset}) has been added, based on the observation of a delayed timing of first water arrival to the water table. Currently for eq. 11, the water table height is governed by instantaneous accretion of the water table, with the *f* parameter augmenting the current time step's active area fraction. This new parameter accounts for the time for the initial pulse of rainfall to hit the land surface, infiltrate and transverse the unsaturated zone. The *f* offset parameter (f_{offset}) is a positive integer that would shift the time step of the *f* parameter that the calculation utilizes within the model's algorithm. The modified eq. 11 is

$$H_{\text{i+1}} = H_i \exp\left(\frac{t_{\text{i}} - t_{\text{i+1}}}{\tau}\right) + \frac{q_{S\text{lim}} f_{\text{i+1}-f_{\text{offset}}}{}^{\tau}}{p_{\text{dp}}} \left[1 - \exp\left(\frac{t_{\text{i}} - t_{\text{i+1}}}{\tau}\right)\right] \qquad [12]$$

2.4 Experimental set-up

In order to run the model for a specific event, a total of eight parameters are necessary: v_{avg}, L, M_{lim}, f, f_{offset}, p_{dp}, v and τ. Based on a previous treatment of maximum water velocity at the site (Chapter 3), the individual average water velocity, v_{avg}, for any single event is calculated with eq. 5. With a known v_{max}, the film thickness L is assumed with the usage of eq. 6. The proportionality constant, τ, is set at 504 hours (three weeks). This rate for the τ constant is based upon long-term observations of recession rates at the site. The *f* parameter is calculated by dividing the current rainfall rate, q_{in}, by q_{Slim}, with

q_{Slim}, a term which is analogous to the infiltration capacity. For instances when the rainfall rate exceeds q_{Slim}, f is set equal to 1. The v parameter, kinematic viscosity of water, is temperature dependent. The average temperature for each event was based on data from the pressure transducer.

The only three unknown parameters remaining are p_{dp} , f_{offset} and M_{lim}. For this study, p_{dp} was fixed and M_{lim} was allowed to vary. The drainable porosity (p_{dp}) was fixed at 0.052, an average p_{dp} based on a narrow range of p_{dp} ratios calculated in chapter 3 under conditions when the water table was close to land surface. The f_{offset} was determined by finding the combination of M_{lim} and f_{offset} that lead to the best goodness-of-fit (discussed in the following section). Given that the f_{offset} only changes the timing of the f parameter, this will not lead to multiple solutions for M_{lim}.

The primary strategy for the model runs was to include as many events from 2007 appropriate for the source-responsive model (within year variability). A second strategy (across year variability) was to run the model for an event that occurred in early May in 2007, 2008, and 2009. The source-responsive model was utilized for a total of 12 events which includes 33 individual observations from the different piezometer at various distances from the subsurface drain. Each individual piezometer water level was modeled for three different values of the maximum water velocity: an average v_{max} value of 1.21 x 10^{-4} m s^{-1}, based on the average of all maximum water velocities calculated from 51 individual rainfall events at the site (Chapter 3); calculated v_{max}, based on the maximum water velocity from the storm being modeled (Chapter 3); rainfall-threshold v_{max}, also calculated from the storm being modeled (Chapter 3). The only difference between the calculated v_{max} and the rainfall-threshold v_{max} was that the difference in time for the

calculated v_{max} was from the first instance of precipitation whereas the rainfall-threshold v_{max} was after at least 1-mm of cumulative precipitation.

2.5 Goodness-of-fit criteria

In addition to visual analysis, two different statistical parameters were added to the Nimmo (2010) model to quantify the model runs to the measured water level. The Nash-Sutcliffe model efficiency coefficient (Nash and Sutcliffe, 1970) and an adapted residual method were both run in order to obtain the best fit of the M_{lim}. The Nash-Sutcliffe model efficiency R^2 (Eq. 13), however, was considered the more robust estimate of goodness-of-fit and the adapted residual method *RF* was only a second check (Eq. 14).

$$E = 1 - \frac{\sum_{i=1}^{N} (H_o^i - H_m^i)^2}{\sum_{i=1}^{N} (H_o^i - H_o^{avg})^2} \quad [13]$$

$$RF = \sum_{i=1}^{N} \mathrm{Abs}(H_m^i - H_o^i) \quad [14]$$

H_o^i represents the individual water level observation, whereas H_m^i represents the modeled output at the corresponding time step, H_o^{avg} is the average water-level for the entire time series, and *N* is the total number of time steps of concern. A value of $E = 1$ indicates a perfect fit and any value below $E = 0$ is considered questionable. For the *RF*, the closer the value is to 0 the better the model fit to the data.

The statistical analysis was only targeted for the section of the time series along the water level rise as shown in Fig. 4.2A-C. The reasoning for only testing part of the modeled results is the water level recession was not of concern for this source-responsive model exercise, given the likelihood water during this period is more likely diffuse flow

and also affected by the subsurface drain. The main concern was the timing and the absolute height of the water level rise.

3. Results

3.1 Active area fraction offset (f_{offset})

Fig. 4.3 illustrates how the f_{offset} affects the model results. A 12.2-mm rain event is shown in Fig. 4.3A with a water table rise of 0.22 m. By invoking a 2.25 hour f_{offset}, the source-responsive model matches the peak rise measured in the 7.6-meter piezometer. Without employing this f_{offset}, the modeled peak rise occurs too early as shown in Fig. 4.3B.

In Table 4.1, the f_{offset} covers a range from zero to 4.25 hours. In theory, the physical basis for f_{offset} is accounting for the delay of the rainfall from the time of the rainfall hits the land surface to the water's arrival to the water table. Without introducing a new relationship into eq. 11, the adapted eq. 12 allows for a threshold amount of rainfall to move through the unsaturated zone and satisfy moisture deficits that would hinder preferential flow due to large matrix suction forces. Overall, the f_{offset} addresses the original concern raised by Nimmo (2010) where he questioned his assumption of instantaneous accretion of the water table.

All of the f_{offset} data was compared against the following parameters in order to see if a simple linear or exponential relationship existed: rainfall amount, pre-event height of piezometer water level, maximum height of piezometer water level during an event, pre-event and event maximum VWC, the calculated and rainfall-threshold v_{max}, and the associated M_{lim} for the three different v_{max} scenarios. The pre-event height of piezometer

water level ($r^2 = 0.31$), maximum height of piezometer water level during an event ($r^2 = 0.33$), and the M_{lim} associated with the calculated v_{max} ($r^2 = 0.26$) stood out as showing at least a weak relationship with f_{offset} (Fig. 4.4A-C). For the remaining parameters, the relationship was non-existent or too weak to consider for further exploration.

3.2 Goodness-of-fit

Two different statistical parameters, the Nash-Sutcliffe model efficiency coefficient and an adapted residual method, were run for every modeling scenario. As alluded to in the methods, only a section of the time series along the water level rise was targeted for both statistical parameters. The box in Fig. 4.2A shows the area of concern for the water level rise up to the maximum event height.

However, many of the modeled scenarios did not have a monotonic rise due to an intermittent rainfall or a non-uniform water level rise. Fig. 4.2B and 4.2C show two different scenarios that yielded a less than ideal goodness-of-fit. Although application of both statistical parameters will not lead to the best demonstration of the source-responsive model's efficiency, as it only targets the water table rise, it at least allows for determination of the best-fit M_{lim} so that the different scenarios can be easily compared.

3.3 Sensitivity analysis

Before running the source-responsive model through the scenarios as outlined in section 3.3, a sensitivity analysis was conducted for M_{lim}, p_{dp}, and v_{max}. Unlike some sensitivity analyses, these results will not try to address the question of the uncertainty of the model parameters themselves (Wilson, 2010), but rather, illustrate how the model output varies over the range of values used in the actual modeling analysis in this study.

Rainfall initiates the model run with no f_{offset}. A kinematic viscosity ν of 1.27 x 10^{-6} m^2 s^{-1} (20°C), the film thickness L controlled by eq. 4, and the proportionality constant (τ) of 504 hours (three weeks) are assumed. For simplicity, the rainfall profile was kept uniform without any breaks during the storm.

As can be seen easily in Fig. 4.5A, an M_{lim} of 1000 m^2 m^{-3} does not adequately represent the observed rise of 0.25 m. An M_{lim} of 2500 m^2 m^{-3}, on the other hand, is very close to the observed rise while the M_{lim} values of 5000 and 10000 m^2 m^{-3} represent a larger magnitude rise greater than the "observed" rise. In the p_{dp} sensitivity analysis, smaller values of p_{dp} will lead to larger magnitude rises, with values below 0.05 extremely sensitive to water level rises. Physically, this is due to the fact that less air-filled pore space is available so that a given amount of infiltrating water will have a larger impact on the water table height for smaller values of p_{dp}. Alternatively, p_{dp} greater than 0.15 will not have much of modeled water level rise, at least for a moderate-sized rainfall event of 25.4 mm (1 in). Finally, larger v_{max} will lead to larger magnitude rises with values >2.0 x 10^{-4} m s^{-1} overshooting this particular case. Physically, this is likely due to faster velocities are more likely the result of water moving through larger pore diameters where flow will less tortuous and unhindered by the smaller pore dynamics and matrix suction.

3.4 Application of different V_{max}

Table 4.1 displays the list of precipitation events included in this study along with the best fit M_{lim} from each model run. The water levels from each piezometer were modeled separately for each event in order to calculate the appropriate facial area density (M_{lim}) for each estimate of the three maximum water velocities: average v_{max}, calculated

v_{max}, and rainfall-threshold v_{max}. Varying the v_{max} to calculate the M_{lim} and f_{offset} required the other four parameters (p_{dp}, L, τ, and f) to remain fixed for the event. As suggested earlier, the drainable porosity ratio, p_{dp}, of 0.052 was utilized for every model run. Film thickness L is dependent on v_{max} through Eq. 6, the proportionality constant τ was fixed at 504 hours (equivalent to three weeks), and active area fraction f was calculated from the ratio of incoming rainfall intensity divided by the q_{Slim} (Eq. 10).

The term the source-responsive model uses to define the amount of preferential flow space contributing to the water flux is M_{lim}. However, in order to make general observations by lumping together all the M_{lim}, it was important to determine whether the subsurface drain had a spatial effect on the M_{lim}. Due to the small number of overall observations, the groups were lumped into two categories: close piezometers (0.3 m, 0.9 m and 3.0 m), and far piezometers (7.6 m and 15.2 m). Using either paired t-tests or Mann-Whitney rank sum tests (depending on the normality of the data), the best fit M_{lim} were not statistically different for the three v_{max} scenarios.

The calculated v_{max} for all available 2007 events and the source-responsive best fit M_{lim} are plotted in Fig. 4.6. Beginning at Julian date 105 (April 15th) up to Julian date 288 (October 15th), the v_{max} trend shows a general increase in v_{max} up to late August (Julian dates 230-245) when a wider distribution of v_{max} was observed. On the other hand, the best fit M_{lim} showed a general decrease from mid-spring (late April, early May) until the late August period where the best fit M_{lim} had the lowest values. Also shown in Fig. 4.6 are the rainfall-threshold v_{max} and best fit M_{lim}, which exhibits the same general decreasing trend as the calculated v_{max}. However, the rainfall-threshold scenarios do not have as large of an M_{lim} range.

Overall, manipulating the M_{lim} by keeping the other parameters fixed for all three water velocities did model all the events in Table 4.1. The fit did vary from run to run, although the Nash-Sutcliffe R^2 (Eq. 12) was generally greater than 0.80 and the *RF* (Eq. 13) was well below 1. The recession period is not included in the modeling exercise since the recession is under the influence of the subsurface drain.

Three different v_{max} scenarios were modeled to help determine which would be the best v_{max} value for use in the source-responsive model. The range in M_{lim} when using an average v_{max} value (Table 4.1) is similar to the other two v_{max} scenarios (calculated, rainfall-threshold). However, it is difficult to determine whether the variations in M_{lim} are due to a varying preferential flow space or another process altogether (Fig. 4.7B). Given the range of v_{max} shown at this site of over two orders of magnitude (Table 4.1), the usage of measured v_{max} (either calculated or rainfall-threshold) is superior if independently available. As illustrated with Fig. 4.5C, varying the v_{max} can have a substantial impact on the resultant water level rise so pinpointing the real v_{max} as much as possible is a better approach.

For the calculated and rainfall-threshold v_{max} scenarios, the results between the two only vary considerably for events with a best fit M_{lim} >10000 m^2 m^{-3} (Fig. 4.7A-7B). For many of the events (Table 4.1), these two v_{max} values are identical as the threshold of 1-mm was often crossed at the onset of precipitation. There are differences between the two values only when a rainfall event starts intermittently and the bulk of the rainfall is delayed by several hours. These are the events with the larger M_{lim} values as shown in Fig. 4.7A. Fig. 4.8 illustrates this with a 1:1 line showing the identical or nearly identical at low M_{lim} values and the sharp difference is at higher M_{lim}.

Overall, the calculated v_{max} show a fairly strong inverse power relationship (Fig. 4.7A, $r^2 = 0.46$). This inverse power relationship improves ($r^2 = 0.71$) by dividing the calculated v_{max} scenarios into two different groups (Fig. 4.7C): a low pre-event VWC (<0.35 m^3 m^{-3}), and a high pre-event VWC (>0.45 m^3 m^{-3}). This suggests that the high pre-event VWC had little available air-filled pore space, so a small input of water would lead to a water level rise similar to the sensitivity analyses of Fig. 4.5B. Conversely, the low pre-event VWC had a much higher available pore space to fill, so either a larger input of water is necessary to get a comparable water table height increase, or a larger M_{lim} would need to be invoked in order to explain the water level rise.

A comparison of a similar time period (early May) for all three years is shown in Fig. 4.9. In this case, only the average and calculated v_{max} are shown along with their best fit M_{lim}. Despite similar moisture condition profiles, these events do seem to have characteristically different M_{lim}, especially in the case of comparing 2007 to 2008 and 2009 for the calculated v_{max} scenarios due to the large difference in the input v_{max}. An important difference between 2007 and 2008 was the shift from soybeans to corn, whereas the 2009 values came from the grassy buffer rather than the field array.

4. Discussion

4.1 Improvements to the source-responsive model

In agricultural areas with soils developed on glacial deposits, the presence of subsurface drainage networks provides additional pathways of water movement to the stream. In this and previous studies (Chapter 2; Chapter 3), preferential flow was shown to be an important pathway of water from the land surface to the subsurface drain. A

challenge to this effort was finding a suitable modeling tool that could incorporate variable preferential flow dynamics, while maintaining a simple approach without including numerous soil specific parameters that are often difficult to determine. The source-responsive model (Nimmo, 2010) was identified as meeting this challenge; however, during the process of utilizing this model, two critical modifications were added in order to maximize its usefulness without adding any complicated logic.

The first modification included adding the new *f* offset parameter (f_{offset}, eq. 12), which changes the time step that the *f* parameter considers. Instead of necessarily staying at the current time step, delaying the *f* parameter allows the water to move through the unsaturated zone without instantly adding water to the water table. Based on the results in Table 4.1, few events did occur where the $f_{offset} = 0$; however, these were all instances where there was only small differences between the pre-event and the event maximum soil VWC, thereby little water was necessary to satisfy soil moisture deficits.

The second modification was the addition of an easy statistical review of the best fit between the modeled results and the measured water table height. The Nash-Sutcliffe model efficiency coefficient has a long history of usage (Nash and Sutcliffe, 1971), and is appropriate for this type of analysis. Without such a parameter, graphical analysis was often difficult to determine the best model results given most of the modeling scenarios look more like Fig. 4.2B and 4.2C rather than Fig. 4.2A.

4.2 Determination of the appropriate v_{max}

The range of v_{max} in Fig. 4.7A-C captures only some of the variability at this site, as the full range from the 51 measured events was greater than two orders of magnitude

(Chapter 3). Given these considerations, it is worth considering the most appropriate v_{max} value to use considering the range in resultant model results (Fig. 4.6C).

A previous attempt was made to consider if preferential flow perhaps falls within a narrow band of average v_{max} (Nimmo, 2007), suggesting that v_{max} can be predicted *a priori* within one order-of-magnitude. From Nimmo (2007), based on the geometric mean of 64 field tests from a variety of field studies with evidence of preferential flow, a value of 1.5×10^{-4} m s^{-1} was found. This is quite close to the average v_{max} utilized in this study of 1.21×10^{-4} m s^{-1}.

However, given the range of calculated v_{max}, it seems that using an average v_{max} is not appropriate for accurately modeling water table fluctuations, especially at the sub-hourly time scale employed with the source-responsive model. Furthermore, the results of from the variable v_{max} are in line with the field results given by Germann and Hensel (2006), where they show a large range of water velocities (>2 orders of magnitude occurred). In fact, German and Hensel reported water velocities that exceeded the rainfall-threshold v_{max}. Therefore, caution must be exercised as varying v_{max} can have a substantial impact on the resultant water table rise utilizing the source-responsive model, so determining the calculated v_{max} from field results is a better approach.

Neither the calculated and rainfall-threshold v_{max} scenarios make a substantial difference for events with smaller M_{lim} on which method to use (Fig. 4.8). However, the upper end of the best fit M_{lim} spectrum, such as those >10000 m^2 m^{-3}, only occurred with the calculated v_{max} because it contains all of the time of transport rather than factoring in an arbitrary period, such as a cumulative total over 1-mm.

4.3 Interpretation of the M_{lim} results

Fig. 4.6 suggests a seasonal trend in the best fit M_{lim}, with three probable explanations: (1) a change in the preferential flow space over time; (2) a change in the amount of preferential flow space utilized changes while the preferential flow space itself remains static; or, (3) the M_{lim} itself is indicative of another phenomenon beyond a measurement of the preferential flow space. Up to Julian date 126 (early May), the best fit M_{lim} is quite variable and reaches some of the largest values. As the summer season sets in, the M_{lim} reaches the lowest values during the summer season when the v_{max} reach some of the largest values.

In Fig 10A-B, two events with extreme M_{lim} are shown (May 6th and October 7th, with best fit M_{lim} of 750 m^2 m^{-3} and 17625 m^2 m^{-3}, respectively). The May 6th event (Fig. 4.10A) had 36.1 mm of rainfall that occurred with two distinct bands, resulting in nearly immediate water table height increase. Over the course of the event, the water table height increased 0.43 m with a maximum height after six hours. In Fig. 4.10B, the rainfall event of October 7th had only 12.2 mm of rainfall. The first substantial water table height increase did not occur for more than 6 hours. This late season event had a maximum water table height increase 0.22 m, half the amount of the other event but with only a third of the same amount of precipitation.

Although these two events differed considerably for the best fit M_{lim}, a clear explanation on whether the cause was due to a variable preferential flow space or just a shift in the amount of a static preferential flow space being utilized was not clear. In comparing these two events, the five different factors that immediately differentiate the two events are the rainfall amount and intensity, v_{max}, f_{offset}, and the difference in the

ground cover. Cumulative rainfall for the May event was three times the October event (36.1 mm vs. 12.2 mm), occurring in two bursts for the May event and only one, more prolonged period for October event. The v_{max} between these two events differs by almost an order of magnitude, and the f_{offset} is 2.5 hours for the October event as opposed to only 0.5 hours for the May event. Finally, the May event occurred on bare soil while the October event occurred on a fully mature soybean field, a factor that could potentially cause a delay. However, it is not clear how any of these five factors could easily explain the first two explanations of the seasonal trend.

4.4 M_{lim} as a continuum of preferential and matrix flow

In the case of the last chapter, it was suggested that the seasonal trends in v_{max} were due to variable preferential flow regime (i.e. M_{lim}), but perhaps the variable M_{lim} is indicative of another phenomenon altogether such as a continuum of preferential and matrix flow. Trying to categorize all of the events of Fig. 4.7A does not seem to fit an overall pattern, as larger and/or higher intensity rainfall events do not always result in lower M_{lim} (example: April 24th, 2007), just as large VWC differences can result in large M_{lim} gaps as in the example of Fig. 4.10A-B. As pointed out in the previous chapter on water velocities, several factors could potentially influence both water velocities and preferential flow space including but not limited to antecedent moisture conditions, storm rainfall intensity and amount, climatological effects, and evapotranspiration.

The seemingly erratic M_{lim} results can make more sense by interpreting the M_{lim} results beyond just a measure of the preferential flow space, but rather as a continuum of preferential and matrix flow. By revisiting the conceptual diagrams of Fig. 4.1, a conceptual picture of the continuum of preferential and matrix flow can be seen. Larger

vertical and horizontal cylinders, considered “classic” macropores, such as biopores (i.e., wormholes), root channels, and soil desiccation cracks (Haria et al., 1994), can be seen in Fig. 4.1. However, on the left side of Fig. 4.1, a close-up view shows the finer aspects of inter-aggregate channels and even flow inside of the aggregates themselves. Simply accounting for the preferential flow via macropores could potentially miss a significant portion of the preferential flow that could occur in spaces illustrated in Fig. 4.1.

For the past 30 years, many of the dual porosity and dual permeability models, as well as the multi-porosity and multi-permeability models, have developed along the paradigm that preferential and matrix flow are distinct regimes. However, during the same period, various distinctions of the different pore sizes, such as what constitutes a macropore, has been vigorously debated. For example, Luxmoore (1981) suggested three porosity classes of micro-, meso-, and macropores, with equivalent pore diameter ranges of <10 μm, 10 to 1,000 μm, and >1,000 μm, respectively. The macropores would be indicative of channel flow through the soil profile, while the micropores would consist of matric pressure gradients for water movement (i.e., matrix flow) and mesopores would be dominated by drainage and gravitational forces for water movement. In response to Luxmoore (1981), Bouma (1982) suggested smaller size limits to the macropore category, with a very fine subclass from 75-1,000 μm. Both authors did note caution in getting caught up in class sizes, as the boundaries of pore classes and therefore flow regimes is much blurrier. Other distinctions of pore sizes have also been considered, of which Perret et al. (1999) summarized at least another 10 classifications.

The lack of consensus potentially points to the fluid nature of the boundaries between what would be considered a macropore, capable of conducting preferential flow,

and smaller micro- and mesopores, more indicative of matrix flow. In that respect, the concept of a continuum of preferential and matrix flow (i.e., source-responsive and diffuse flow) is warranted. As Nimmo (2010) suggested, strict adherence to a particular set of pore sizes narrows the scope of the distinguishing preferential flow from matrix flow dynamics, as preferential flow in all likelihood occurs at smaller pore diameters than previous designations of macropore classes.

So, ignoring size limits for a moment, a consideration for the physical meaning of different values of M_{lim} was analyzed in order to determine what could constitute realistic lower size limits for the typical preferential flow, ranges that could potentially expand the paradigm of preferential flow, and limits to realistic preferential flow. For simplification in these calculations, the facial area density was calculated by taking an average pore width and multiplying it by the number of pores of that size in unit volume (m^3), divided by the unit volume. For example, in the case of pores with a 0.1 mm diameter and a unit length of 1 m, the number of pores per unit volume to reach an M_{lim} of 100 was 3.2×10^5 pores. Continuing with the same unit length of the average pore as 1 m in length, the pore size was varied between 30 μm and 10 mm as the macropore diameter size lower limits are generally 30 μm (Perret et al., 1999). Furthermore, the end area of all the average pore diameters was quantified in order to calculate the percentage of a unit area was occupied by macropores. So, to reach an M_{lim} of 100 with 3.2×10^5 pores and average pore diameter of 0.1 mm, 0.1% of the surface area would be covered by these pores. Literature estimates of typical macropore densities range from below 0.5% up to 5% or more in typical agricultural soils (Richard and Steenhuis, 1988), although this number is biased by whatever the particular study defines as a macropore or how the density was

quantified. For example, Perret et al. (1999) utilized CAT scanning with 3-D reconstruction to quantify macropore densities, while other methods include image analysis (Moran and McBratney, 1999), breakthrough curves (Villholth et al., 1998), tracers (Everts and Kanwar, 1990), and tension infiltrometers (Everts, and Kanwar, 1993). However, all visual techniques will likely have a difficult time quantifying the lower pore size limits.

So, the question remains, do M_{lim} values of up to 18000 m^2 m^{-3} calculated in this study realistically represent true preferential flow, or does the M_{lim} parameter inherently contain an aspect of diffuse (i.e., matrix flow) imbedded within the term? Germann's (2010) comments on Nimmo (2010) and Germann and Hensel (2006) showed that v_{max} of up to 5.5 x 10^{-3} m s^{-1} could be modeled with pore radii below current macropore size limits and therefore concluded that macropores were not required to initiate preferential flow. On the other hand, Bouma (1982) found considerable water flow through planar pores of 90 μm, constituting 2.4% of the total unit volume.

A true spectrum of macropore sizes would include much larger pore diameter openings, rather than the hypothetically small "average" pore diameters in fig. 4.11, which would bring the overall M_{lim} farther down. Even if a lower limit is reached that constitutes a boundary between preferential/source-responsive and matrix/diffuse flow, the water velocity through a 1-μm diameter pore would be different than the water velocity (v_{max}) through a 1-mm diameter pore so utilizing a single water velocity would not necessarily pinpoint the M_{lim} and, therefore, the size limits of the preferential flow space.

However, a lower limit for the size of a macropore opening (i.e., diameter of cylinder or plane) must be reached for the source-responsive domain. This lower limit is governed by the frictional and matric forces that would impede a source-responsive (i.e., preferential flow) response. Identifying such a limit can be aided by consideration of Fig. 4.11; however, an exact number cannot be as easily stated given the assumed lower limit of preferential flow (i.e., macropores) has increased over time with improved visualization techniques and might continue to do so. Aggregation in soils with high-clay content constitutes a huge potential for inter-aggregate flow, as preferential flow pathways along planes of weakness can occur down to extremely small aggregate sub-units (Jarvis and Dubus, 2006).

Based on the quickness and magnitude of the water table height increase in this study, M_{lim} values over 3000 m^2 m^{-3} likely constitute a mixture of preferential and matrix flow, with an increased amount of matrix flow beyond 5000 m^2 m^{-3}. As shown in Fig 4.11, beyond an M_{lim} of 5000 m^2 m^{-3}, the required density of macropores goes beyond 5% to increasingly unrealistic macropore densities. The suspension of the diffuse flow for the source-responsive model in this study likely caused the source-responsive component of the model to artificially behave as a mixture of both source-responsive flow (i.e., preferential flow) and diffuse flow (i.e., matrix flow). For this reason, suspension of the diffuse flow component is probably only valid for larger, more intense rainfall events or periods with elevated soil moisture conditions.

As a final note in this particular study, the p_{dp} held constant at 0.052 (Chapter 3). Instead of keeping the p_{dp} constant, the p_{dp} could have been varied which is probably more realistic. Studies such as Shah and Ross (2009) suggest that p_{dp} would be expected

to vary both temporally and spatially. By decreasing the p_{dp} as in Fig. 4.6C, the necessary M_{lim} to match the magnitude of the measured water table height would be lowered. For example, by decreasing the p_{dp} from 0.052 to 0.03, the calculated M_{lim} would almost be three times smaller.

5. Conclusions

In this study, water table fluctuations adjacent to a subsurface drain were used to calibrate the source-responsive model. A total of 12 events (33 individual observations) were modeled with the source-responsive model for three different scenarios to order calculate M_{lim}: average v_{max} and two different calculated v_{max} using a fixed drainable porosity. Output from the model included the facial area density (M_{lim}), a property of the medium analogous to other macropore and preferential flow pathway density quantifications. By calibrating to known parameters, an indication of the facial area density both spatially and temporally was determined. Testing the best maximum water velocity for future usage in the source-responsive model, the model results support the usage of calculated v_{max} when available rather than an average v_{max}.

As an improvement to the performance of the source-responsive model, two different additions to the model were completed, one which affected the behavior of the model and the other addition helped qualify the goodness-of-fit of the model's output. The first addition, the f_{offset} parameter, delays the water infiltrating water by the required time increment for a best fit. This new parameter effectively accounts delay to an unknown threshold rainfall amount to move through the unsaturated zone and satisfy moisture deficits that would normally hinder preferential flow due to large matrix suction forces.

The second addition included two statistical parameters to judge the model output's best fit to the measured data: the Nash-Sutcliffe model efficiency coefficient (Nash and Sutcliffe, 1970) and an adapted residual method.

Model results showed a weak trend towards a more focused preferential flow space during mid-summer, without any statistical difference between distance away from the subsurface drain. Otherwise, the model results reflect a more complicated interplay with the conducting medium itself, with larger M_{lim} indicative of preferential flow intermixed with matrix flow. Although these results seem counter-intuitive compared to the original premise of M_{lim} indicating the size of the preferential flow space, this instead highlights the likely continuum between pore sizes that behave in a more source-responsive manner (i.e., preferential flow) versus diffuse flow (i.e., matrix flow). This also is a result of suspension of the diffuse flow component in this analysis, which is probably only valid for larger, more intense rainfall events or periods with elevated soil moisture conditions.

References

Ahuja, L.R., D.G. Decoursey, B.B. Barnes, and K.W. Rojas. 1993. Characteristics of macropore transport studied with the ARS Root-Zone Water-Quality Model. Trans. ASAE 36:369–380.

Allaire, S.E., S. Roulier, and A.J. Cessna. 2009. Quantifying preferential flow in soils: A review of different techniques. J. Hydrol. 78: 179-204.

Bettis III, E.A., D.J. Quade, and T.J. Kemmis. 1996. Hogs, Bogs, and Logs: Quaternary Deposits and Environmental Geology of the Des Moines Lobe. Geological Survey

Bureau Guidebook Series No. 18. Ames, Iowa: Iowa Department of Natural Resources.

Beven, K. and P. Germann. 1982. Macropores and water flow in soils. Water Resour. Res. 18: 1311–1325.

Bird, R.B., W.E. Stewart, and E.N. Lightfoot. 2002. Transport phenomena. 2nd ed. John Wiley & Sons, New York.

Bouma, J. 1981. Soil morphology and preferential flow along macropores. Ag. Water Manage. 3: 235–250.

Bouma, J., C.F.M. Belmans, and L.W. Dekker. 1982. Water infiltration and redistribution in a silt loam subsoil with vertical worm channels. Soil Sci. Soc. Am. J. 46: 917-921.

Cey, E.E. and D.L. Rudolph. 2009. Field study of macropore flow processes using tension infiltration of a dye tracer in partially saturated soils. Hydrol. Proc. 23: 1768-1779.

Dideriksen, R.O. 1986. Soil survey of Hamilton County, Iowa. United States Department of Agriculture Soil Conservation Service, 157 p.

Ebel, B.A., and J.R. Nimmo. 2009. Estimation of unsaturated zone traveltimes for Rainier Mesa and Shoshone Mountain, Nevada Test Site, Nevada, using a source-responsive preferential-flow model. Open-File Rep. 2009-1175. USGS, Menlo Park, CA.

Everts, C.J. and R.S. Kanwar. 1990. Estimating preferential flow to a subsurface drain with tracers. Trans. ASAE 33: 451-457.

Everts, C.J., and R.S.Kanwar. 1993. Interpreting tension-infiltrometer data for quantifying soil macropores: Some particle considerations. Tran. ASAE 36:423–428.

Gerke, H.H., and M. Th. van Genuchten. 1993. A dual-porosity model for simulating the preferential movement of water and solutes in structured porous media. Water Resour. Res. 29:305–319.

Germann, P.F. and K. Beven. 1985. Kinematic wave approximation to infiltration into soils with sorbing macropores. Water Resour. Res. 21: 990-996.

Germann, P. 2010. Comment on "Theory for source-responsive and free-surface film modeling of unsaturated flow". Vadose Zone Journal 9: 1100-1101.

Germann, P.F. and D. Hensel. 2006. Poiseuille flow geometry inferred from velocities of wetting fronts in soils. Vadose Zone Journal 5: 867-876.

Haria, A.H., A.C. Johnson, J.P. Bell, and C.H. Batchelor. 1994. Water movement and isoproturon behaviour in a drained heavy clay soil: 1. Preferential flow processes. J. Hydrol. 163: 203–216.

Iowa Department of Transportation. 2011. Available at http://mesonet.agron.iastate.edu/AWOS/ (verified 25 July 2011).

Jarvis, N.J., 1991. MACRO -- A model of water movement and solute transport in macroporous soils. PhD Dissertation. Uppsala, Sweden: Swedish University of Agricultural Sciences, Department of Soil Science.

Jarvis N.J. and I.G. Dubus. 2006. State-of-the-art review on preferential flow. Report DL#6 of the FP6 EU-funded FOOTPRINT project [www.eu-footprint.org], 60 p.

Jury, W. and R. Horton. 2004. Soil Physics (6th edition). Hoboken, NJ: John Wiley and Sons, Inc.

Kumar, A., R.S. Kanwar, and G.R. Hallberg. 1997. Separating preferential and matrix flows using subsurface tile flow data. J. of Environ. Sci. and Health, Part A: Toxic/Hazardous Substances and Environ. Engineering 32: 1711–1729.

Kung, K.-J.S., E.J. Kladivko, T.J. Gish, T.S. Steenhuis, G. Bubenzer, and C.S. Helling. 2000. Quantifying preferential flow by breakthrough of sequentially applied tracers: Silt loam soil. Soil Sci. Soc. Am. J. 64: 1296-1304.

Larsbo, M. and N. Jarvis. 2007. MACRO 5.0: A model of water flow and solute transport in macroporous soil. Technical description, Swedish University of Agricultural Sciences: 49 p.

Luxmoore, R.J. 1981. Micro-, meso-, and macroporosity of soil. Soil Sci. Soc. Am. J. 45: 671-672.

McCarthy, K.A., C.E. Rose, and S.J. Kalkhoff. 2012. Environmental Settings of the South Fork Iowa River basin, Iowa, and the Bogue Phalia basin, Mississippi, 2006-10. U.S. Geological Survey Scientific Investigations Report 2012-5021, 30 p.

Mein, R.G. and C.L. Larson. 1973. Modeling infiltration during a steady rain. Water Resour. Res. 9: 384-394.

Moran, C.J., and A.B. McBratney. 1992. Acquisition and analysis of three component digital images of soil pore structure: I. Method. J. Soil Sci. 43:541–549.

Narasimhan, T.N. 1998. Something to think about...Darcy-Buckingham's Law. Ground Water 36: 194-195.

Nash, J.E. and I.V. Sutcliffe. 1970. River flow forecasting through conceptual models Part 1 - A Discussion of principles. J. Hydrol. 10: 282-290.

Nimmo, J.R. 2007. Simple predictions of maximum transport rate in unsaturated soil and rock. Water Resour. Res. 43: 1-11.

Nimmo, J.R. 2010. Theory for source-responsive and free-surface film modeling of unsaturated flow. Vadose Zone Journal 9: 295–306.

Perret, J., S.O. Prasher, A. Kantzas, and C. Langford. 1999. Three-dimensional quantification of macropore networks in undisturbed soil cores. Soil Sci. Soc. Am. J. 63: 1530-1543.

Pilgrim, D.H., D.D. Huff, and T.D. Steele. 1979. Use of specific conductance and contact time relations for separating flow components in storm runoff. Water Resour. Res. 15: 329–339.

Richard, T.L. and T.S. Steenhuis. 1988. Tile drain sampling of preferential flow on a field scale. J. Contam. Hydrol. 3: 307-325.

Richards, L.A. 1931. Capillary conduction of liquids through porous materials. Physics 1:318–333.

Roth , J. 2010. The hydrology of a drained topographical depression within an agricultural field in north central Iowa. MS Thesis. Minneapolis, MN: University of Minnesota, Dept. of Civil Engineering.

Schilling, K.E. and M. Helmers. 2008. Tile drainage as karst: Conduit flow and diffuse flow in a tile-drained watershed. J. Hydrol. 349: 291–301.

Shah, N. and M. Ross. 2009. Variability in specific yield under shallow water table conditions. J. Hydrol. Eng. 14: 1290-1298.

Shipitalo, M.J. and W.M. Edwards. 1996. Effects of initial water content on macropore/matrix flow and transport of surface-applied chemicals. J. Environ. Qual. 25: 662–670.

Šimůnek, J., T. Vogel, and M. Th. van Genuchten. 1994. The SWMS_2D code for simulating water flow and solute transport in two-dimensional variably saturated media. Riverside, CA, USDA-ARS U.S Salinity Laboratory, 197 p.

Šimůnek, J., N.J. Jarvis, M. Th. van Genuchten, and A. Gärdenäs. 2003. Review and comparison of models for describing non-equilibrium and preferential flow and transport in the vadose zone. J. Hydrol. 272: 14-35.

Stone, W.W. and J.T. Wilson. 2006. Preferential flow estimates to an agricultural drain with implications for glyphosate transport. J. Environ. Qual. 35: 1825-1835.

Villholth, K.G., K.H. Jensen, and J. Fredericia. 1998. Flow and transport processes in a macroporous subsurface-drained glacial till soil I: Field investigations. J. Hydrol. 207: 98–120.

Wilson, B.N. 2009. Lecture Notes for BBE 8513: Hydrologic Modeling of Small Watersheds. St. Paul, MN: University of Minnesota, Department of Bioproducts and Biosystems Engineering.

Table 4.1: Summary of facial area density (M_{lim}) values for 12 events (33 individual observations) from 2007-2009.

Event Date	Distance from SD[1]	Total Rainfall	Mean V_{max}[2]	Mean M_{lim}	Calc. V_{max}[3]	Calc. M_{lim}	RT V_{max}[4]	RT M_{lim}	f_{offset}	WT rise (max)	VWC, before event[5]	VWC, max. event
	m	mm	m/s	m^2/m^3	m/s	m^2/m^3	m/s	m^2/m^3	/h	m	m^3/m^3	m^3/m^3
4/24/2007	7.6	30.7	$1.22x10^{-4}$	3325	$5.30x10^{-5}$	10525	$6.85x10^{-5}$	7150	2.00	0.43	0.318	0.471
4/24/2007	15.2	30.7	$1.22x10^{-4}$	2050	$5.01x10^{-5}$	7450	$6.27x10^{-5}$	5375	3.00	0.41	0.318	0.471
4/24-4/25/2007	0.3	13.2	$1.22x10^{-4}$	2050	$1.05x10^{-4}$	2475	$1.31x10^{-4}$	1600	1.50	0.21	0.471	0.491
4/24-4/25/2007	0.9	13.2	$1.22x10^{-4}$	2075	$7.16x10^{-4}$	2275	$1.40x10^{-4}$	1625	1.50	0.21	0.471	0.491
4/24-4/25/2007	3.0	13.2	$1.22x10^{-4}$	2075	$6.85x10^{-5}$	4425	$8.47x10^{-5}$	3425	1.50	0.20	0.471	0.491
4/24-4/25/2007	7.6	13.2	$1.22x10^{-4}$	2500	$8.77x10^{-5}$	3900	$1.13x10^{-4}$	2675	0.00	0.27	0.471	0.491
4/25-4/26/2007	0.3	14.0	$1.22x10^{-4}$	1550	$8.68x10^{-5}$	2550	$1.19x10^{-4}$	1575	0.00	0.33	0.491	0.495
4/25-4/26/2007	0.9	14.0	$1.22x10^{-4}$	1550	$9.33x10^{-5}$	2300	$1.28x10^{-4}$	1425	0.00	0.33	0.491	0.495
4/25-4/26/2007	7.6	14.0	$1.22x10^{-4}$	925	$1.11x10^{-4}$	1075	$2.21x10^{-4}$	375	0.00	0.19	0.491	0.495
5/6/2007	7.6	26.0	$1.22x10^{-4}$	1950	$3.46x10^{-5}$	12700	$6.92x10^{-5}$	4500	3.00	0.17	0.328	0.430
5/6/2007	15.2	26.0	$1.22x10^{-4}$	1825	$3.21x10^{-5}$	13325	$5.77x10^{-5}$	5475	4.25	0.17	0.328	0.430
6/6-6/7/2007	3.0	24.1	$1.22x10^{-4}$	2000	$7.96x10^{-5}$	4025	$7.96x10^{-5}$	4025	2.00	0.15	0.340	0.483
6/6-6/7/2007	7.6	24.1	$1.22x10^{-4}$	2125	$8.06x10^{-5}$	4175	$8.06x10^{-5}$	4175	0.75	0.16	0.340	0.483
6/6-6/7/2007	15.2	24.1	$1.22x10^{-4}$	1575	$7.41x10^{-5}$	3500	$7.41x10^{-5}$	3500	1.75	0.13	0.340	0.483
8/19-8/20/2007	7.6	44.2	$1.22x10^{-4}$	6200	$3.11x10^{-4}$	1750	$3.11x10^{-4}$	1750	1.00	0.35	0.371	0.519
8/20-8/21/2007	0.3	18.3	$1.22x10^{-4}$	18050	$4.52x10^{-4}$	2900	$4.52x10^{-4}$	2900	2.25	0.32	0.518	0.529
8/20-8/21/2007	0.9	18.3	$1.22x10^{-4}$	16950	$4.69x10^{-4}$	2625	$4.69x10^{-4}$	2625	2.00	0.30	0.518	0.529
8/20-8/21/2007	3.0	18.3	$1.22x10^{-4}$	12825	$2.86x10^{-4}$	4175	$2.86x10^{-4}$	4175	2.00	0.24	0.518	0.529
8/20-8/21/2007	7.6	18.3	$1.22x10^{-4}$	8275	$2.84x10^{-4}$	2675	$2.84x10^{-4}$	2675	2.00	0.15	0.518	0.529

Event Date	Distance from SD[1]	Total Rainfall	Mean V_{max}[2]	Mean M_{lim}	Calc. V_{max}[3]	Calc. M_{lim}	RT V_{max}[4]	RT M_{lim}	f_{offset}	WT rise (max)	VWC, before event[5]	VWC, max. event
	m	mm	m/s	m^2/m^3	m/s	m^2/m^3	m/s	m^2/m^3	/h	m	m^3/m^3	m^3/m^3
8/21-8/22/2007	0.3	18.5	$1.22x10^{-4}$	9925	$4.83x10^{-4}$	1450	$4.83x10^{-4}$	1450	1.00	0.36	0.416	0.523
8/21-8/22/2007	0.9	18.5	$1.22x10^{-4}$	8475	$3.32x10^{-4}$	2175	$3.32x10^{-4}$	2175	1.00	0.34	0.416	0.523
8/21-8/22/2007	3.0	18.5	$1.22x10^{-4}$	5950	$2.26x10^{-4}$	2750	$2.26x10^{-4}$	2750	1.00	0.27	0.416	0.523
8/21-8/22/2007	7.6	18.5	$1.22x10^{-4}$	5050	$2.13x10^{-4}$	2525	$2.13x10^{-4}$	2525	1.00	0.20	0.416	0.523
8/28-8/29/2007	3.0	23.1	$1.22x10^{-4}$	1700	$1.53x10^{-4}$	1375	$1.53x10^{-4}$	1375	1.00	0.15	0.379	0.385
8/28-8/29/2007	7.6	23.1	$1.22x10^{-4}$	2125	$1.21x10^{-4}$	2425	$1.21x10^{-4}$	2425	0.00	0.17	0.379	0.385
10/7-10/8/2007	3.0	12.2	$1.22x10^{-4}$	5550	$6.06x10^{-5}$	17625	$1.41x10^{-4}$	4950	2.50	0.22	0.370	0.498
10/7-10/8/2007	7.6	12.2	$1.22x10^{-4}$	5100	$6.15x10^{-5}$	15850	$1.54x10^{-4}$	4000	2.25	0.22	0.370	0.498
5/6-5/7/2008	3.0	36.1	$1.22x10^{-4}$	2325	$1.25x10^{-4}$	2175	$1.25x10^{-4}$	2175	1.50	0.26	0.349	0.487
5/6-5/7/2008	7.6	36.1	$1.22x10^{-4}$	6450	$4.91x10^{-4}$	750	$4.91x10^{-4}$	750	0.50	0.43	0.349	0.487
5/6-5/7/2008	15.2	36.1	$1.22x10^{-4}$	15550	$3.41x10^{-4}$	3125	$3.41x10^{-4}$	3125	0.75	0.59	0.349	0.487
5/5-5/6/2009	0.3	11.2	$1.22x10^{-4}$	1900	$1.66x10^{-4}$	1150	$1.66x10^{-4}$	1150	3.25	0.15	--	--
5/5-5/6/2009	0.9	11.2	$1.22x10^{-4}$	2400	$1.92x10^{-4}$	1175	$1.92x10^{-4}$	1175	3.25	0.16	--	--
5/5-5/6/2009	7.6	11.2	$1.22x10^{-4}$	3725	$1.37x10^{-4}$	2975	$1.37x10^{-4}$	2975	2.00	0.31	--	--

[1] Subsurface Drain; [2] Mean v_{max} (Chapter 3); [3] Calculated v_{max} (Chapter 3); [4] Rainfall-threshold v_{max} (Chapter 3); [5] Volumetric Water Content

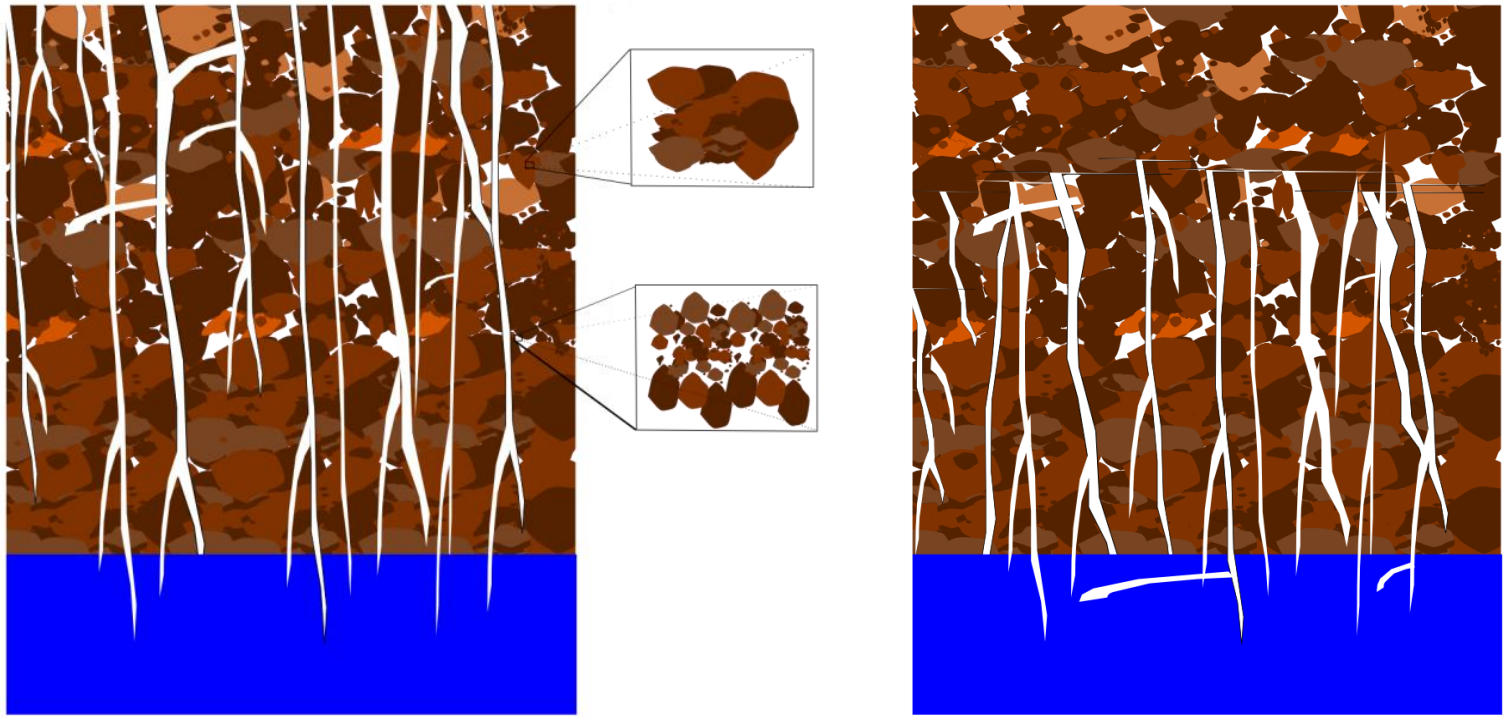

Fig. 4.1: On the left, primary and secondary cracks (caused by wetting/drying cycles), macropores, macroaggregates, and higher porosity in the upper unsaturated zone. Some surface cracks and macropores are directly connected to the shallow water table. Two inset boxes show microaggregates (top) and inter-aggregate pores (bottom). On the right, tillage resets macropore connectivity.

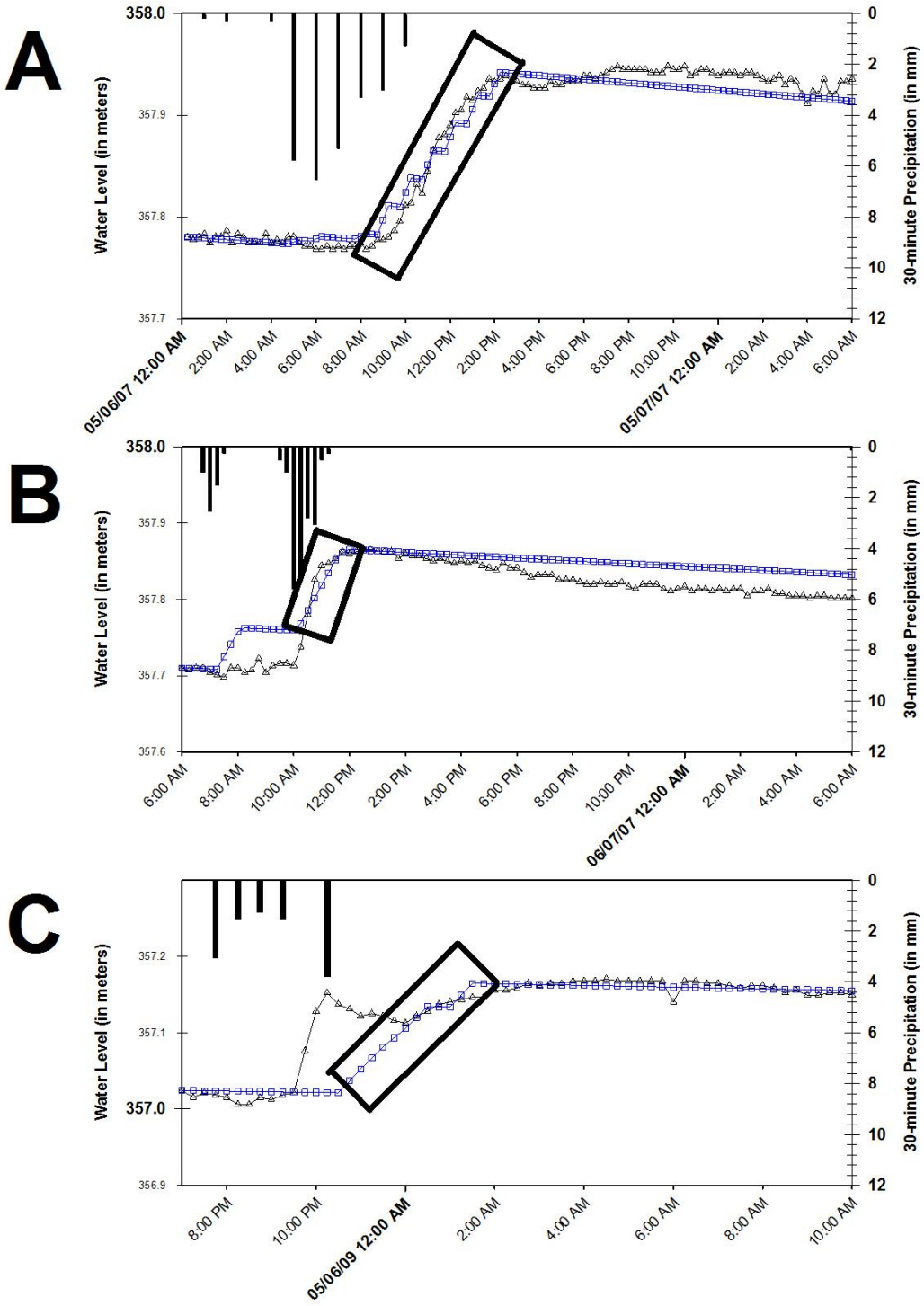

Fig. 4.2: Comparison of the various approaches to the application of the goodness-of-fit parameters, with (A) an ideal application with an even water level rise, (B) intermittent rainfall leading to an uneven modeled rise, and (C) uneven measured water level rise.

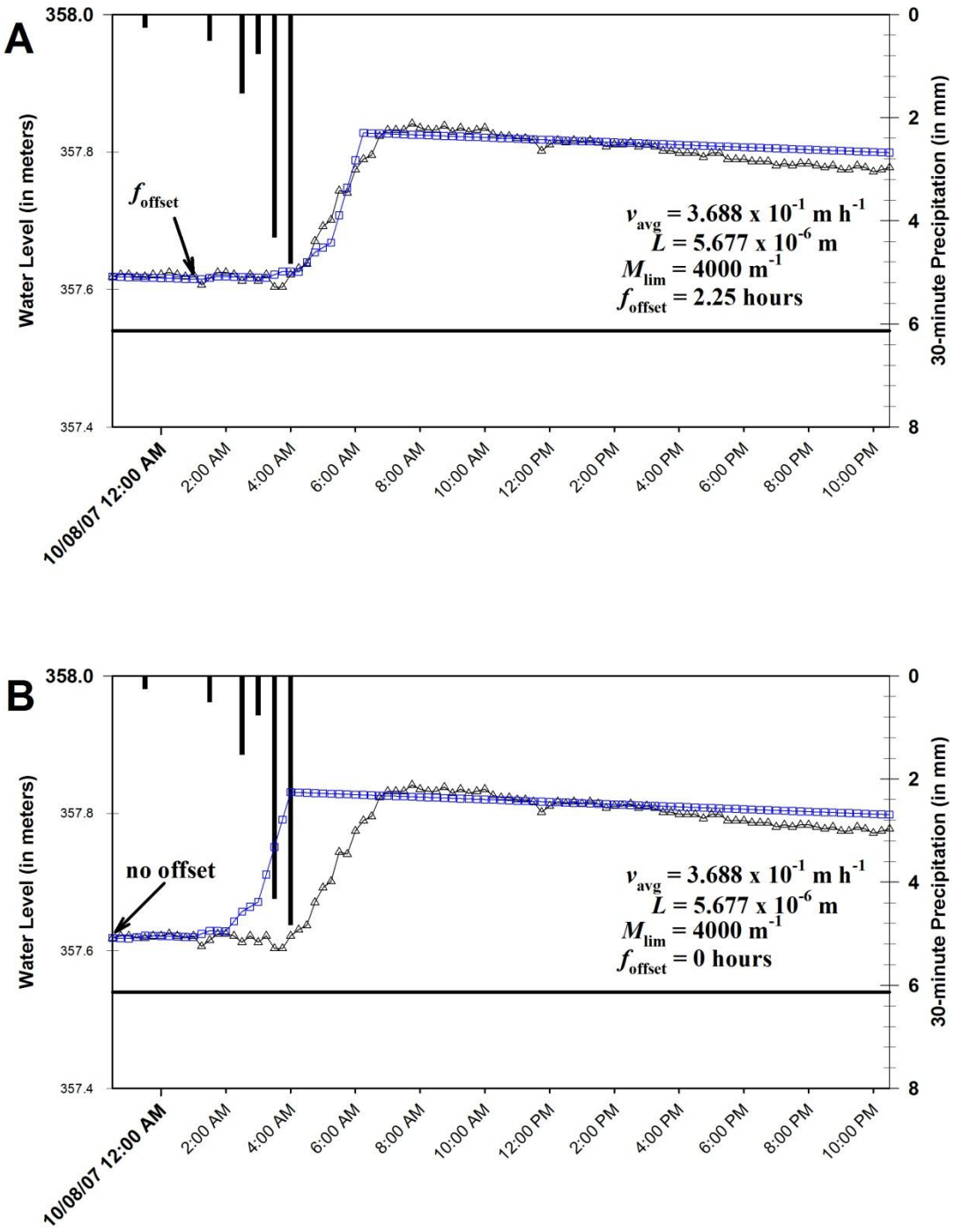

Fig. 4.3: The same storm is modeled with the source-responsive model with the same input parameters with the exception of a 2.25 hour f_{offset} in (A) and no offset for (B).

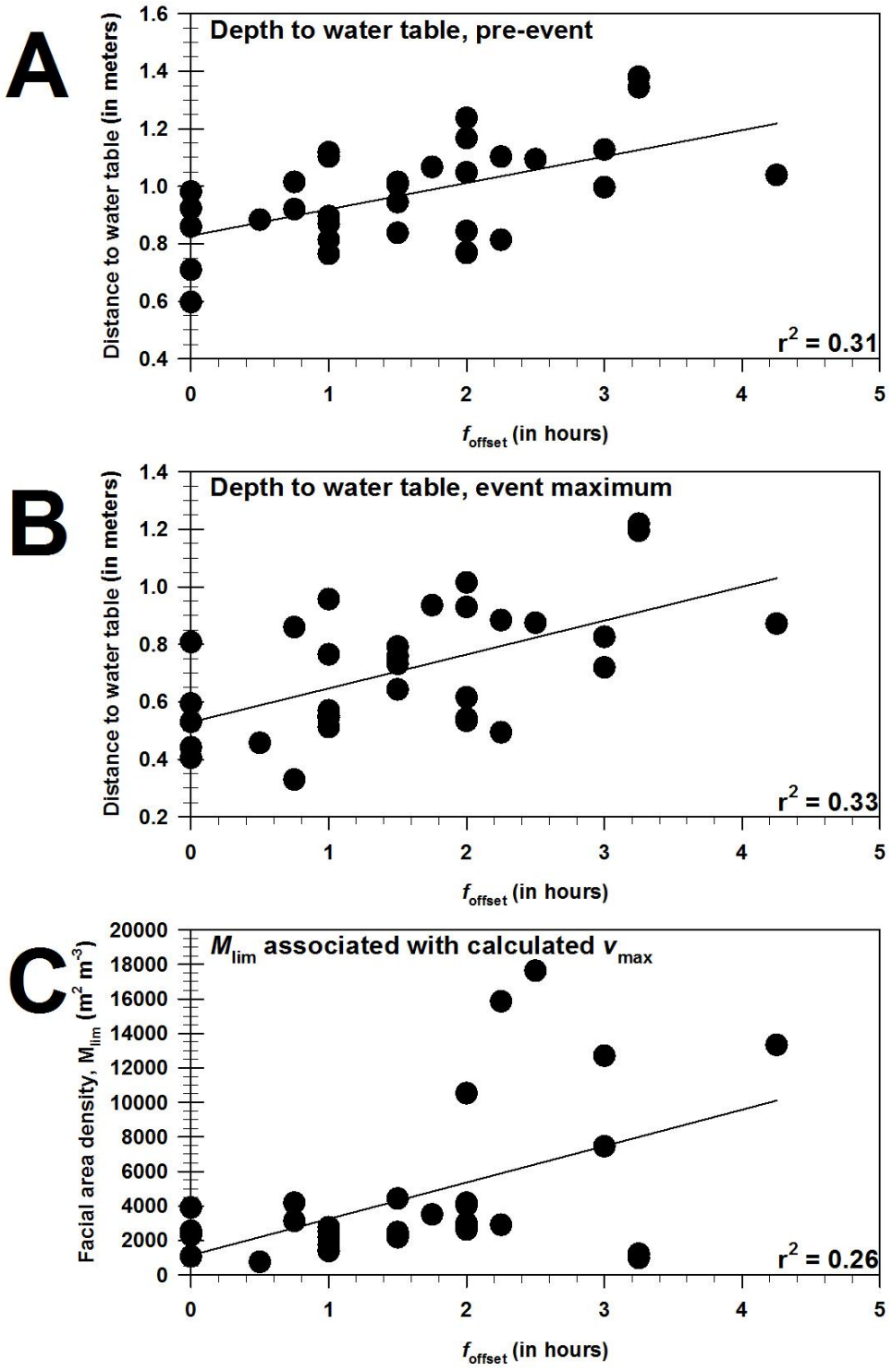

Fig. 4.4: Comparison of the f_{offset} parameter with the (A) depth to the water table (pre-event), (B) depth to the water table (event maximum), and (C) the M_{lim} associated with the calculated v_{max}. Additionally, the linear regression and r^2 is shown.

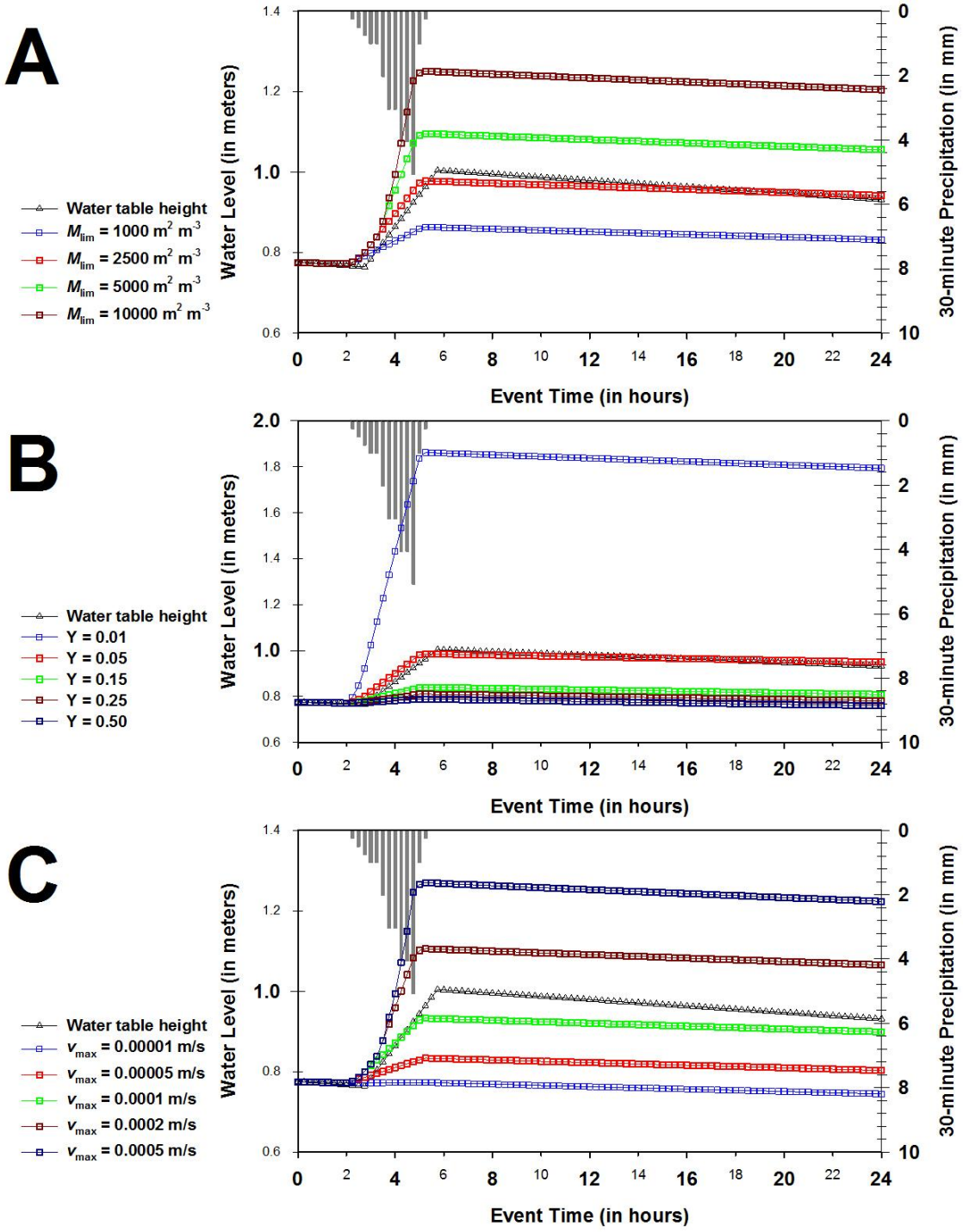

Fig. 4.5: Modeled water table height in comparison to an ideal water table rise and rainfall event of 26.1 mm. Results of (A) varying the M_{lim} (v_{max} = 1.21 x 10^{-4} m s^{-1}; p_{dp} = 0.052), (B) varying the p_{dp} (v_{max} = 1.21 x 10^{-4} m s^{-1}; M_{lim} = 2500 m^2 m^{-3}), and (C) varying the v_{max} (M_{lim} = 2500 m^2 m^{-3}; p_{dp} = 0.052).

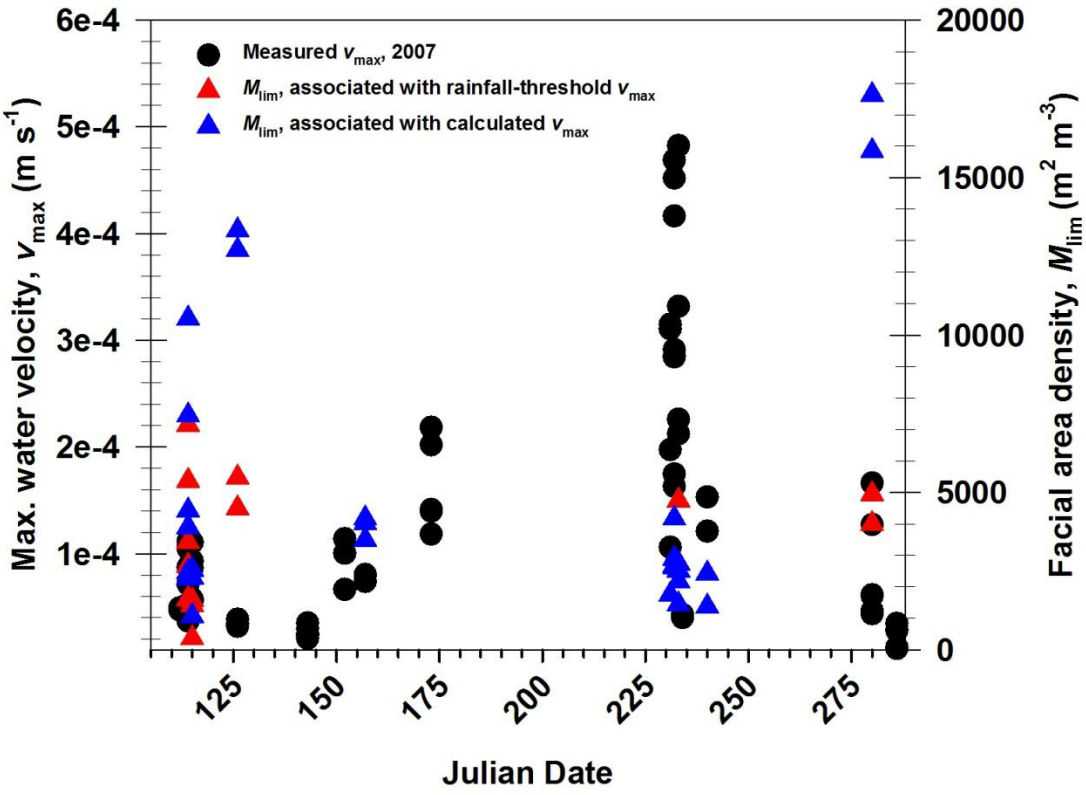

Fig. 4.6: Maximum water velocity v_{max} (circles) and facial area density Ml_{im} (triangles) for all individual observations in 2007, including both the field and buffer array piezometers, plotted against the Julian date.

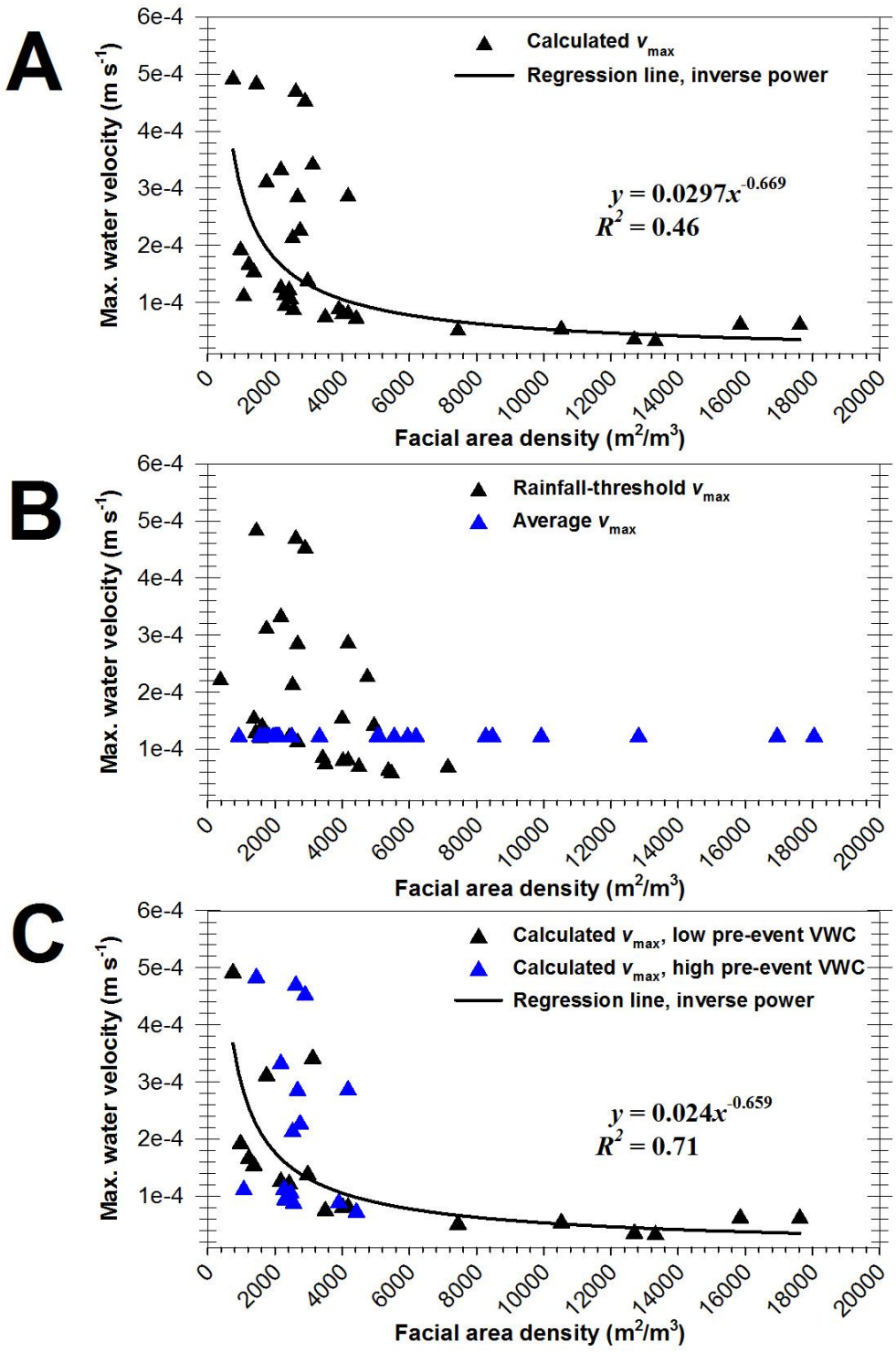

Fig. 4.7: Facial area density (M_{lim}) plotted against the (A) calculated V_{max} along with the inverse power relationship, (B) rainfall-threshold V_{max} and average V_{max}, and (C) the calculated V_{max} split into two categories (low pre-event VWC, high pre-event VWC). By splitting the calculated V_{max} into two categories, the inverse power relationship improves from an $r^2 = 0.46$ in (A) to an $r^2 = 0.71$ (C).

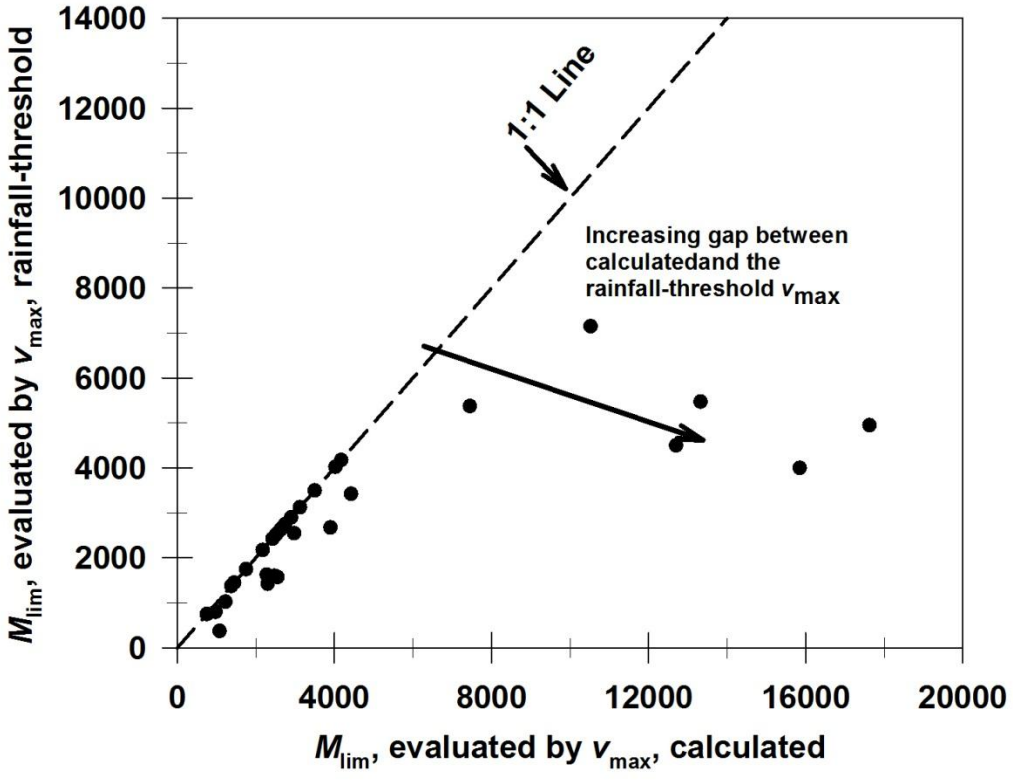

Fig. 4.8: M_{lim} results evaluated by the calculated v_{max} and the rainfall-threshold v_{max} plotted against each other. The increasing gap at higher M_{lim} is due to the larger M_{lim} necessary to accommodate water flux by the slower, calculated v_{max}.

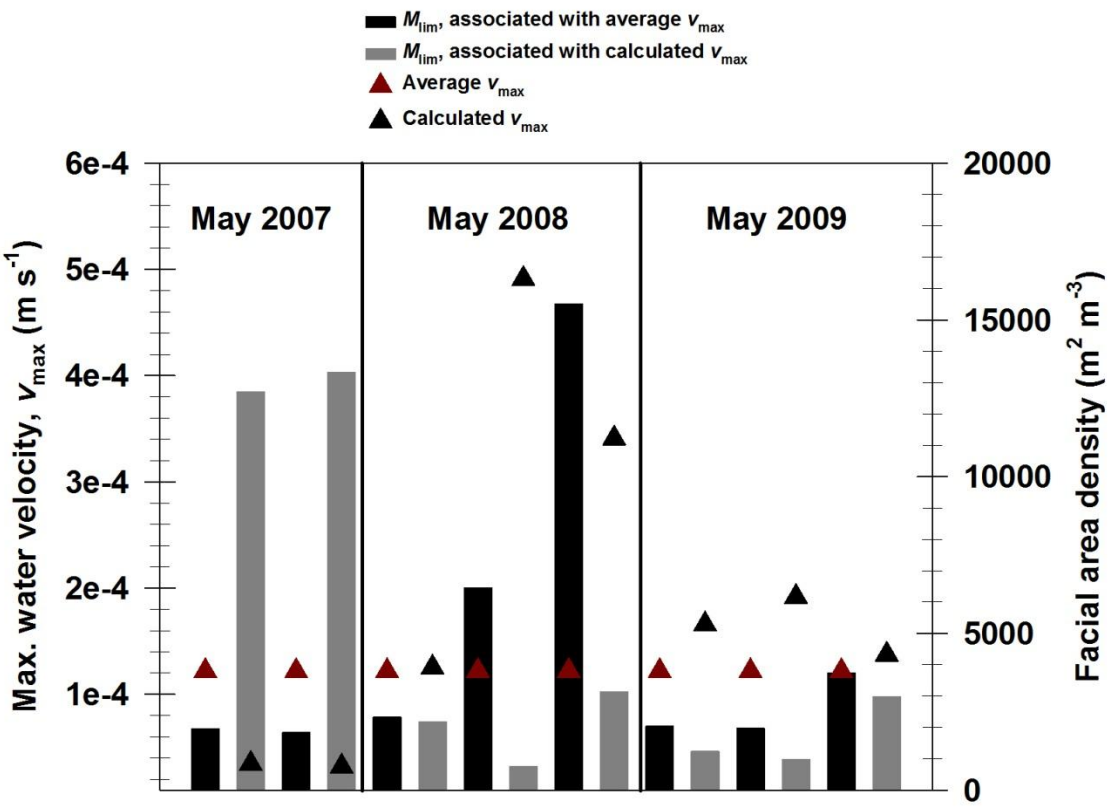

Fig. 4.9: Maximum water velocity, v_{max}, (m s^{-1}) and facial area density, M_{lim}, (m^2 m^{-3}) for events with similar dates for May 2007-2009.

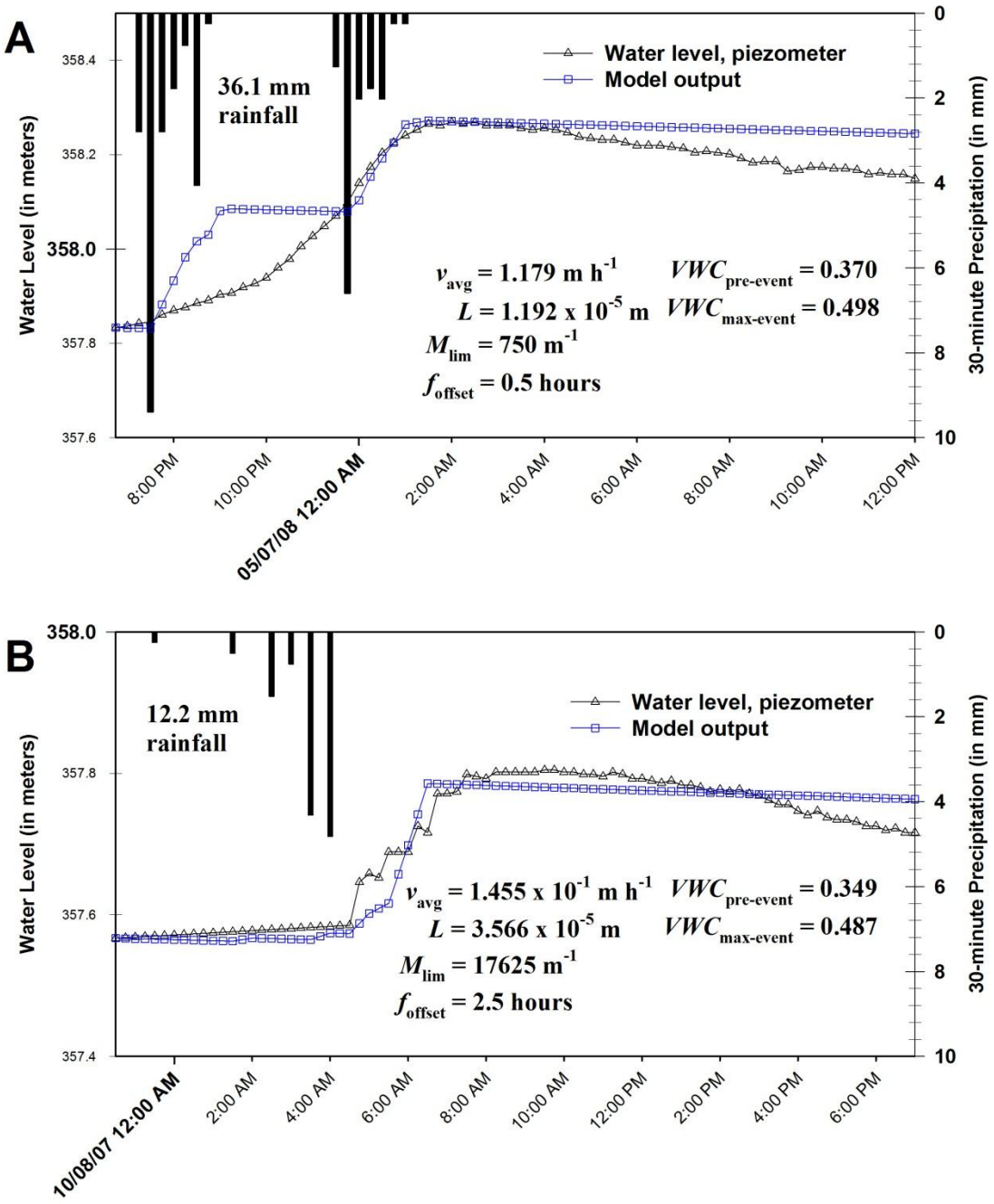

Fig. 4.10A-B: Two different rainfall events, illustrating an example of a low M_{lim} from an early season, high intensity storm (A) and a high M_{lim} from a late season rainfall event (B).

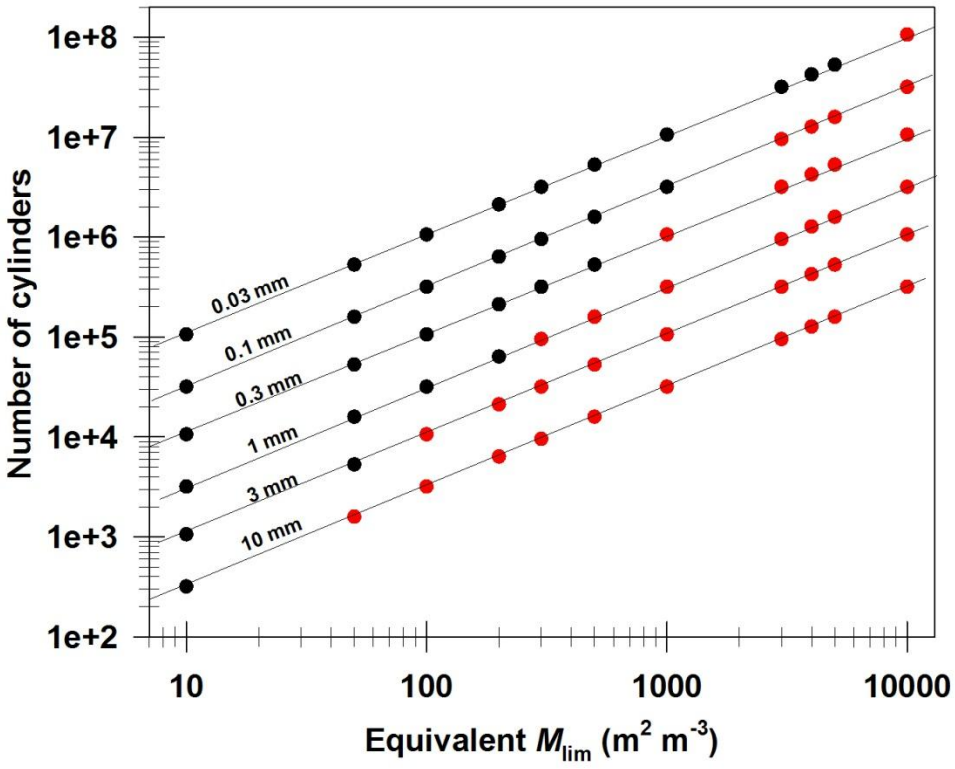

Fig. 4.11: Calculations of the number of pores of an average pore-size diameter for different M_{lim} values. Red denotes values with equivalent surface area coverage (over a unit area of 1 m^2) >5%, beyond literature values of maximum macropore densities.

Chapter 5: Predictive effects of variable drain spacing on subsurface drainage

Abstract

The extent of preferential flow was studied utilizing the specific conductance (SC) end-member mixing analysis (EMMA) and source-responsive models for two separate events at a 38.8 hectare field site, close to the headwaters of the South Fork of the Iowa River (north-central Iowa). A third model, a subsurface drain flow calculator based on the Green-Ampt and Hooghoudt equations (DRAIN-Pro), was tested for the same two events. All three models were found to effectively simulate both rainfall events. EMMA described the preferential flow by dividing the subsurface drain outflow into water sourced from fast (i.e., preferential flow) and slow (i.e., matrix flow) flow sources. The source-responsive model described the size of the preferential flow space necessary to accommodate preferential flow. DRAIN-Pro accounted for preferential flow by estimating both the effective vertical and horizontal hydraulic conductivities. DRAIN-Pro was found to be better suited for the larger of the two rainfall events with already saturated antecedent moisture conditions, whereas EMMA worked better for the small and short-duration rainfall event and the source-responsive model worked equally well for both rainfall events. With the usage of DRAIN-Pro, the effect of lateral drain spacing distance (10 to 100 m) between adjacent subsurface drains was assessed. The hypothetical drain spacing scenarios found little difference between the expected drainage efficiency (percentage of total subsurface drain outflow to cumulative precipitation) of any of the K_v and K_h combinations when the drain spacing distance was >60 m. At and below 20 m between adjacent drain spacings, the drainage efficiency

quickly increased with a transitional zone between >20 and 60 m. Finally, a preferential flow contributing area between 2.7 to 4.8 m wide was calculated from four preferential flow events. This preferential flow contributing area helped contextualize the hypothetical drain spacing scenarios by illustrating that nearly 40% of the subsurface drain contributing area would be connected by preferential flow pathways at a lateral drain spacing of 40 feet (12 m).

1. Introduction

Preferential flow is water movement that is relatively fast, non-equilibrium water movement through the unsaturated zone. The water moves through a subset of the total pore spaces in the soil matrix. Accurate prediction of preferential flow is hampered by dynamic shifts in antecedent moisture conditions, rainfall intensity, evapotranspiration, soil characteristics, biological activity, and tillage management, all of which influence preferential flow. Preferential flowpaths can dramatically influence the residence time of water in the soil. Therefore, its inclusion into hydrologic models is critical to their success (Šimůnek et al., 2003). This is particularly important for agricultural fields with subsurface drainage close to the land surface, as the preferential flowpaths quickly move water to the water table and can enhance agrichemical export to nearby streams via the subsurface drain (Kladivko et al., 1999).

The two components of unsaturated zone water flow, preferential and matrix flow, are exceedingly difficult to differentiate. However, several approaches do exist to discriminate these two types of flows. For example, approaches such as hydrograph separation (e.g. Stone and Wilson, 2006; Schilling and Helmers, 2008), laboratory investigations (e.g. Wildenschild et al., 1994; Allaire-Leung et al., 2000), field dye-

tracing studies (e.g. Richard and Steenhuis, 1988; Cey and Rudolph, 2009), or modeling analysis (e.g. Germann and Beven, 1985; Jarvis et al., 1991; Van Genuchten and Šimůnek, 2004) have been used to distinguish preferential flow from matrix flow in space and time.

One approach to studying preferential flow dynamics is end-member mixing analysis (EMMA). EMMA uses conservative tracers in a mixing model to differentiate between two or more distinct water sources. One such tracer is specific conductance, which exploits the characteristic specific conductance (SC) values for distinct flowpaths to differentiate fast flow sources from slow flow sources (Chapter 2; Schilling and Helmers, 2008; Kobayashi, 1986). SC works as a simple tracer because the ionic content of the water changes based on the contact time and degree of interaction with the soil (Pilgrim et al., 1979). An advantage of SC is the capability to record continuous measurements at several locations without the need for continuous sampling and expensive laboratory analysis. Given characteristic SC values of different flowpaths or water sources (i.e., overland flow, rainfall, unsaturated zone soil water, groundwater), EMMA of subsurface drainage during and after a rainfall event can be used to decipher the percentage of preferential flow.

Another approach to studying preferential flow dynamics is the source-responsive model (Nimmo, 2010; Ebel and Nimmo, 2009), which requires only a few parameters to predict preferential flow dynamics. Unlike a dual permeability strategy, such as MACRO (Larsbo and Jarvis, 2007) and RZWQM (Ahuja et al., 1993) where preferential and matrix flow are discretized into separate, but exchangeable domains, the source-responsive model is envisioned as a single, continuum approach of source-responsive

flow (i.e., preferential flow) and diffuse flow (i.e., matrix flow). The product of the source-responsive model is an estimate of the amount of preferential flow pathways (surface area per unit volume) participating in preferential flow. This estimate is known as the facial area density (M_{lim}) (Nimmo, 2010).

Preferential flow dynamics can also be partially discerned by applying a one-dimensional, non-steady state unsaturated zone model based on the Green-Ampt and Hooghoudt equations. Contrasting differences in drain flow as a function of precipitation, soil type, slope, soil water content and drain system design can help differentiate the amount of preferential flow necessary to explain drain flow differences and water table height fluctuations over time. This approach has been incorporated into previous models, such as the Water Erosion Prediction Project (WEPP) model (Flanagan et al., 1995). This type of model provides a prediction of subsurface drain outflow and the water table height at the apex between two parallel drains which can be compared to the water table height from field piezometers.

This chapter utilized these three (EMMA, source-responsive, and Green-Ampt/Hoodhoudt) approaches to describe two example rainfall events that led to both water table rises and increased subsurface drainage. The quick movement of water in the unsaturated zone during both events was attributed to preferential flow. Each approach brought a unique perspective on characterizing preferential flow that in isolation would yield an incomplete picture of the underlying preferential flow dynamics (Chapters 2-4). Furthermore, the Green-Ampt/Hooghoudt (DRAIN-Pro) approach was utilized to consider the influence of drain spacing on drainage efficiency (percentage of drain flow to cumulative precipitation) within the first 48 hours after a rainfall event by applying

expected hydraulic conductivity ranges from the study site. These results identified a critical zone (>60 m) beyond which drain spacing distance did not have a significant impact on the amount of subsurface drainage. For the zone of drain spacing distances <40 m (increased drainage efficiencies), a second zone identified as the preferential flow contribution area to the subsurface drain was identified. This preferential flow contribution area helped contextualize the importance of drain spacing extent to the expected preferential flow after a rainfall.

2. Site Description

Detailed site descriptions for the 38.8 hectare study field (Fig. 5.1), located in Hamilton County, Iowa in the upper South Fork of the Iowa River sub-watershed, have been documented in other reports including McCarthy et al. (2011), Chapter 2, and Chapter 3. As a brief summary, the field site is highlighted by two active subsurface drains, both estimated in location and extent on Fig. 5.1. The primary subsurface drain in this study is located approximately 150 m SE of a USGS stream gage. Land use is row-cropped agriculture (corn or soybeans) and a grassy buffer strip (25 m wide, separating the field from the South Fork of the Iowa River). The study site is underlain by silty loam and clay loam soils of the Clarion-Nicollet-Webster soil catena (Dideriksen, 1986), noted for its flat to gentle slope (0 to 3 percent) and poor drainage. Soil cores from the field site confirmed the typical soil profile is 1.8 to 2 m in depth, underlain by an effective confining layer made up of glacial deposits of the Des Moines Lobe (Bettis et al., 1996). Water transport is primarily limited to the upper soil layer due to both the effectiveness of the Des Moines lobe deposits as a confining layer and the active subsurface drainage which is about 1 meter deep.

3. Methods

3.1 Rain events

Two rainfall events centered on May 6, 2007 and May 29, 2008 had 15-minute resolution specific conductivity (SC) and temperature measurements at the primary subsurface drain outlet (Fig. 5.1). Subsurface drainage discharge (Q_{DF}, $m^3\ s^{-1}$) was calculated at the same location by an area velocity module (Teledyne ISCO 2150. Rainfall amounts were measured with a 20.3-cm diameter tipping bucket rain gage (Texas Electronics TE525WS), located adjacent to the nearby USGS stream gage.

Before, during, and after the two rainfall events, 15-minute continuous water level and temperature data was collected from a 2.54-cm diameter piezometer. The polyvinyl chloride-constructed piezometer, installed by a direct push machine (Geoprobe™ Model 540MT), was bottom screened between 0.9-1.2 m below land surface. The piezometer was located 15.2 m away from the subsurface drain. The measured water level in this piezometer approximates the expected water table height apex.

3.2 Model analysis

Briefly from Chapter 2, EMMA for these two events was divided into two flow components, fast flow (Q_{FF}) and slow flow (Q_{SF}), regarded as the two primary inputs into the subsurface drain (Q_{DF}). Fast flow (Q_{FF}) sources lump together water from both ponded water runoff (via vertical inlets into the subsurface drain) and preferential flow. Slow flow (Q_{SF}) sources lump together soil matrix flow and groundwater inputs. The SC end-members for the hydrograph separation, SC_{FF} (fast flow) and SC_{SF} (slow flow), were based on the mean values of precipitation and groundwater, with mean values of 12

μS/cm and 863 μS/cm, respectively (Chapter 2). Another input parameter, the event onset SC (SC_{EO}), was the mean SC value over a two-hour period prior to the first recorded precipitation of any given rainfall event. In the case of the two events being modeled, the SC_{EO} was substituted for the SC_{SF}, assuming that all the subsurface drain flow was derived from slow flow sources prior to the rainfall event. This substitution will allow for more accurate determinations of the percentage of preferential flow during the duration of the event. The length of the events was measured from the first rainfall until the SC value returned to 90% of the SC_{EO}.

As shown in Chapters 3 and 4, the observed water table fluctuations after rainfall events can be described by the source-responsive model as water that quickly flows through the unsaturated zone along preferential flow pathways (Nimmo, 2010; Chapter 4). Water table fluctuations within the source-responsive model are due to two competing mechanisms: recession and accretion. Recession and accretion are the first and second terms, respectively, in the following equation

$$\frac{dH}{dt} = -\frac{H}{\tau} + \frac{q_{S_{\mathrm{lim}}} f}{p_{\mathrm{dp}}} \qquad [1]$$

where H is the rise above the water table height before the event and τ is the proportionality constant which encompasses the linear rate of recession, in hours. The water flux, q_{Slim}, is the maximum rate of recharge that can be accommodated for any particular event, analogous to the infiltration capacity. The water flux can only move through available pore space, so the water flux is divided by the medium's drainable porosity ratio, p_{dp}. Flow does not occur in all available source-responsive domain space for every event, so a dimensionless factor f (active area fraction) modulates q_{Slim} to adjust

for variable source-responsive flow. In order to solve for *H* incrementally over the course of a storm event, the solution is

$$H_{i+1} = H_i \exp\left(\frac{t_i - t_{i+1}}{\tau}\right) + \frac{q_{s_{lim}} f_{i+1} - f_{offset}}{p_{dp}} \tau \left[1 - \exp\left(\frac{t_i - t_{i+1}}{\tau}\right)\right] \quad [2]$$

where H_i is a starting level. The *f* offset parameter (f_{offset}) has been added to account for the observation of delayed timing of first water arrival to the water table.

Finally, the water table fluctuations can be predicted based on theoretical or empirical relations and the physical characteristics of the system including the soil fractional composition (i.e., sand, silt, clay, organic content), soil moisture content slope, and drain system design. DRAIN-Pro is a subsurface drain flow calculator that employs the modified Green-Ampt equation for soil infiltration (Mein and Larson, 1973) and the Hooghoudt's equation (Skaggs, 1978) for subsurface flow to artificial drain tubes (Jason Roth, pers. comm., 23 Oct 2011). The Green-Ampt equation was modified to set the infiltration rate equal to the rainfall rate when the calculated infiltration rate is greater than the rainfall rate (Mein and Larson, 1973) and to account for an unsteady hyetograph (Chu, 1978). Algorithms for application of the Green-Ampt model were derived from the WEPP model (Alberts et al, 1995) and Wilson (2009). Subsurface drainage equations within DRAIN-Pro are the same as in WEPP (Savabi et al., 1995), which are based on DRAINMOD (Skaggs, 1978). The soil properties, including the effective porosity, total porosity, residual water content, field capacity, soil pore size distribution, and the bubbling pressure, were based on relations of soil moisture content and soil fractional composition (i.e., sand, silt, clay, organic content) following the WEPP manual (Alberts et al., 1995) and Wilson (2009).

3.3 Calculation of contributing area to subsurface drainage

Total subsurface drain outflow was calculated after four separate rainfall events in 2008 (Aug. 27, Sept. 8, Oct. 14-15, and Oct. 24) to calculate the contributing surface area surrounding the subsurface drain necessary to explain increased water flux shortly after the rainfall onset. The four events all occurred during a period of relatively dry conditions, so later in the year than the two example rainfall events. Two late summer events occurred on Aug. 27 and Sept. 8 with 7.62 and 9.91 cm of cumulative rainfall, respectively. The other two events occurred shortly before harvest, on Oct. 14-15 and Oct. 28 with 21.08 and 3.56 of cumulative rainfall, respectively. Due to the small size of these rainfall events onto relatively dry soils, none of these events had any overland flow so all of the increase in subsurface drain discharge was due to the rain water moving through fast flowpaths (i.e., preferential flow). Each event had an appreciable amount of rainfall, and no rainfall in the previous 24 hours. The drain outflow returned to the same outflow as prior to the event so that the storm flow could easily be tabulated. To calculate the contributing surface area, the total storm flow (in m^3 for the storm length) was divided by the equivalent water depth for the incoming rainfall. To convert from contributing area to an average width of contributing area, the subsurface drain length was set to 600 m (length of subsurface drain calculated from GIS coverage).

3.4 Effect of drain spacing on extent and timing of drain flow

DRAIN-Pro was utilized to simulate water table and subsurface drain outflow for six different subsurface drain spacings: 10 m, 20 m, 40 m, 60 m, 80 m, and 100 m across the potential range of vertical (K_v) and horizontal (K_h) effective hydraulic conductivities (0.5 cm/hr, 1 cm/hr, 5 cm/hr, 15 cm/hr, 25 cm/hr, and 100 cm/hr) from the field site. This

spectrum of hydraulic conductivities and drain spacing predicted the effects on the subsurface drain outflow (magnitude and timing). Subsurface drainage efficiency (subsurface drain outflow as a percent of total precipitation) was used to compare the various scenarios. Every unique combination of K_v and K_h were modeled for all six drain spacing distances.

A simulated rain storm was generated from the early portion of the rain storm on May 29, 2008 (generated rain event = 5.54 cm) to initiate subsurface drainage. The lower boundary for the model was assigned as 1.8 m, the average depth of the confining layer of the Des Moines Lobe glacial deposits at this location. The Canisteo silty clay loam, the most common soil type at the field site, was used in the model for the soil properties of sand content (40.85%), clay content (27.43%), percentage of organic matter (2.22%), and the cation exchange (19.1 meq/100g). These soil properties were used to automatically calculate parameters such as the effective porosity, total porosity, residual water content, and field capacity. The simulated subsurface drain was based on the field site (1% slope, 21-cm inner diameter, 1 m depth, and an estimated Manning's roughness of 0.015 $s/m^{1/3}$). Each scenario was initiated with a starting water table height of 1 m and an initial water content of 26.55% (calculated field capacity for the Canisteo soil) in order to minimize the contribution of water from the pre-event soil profile to the subsurface drain outflow.

4. Results

4.1 Results of the three modeling approaches

Table 5.1 highlights the critical environmental observations for both rainfall events. Total cumulative precipitation was considerably different for the two events (26 mm vs.

Table 5.1: Environmental observations and results of the three modeling approaches for the two example rainfall events.

	May 6, 2008	May 29, 2008
Environmental Observations		
Total cumulative precipitation (mm)	26	77
Time to maximum water table (min)	1125	1575
Initial volumetric water content (percent)	25.5	26.7
Change in water table at maximum fluctuation (mm)	171	570
Ratio of total precip. to water table height diff. (percent)	15.2	13.5
Time to initial change in specific conductance (SC) (min)	390	75
Time to first minimum SC (min)	480	75
Change in SC at minimum SC (uS/cm)	98	410, 618, 614[1]
Change in drain discharge at minimum SC (L/sec)	5	0, 0, 0[1]
EMMA Model		
Percent due to fast flow at minimum SC	41	67, 100, 100[1]
Percent due to fast flow for whole event	15	28
Source-Responsive Model		
v_{max} (cm/hr)	7.7	22
Facial are density (m^2/m^3)	13325	2425
L (cm)	$3x10^{-4}$	$5x10^{-4}$
f-offset (minutes)	255	180
Drain-Pro		
Calculated K_v (cm/hr) at initial water content of 27%	11	8
Calculated K_h (cm/hr) at initial water content of 27%	30	144
Calculated K_v (cm/hr) at initial water content of 30%	1	0.5
Calculated K_h (cm/hr) at initial water content of 30%	0.5	402

[1] Three different SC maxima occurred during the course of the rainfall event.

77 mm), whereas initial soil moisture content (in terms of volumetric water content) was similar (25.5% vs. 26.7%). The timing of the SC minimum was faster for the May 29 event at only 75 minutes as opposed to 390 minutes for the May 7 event. The SC minimum was also larger, with three separate minima for the May 29 event. The two events were similar in the ratio of total cumulative precipitation to the maximum water table height difference at 15.2% and 13.5% for the May 7 and May 29 events, respectively. Also, the time from the beginning of the event to the maximum water table was also high for both events at 1125 (18 h, 15 min) and 1575 minutes (26 h, 15 min) for the May 7 and May 29 events, respectively.

The two rainfall events were separated into fast flow and slow flow utilizing the EMMA model (Fig. 5.2A-B). The percentage of fast flow was differentiated from the slow flow through the application of the characteristic SC values for using rainfall for fast flow and the pre-event drain flow as slow flow (Table 1). The peak Q_{FF} of 41% for the May 7 event was smaller than the three peaks in Q_{FF} (67%, 100%, 100%) for the May 29 event. Both events exhibited a similar and sustained increase in overall Q_{DF}. However, due to the more sustained Q_{FF} during the May 29 event, the overall Q_{FF} for the entire event was larger at 28% as opposed to 15% for the May 7 which tailed off quickly.

The source-responsive model yielded information on the transport velocities (v_{max}), the facial area density of the preferential flow space (M_{lim}) and the offset time for the two rain events (Table 5.1). Based on independently calculated transport velocities (v_{max}) from Chapter 3, the v_{avg} and L were calculated based on their relationship to v_{max} through laminar flow principles (Nimmo, 2010). The drainable porosity (p_{dp}) and the proportionality constant (τ,) were set to 0.052 (5.2%) and 504 hours, respectively. With the fixed parameters of v_{avg}, L, p_{dp}, and τ, the M_{lim} and f_{offset} were calculated for the two events. The best-fit results are shown in Fig. 5.3A and 5.3B which were determined by an adaptation of the Nash-Sutcliffe model efficiency coefficient (Nash and Sutcliffe, 1970).

For the event that occurred on May 7, 2007, the v_{max} and L were 7.699 x 10^{-2} m/hr (7.7 cm/hr) and 2.919 x 10^{-6} m (2.919 μm). The facial area density (M_{lim}) was 2425 m^{-1}. The Nash-Sutcliffe model efficiency coefficient was 0.98 for the water level rise, with the model matching within 0.01 m both the initiation and maximum water table rise measured in the piezometer. Also, with an f_{offset} of 4.25 h, the timing of the modeled water level rise matched the piezometer data.

For the event that occurred on May 29, 2008, the v_{max} and L were 2.200 x 10^{-1} m/hr (22 cm/hr) and 4.866 x 10^{-6} m (4.866 μm). The facial area density (M_{lim}) was 13325 m^{-1}. The Nash-Sutcliffe model efficiency coefficient was 0.90 for the water level rise, with the model matching within 0.01 m both the initiation and maximum water table rise measured in the piezometer. With an f_{offset} of 3.00 h, the timing of the modeled water level rise matched the piezometer data; however, the water level rise did not match as well as the May 7, 2007 event mainly due to the more complicated rainfall pattern.

The water table height was accurately predicted for both events utilizing the DRAIN-Pro model. Various combinations of vertical and horizontal hydraulic conductivities were attempted until the best-fit Nash-Sutcliffe for the entire time interval was >0.85 for initial water contents ranging from 27% to 30%. For both events, the required K_v and K_h to attain the same water level rise decreased with increasing initial water content with the exception of K_h for the May 2008 event.

For the event on May 7, 2007 (Fig. 5.4A), starting at an initial water content of 27%, the required K_v was 11 cm/hr and K_h of 30 cm/hr up to 30% with a K_v of 1cm/hr and K_h of 0.5 cm/hr. The range in the Nash-Sutcliffe model efficiency coefficient was 0.85 to 0.88. Although the final water table height was predicted accurately, the initiation of the water table rise was too early and did not capture the steepness of the rise. In the case of this event, the source-responsive model did a better job of accurately predicting the water table rise.

For the event on May 29, 2007 (Fig. 5.4B), starting at an initial water content of 27%, the required K_v was 8 cm/hr up to 30% with a K_v of 0.5 cm. However, in the case of K_h, a much larger and increasing range of K_h (144 cm/hr to 402 cm/hr) was necessary to

accurately predict the water table rise when increasing the initial water content from 27% to 30%. The range in the Nash-Sutcliffe model efficiency coefficient was 0.93 to 0.98. In this case, the water table height rise initiation, water table height slope, and final water table height were better predicted with DRAIN-Pro than either the other rainfall event or the source-responsive model's prediction for this event.

4.2 Area contributing to subsurface drain

Four rainfall events between August and October 2008 were utilized to calculate the area above the subsurface drain directly contributing to preferential flow (Fig. 5.5A-D). For each of the four rainfall events, the contributing area was calculated by dividing the total drain storm flow volume by the rainfall volume, and then subsequently dividing by the calculated length of the subsurface drain to yield the average width of the contributing area. Each of the four events started with very small sustained baseflow on the order of 3.7×10^{-5} m^3/s and returned to the same baseflow after brief storm peaks. This calculation resulted in a range of preferential flow contribution areas between 2.7 to 4.8 m wide. All four of these events were too small to initiate any overland runoff. Although limited to only four events across a period of two months, these results suggest a strong preferential flow connection directly to the subsurface drain given that the drain outflow hydrograph peaks within hours after the rainfall event for even these small rainfall events.

4.3 Effect of drain spacing on extent and timing of drain flow

The variable drain spacing and soil hydraulic conductivity scenarios indicated increased drainage intensity (drainage efficiency) in the first 24 hours with narrower spacing between parallel subsurface drains (Fig. 5.6A-F) for all of the different combinations of vertical (K_v) and horizontal hydraulic conductivity (K_h). The magnitude

of the hydraulic conductivities did affect the magnitude of the drainage efficiency. The results are plotted by individual K_h, such that all the different K_v scenarios for that K_h are shown for all six distances (Fig. 5.6A-F).

There is minimal difference between the predicated drainage efficiency for any of K_v and K_h when the drain spacing distance is >60 m (with the exception of a K_h of 100 cm/hr (Fig. 5.6F)). The maximum drainage efficiency is <15% (Fig. 5.6A-E) for spacing distances >60 m (Fig. 5.6A-E). At distances >60 m, the majority of water from a single rainfall event will not drain find its way to the subsurface drain in the first 24 hours (assuming field capacity and an initial water table at the same height as the subsurface drain). This result is also apparent in Fig. 5.7, where the K_v is plotted against the drainage efficiency, with each line indicating a different K_h and each graph showing a different spacing.

At drain spacing distances of 10 m and 20 m, strong differences in the drainage efficiency exist for the various combinations of K_v and K_h (Fig. 5.6). For example, the range in drainage efficiency goes from 6.7% (K_v = 0.5 cm/hr) to 87.5% (K_v = 100 cm/hr) with a K_h of 100 cm/hr and 10 m drain spacing. The greatest increase in drainage efficiency for all K_h scenarios occurs up to K_v values of ~30 cm/hr. This illustrates the increased importance of K_h over K_v, which is logical given the distance water must travel is generally much greater in the horizontal direction than in the vertical direction for fields with shallow water tables.

Along with the increased drainage efficiency in the first 24 hours, the expected time to peak flow is faster for narrower drain spacing. Fig. 5.8 illustrates the time to peak flow for all scenarios that reached peak flow in less than 48 hours. These results illustrate the

short time in which high peak flow can occur for drain spacing <40 m. As with the results for drainage efficiency, the higher the K_v and K_h values, the faster the time to peak flow especially when both values are at least 15 cm/hr. There is an important difference between the drain spacing distances, <40 m and >40 m.

5. Discussion

5.1 Similarity and differences of the three different models

In this study, three different models were used to model two different rainfall events with a high preferential flow component. All three models were utilized as a proof of preferential flow at the field site. The smaller of the two rainfall events (May 2007) was found to have a single, high preferential flow pulse, well characterized by both the EMMA and the source-responsive models. This smaller rainfall event was not as well characterized by the DRAIN-Pro model. This model missed the steep and fast water table rise, but successfully predicted the maximum water table height. The larger rainfall event (May 2008) was best characterized by the DRAIN-Pro model. The source-responsive model also performed well for this event, but the EMMA underpredicted some of the later preferential flow.

Estimates of preferential flow were independently obtained from the EMMA, the source-responsive model, and DRAIN-Pro for two rainfall events from the study site (Table 1). The EMMA described the preferential flow by dividing the subsurface drain outflow into water sourced from fast (i.e., preferential flow) and slow (i.e., matrix flow) sources. This approach not only calculated the maximum preferential flow percentage, but the overall flow attributed to preferential flow during an event. In the case of the source-responsive model, the facial area density (M_{lim}) provided an estimate of the

amount of source-responsive domain participating in the event. The delay of preferential flow to the subsurface drain is also described through the source-responsive model with the f_{offset} parameter. DRAIN-Pro indirectly ascribed preferential flow through the estimated saturated effective hydraulic conductivities which were larger than the expected values for the soils at the study site (maximum effective maximum hydraulic conductivity for the soils is 3.6 cm/hr, Dideriksen, 1986).

For the EMMA approach, the two events illustrated very different preferential flow dynamics. As the first event was a small event without any likelihood of, surface inflows into vertical inlets were thereby eliminated as a viable pathway leaving preferential flow as the only alternative. The EMMA also ascribed fast flow as the mechanism for the large spikes in the early stages of the second event. However, unlike the first rainfall event with a clear preferential flow flux, the second event is more pulsed for the fast flow component (i.e., preferential flow). Many of the increases in fast flow do correspond with or occur shortly after the rainfall bursts; however, the size of the fast flow flux did not increase (as otherwise indicated by lower SC water) with the large and sustained increase in overall subsurface drainage. This makes interpretation of the fast flow as only preferential flow more difficult. In the early stages of an event, EMMA can clearly calculate the percentage of preferential flow but this technique becomes weaker over time because of the chemical interactions with the surrounding soil matrix.

For the source-responsive model, starting with the larger second event, the M_{lim} of 2425 m^{-1} seems reasonable to suggest preferential flow based on the discussion of Chapter 4. The match between the simulation results and the measured data was very high with a Nash-Sutcliffe coefficient of 0.98. However, the first event had an applied

M_{lim} of 13325 m^{-1}. As highlighted in Chapter 4, it was suggested that M_{lim} might not only be an indicator of preferential flow space, as implied by the source-responsive domain M_{lim} describes, but as a continuum of preferential and matrix flow. In this case, it would be unreasonable to assume the large M_{lim} is suggesting a very large preferential flow space, at least as defined in contemporary terms. The average pore diameter size would need to be much smaller, to sizes suggested as the lower limit of 30 μm for macropores under the classification schemes of McIntyre (1974) and Marshall (1959). This does not suggest that preferential flow is not possible, but natural velocity limits set by very small pore sizes with tortuous flowpaths cannot be ignored.

For DRAIN-Pro, both simulations were able to predict the maximum water table height. However, only the second simulation was able to follow the water table rise closely, both in its timing and slope. The first event only seems to average the response and does not seem to capture the fast water level rise which starts after 8:00 AM. As the fast flow flux increases at this time for the EMMA results, this is preferential flow that is not adequately captured with DRAIN-Pro as it does not have an explicit preferential flow domain. The second event (May 29) has a high correlation between the simulation and measured results. Soil moisture conditions were extremely wet at this time, so the large flux of rainfall into the Green-Ampt module of DRAIN-Pro makes it ideal for such an event. As is it well known that the hydraulic conductivity can range over several orders of magnitude with increasing moisture content, especially for soils with high clay content, the large horizontal hydraulic conductivity (K_h) to simulate the conditions would be expected (Chow et al., 1988).

Overall, the goal of using all three models to characterize the nature of preferential flow for the two different rainfall events was met. Each approach brings a unique perspective of preferential flow that, when combined, can elucidate a more complete picture of the underlying preferential flow dynamics. The smaller rainfall event (May 7) seemed to be characterized by a single, preferential flow pulse as characterized by both the SC EMMA and source-responsive model. In the case of the source-responsive model, the required lower limits of pore size in the source-responsive domain are small but still conceivable by some classification schemes. DRAIN-Pro seemed unable to capture the fast water level rise for the smaller rainfall event, but worked extremely well under wet antecedent moisture conditions with the larger rainfall event.

5.2 Drainage expectations given calculated contributing area

The contributing area calculated from the four preferential flow events in 2008 was a zone between 2.7 to 4.8 m wide. This is a conservative estimate, as this assumes that all rainfall reaches the subsurface drain during the subsurface drain flux increase and ignoring other losses such as evapotranspiration. The importance of drain spacing is highlighted by considering the larger contributing area of 4.8 m in the context drain spacing scenarios. For example, if the drain spacing is 20 m and the contributing area is 4.8 m, nearly 25% of the water falling on the field area would be drained in a very short time via preferential flow pathways to the water table and removal through the drain. For common drain spacing of 40 feet (12 m) nearly 40% of the field area would be connected to the subsurface drain via preferential flow pathways.

In the context of agrochemical transport for a subsurface tile-drained landscape, it is clear that preferential flowpaths can have a dominant influence on water transport in the

24 to 48 hours after a rainfall event. Maximum peak flow occurs in <24 hours and drainage efficiencies >40% for combinations of K_h and K_v with values greater than 15 cm/hr for the 10 and 20 m drain spacings (Fig. 5.8). In turn, chemicals such as fertilizer and pesticides that are carried by the water will have little opportunity for either utilization or natural attenuation.

Overall, management decisions must weigh two opposing concerns in relation to the distances between subsurface drains. On the one hand, closer lateral spacing allows for more efficient drainage of the field after a large rainfall event. However, wider drain spacing distances limit the area contributing to drain flow immediately after the rainfall event and retains more soil moisture for crop use in the unsaturated zone. Based on the hypothetical spacing scenarios, the transitional zone between 20 to 60 m will at least offer more enhanced drainage while limiting the overall percentage of preferential flow.

5.3 Drainage expectations given drain spacing

Two conditions were captured with the hypothetical drain spacing scenarios: (1) changes in velocity due to the natural conditions, such as shifts in K_h and K_v; (2) drain water management, in terms of the lateral spacing of subsurface drains. The hypothetical drain spacing scenarios found little difference between the expected drainage efficiency of any of the range of K_v and K_h values when the distance was >60 m. For distances of drain spacing <20 m, the drainage efficiency quickly increased for most combinations of K_v and K_h with a transitional zone between >20 and 60 m.

If the rapid increase in subsurface drainage occurs <20 m, than lateral spacing beyond this threshold will lower the immediate response of drainage networks. However, at high K_h and/or K_v values ≥100 cm/hr, lateral spacing up to 60 m was shown to

potentially have high drainage efficiencies (Fig. 5.6F, Fig. 5.7) and short times to peak flow.

In terms of generating larger drain fluxes, the magnitude of K_h was more important. This is due to the distance that must be traveled by the water. The vertical distance to the water table is much shorter (~1 m) as opposed to the horizontal distance (half of the distance of the drain spacing).

As these silt clay loam have a high potential for preferential flow pathways, especially in close proximity to the subsurface drains based on the calculated contributing area, the application of high effective hydraulic conductivities up to 100 cm/hr was reasonable. This is especially apparent in the early spring season with wet antecedent moisture conditions and after periods of high precipitation (March-early June 2008, Chapters 2-3). One of the primary conclusions of Chapter 2, utilizing specific conductance to track fast/preferential flow, was that more preferential flow occurs in the spring with less preferential flow observed later in the year (late summer to fall) except for after large storms. Chapter 3, which characterized the maximum water velocities, found consistently high water velocities in the spring with a second maximum in the late summer.

During certain periods of the year, the influence of preferential flowpaths causes these soils to behave less like silty clay loam soils and more like well-sorted sand and gravel (Bear, 1972) due to several conditions, including the antecedent moisture conditions, storm rainfall intensity, evapotranspiration, crop growth, and the soil surface conditions (i.e., surface cracks, sealing). On the other hand, this behavior has limits given these are silty clay loam soils which also have a capacity for swelling between the soil

aggregate boundaries under saturated conditions. Therefore, the likelihood of preferential flowpaths along aggregate boundaries needs to be counterbalanced with the possibility of swelling soils that would limit water transport over longer distances.

6. Conclusions

Each of the three approaches (EMMA, source-responsive, DRAIN-Pro) brought a unique perspective to describe preferential flow that, when combined, elucidated a more complete picture of the underlying preferential flow dynamics. The timing, extent, and variability of preferential flow using all three approaches was limited to only two actual rainfall events in this chapter. However, variability using a single approach across the entire year was assessed in previous chapters, with EMMA in Chapter 2, maximum water velocities in Chapter 3, the source-responsive model in Chapter 4, and the DRAIN-Pro model in this chapter.

EMMA described the preferential flow by dividing the subsurface drain outflow into water sourced from fast (i.e., preferential flow) and slow (i.e., matrix flow) flow sources. This approach not only calculated the maximum preferential flow percentage, but the overall flow attributed to preferential flow during an event. The source-responsive model described the size of the preferential flow space (M_{lim}) necessary to accommodate preferential flow for any single event. The delay of preferential flow to the subsurface drain was also described through the source-responsive model with the f_{offset} parameter. DRAIN-Pro accounted for preferential flow by estimating both the effective K_v and K_h, which contains an embedded preferential flow hydraulic conductivity when the K_v and K_h are greater than hydraulic conductivities expected for matrix flow only.

Varying the lateral drain spacing distance from 10 to 100 m by applying the DRAIN-Pro model found a critical zone <20 m where drainage efficiency, as a ratio of the subsurface drain outflow to the total precipitation, markedly increased. The drain spacing distances >20 m did not have such dramatic increases, and drain spacing distances >60 m had low drainage efficiencies (Fig. 5.6, Fig. 5.7) and long periods before peak flow (Fig. 5.8). A transitional zone between 20 m to 60 m did have enhanced drainage, but often required much higher combinations of K_v and K_h.

Finally, the preferential flow contributing area calculated from four isolated rainfall events was found to be between 2.7 to 4.8 m in width. This calculated preferential flow contributing area contextualizes the hypothetical drain spacing results. Narrow drain spacing distances (<20 m) will be expected to have a high overall preferential flow component (up to 40%). Management decisions considering the lateral spacing of subsurface drains should consider wider spacing, if possible, beyond this critical 20 m zone given the enhanced agrochemical transport potential via preferential flow.

References

Ahuja, L.R., D.G. Decoursey, B.B. Barnes, and K.W. Rojas. 1993. Characteristics of macropore transport studied with the ARS Root-Zone Water-Quality Model. Trans. ASAE 36:369–380.

Allaire-Leung, S.E., S.C. Gupta, and J.F. Moncrief. 2000. Water and solute movement in soil as influenced by macropore characteristics - 1. Macropore continuity. J. Cont. Hydrol. 41(3-4): 283-301.

Bear, J. 1972. Dynamics of Fluids in Porous Media. Dover Publications.

Bettis III, E.A., D.J. Quade, and T.J. Kemmis. 1996. Hogs, Bogs, and Logs: Quaternary Deposits and Environmental Geology of the Des Moines Lobe. Geological Survey Bureau Guidebook Series No. 18. Ames, Iowa: Iowa Department of Natural Resources.

Cey, E.E. and D.L. Rudolph. 2009. Field study of macropore flow processes using tension infiltration of a dye tracer in partially saturated soils. Hydrol. Proc. 23: 1768-1779.

Chu, S.T. 1978. Infiltration during an unsteady rain. Water Res. Res. 14(3): 461-466.

Dideriksen, R.O. 1986. Soil survey of Hamilton County, Iowa. United States Department of Agriculture Soil Conservation Service, 157 p.

Ebel, B.A., and J.R. Nimmo. 2009. Estimation of unsaturated zone traveltimes for Rainier Mesa and Shoshone Mountain, Nevada Test Site, Nevada, using a source-responsive preferential-flow model. Open-File Rep. 2009-1175. USGS, Menlo Park, CA.

Flanagan, D. C., and M. A. Nearing, eds. 1995. USDA Water Erosion Prediction Project hillslope and watershed model documentation. NSERL Report No. 10. West Lafayette, Ind.: USDA-ARS National Soil Erosion Research Laboratory.

Germann, P.F. and K. Beven. 1985. Kinematic wave approximation to infiltration into soils with sorbing macropores. Water Resour. Res. 21: 990-996.

Jarvis, N., P-E. Jansson, P.E. Dik, and I. Messing. 1991. Modeling water and solute transport in macroporous soil. I. Model description and sensitivity analysis. J. Soil Sci. 42: 59-70.

Kladivko, E.J., J. Grochulska, R.F. Turco, G.E. Van Scoyoc, and J.D. Eigel. 1999. Pesticide and nitrate transport into subsurface tile drains of different spacings. J. Environ. Qual. 28(3): 997-1004.

Kobayashi, D. 1986. Separation of a snowmelt hydrograph by stream conductance. J. Hydrol. 84: 157–165.

Larsbo, M. and N. Jarvis. 2007. MACRO 5.0: A model of water flow and solute transport in macroporous soil. Technical description, Swedish University of Agricultural Sciences: 49 p.

Marshall, T.J. 1959. Relations between water and soil. Tech. commun. 50, Commonw. Agric. Bur., Farnham Royal, UK.

McCarthy, K.A., C.E. Rose, and S.J. Kalkhoff. 2011. Environmental Settings of the South Fork Iowa River basin, Iowa, and the Bogue Phalia basin, Mississippi. U.S. Geological Survey Scientific Investigations Report 12-xxxx, xx p.

McIntyre, D.S. 1974. Pore space and aeration determinations. p. 67–74. *In* J. Loveday (ed.) Methods for analysis of irrigated Soils. Commonw. Agric. Bur., Farnham Royal, UK.

Mein, R.G. and C.L. Larson. 1973. Modeling infiltration during a steady rain. Water Resour. Res. 9: 384-394.

Nash, J.E. and I.V. Sutcliffe. 1970. River flow forecasting through conceptual models Part 1 - A Discussion of principles. J. Hydrol. 10: 282-290.

Nimmo, J.R. 2010. Theory for source-responsive and free-surface film modeling of unsaturated flow. Vadose Zone Journal 9: 295–306.

Pilgrim, D.H., D.D. Huff, and T.D. Steele. 1979. Use of specific conductance and contact time relations for separating flow components in storm runoff. Water Resour. Res. 15: 329–339.

Richard, T.L. and T.S. Steenhuis. 1988. Tile drain sampling of preferential flow on a field scale. J. Contam. Hydrol. 3: 307-325.

Roth , J. 2010. The hydrology of a drained topographical depression within an agricultural field in north central Iowa. MS Thesis. Minneapolis, MN: University of Minnesota, Dept. of Civil Engineering.

Schilling, K.E. and M. Helmers. 2008. Tile drainage as karst: Conduit flow and diffuse flow in a tile-drained watershed. J. Hydrol. 349: 291–301.

Skaggs, R.W. 1978. A Water Management Model for Shallow Water Table Soils. Report No. 134. Water Resources Research Institute of the University of North Carolina.

Šimůnek, J., N.J. Jarvis, M. Th. van Genuchten, and A. Gärdenäs. 2003. Review and comparison of models for describing non-equilibrium and preferential flow and transport in the vadose zone. J. Hydrol. 272: 14-35.

Stone, W.W. and J.T. Wilson. 2006. Preferential flow estimates to an agricultural drain with implications for glyphosate transport. J. Environ. Qual. 35: 1825-1835.

Van Genuchten, M. Th. and J. Šimůnek. 2004. Integrated modeling of vadose-zone flow and transport processes. *In* R.A. Feddes, G.H. de Rooij, and J.C. van Dam (eds.) Unsaturated-zone modeling: Progress, challenges, and applications. Kluwer Academic Publishers: Dordrecht, The Netherlands.

Wildenschild, D., Jensen, K.H., Villholth, K., and Illangasekare, T.H. 1994. A laboratory analysis of the effect of macropores on solute transport. Ground Water 32(3): 381-389.

Wilson, B.N. 2009. Lecture Notes for BBE 8513: Hydrologic Modeling of Small Watersheds. St. Paul, MN: University of Minnesota, Department of Bioproducts and Biosystems Engineering.

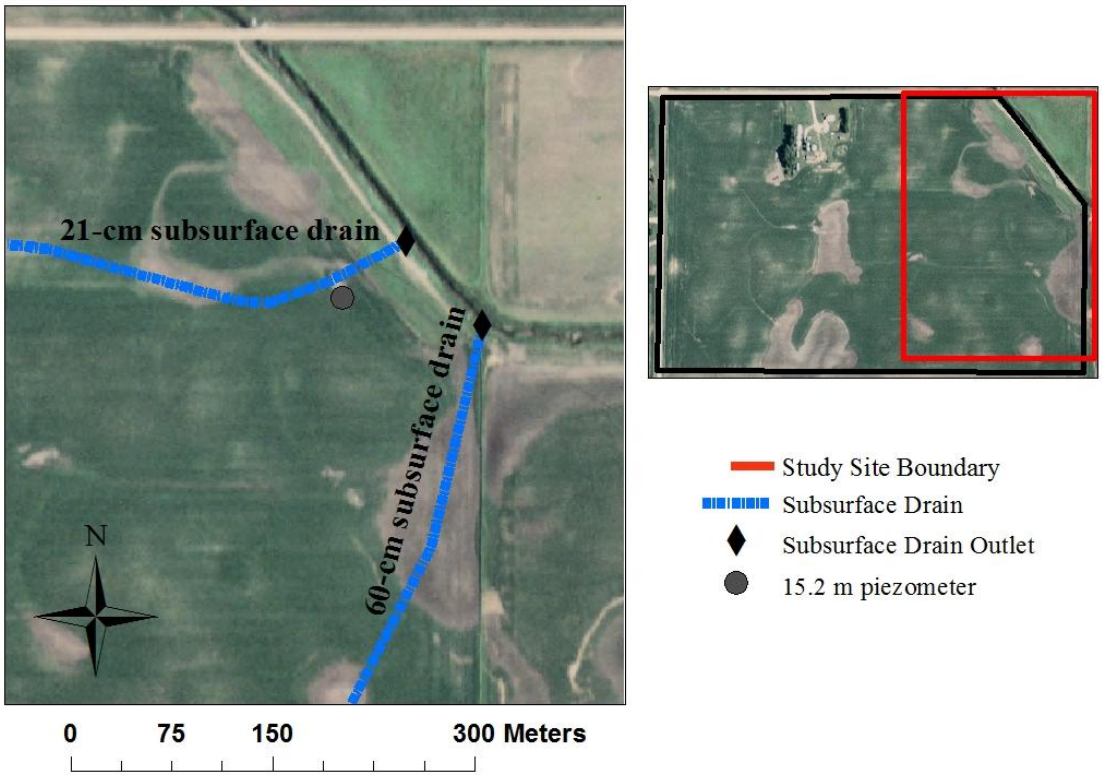

Fig. 5.1: The right-hand map shows the field boundary for the 38.8 hectare field, with a smaller red box highlighting the inset map on the left. For the left-hand map, the pertinent site locations for this study are shown, including the 15.2 m piezometer (distance from subsurface drain), the two subsurface drain locations, and subsurface drain outlets.

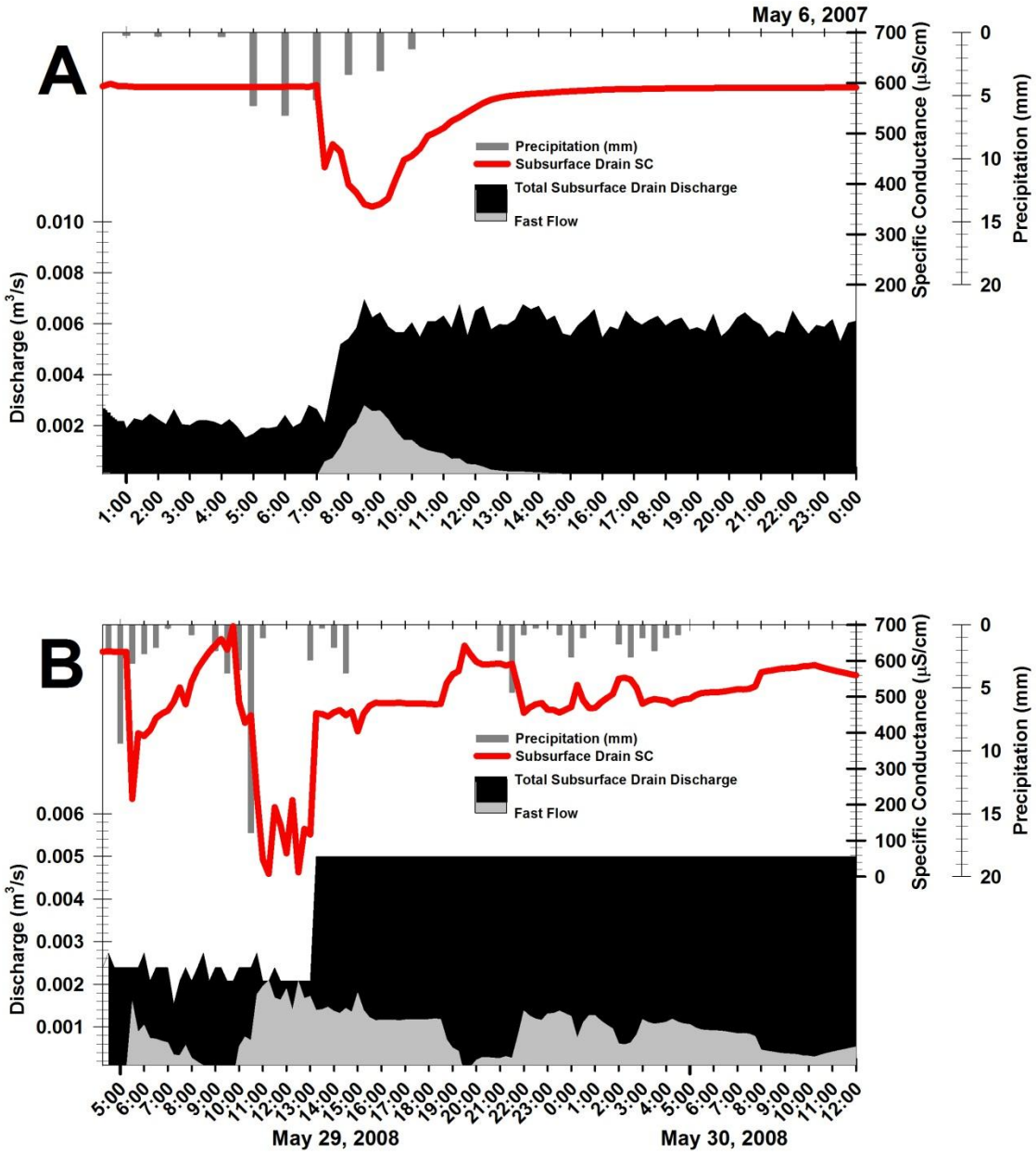

Fig. 5.2A-B: Precipitation (mm), subsurface drain SC (µS/cm), total subsurface drain discharge (m^3/s), and calculated preferential flow (m^3/s), for 21-cm subsurface drain for (A) May 6, 2007 and (B) May 29-30, 2008.

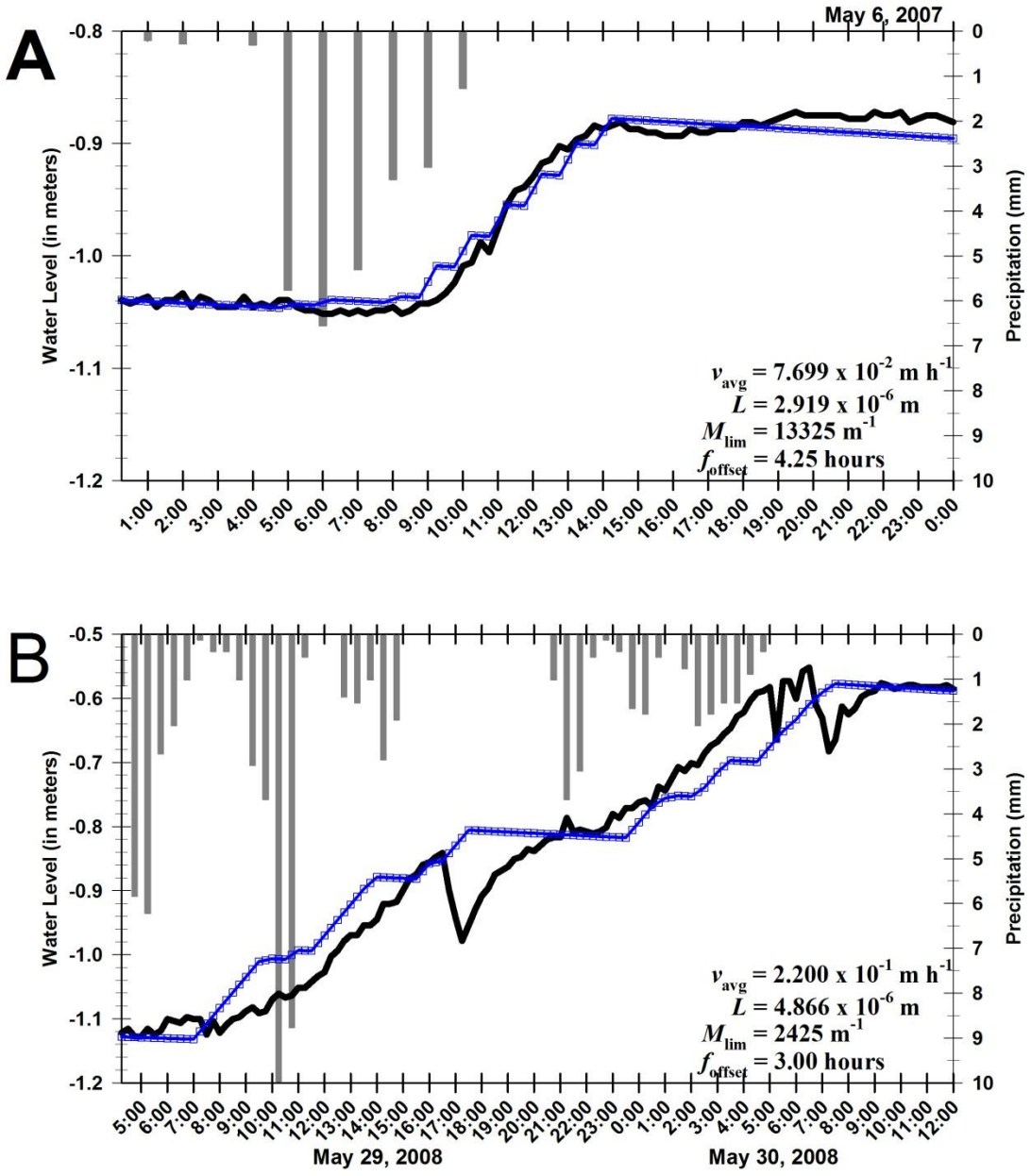

Fig. 5.3A-B: Precipitation (mm), measured water table/level (m), and the source-responsive model best-fit results for the field piezometer located 15.2 m away from the subsurface drain for (A) May 6, 2007 and (B) May 29-30, 2008. Also shown in the lower inset are the input parameters.

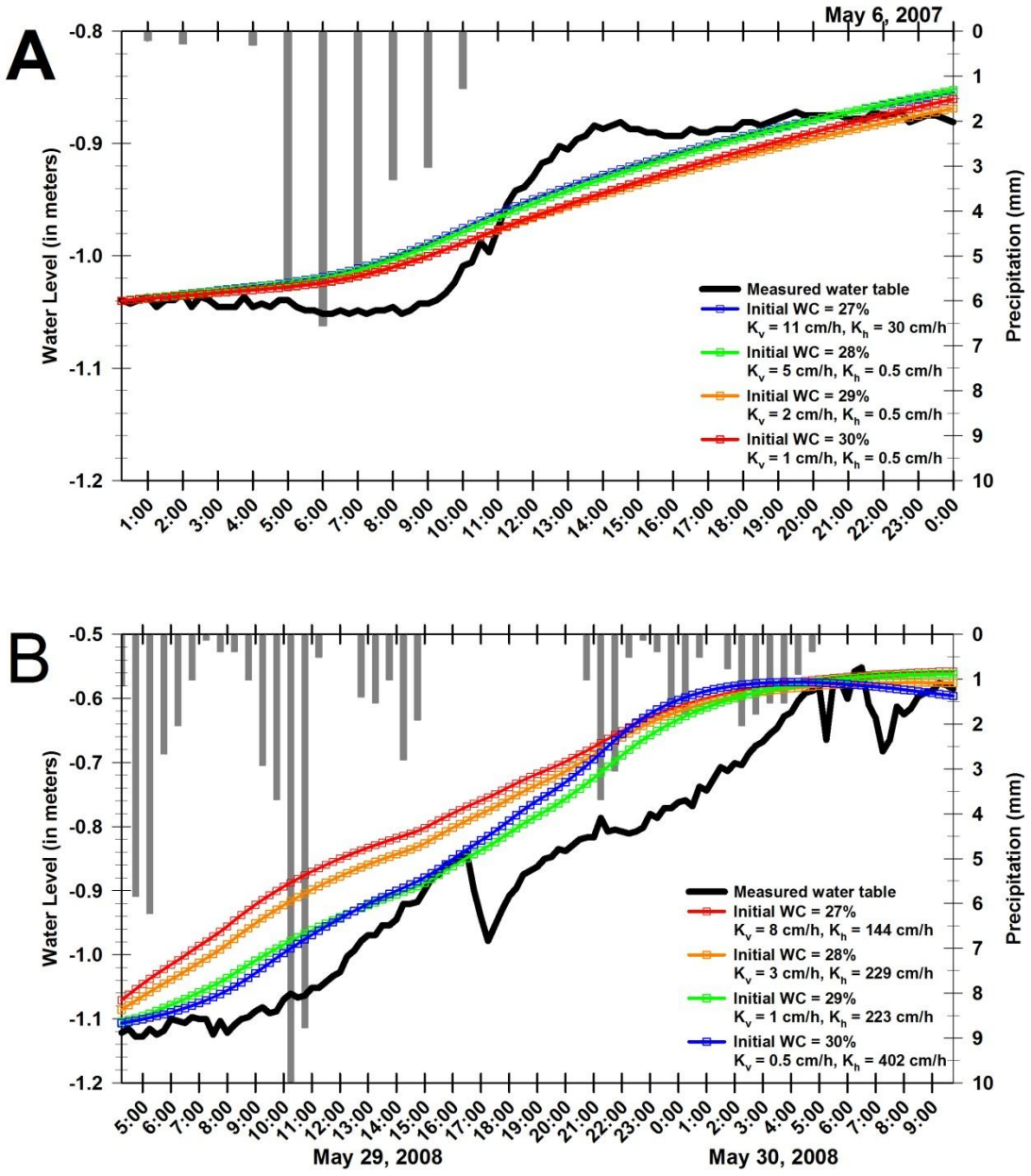

Fig. 5.4A-B: Precipitation (mm), measured water table/level (m), and the DRAIN-Pro model best-fit results for the field piezometer located 15.2 m away from the subsurface drain for (A) May 6, 2007 and (B) May 29-30, 2008. Best-fit results are shown for initial water content (WC) from 27% to 30%.

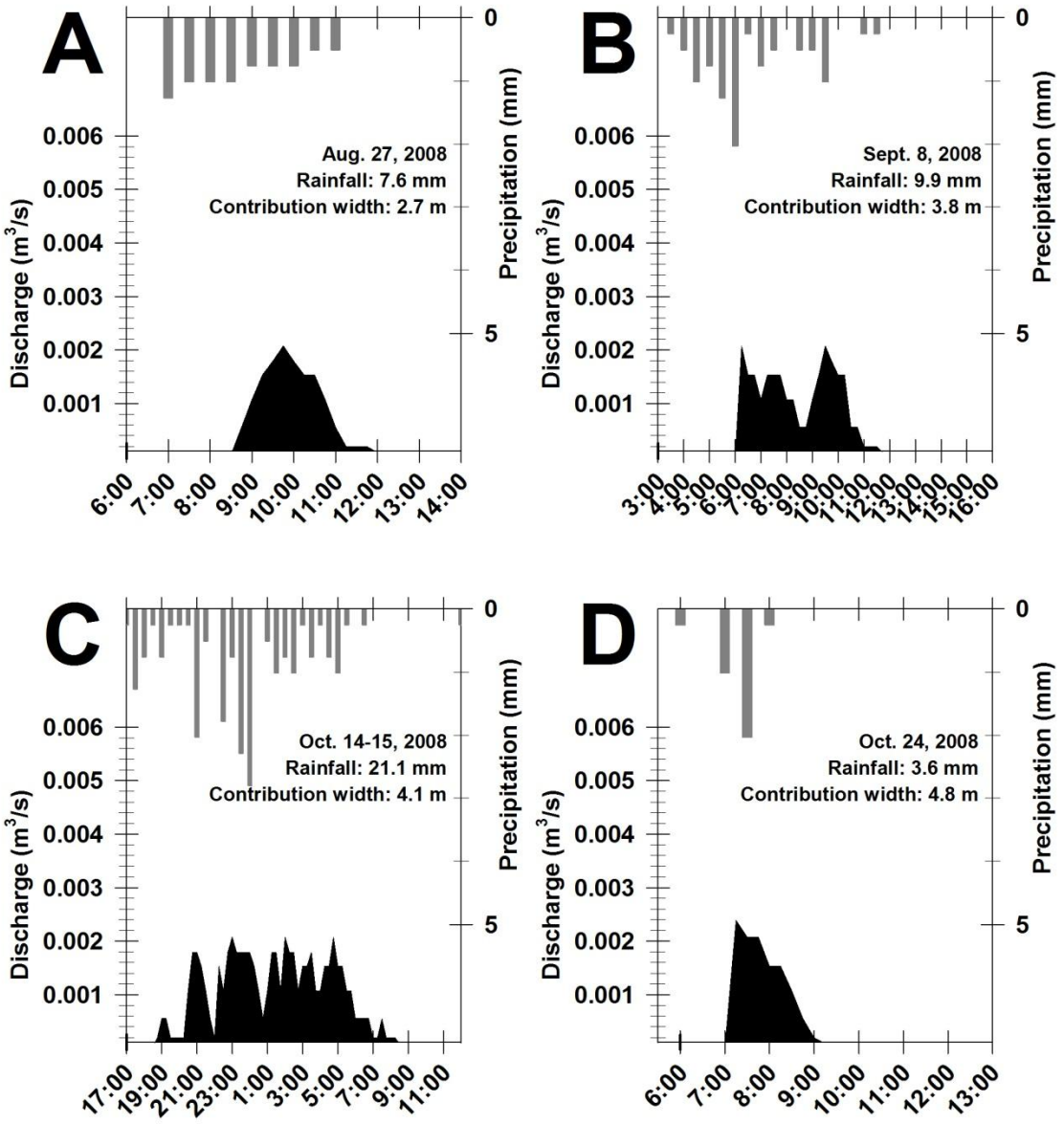

Fig. 5.5A-D: Four mid-to-late season rainfall events with increased subsurface drain discharge, sourced entirely from preferential flow, from (A) August 27, 2008; (B) Sept. 8, 2008; (C) Oct.14-15, 2008; (D) Oct. 24, 2008. Also shown is the cumulative rainfall at the calculated contribution area perpendicular to the entire length of the subsurface drain.

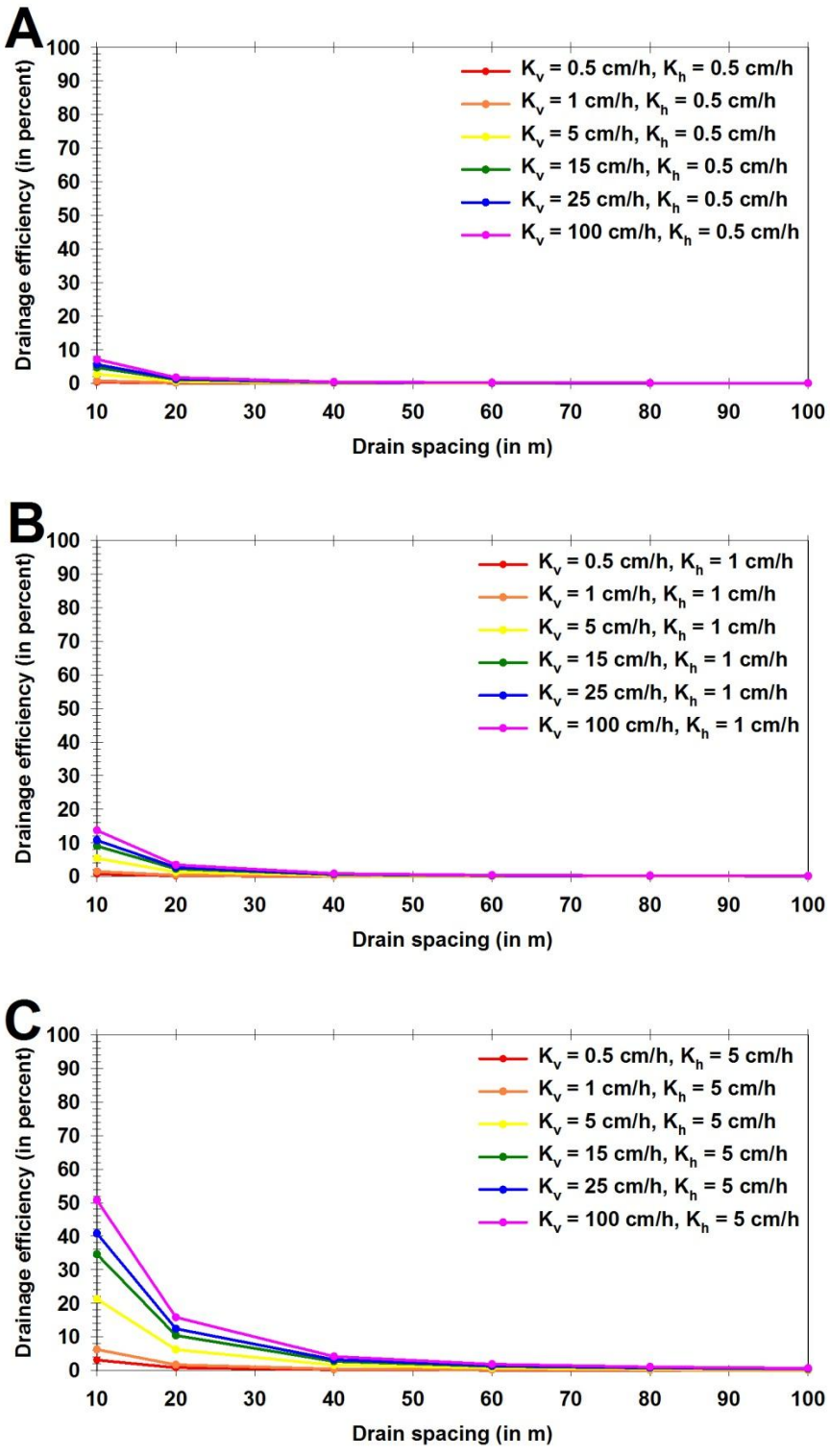

Fig. 5.6A-C: Hypothetical drainage efficiency after 24 hours utilizing DRAIN-Pro (5.54-cm cumulative rainfall), plotted with distance between adjacent subsurface drains. The lines denote different combinations of horizontal and vertical hydraulic conductivity.

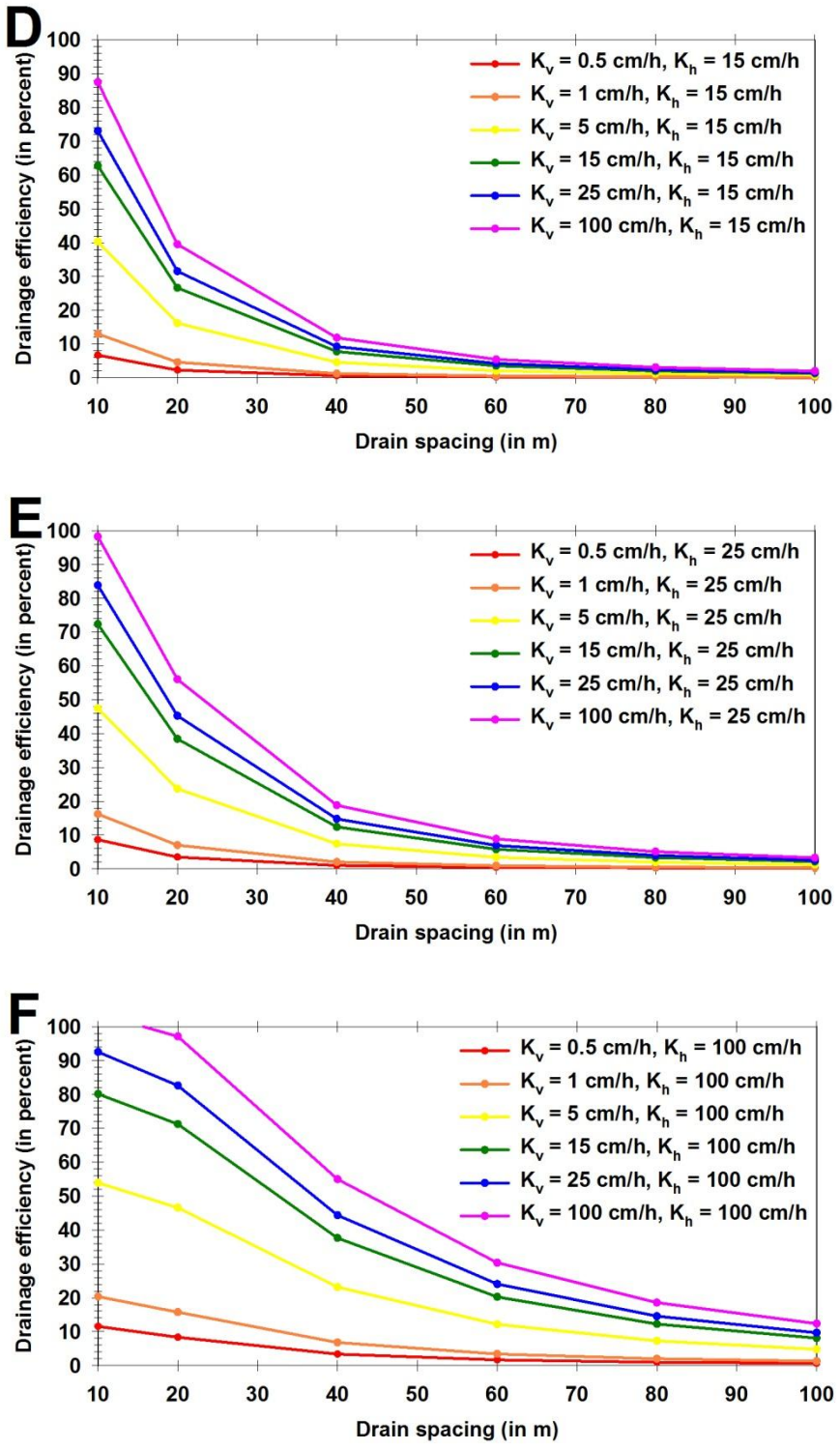

Fig. 5.6D-F (cont.): Hypothetical drainage efficiency after 24 hours utilizing DRAIN-Pro (5.54-cm cumulative rainfall), plotted with distance between adjacent subsurface drains. The lines denote different combinations of horizontal and vertical hydraulic conductivity.

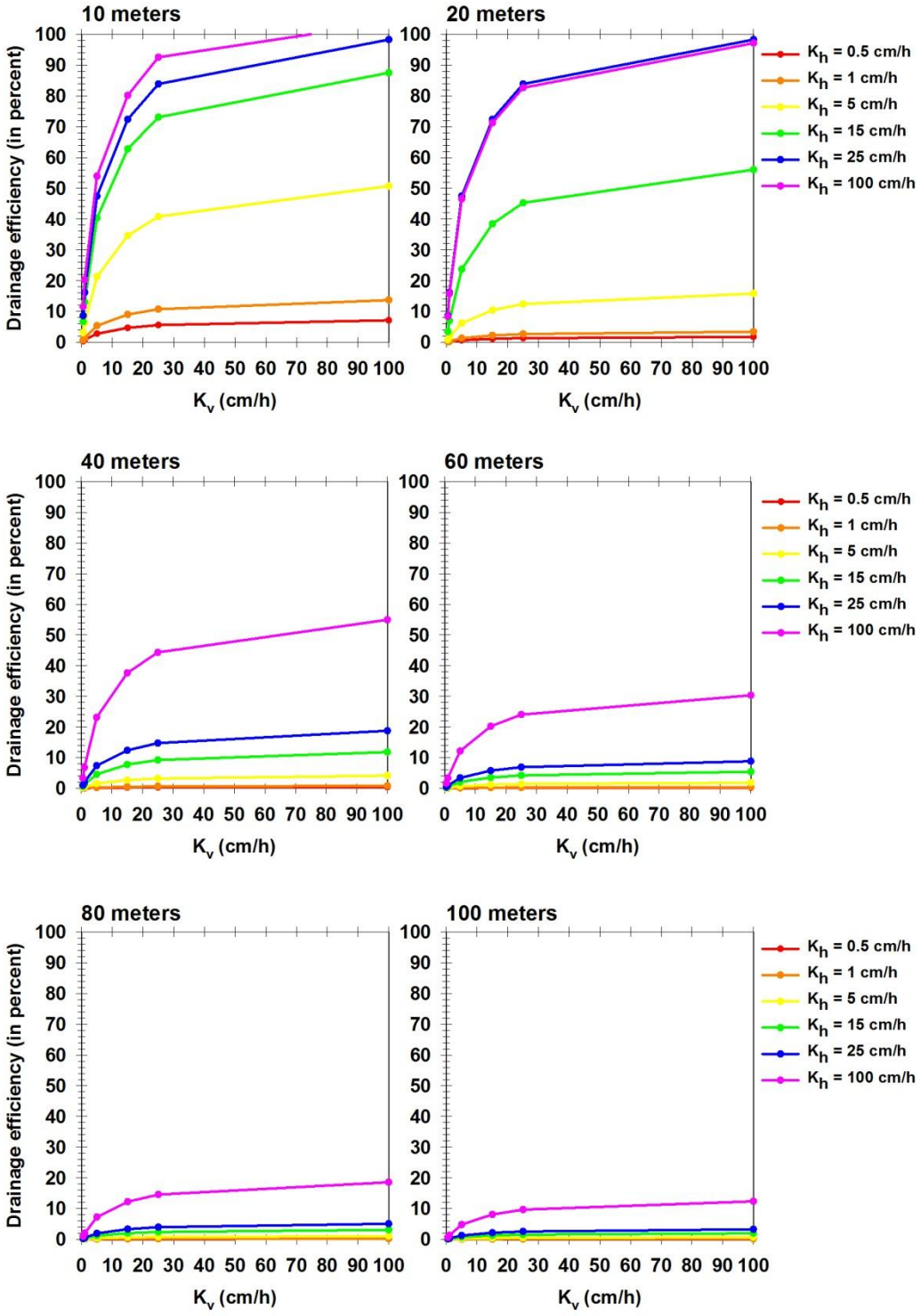

Fig. 5.7: Hypothetical drainage efficiency after 24 hours utilizing DRAIN-Pro (5.54-cm cumulative rainfall) at different vertical hydraulic conductivities (0.5 cm/hr, 1 cm/h, 5 cm/h, 15 cm/h, 25 cm/h, 100 cm/h). Each different line represents a different horizontal hydraulic conductivity.

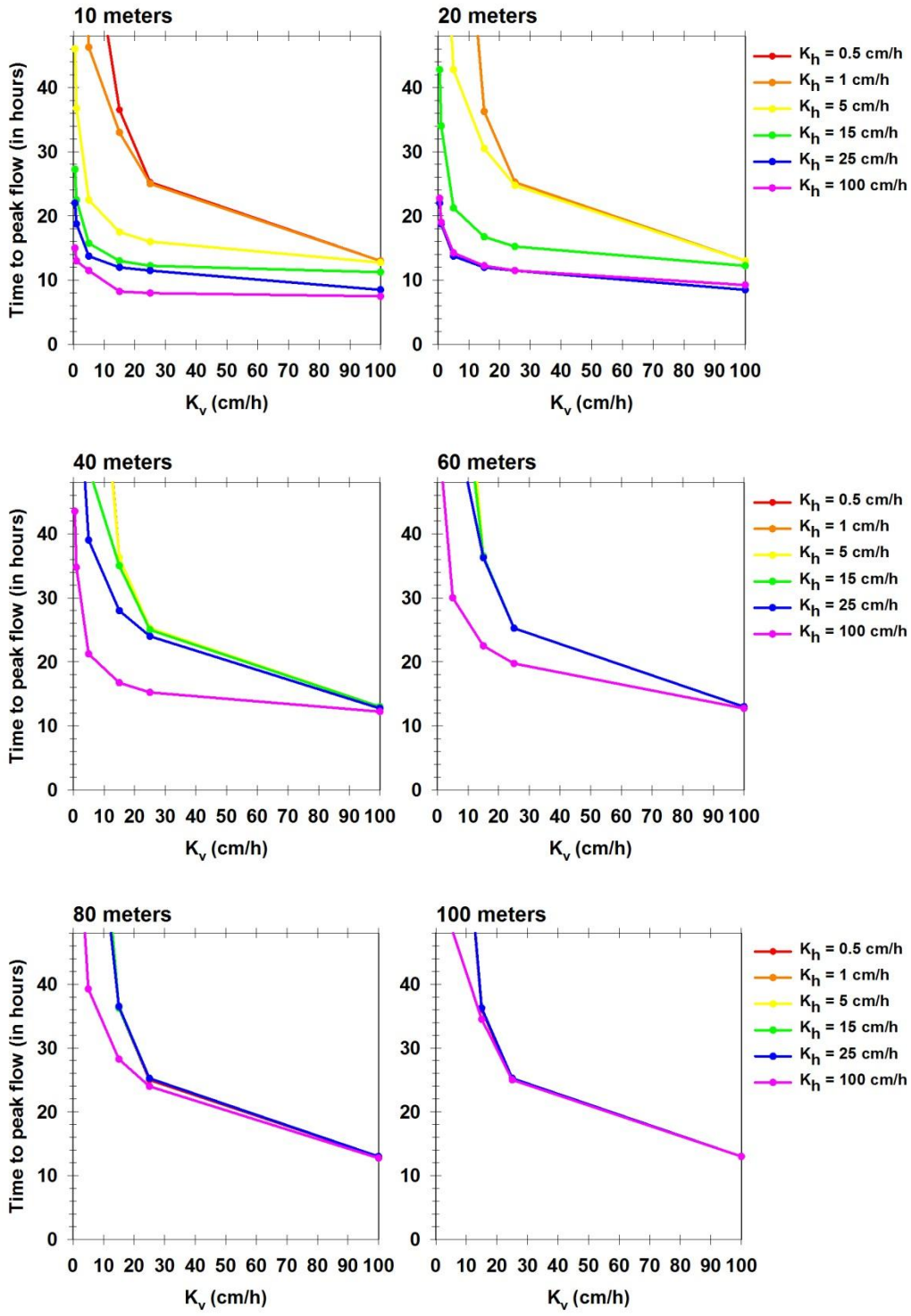

Fig. 5.8: Hypothetical time to peak flow (in hours) utilizing DRAIN-Pro (5.54-cm cumulative rainfall) at different vertical hydraulic conductivities (0.5 cm/hr, 1 cm/h, 5 cm/h, 15 cm/h, 25 cm/h, 100 cm/h). Each different line represents a different horizontal hydraulic conductivity.

Chapter 6: Bibliography

Ahuja, L.R., D.G. Decoursey, B.B. Barnes, and K.W. Rojas. 1993. Characteristics of macropore transport studied with the ARS Root-Zone Water-Quality Model. Trans. ASAE 36:369–380.

Alexander, R.B., R.A. Smith, G.E. Schwarz, E.W. Boyer, J.V. Nolan, and J.W. Brakebill. 2008. Differences in phosphorus and nitrogen delivery to the Gulf of Mexico from the Mississippi River basin. Environ. Sci. Technol. 42: 822–830.

Allaire, S.E., S. Roulier, and A.J. Cessna. 2009. Quantifying preferential flow in soils: A review of different techniques. J. Hydrol. 78: 179-204.

Allaire-Leung, S.E., S.C. Gupta, and J.F. Moncrief. 2000. Water and solute movement in soil as influenced by macropore characteristics - 1. Macropore continuity. J. Cont. Hydrol. 41(3-4): 283-301.

Allen, R.G., L.S. Pereira, D. Raes, and M. Smith. 1998. Crop evapotranspiration: guidelines for computing crop water requirements. Food and Agriculture Organization Irrigation and Drainage Paper No. 56.

Andreini, M.S. and T.S. Steenhuis. 1990. Preferential paths of flow under conventional and conservation tillage. Geoderma 46: 85–102.

Assouline, S. 2004. Rainfall-induced soil surface sealing: A critical review of observations, conceptual models, and solutions. Vadose Zone J. 3: 570-591.

Bear, J. 1972. Dynamics of Fluids in Porous Media. Dover Publications.

Benoit, G.R., S. Mostaghimi, R.A. Young, and M.J. Lindstrom. 1986. Tillage-residue effects on snow cover, soil-water, temperature and frost. Trans. ASAE 29: 473–479.

Bergström, L., N. Jarvis, M. Larsson, F. Djodjic, and A. Shirmohammadi. 2001. Factors affecting the significance of macropore flow for leaching of agrochemicals. Preferential Flow Water: Movement and Chemical Transport in the Environment, Proc. 2nd Intl. Symp. (3–5 January 2001). Am. Soc. Agric. Biol. Eng., St. Joseph, MI.

Bettis III, E.A., D.J. Quade, and T.J. Kemmis. 1996. Hogs, Bogs, and Logs: Quaternary Deposits and Environmental Geology of the Des Moines Lobe. Geological Survey Bureau Guidebook Series No. 18. Ames, Iowa: Iowa Department of Natural Resources.

Beven, K. and P. Germann. 1982. Macropores and water flow in soils. Water Resour. Res. 18: 1311–1325.

Beven, K.J. and R.T. Clarke. 1986. On the variation of Infiltration into a homogeneous soil matrix containing a population of macropores. Water Resour. Res. 22: 383-388.

Bird, R.B., W.E. Stewart, and E.N. Lightfoot. 2002. Transport phenomena. 2nd ed. John Wiley & Sons, New York.

Blake, G.R., and K.H. Hartge. 1986. Particle density. p. 377-382. *In* A. Klute (ed.) Methods of soil analysis. Part 1. Physical and mineralogical methods. SSSA, Madison, WI.

Blann, K.L., J.L. Anderson, G.R. Sands, and B. Vondracek. 2009. Effects of agricultural drainage on aquatic ecosystems: a review. Crit. Rev. Environ. Sci. Technol. 39: 909–1001.

Bouma, J. 1981. Soil morphology and preferential flow along macropores. Ag. Water Manage. 3: 235–250.

Bouma, J., C.F.M. Belmans, and L.W. Dekker. 1982. Water infiltration and redistribution in a silt loam subsoil with vertical worm channels. Soil Sci. Soc. Am. J. 46: 917-921.

Braun, H.M.H, and R. Kruijne. 1994. Soil conditions. p. 77-110. *In* H.P. Ritzema (ed.) Drainage principles and applications. International Institute for Land Reclamation and Improvement, Wageningen, The Netherlands.

Burkhart, M. and D. James. 1999. Agricultural-nitrogen contributions to hypoxia in the Gulf of Mexico. J. Environ. Qual. 28: 850–859.

Capel, P.D., K.A. McCarthy, and J.E. Barbash. 2008. National, holistic, watershed-scale approach to understand the sources, transport, and fate of agricultural chemicals. J. Environ. Qual. 37: 983-993.

Cey, E.E. and D.L. Rudolph. 2009. Field study of macropore flow processes using tension infiltration of a dye tracer in partially saturated soils. Hydrol. Proc. 23: 1768-1779.

Chikhaoui, M., C. Madramootoo, M. Eastman, and A. Michaud. 2008. Estimating preferential flow to agricultural tile drains, Proc. 2008 ASABE Ann. Intl. Meet. (29 June–2 July 2008). Am. Soc. Agric. Biol. Eng., St. Joseph, MI.

Chu, S.T. 1978. Infiltration during an unsteady rain. Water Res. Res. 14(3): 461-466.

Dideriksen, R.O. 1986. Soil survey of Hamilton County, Iowa. United States Department of Agriculture Soil Conservation Service, 157 p.

Ebel, B.A., and J.R. Nimmo. 2009. Estimation of unsaturated zone traveltimes for Rainier Mesa and Shoshone Mountain, Nevada Test Site, Nevada, using a source-responsive preferential-flow model. Open-File Rep. 2009-1175. USGS, Menlo Park, CA.

Edwards, W.M., M.J. Shipitalo, L.B. Owens, and W.A. Dick. 1993. Factors affecting preferential flow of water and atrazine through earthworm burrows under continuous no-till corn. J. Environ. Qual. 22: 453–457.

Ehlers, W. 1976. Rapid determination of undisturbed hydraulic conductivity in tilled and untilled loess soil. Soil Sci. Soc. Am. J. 40: 837–840.

Elrick, D.E., W.D. Reynolds, and K.A. Tan. 1989. Hydraulic conductivity measurements in the unsaturated zone using improved well analyses. Ground Water Monit. Rev. 9:184–193.

Everts, C.J. and R.S. Kanwar. 1990. Estimating preferential flow to a subsurface drain with tracers. Trans. ASAE 33: 451-457.

Everts, C.J., and R.S.Kanwar. 1993. Interpreting tension-infiltrometer data for quantifying soil macropores: Some particle considerations. Tran. ASAE 36:423–428.

Fenelon, J.M. and R.C. Moore. 1998. Transport of agrichemicals to ground and surface water in a small central Indiana watershed. J. Environ. Qual. 27: 884–894.

Fisher, L.H. and R.W. Healy. 2008. Water movement within the unsaturated zone in four agricultural areas of the United States. J Environ. Qual. 37: 1051-1063.

Flanagan, D. C., and M. A. Nearing, eds. 1995. USDA Water Erosion Prediction Project hillslope and watershed model documentation. NSERL Report No. 10. West Lafayette, Ind.: USDA-ARS National Soil Erosion Research Laboratory.

Flury, M., H. Fluhler, W.A. Jury, and J. Leuenberger. 1994. Susceptibility of soils to preferential flow of water: a field study. Water Resour. Res. 30: 1945-1954.

Fox. G.A., R. Malone, G.J. Sabbagh, and K. Rojas. 2004. Interrelationship of macropores and subsurface drainage for conservative tracer and pesticide transport. J. Environ. Qual. 33: 2281-2289.

Gerke, H.H., and M. Th. van Genuchten. 1993. A dual-porosity model for simulating the preferential movement of water and solutes in structured porous media. Water Resour. Res. 29:305–319.

Gerla, P.J. and R.K. Matheney. 1996. Seasonal variability and simulation of groundwater flow in a prairie wetland. Hydrological Processes 10: 903-920.

Germann, P.F. and K. Beven. 1985. Kinematic wave approximation to infiltration into soils with sorbing macropores. Water Resour. Res. 21: 990-996.

Germann, P.F. and D. Hensel. 2006. Poiseuille flow geometry inferred from velocities of wetting fronts in soils. Vadose Zone Journal 5: 867-876.

Germann, P., A. Helbling, and T. Vadilonga. 2007. Rivulet approach to rates of preferential infiltration. Vadose Zone J. 6: 207-220.

Germann, P. 2010. Comment on "Theory for source-responsive and free-surface film modeling of unsaturated flow". Vadose Zone Journal 9: 1100-1101.

Gowdish, L. and R. Muñoz-Carpena. 2009. An improved Green-Ampt infiltration and redistribution method for uneven multistorm series. Vadose Zone J. 8: 470-479.

Grossman, W.D., and T.G. Reinsch. 2002. Saturated and field-saturated water flow parameters. p. 201-228. *In* J.H. Dane and G.C. Topp (ed.) Methods of soil analysis. Part 4. Physical methods. SSSA, Madison, WI.

Haria, A.H., A.C. Johnson, J.P. Bell, and C.H. Batchelor. 1994. Water movement and isoproturon behaviour in a drained heavy clay soil: 1. Preferential flow processes.J. Hydrol. 163: 203–216.

Heard, J.R., E.J. Kladivko, and J.V. Mannering. 1988. Soil macroporosity, hydraulic conductivity and air permeability of silty soils under long-term conservation tillage in Indiana. Soil Tillage Res. 11: 1–18.

Heath, R.C. 1983. Basic ground-water hydrology. USGS Water Supply Paper 2220. USGS, Denver, CO.

Heppell, C.M., T.J. Burt, and R.J. Williams. 2000. Variations in the hydrology of an underdrained clay hillslope. J. Hydrol. 227: 236-256.

Heppell, C.M. and A.S. Chapman. 2006. Analysis of a two-component hydrograph separation model to predict herbicide runoff in drained soils. Ag. Water Manage. 79: 177–207.

Heppell, C.M., F. Worrall, T.P. Burt, and R.J. Williams. 2002. A classification of drainage and macropore flow in an agricultural catchment. Hydrol. Processes 16: 27–46.

Hillaker, H.J. 2008. Iowa annual weather summary – 2008. Des Moines, IA: Iowa Dept. of Ag. and Land Stewardship. Available at http://www.iowaagriculture.gov/climatology/weatherSummaries/2008/fas2008.pdf (verified 21 March 2011).

Iowa DNR. 2008. 2008 National Agriculture Imagery Program (NAIP) Aerial Photography Mosaic of Hamilton County, Iowa. Iowa Geological Survey, DNR, GIS Section. Iowa City, Iowa.

Iowa Department of Transportation. 2011. Available at http://mesonet.agron.iastate.edu/AWOS/ (verified 25 July 2011).

James, H.R. and T.E. Fenton. 1993. Water tables in paired artificially drained and undrained soil catenas in Iowa. Soil Sci. Soc. Am. J. 57: 774-781.

Jarvis, N., P-E. Jansson, P.E. Dik, and I. Messing. 1991. Modeling water and solute transport in macroporous soil. I. Model description and sensitivity analysis. J. Soil Sci. 42: 59-70.

Jarvis, N.J., 1991. MACRO -- A model of water movement and solute transport in macroporous soils. PhD Dissertation. Uppsala, Sweden: Swedish University of Agricultural Sciences, Department of Soil Science.

Jarvis N.J. and I.G. Dubus. 2006. State-of-the-art review on preferential flow. Report DL#6 of the FP6 EU-funded FOOTPRINT project [www.eu-footprint.org], 60 p.

Jaynes, D.B., J.L. Hatfield, and D.W. Meek. 1999. Water quality in Walnut Creek Watershed: Herbicides and nitrate in surface waters. J. Environ. Qual. 28: 45–59.

Jaynes, D.B., S.I. Ahmed, K.-J.S. Kung, and R.S. Kanwar. 2001. Temporal dynamics of preferential flow to a subsurface drain. Soil Sci. Soc. Am. J. 65: 1368-1376.

Jury, W. and R. Horton. 2004. Soil Physics (6th edition). Hoboken, NJ: John Wiley and Sons, Inc.

Kalkhoff, S.J., K.E. Lee, S.D. Porter, P.J. Terrio, and E.M. Thurman. 2003. Herbicides and herbicide degradation products in upper Midwest agricultural streams during August base-flow conditions. J. Environ. Qual. 32: 1025–1035.

Kanwar, R.S., R.M. Cruse, M. Ghaffarzadeh, A. Bakhsh, D.L. Karlen, and T.B. Bailey. 2005. Corn–soybean and alternative cropping systems effects on NO_3-N leaching losses in subsurface drainage water. Appl. Eng. Agric. 21: 181–188.

Kao, C., S. Bouarfa, and D. Zimmer. 2001. Steady state analysis of unsaturated flow above a shallow water-table aquifer drained by ditches. J. Hydrol. 250: 122-133.

Kladivko, E.J., G.E. Van Scoyoc, E.J. Monke, K.M. Oates, and W. Pask. 1991. Pesticide and nutrient movement into subsurface tile drains on a silt loam soil in Indiana. J. Environ. Qual. 20: 264–270.

Kladivko, E.J., J. Grochulska, R.F. Turco, G.E. Van Scoyoc, and J.D. Eigel. 1999. Pesticide and nitrate transport into subsurface tile drains of different spacings. J. Environ. Qual. 28: 997-1004.

Kladivko, E.J., L.C. Brown, and J.L. Baker. 2001. Pesticide transport to subsurface tile drains in humid regions of North America. Crit. Rev. Environ. Sci. Technol. 31: 1–62.

Kladivko, E.J., J.R. Frankenberger, D.B. Jaynes, D.W. Meek, B.J. Jenkinson, and N.R. Fausey. 2004. Nitrate leaching to subsurface drains as affected by drain spacing and changes in crop production system. J. Environ. Qual. 33: 1803–1813.

Kobayashi, D. 1986. Separation of a snowmelt hydrograph by stream conductance. J. Hydrol. 84: 157–165.

Krajewski, W.F. and R. Mantilla. 2010. Why were the 2008 floods so large?. p. 19-30. *In* C.F. Mutel (ed.) A watershed year: Anatomy of the Iowa floods of 2008. University of Iowa Press. Iowa City, IA.

Kumar, A., R.S. Kanwar, and G.R. Hallberg. 1997. Separating preferential and matrix flows using subsurface tile flow data. J. of Environ. Sci. and Health, Part A: Toxic/Hazardous Substances and Environ. Engineering 32: 1711–1729.

Kung, K.-J.S., T.S. Steenhuis, E.J. Kladivko, T.J. Gish, G. Bubenzer, and C.S. Helling. 2000. Impact of preferential flow on the transport of adsorbing and non-adsorbing tracers. Soil Sci. Soc. Am. J. 64: 1290-1296.

Kung, K.-J.S., E.J. Kladivko, T.J. Gish, T.S. Steenhuis, G. Bubenzer, and C.S. Helling. 2000. Quantifying preferential flow by breakthrough of sequentially applied tracers: Silt loam soil. Soil Sci. Soc. Am. J. 64: 1296-1304.

Larsbo, M. and N. Jarvis. 2007. MACRO 5.0: A model of water flow and solute transport in macroporous soil. Technical description, Swedish University of Agricultural Sciences: 49 p.

Laudon, H. and O. Slaymaker. 1997. Hydrograph separation using stable isotopes, silica and electrical conductivity: an alpine example. J. Hydrol. 201: 82–101.

Leeds–Harrison, P.B., C.J.P. Shipway, N.J. Jarvis, and E.G. Youngs. 1986. The influence of soil macroporosity on water retention, transmission and drainage in a clay soil. Soil Use and Manage. 2: 47–50.

Logsdon, S.D. 1995. Flow mechanisms through continuous and buried macropores. Soil Science 160: 237-242.

Luxmoore, R.J. 1981. Micro-, meso-, and macroporosity of soil. Soil Sci. Soc. Am. J. 45: 671-672.

Madramootoo, C.A., W.R. Johnston, J.E. Ayars, R.O. Evans, and N.R. Fausey. 2007. Agricultural drainage management, quality and disposal issues in North America. Irr. Drain. 56: S35–S45.

Marshall, T.J. 1959. Relations between water and soil. Tech. commun. 50, Commonw. Agric. Bur., Farnham Royal, UK.

McCarthy, K.A., C.E. Rose, and S.J. Kalkhoff. 2012. Environmental Settings of the South Fork Iowa River basin, Iowa, and the Bogue Phalia basin, Mississippi, 2006-10. U.S. Geological Survey Scientific Investigations Report 2012-5021, 30 p.

McIntyre, D.S. 1974. Pore space and aeration determinations. p. 67–74. *In* J. Loveday (ed.) Methods for analysis of irrigated Soils. Commonw. Agric. Bur., Farnham Royal, UK.

Meadows, M., R. Bales, J. Hopmans, P. Hartsough, T. O'Geen, and P. Kirchner. 2009. Soil moisture response to snowmelt and rainfall across elevation, aspect and canopy cover in the Southern Sierra Nevada. Eos Trans. AGU 90, Fall Meet. Suppl.: Abstract H33A–0856.

Mein, R.G. and C.L. Larson. 1973. Modeling infiltration during a steady rain. Water Resour. Res. 9: 384-394.

Mohanty, B.P., M.D. Ankeny, R. Horton, and R.S. Kanwar. 1994. Spatial-analysis of hydraulic conductivity measured using disc infiltrometers. Water Resour. Res. 30: 2489–2498.

Moran, C.J., and A.B. McBratney. 1992. Acquisition and analysis of three component digital images of soil pore structure: I. Method. J. Soil Sci. 43:541–549.

Muñoz-Carpena, R. 2004. Field devices for monitoring soil water content. Homestead, FL, Department of Agricultural and Biological Engineering, Florida Cooperative Extension Service, Institute of Food and Agricultural Sciences, University of Florida**:** 17.

Narasimhan, T.N. 1998. Something to think about...Darcy-Buckingham's Law. Ground Water 36: 194-195.

Nash, J.E. and I.V. Sutcliffe. 1970. River flow forecasting through conceptual models Part 1 - A Discussion of principles. J. Hydrol. 10: 282-290.

National Atmospheric Deposition Program. 2011. National Atmospheric Deposition Program Office. Champaign, IL: Illinois State Water Survey. Available at http://nadp.sws.uiuc.edu/sites/siteinfo.asp?net=NTN&id=IA08 (verified 10 February 2011).

NCDC. 2010. Climate Record for Webster City, IA, United States. Webster City, IA: National Climatic Data Center. Available at http://www4.ncdc.noaa.gov/cgi-win/wwcgi.dll?wwDI~StnSrch~StnID~12001856 (verified 17 December 2010).

Nicks, A.D. 1985.Generation of climate data. Proceedings of the Natural Resources Modeling Symposium. USDA–ASA ARS, 30:297–300.

Nimmo, J.R. 2003. How fast does water flow in an unsaturated macropore?: Evidence from field and lab experiments. *In* J. Álvarez-Benedí and P. Marinero (ed.) Estudios de la Zona No Saturada del Suelo, Vol. 6.

Nimmo, J.R. 2007. Simple predictions of maximum transport rate in unsaturated soil and rock. Water Resour. Res. 43: 1-11.

Nimmo, J.R., K.M. Schmidt, K.S. Perkins, and J.D. Stock. 2009. Rapid measurement of field-saturated hydraulic conductivity for areal characterization. Vadose Zone J. 8: 142-149.

Nimmo, J.R. 2010. Theory for source-responsive and free-surface film modeling of unsaturated flow. Vadose Zone Journal 9: 295–306.

Ogden, C.B., H.M. van Es, R.J. Wagenet, and T.S. Steenhuis. 1999. Spatial-temporal variability of preferential flow in a clay soil under no-till and plow-till. J. Environ. Qual. 28: 1264-1273.

Øygarden, L., J. Kværner, and P.D. Jenssen. 1997. Soil erosion via preferential flow to drainage systems in clay soils. Geoderma 76: 65–86.

Perret, J., S.O. Prasher, A. Kantzas, and C. Langford. 1999. Three-dimensional quantification of macropore networks in undisturbed soil cores. Soil Sci. Soc. Am. J. 63: 1530-1543.

Pilgrim, D.H., D.D. Huff, and T.D. Steele. 1979. Use of specific conductance and contact time relations for separating flow components in storm runoff. Water Resour. Res. 15: 329–339.

Prior, J.C. 1991. Landforms of Iowa (1st edition). Iowa City, IA: University of Iowa Press.

Quade, J., J.D. Giglierano, E.A. Bettis, and R.J. Wisner. 2000. Surficial geologic map of the Des Moines Lobe of Iowa: Hamilton and Webster Counties. Geological Survey Bureau Open File Map 2000–1.

Randall, G.W. and D.J. Mulla. 2001. Nitrate-nitrogen in surface waters as influenced by climatic conditions and agricultural practices. J. Environ. Qual. 30: 337-344.

Rawls, W.J., D.L. Brakensiek, and N. Miller. 1983. Green-Ampt infiltration parameters from soils data. J. Hydr. Eng. 109: 62–70.

Reynolds, W.D., and D.E. Elrick. 1990. Ponded infiltration from a single ring. I. Analysis of steady flow. Soil Sci. Soc. Am. J. 54:1233–1241.

Reynolds, W.D., D.E. Elrick, E.G. Youngs, and A. Amoozegar. 2002. Field methods (vadose and saturated zone techniques). p. 817. In J.H. Dane and G.C. Topp (ed.) Methods of soil analysis. Part 4. Physical methods. SSSA, Madison, WI.

Richard, T.L. and T.S. Steenhuis. 1988. Tile drain sampling of preferential flow on a field scale. J. Contam. Hydrol. 3: 307-325.

Richards, L.A. 1931. Capillary conduction of liquids through porous materials. Physics 1:318–333.

Roth, J. 2010. The hydrology of a drained topographical depression within an agricultural field in north central Iowa. MS Thesis. Minneapolis, MN: University of Minnesota, Dept. of Civil Engineering.

Sands, G.R. 2001. Soil water concepts. Agricultural Drainage Publication Series. University of Minnesota. St. Paul, MN.

Schilling, K.E. and M. Helmers. 2008. Tile drainage as karst: Conduit flow and diffuse flow in a tile-drained watershed. J. Hydrol. 349: 291–301.

Shah, N. and M. Ross. 2009. Variability in specific yield under shallow water table conditions. J. Hydrol. Eng. 14: 1290-1298.

Shipitalo, M.J. and W.M. Edwards. 1996. Effects of initial water content on macropore/matrix flow and transport of surface-applied chemicals. J. Environ. Qual. 25: 662–670.

Sidle, R.C., Y. Tsuboyama, S. Noguchi, I. Hosoda, M. Fujieda, and T. Shimizu. 2000. Stormflow generation in steep forested headwaters: a linked hydrogeomorphic paradigm. Hydrol. Processes 14: 369–385.

Šimůnek, J., T. Vogel, and M. Th. van Genuchten. 1994. The SWMS_2D code for simulating water flow and solute transport in two-dimensional variably saturated media. Riverside, CA, USDA-ARS U.S Salinity Laboratory, 197 p.

Šimůnek, J., N.J. Jarvis, M. Th. van Genuchten, and A. Gärdenäs. 2003. Review and comparison of models for describing non-equilibrium and preferential flow and transport in the vadose zone. J. Hydrol. 272: 14-35.

Skaggs, R.W. 1976. Determination of the hydraulic conductivity—drainable porosity ratio from water table measurements. Trans. ASAE 25: 73-84.

Skaggs, R.W. 1978. A Water Management Model for Shallow Water Table Soils. Report No. 134. Water Resources Research Institute of the University of North Carolina.

Stone, W.W. and J.T. Wilson. 2006. Preferential flow estimates to an agricultural drain with implications for glyphosate transport. J. Environ. Qual. 35: 1825-1835.

Swanson, H. 2003. Using quantitative landscape modeling and scientific visualization to characterize soil hydrology dynamics. MS Thesis. St. Paul, MN: University of Minnesota.

Thomas, G.W. and R.E. Phillips. 1979. Consequences of water-movement in macropores. J. Environ. Qual. 8: 149–152.

Thornburg, J. 2009. Temporal and spatial variability in nitrate and water quality parameters of subsurface drains in an agricultural stream. MS Thesis. St. Paul, MN: University of Minnesota, Water Resources Science.

Tomer, M.D. and D.E. James. 2004. Do soil surveys and terrain analyses identify similar priority sites for conservation? Soil Sci. Soc. Am. J. 68: 1905-1915.

Tomer, M.D., T.B. Moorman, and C.G. Rossi. 2008. Assessment of the Iowa River's South Fork watershed: Part 1. Water Quality. J. Soil Water Conserv. 63: 360–370.

Topp, G.C.and Ferre. 2002. Saturated and field-saturated water flow parameters. p. 422–424. *In* J.H. Dane and G.C. Topp (ed.) Methods of soil analysis. Part 4. Physical methods. SSSA, Madison, WI.

USDA National Resource Conservation Service. 2009. Soil Survey Geographic (SSURGO) database for Hamilton County, Iowa. Fort Worth, Texas. Available at http://datagateway.nrcs.usda.gov/ (verified 10 February 2011).

Van Genuchten, M. Th. and J. Šimůnek. 2004. Integrated modeling of vadose-zone flow and transport processes. *In* R.A. Feddes, G.H. de Rooij, and J.C. van Dam (eds.) Unsaturated-zone modeling: Progress, challenges, and applications. Kluwer Academic Publishers: Dordrecht, The Netherlands.

Villholth, K.G., K.H. Jensen, and J. Fredericia. 1998. Flow and transport processes in a macroporous subsurface-drained glacial till soil I: Field investigations. J. Hydrol. 207: 98–120.

Warner, G.S. and R.A. Young. 1991. Measurement of preferential flow beneath mature corn. *In* T.J. Gish and A. Shirmohammadi (ed.) Proceedings of the National Symposium on Preferential Flow. American Society of Agricultural Engineers. St. Joseph, MI.

Watson, K.W. and R.J. Luxmoore. 1986. Estimating macroporosity in a forest watershed by use of a tension infiltrometer. Soil Sci. Soc. Am. J. 50: 578–582.

Werellagama, D.R.I.B., U. Matsubayahsi, and F. Takagi. 1997. Hysteresis observed in SC vs. Q relationships and its implications on flowpath identification. Ann. J. Hydr. Eng. 41: 197–202.

Wildenschild, D., Jensen, K.H., Villholth, K., and Illangasekare, T.H. 1994. A laboratory analysis of the effect of macropores on solute transport. Ground Water 32(3): 381-389.

Williams, A.G., J.F. Dowd, D. Scholefield, N.M. Holden and L.K. Deeks. 2003. Preferential flow variability in a well-structured soil. Soil Sci. Soc. Am. J. 67: 1272-1281.

Wilson, B.N. 2009. Lecture Notes for BBE 8513: Hydrologic Modeling of Small Watersheds. St. Paul, MN: University of Minnesota, Department of Bioproducts and Biosystems Engineering.

Winter, T.C. 1998. Relation of streams, lakes, and wetlands to groundwater flow systems. Hydrogeology Journal 7: 28-45.

Woo, M. K. and R.D. Rowsell. 1993. Hydrology of a Prairie Slough. J. Hydrol. 146: 175–207.

Zhang, Y.K. and K.E. Schilling. 2006. Effects of land cover on water table, soil moisture, evapotranspiration, and groundwater recharge: A Field observation and analysis. J. Hydrol. 319: 328-338.

Appendix A

Summary of the 54 SC events, including all of the time and SC parameters.

Date/Time, τ_S	τ_{EO} (min)	τ_{EM} (min)	τ_{50} (min)	τ_{90} (min)	SC_{EO} (μS/cm)	SC_{EM} (μS/cm)	SC_{50} (μS/cm)	SC_{90} (μS/cm)
2006-12-11 18:30	180	420	468	588	719	358	538	683
2006-12-20 13:30	180	420	509	855	736	409	572	703
2006-12-21 04:00	135	210	259	438	723	521	622	703
2007-01-03 11:00	255	270	461	495	705	615	660	696
2007-01-26 12:15	195	225	281	529	707	605	656	696
2007-02-19 10:15	285	360	492	723	704	507	605	684
2007-02-20 09:30	330	360	572	788	707	622	665	699
2007-02-21 09:45	300	540	819	1365	701	580	640	689
2007-02-24 03:00	180	195	260	466	703	517	610	685
2007-03-08 14:00	150	225	400	612	728	516	622	707
2007-03-09 10:15	240	435	549	779	724	414	569	693
2007-03-10 10:00	135	255	521	736	732	339	535	692
2007-03-29 22:00	75	75	125	183	662	554	608	651
2007-03-30 03:30	45	60	88	150	668	498	583	651
2007-03-30 14:00	105	210	240	287	667	569	618	657
2007-03-31 02:00	105	195	224	343	668	372	520	639
2007-03-31 07:30	135	180	228	330	638	486	562	622
2007-04-10 17:30	1035	1155	1139	1655	559	454	507	548
2007-04-22 12:30	105	135	192	--	655	439	547	633
2007-04-22 17:00	60	90	128	161	620	325	473	590
2007-05-07 04:00	195	285	377	518	593	355	474	569
2007-05-14 18:00	75	90	113	141	617	529	573	608
2007-06-21 16:00	90	90	133	171	638	552	595	629
2007-06-22 02:30	90	120	509	--	640	303	471	606
2007-07-09 02:00	135	150	230	422	628	563	595	622
2007-07-18 14:30	165	180	259	425	666	234	450	623
2007-07-26 19:30	105	135	293	438	690	353	522	657
2007-08-04 06:30	90	210	377	669	731	168	449	675
2007-10-02 07:30	150	285	577	614	518	420	469	509
2007-10-05 08:30	165	195	245	316	732	595	664	719

Date/Time, τ_S	τ_{EO} (min)	τ_{EM} (min)	τ_{50} (min)	τ_{90} (min)	SC_{EO} (µS/cm)	SC_{EM} (µS/cm)	SC_{50} (µS/cm)	SC_{90} (µS/cm)
2008-01-07 13:30	45	60	151	307	701	284	493	663
2008-04-10 10:30	105	165	248	302	677	570	623	666
2008-04-10 15:30	90	90	111	--	662	535	598	649
2008-04-10 17:30	45	60	85	115	626	453	539	608
2008-04-17 08:30	120	135	176	212	656	570	613	647
2008-04-18 10:30	90	195	233	333	658	401	530	633
2008-04-22 02:30	75	75	118	186	652	496	574	637
2008-05-23 06:00	60	75	145	201	622	442	532	604
2008-05-29 04:30	60	60	111	229	626	216	421	585
2008-06-27 17:00	15	60	102	441	634	165	399	587
2008-07-06 18:30	135	150	224	324	651	580	615	644
2008-07-07 16:00	15	60	95	176	650	180	415	603
2008-07-09 14:30	90	90	140	198	652	513	583	638
2008-07-17 14:15	15	30	611	1005	677	46	361	614
2008-07-19 18:00	60	75	113	143	590	137	364	545
2008-07-21 01:30	105	150	219	264	595	470	533	582
2008-07-24 05:30	165	210	224	303	667	499	583	651
2008-08-12 07:00	240	300	437	572	714	353	533	678
2008-08-27 07:00	210	225	272	--	799	382	590	757
2008-09-08 03:30	270	285	309	433	824	153	488	757
2008-10-13 12:00	240	270	329	--	853	124	488	780
2008-10-14 17:00	330	480	980	1298	718	163	440	662
2008-10-23 10:30	255	300	392	491	795	410	602	756
2008-10-24 06:00	60	240	674	839	799	261	530	745

Appendix B1

End member mixing analysis (EMMA) for the May 6, 2007 event.

Date/Time, τ_S	T_{DF} (°C)	SC_{DF} (µS/cm)	Q_{DF} (m^3/s)	Q_{FF} (m^3/s)	Q_{SF} (m^3/s)	Q_{FF} (%)	Q_{SF} (%)
2007-05-06 02:30	8.4	592	2.631E-03	3.849E-06	2.627E-06	0.15	99.85
2007-05-06 02:45	8.4	592	2.044E-03	2.287E-06	2.042E-06	0.11	99.89
2007-05-06 03:00	8.4	592	2.006E-03	2.590E-06	2.004E-06	0.13	99.87
2007-05-06 03:15	8.4	592	2.189E-03	2.826E-06	2.186E-06	0.13	99.87
2007-05-06 03:30	8.4	592	2.208E-03	2.851E-06	2.205E-06	0.13	99.87
2007-05-06 03:45	8.4	592	2.145E-03	3.508E-06	2.142E-06	0.16	99.84
2007-05-06 04:00	8.4	592	2.019E-03	3.301E-06	2.016E-06	0.16	99.84
2007-05-06 04:15	8.4	592	2.240E-03	2.891E-06	2.237E-06	0.13	99.87
2007-05-06 04:30	8.4	592	1.943E-03	1.840E-06	1.941E-06	0.09	99.91
2007-05-06 04:45	8.4	592	1.520E-03	1.963E-06	1.519E-06	0.13	99.87
2007-05-06 05:00	8.4	592	1.666E-03	2.437E-06	1.663E-06	0.15	99.85
2007-05-06 05:15	8.4	592	1.905E-03	2.460E-06	1.903E-06	0.13	99.87
2007-05-06 05:30	8.4	592	1.886E-03	2.435E-06	1.884E-06	0.13	99.87
2007-05-06 05:45	8.4	592	1.949E-03	2.852E-06	1.947E-06	0.15	99.85
2007-05-06 06:00	8.4	593	2.397E-03	1.444E-06	2.396E-06	0.06	99.94
2007-05-06 06:15	8.4	593	1.931E-03	-8.308E-07	1.931E-07	-0.04	100.04
2007-05-06 06:30	8.5	593	2.101E-03	1.808E-07	2.101E-07	0.01	99.99
2007-05-06 06:45	8.5	592	2.795E-03	3.127E-06	2.792E-06	0.11	99.89
2007-05-06 07:00	8.5	596	2.637E-03	-1.430E-05	2.651E-05	-0.54	100.54
2007-05-06 07:15	8.5	433	2.095E-03	5.771E-04	1.518E-04	27.55	72.45
2007-05-06 07:30	8.7	479	3.647E-03	7.178E-04	2.929E-04	19.68	80.32
2007-05-06 07:45	8.8	464	5.186E-03	1.154E-04	4.032E-04	22.25	77.75
2007-05-06 08:00	9.0	398	5.401E-03	1.809E-03	3.592E-04	33.49	66.51
2007-05-06 08:15	9.2	383	5.823E-03	2.108E-03	3.715E-04	36.21	63.79
2007-05-06 08:30	9.3	360	6.940E-03	2.786E-03	4.154E-04	40.15	59.85
2007-05-06 08:45	9.4	355	6.233E-03	2.555E-03	3.678E-04	40.99	59.01
2007-05-06 09:00	9.4	360	6.435E-03	2.583E-03	3.853E-04	40.13	59.87
2007-05-06 09:15	9.4	371	5.886E-03	2.247E-03	3.639E-04	38.17	61.83
2007-05-06 09:30	9.3	411	5.653E-03	1.772E-03	3.880E-04	31.35	68.65
2007-05-06 09:45	9.2	448	5.666E-03	1.417E-03	4.248E-04	25.02	74.98

Date/Time, τ_S	T_{DF} (°C)	SC_{DF} (µS/cm)	Q_{DF} (m^3/s)	Q_{FF} (m^3/s)	Q_{SF} (m^3/s)	Q_{FF} (%)	Q_{SF} (%)
2007-05-06 10:00	9.2	456	6.038E-03	1.426E-03	4.611E-03	23.63	76.37
2007-05-06 10:15	9.2	470	5.470E-03	1.158E-03	4.312E-03	21.16	78.84
2007-05-06 10:30	9.2	495	6.088E-03	1.025E-03	5.063E-03	16.84	83.16
2007-05-06 10:45	9.2	502	6.088E-03	9.500E-04	5.138E-03	15.60	84.40
2007-05-06 11:00	9.1	511	6.309E-03	8.921E-04	5.417E-03	14.14	85.86
2007-05-06 11:15	9.1	524	5.823E-03	6.871E-04	5.136E-03	11.80	88.20
2007-05-06 11:30	9.1	533	6.751E-03	7.013E-04	6.049E-03	10.39	89.61
2007-05-06 11:45	9.1	542	5.514E-03	4.807E-04	5.033E-03	8.72	91.28
2007-05-06 12:00	9.1	551	6.498E-03	4.648E-04	6.034E-03	7.15	92.85
2007-05-06 12:15	9.0	561	6.688E-03	3.735E-04	6.314E-03	5.59	94.41
2007-05-06 12:30	9.0	567	5.766E-03	2.576E-04	5.509E-03	4.47	95.53
2007-05-06 12:45	9.0	571	5.968E-03	2.255E-04	5.743E-03	3.78	96.22
2007-05-06 13:00	9.0	574	5.949E-03	1.951E-04	5.754E-03	3.28	96.72
2007-05-06 13:15	9.0	576	6.151E-03	1.826E-04	5.969E-03	2.97	97.03
2007-05-06 13:30	8.9	577	6.751E-03	1.819E-04	6.569E-03	2.69	97.31
2007-05-06 13:45	8.9	579	6.561E-03	1.621E-04	6.399E-03	2.47	97.53
2007-05-06 14:00	8.9	580	6.688E-03	1.537E-04	6.534E-03	2.30	97.70
2007-05-06 14:15	8.9	581	6.132E-03	1.314E-04	6.001E-03	2.14	97.86
2007-05-06 14:30	8.9	582	6.309E-03	1.222E-04	6.187E-03	1.94	98.06
2007-05-06 14:45	8.9	583	5.602E-03	9.788E-05	5.505E-03	1.75	98.25
2007-05-06 15:00	8.9	584	5.527E-03	8.895E-05	5.438E-03	1.61	98.39
2007-05-06 15:15	8.9	585	5.956E-03	8.663E-05	5.869E-03	1.45	98.55
2007-05-06 15:30	8.9	585	6.221E-03	8.406E-05	6.137E-03	1.35	98.65
2007-05-06 15:45	8.8	586	6.561E-03	7.849E-05	6.483E-03	1.20	98.80
2007-05-06 16:00	8.8	587	5.445E-03	5.764E-05	5.387E-03	1.06	98.94
2007-05-06 16:15	8.8	587	5.880E-03	5.617E-05	5.824E-03	0.96	99.04
2007-05-06 16:30	8.8	588	5.766E-03	5.211E-05	5.714E-03	0.90	99.10
2007-05-06 16:45	8.8	588	6.498E-03	5.537E-05	6.443E-03	0.85	99.15
2007-05-06 17:00	8.8	588	6.132E-03	4.908E-05	6.083E-03	0.80	99.20
2007-05-06 17:15	8.8	589	5.956E-03	4.562E-05	5.910E-03	0.77	99.23
2007-05-06 17:30	8.8	589	6.151E-03	4.288E-05	6.108E-03	0.70	99.30
2007-05-06 17:45	8.8	589	6.296E-03	4.281E-05	6.254E-03	0.68	99.32

Date/Time, τ_S	T_{DF} (°C)	SC_{DF} (µS/cm)	Q_{DF} (m^3/s)	Q_{FF} (m^3/s)	Q_{SF} (m^3/s)	Q_{FF} (%)	Q_{SF} (%)
2007-05-06 18:00	8.8	589	5.912E-03	3.714E-05	5.874E-03	0.63	99.37
2007-05-06 18:15	8.8	590	6.126E-03	3.533E-05	6.091E-03	0.58	99.42
2007-05-06 18:15	8.8	590	6.126E-03	3.533E-05	6.091E-03	0.58	99.42
2007-05-06 18:30	8.8	590	6.221E-03	3.159E-05	6.189E-03	0.51	99.49
2007-05-06 18:45	8.7	590	5.760E-03	2.826E-05	5.732E-03	0.49	99.51
2007-05-06 19:00	8.7	590	5.848E-03	2.970E-05	5.819E-03	0.51	99.49
2007-05-06 19:15	8.7	590	5.703E-03	2.896E-05	5.674E-03	0.51	99.49
2007-05-06 19:30	8.7	590	6.372E-03	3.126E-05	6.341E-03	0.49	99.51
2007-05-06 19:45	8.7	590	5.489E-03	2.409E-05	5.465E-03	0.44	99.56
2007-05-06 20:00	8.7	590	5.779E-03	2.537E-05	5.754E-03	0.44	99.56
2007-05-06 20:15	8.7	590	6.233E-03	2.843E-05	6.205E-03	0.46	99.54
2007-05-06 20:30	8.7	591	6.435E-03	2.714E-05	6.408E-03	0.42	99.58
2007-05-06 20:45	8.7	591	6.139E-03	2.483E-05	6.114E-03	0.40	99.60
2007-05-06 21:00	8.7	591	5.949E-03	2.407E-05	5.925E-03	0.40	99.60
2007-05-06 21:15	8.7	591	5.464E-03	2.116E-05	5.442E-03	0.39	99.61
2007-05-06 21:30	8.7	591	5.716E-03	2.214E-05	5.694E-03	0.39	99.61
2007-05-06 21:45	8.7	591	5.628E-03	2.276E-05	5.605E-03	0.40	99.60
2007-05-06 22:00	8.7	591	6.498E-03	2.629E-05	6.472E-03	0.40	99.60
2007-05-06 22:15	8.7	591	5.981E-03	2.213E-05	5.959E-03	0.37	99.63
2007-05-06 22:30	8.7	591	5.590E-03	2.069E-05	5.569E-03	0.37	99.63
2007-05-06 22:45	8.7	591	5.937E-03	2.197E-05	5.915E-03	0.37	99.63
2007-05-06 23:00	8.7	591	5.867E-03	2.070E-05	5.847E-03	0.35	99.65
2007-05-06 23:15	8.7	591	6.170E-03	2.071E-05	6.150E-03	0.34	99.66
2007-05-06 23:30	8.7	591	5.293E-03	1.686E-05	5.276E-03	0.32	99.68
2007-05-06 23:45	8.7	591	6.025E-03	1.919E-05	6.006E-03	0.32	99.68
2007-05-07 00:00	8.7	591	6.101E-03	1.943E-05	6.081E-03	0.32	99.68

Appendix B2

End member mixing analysis (EMMA) for the October 14-15, 2008 event.

Date/Time, τ_S	T_{DF} (°C)	SC_{DF} (µS/cm)	Q_{DF} (m^3/s)	Q_{FF} (m^3/s)	Q_{SF} (m^3/s)	Q_{FF} (%)	Q_{SF} (%)
2008-10-14 17:00	14.1	711	7.929E-06	7.305E-08	7.856E-06	0.92	99.08
2008-10-14 17:15	13.7	711	1.189E-05	1.096E-07	1.178E-05	0.92	99.08
2008-10-14 17:30	13.4	715	1.699E-05	6.021E-08	1.693E-05	0.35	99.65
2008-10-14 17:45	13.4	718	1.699E-05	-1.204E-08	1.700E-05	-0.07	100.07
2008-10-14 18:00	13.3	717	1.699E-05	1.204E-08	1.698E-05	0.07	99.93
2008-10-14 18:15	13.3	720	1.444E-05	-5.118E-08	1.449E-05	-0.35	100.35
2008-10-14 18:30	14.1	723	1.444E-05	-1.126E-07	1.455E-05	-0.78	100.78
2008-10-14 18:45	14.4	721	1.982E-04	-9.834E-07	1.992E-04	-0.50	100.50
2008-10-14 19:00	14.4	718	5.550E-04	-3.933E-07	5.554E-04	-0.07	100.07
2008-10-14 19:15	14.7	712	5.550E-04	4.327E-06	5.507E-04	0.78	99.22
2008-10-14 19:30	14.4	714	1.982E-04	9.834E-07	1.972E-04	0.50	99.50
2008-10-14 19:45	14.6	715	1.982E-04	7.024E-07	1.975E-04	0.35	99.65
2008-10-14 21:45	14.5	694	5.550E-04	1.833E-05	5.367E-04	3.30	96.70
2008-10-14 22:30	14.4	466	1.076E-03	3.837E-04	6.923E-04	35.66	64.34
2008-10-14 22:45	14.4	344	1.794E-03	9.508E-04	8.428E-04	53.01	46.99
2008-10-14 23:00	14.3	335	2.080E-03	1.129E-03	9.506E-04	54.29	45.71
2008-10-14 23:15	14.3	334	1.794E-03	9.742E-04	8.194E-04	54.32	45.68
2008-10-14 23:30	14.1	341	1.794E-03	9.582E-04	8.354E-04	53.42	46.58
2008-10-14 23:45	14.1	356	1.794E-03	9.188E-04	8.748E-04	51.23	48.77
2008-10-15 00:00	14.0	381	1.794E-03	8.552E-04	9.384E-04	47.68	52.32
2008-10-15 00:15	13.7	304	1.535E-03	8.991E-04	6.357E-04	58.58	41.42
2008-10-15 00:30	13.3	264	1.076E-03	6.923E-04	3.837E-04	64.34	35.66
2008-10-15 00:45	13.0	201	5.550E-04	4.063E-04	1.487E-04	73.21	26.79
2008-10-15 01:00	12.9	163	1.076E-03	8.451E-04	2.309E-04	78.54	21.46
2008-10-15 01:30	13.1	207	1.794E-03	1.297E-03	4.968E-04	72.30	27.70
2008-10-15 01:45	13.3	208	1.076E-03	7.779E-04	2.982E-04	72.29	27.71
2008-10-15 02:00	13.3	206	2.080E-03	1.509E-03	5.707E-04	72.56	27.44
2008-10-15 02:15	13.3	217	1.794E-03	1.272E-03	5.217E-04	70.91	29.09
2008-10-15 02:30	13.3	244	1.794E-03	1.205E-03	5.890E-04	67.16	32.84
2008-10-15 03:00	13.4	347	1.535E-03	8.056E-04	7.292E-04	52.49	47.51

Date/Time, τ_S	T_{DF} (°C)	SC_{DF} (µS/cm)	Q_{DF} (m^3/s)	Q_{FF} (m^3/s)	Q_{SF} (m^3/s)	Q_{FF} (%)	Q_{SF} (%)
2008-10-15 03:15	13.4	277	1.535E-03	9.589E-04	5.758E-04	62.48	37.52
2008-10-15 03:30	13.4	266	1.794E-03	1.147E-03	6.463E-04	63.97	36.03
2008-10-15 03:45	13.4	327	1.076E-03	5.962E-04	4.798E-04	55.41	44.59
2008-10-15 04:00	13.4	298	1.076E-03	6.395E-04	4.365E-04	59.43	40.57
2008-10-15 04:15	13.4	303	1.535E-03	9.019E-04	6.328E-04	58.77	41.23
2008-10-15 04:30	13.4	290	1.535E-03	9.307E-04	6.041E-04	60.64	39.36
2008-10-15 04:45	13.5	284	2.080E-03	1.278E-03	8.018E-04	61.45	38.55
2008-10-15 05:00	13.5	289	1.535E-03	9.313E-04	6.035E-04	60.68	39.32
2008-10-15 05:15	13.5	307	1.535E-03	8.921E-04	6.426E-04	58.13	41.87
2008-10-15 05:30	13.5	364	1.076E-03	5.399E-04	5.361E-04	50.18	49.82
2008-10-15 05:45	13.5	335	1.076E-03	5.831E-04	4.929E-04	54.19	45.81
2008-10-15 06:00	13.5	409	5.550E-04	2.431E-04	3.119E-04	43.80	56.20
2008-10-15 06:15	13.5	368	5.550E-04	2.750E-04	2.800E-04	49.55	50.45
2008-10-15 06:30	13.5	339	5.550E-04	2.976E-04	2.574E-04	53.62	46.38
2008-10-15 06:45	13.6	313	5.550E-04	3.181E-04	2.369E-04	57.32	42.68
2008-10-15 07:00	13.6	316	1.982E-04	1.127E-04	8.547E-05	56.88	43.12
2008-10-15 07:15	13.6	320	1.982E-04	1.117E-04	8.651E-05	56.36	43.64
2008-10-15 07:30	13.7	315	5.550E-04	3.170E-04	2.380E-04	57.12	42.88
2008-10-15 07:45	13.7	304	1.982E-04	1.161E-04	8.215E-05	58.55	41.45
2008-10-15 08:00	13.7	302	1.982E-04	1.167E-04	8.153E-05	58.87	41.13
2008-10-15 08:15	13.8	308	1.982E-04	1.152E-04	8.305E-05	58.10	41.90
2008-10-15 08:30	13.8	319	8.495E-05	4.802E-05	3.693E-05	56.53	43.47
2008-10-15 08:45	13.8	335	8.495E-05	4.611E-05	3.884E-05	54.27	45.73
2008-10-15 09:00	13.9	356	8.495E-05	4.352E-05	4.143E-05	51.23	48.77
2008-10-15 09:15	13.9	418	8.495E-05	3.605E-05	4.890E-05	42.44	57.56
2008-10-15 09:30	13.9	485	8.495E-05	2.795E-05	5.700E-05	32.90	67.10
2008-10-15 09:45	13.9	484	8.495E-05	2.808E-05	5.687E-05	33.05	66.95
2008-10-15 10:00	14.0	488	5.097E-05	1.660E-05	3.437E-05	32.57	67.43
2008-10-15 10:15	14.0	494	5.097E-05	1.613E-05	3.484E-05	31.65	68.35
2008-10-15 10:30	14.0	501	5.097E-05	1.565E-05	3.532E-05	30.70	69.30
2008-10-15 10:45	14.0	509	5.097E-05	1.503E-05	3.594E-05	29.50	70.50
2008-10-15 11:00	14.1	528	5.097E-05	1.368E-05	3.729E-05	26.83	73.17

Date/Time, τ_S	T_{DF} (°C)	SC_{DF} (µS/cm)	Q_{DF} (m^3/s)	Q_{FF} (m^3/s)	Q_{SF} (m^3/s)	Q_{FF} (%)	Q_{SF} (%)
2008-10-15 11:15	14.1	579	5.097E-05	9.977E-06	4.099E-05	19.57	80.43
2008-10-15 11:30	14.1	579	5.097E-05	9.985E-06	4.099E-05	19.59	80.41
2008-10-15 11:45	14.1	566	5.097E-05	1.098E-05	3.999E-05	21.55	78.45
2008-10-15 12:00	14.1	567	3.681E-05	7.858E-06	2.895E-05	21.35	78.65
2008-10-15 12:15	14.2	576	5.097E-05	1.023E-05	4.074E-05	20.07	79.93
2008-10-15 12:30	14.1	588	5.097E-05	9.385E-06	4.159E-05	18.41	81.59
2008-10-15 12:45	14.2	592	5.097E-05	9.053E-06	4.192E-05	17.76	82.24
2008-10-15 13:00	14.2	591	5.097E-05	9.118E-06	4.185E-05	17.89	82.11
2008-10-15 13:15	14.2	587	5.097E-05	9.464E-06	4.151E-05	18.57	81.43
2008-10-15 13:30	14.2	585	5.097E-05	9.573E-06	4.140E-05	18.78	81.22
2008-10-15 13:45	14.2	592	5.097E-05	9.081E-06	4.189E-05	17.82	82.18
2008-10-15 14:00	14.2	609	5.097E-05	7.853E-06	4.312E-05	15.41	84.59
2008-10-15 14:15	14.2	631	5.097E-05	6.264E-06	4.471E-05	12.29	87.71
2008-10-15 14:30	14.2	653	5.097E-05	4.696E-06	4.627E-05	9.21	90.79
2008-10-15 14:45	14.2	670	5.097E-05	3.403E-06	4.757E-05	6.68	93.32
2008-10-15 15:00	14.2	686	5.097E-05	2.283E-06	4.869E-05	4.48	95.52
2008-10-15 15:15	14.3	699	5.097E-05	1.344E-06	4.963E-05	2.64	97.36
2008-10-15 15:30	14.3	710	3.681E-05	3.913E-07	3.642E-05	1.06	98.94

Appendix B3

End member mixing analysis (EMMA) for the May 29-30, 2008 event.

Date/Time, τ_S	T_{DF} (°C)	SC_{DF} (µS/cm)	Q_{DF} (m^3/s)	Q_{FF} (m^3/s)	Q_{SF} (m^3/s)	Q_{FF} (%)	Q_{SF} (%)
2008-05-29 03:30	9.2	626	2.394E-03	--	--	--	--
2008-05-29 03:45	9.2	625	2.394E-03	--	--	--	--
2008-05-29 04:00	9.3	626	2.394E-03	--	--	--	--
2008-05-29 04:15	9.3	626	2.394E-03	4.877E-08	2.394E-03	0.00	100.00
2008-05-29 04:45	9.3	626	2.394E-03	4.877E-08	2.394E-03	0.00	100.00
2008-05-29 05:00	9.3	626	2.394E-03	4.877E-08	2.394E-03	0.00	100.00
2008-05-29 05:15	9.3	625	2.394E-03	1.609E-06	2.392E-03	0.07	99.93
2008-05-29 05:30	9.6	216	2.394E-03	1.598E-03	7.959E-04	66.75	33.25
2008-05-29 05:45	10.0	398	2.394E-03	8.861E-04	1.508E-03	37.02	62.98
2008-05-29 06:00	10.1	391	2.737E-03	1.047E-03	1.690E-03	38.26	61.74
2008-05-29 06:15	10.1	407	2.080E-03	7.397E-04	1.340E-03	35.57	64.43
2008-05-29 06:30	10.1	441	2.394E-03	7.203E-04	1.673E-03	30.09	69.91
2008-05-29 06:45	10.1	453	2.394E-03	6.727E-04	1.721E-03	28.10	71.90
2008-05-29 07:00	10.1	462	2.394E-03	6.391E-04	1.755E-03	26.70	73.30
2008-05-29 07:15	10.0	486	1.535E-03	3.483E-04	1.187E-03	22.69	77.31
2008-05-29 07:30	10.1	526	2.080E-03	3.366E-04	1.743E-03	16.19	83.81
2008-05-29 07:45	10.0	479	2.394E-03	5.712E-04	1.822E-03	23.86	76.14
2008-05-29 08:00	9.9	543	2.080E-03	2.814E-04	1.798E-03	13.53	86.47
2008-05-29 08:15	9.8	578	2.394E-03	1.854E-04	2.208E-03	7.74	92.26
2008-05-29 08:30	9.8	603	2.737E-03	1.018E-04	2.636E-03	3.72	96.28
2008-05-29 08:45	9.7	626	2.080E-03	4.237E-08	2.080E-03	0.00	100.00
2008-05-29 09:00	9.7	644	2.394E-03	-7.096E-05	2.465E-03	-2.96	102.96
2008-05-29 09:15	9.7	661	2.394E-03	-1.365E-04	2.530E-03	-5.70	105.70
2008-05-29 09:30	9.6	631	2.080E-03	-1.860E-05	2.098E-03	-0.89	100.89
2008-05-29 09:45	9.7	696	2.080E-03	-2.403E-04	2.320E-03	-1155	111.55
2008-05-29 10:00	9.9	486	2.394E-03	5.451E-04	1.849E-03	22.77	77.23
2008-05-29 10:15	10.0	428	2.394E-03	7.714E-04	1.622E-03	32.23	67.77
2008-05-29 10:30	10.1	449	2.394E-03	6.898E-04	1.704E-03	28.82	71.18
2008-05-29 10:45	10.1	230	2.737E-03	1.765E-03	9.727E-04	64.47	35.53

Date/Time, τ_S	T_{DF} (°C)	SC_{DF} (µS/cm)	Q_{DF} (m^3/s)	Q_{FF} (m^3/s)	Q_{SF} (m^3/s)	Q_{FF} (%)	Q_{SF} (%)
2008-05-29 11:00	10.0	48	2.080E-03	1.958E-03	1.218E-04	94.14	5.86
2008-05-29 11:15	10.0	8	2.080E-03	2.094E-03	-1.430E-05	100.6	-0.69
2008-05-29 11:30	10.0	193	2.394E-03	1.687E-03	7.066E-04	70.48	29.52
2008-05-29 11:45	10.0	143	2.080E-03	1.636E-03	4.440E-04	78.65	21.35
2008-05-29 12:00	9.9	65	2.080E-03	1.901E-03	1.788E-04	91.40	8.60
2008-05-29 12:15	9.9	213	2.080E-03	1.399E-03	6.806E-04	67.27	32.73
2008-05-29 12:45	9.9	133	2.080E-03	1.669E-03	4.101E-04	80.28	19.72
2008-05-29 13:00	10.0	117	2.080E-03	1.724E-03	3.556E-04	82.90	17.10
2008-05-29 13:15	10.0	454	5.000E-03	1.395E-03	3.605E-03	27.91	72.09
2008-05-29 13:30	10.0	452	5.000E-03	1.413E-03	3.587E-03	28.27	71.73
2008-05-29 13:45	10.0	445	5.000E-03	1.470E-03	3.530E-03	29.39	70.61
2008-05-29 14:00	10.0	457	5.000E-03	1.375E-03	3.625E-03	27.50	72.50
2008-05-29 14:15	10.0	463	5.000E-03	1.324E-03	3.676E-03	26.47	73.53
2008-05-29 14:30	10.0	449	5.000E-03	1.442E-03	3.558E-03	28.84	71.16
2008-05-29 14:45	10.0	459	5.000E-03	1.356E-03	3.644E-03	27.12	72.88
2008-05-29 15:00	10.0	404	5.000E-03	1.805E-03	3.195E-03	36.11	63.89
2008-05-29 15:15	10.1	454	5.000E-03	1.400E-03	3.600E-03	28.00	72.00
2008-05-29 15:30	10.0	475	5.000E-03	1.227E-03	3.773E-03	24.53	75.47
2008-05-29 15:45	10.1	483	5.000E-03	1.158E-03	3.842E-03	23.16	76.84
2008-05-29 16:00	10.1	483	5.000E-03	1.166E-03	3.834E-03	23.31	76.69
2008-05-29 16:15	10.1	483	5.000E-03	1.163E-03	3.837E-03	23.26	76.74
2008-05-29 16:30	10.2	482	5.000E-03	1.168E-03	3.832E-03	23.36	76.64
2008-05-29 16:45	10.2	484	5.000E-03	1.154E-03	3.846E-03	23.08	76.92
2008-05-29 17:00	10.2	482	5.000E-03	1.170E-03	3.830E-03	23.41	76.59
2008-05-29 17:15	10.3	481	5.000E-03	1.177E-03	3.823E-03	23.54	76.46
2008-05-29 17:30	10.3	481	5.000E-03	1.178E-03	3.822E-03	23.55	76.45
2008-05-29 17:45	10.4	481	5.000E-03	1.179E-03	3.821E-03	23.57	76.43
2008-05-29 18:00	10.4	481	5.000E-03	1.181E-03	3.819E-03	23.62	76.38
2008-05-29 18:15	10.4	479	5.000E-03	1.195E-03	3.805E-03	23.90	76.10
2008-05-29 18:30	10.4	480	5.000E-03	1.184E-03	3.816E-03	23.69	76.31
2008-05-29 18:45	10.4	538	5.000E-03	7.099E-04	4.290E-03	14.20	85.80
2008-05-29 19:00	10.1	562	5.000E-03	5.144E-04	4.486E-03	10.29	89.71

Date/Time, τ_S	T_{DF} (°C)	SC_{DF} (µS/cm)	Q_{DF} (m^3/s)	Q_{FF} (m^3/s)	Q_{SF} (m^3/s)	Q_{FF} (%)	Q_{SF} (%)
2008-05-29 19:15	10.0	572	5.000E-03	4.394E-04	4.561E-03	8.79	91.21
2008-05-29 19:45	9.9	618	5.000E-03	6.530E-05	4.935E-03	1.31	98.69
2008-05-29 20:00	9.9	598	5.000E-03	2.275E-04	4.773E-03	4.55	95.45
2008-05-29 20:15	9.9	590	5.000E-03	2.894E-04	4.711E-03	5.79	94.21
2008-05-29 20:30	9.8	590	5.000E-03	2.886E-04	4.711E-03	5.77	94.23
2008-05-29 20:45	9.8	592	5.000E-03	2.764E-04	4.724E-03	5.53	94.47
2008-05-29 21:00	9.8	593	5.000E-03	2.674E-04	4.733E-03	5.35	94.65
2008-05-29 21:15	9.8	587	5.000E-03	3.147E-04	4.685E-03	6.29	93.71
2008-05-29 21:30	9.8	592	5.000E-03	2.731E-04	4.727E-03	5.46	94.54
2008-05-29 21:45	9.8	527	5.000E-03	8.029E-04	4.197E-03	16.06	83.94
2008-05-29 22:00	10.6	455	5.000E-03	1.386E-03	3.614E-03	27.73	72.27
2008-05-29 22:15	10.6	471	5.000E-03	1.263E-03	3.737E-03	25.27	74.73
2008-05-29 22:30	10.6	479	5.000E-03	1.194E-03	3.806E-03	23.88	76.12
2008-05-29 22:45	10.6	483	5.000E-03	1.163E-03	3.837E-03	23.26	76.74
2008-05-29 23:00	10.7	464	5.000E-03	1.313E-03	3.687E-03	26.26	73.74
2008-05-29 23:15	10.8	464	5.000E-03	1.320E-03	3.680E-03	26.41	73.59
2008-05-29 23:30	10.8	456	5.000E-03	1.381E-03	3.619E-03	27.61	72.39
2008-05-29 23:45	10.8	464	5.000E-03	1.318E-03	3.682E-03	26.36	73.64
2008-05-30 00:00	10.8	472	5.000E-03	1.253E-03	3.747E-03	25.05	74.95
2008-05-30 00:15	10.6	533	5.000E-03	7.507E-04	4.249E-03	15.01	84.99
2008-05-30 00:30	10.6	490	5.000E-03	1.105E-03	3.895E-03	22.10	77.90
2008-05-30 00:45	10.8	469	5.000E-03	1.278E-03	3.722E-03	25.56	74.44
2008-05-30 01:00	10.8	469	5.000E-03	1.275E-03	3.725E-03	25.49	74.51
2008-05-30 01:15	10.7	485	5.000E-03	1.149E-03	3.851E-03	22.98	77.02
2008-05-30 01:30	10.7	497	5.000E-03	1.051E-03	3.949E-03	21.01	78.99
2008-05-30 01:45	10.6	507	5.000E-03	9.642E-04	4.036E-03	19.28	80.72
2008-05-30 02:00	10.4	550	5.000E-03	6.130E-04	4.387E-03	12.26	87.74
2008-05-30 02:15	10.3	553	5.000E-03	5.885E-04	4.411E-03	11.77	88.23
2008-05-30 02:30	10.3	548	5.000E-03	6.325E-04	4.367E-03	12.65	87.35
2008-05-30 02:45	10.4	525	5.000E-03	8.183E-04	4.182E-03	16.37	83.63
2008-05-30 03:00	10.7	480	5.000E-03	1.183E-03	3.817E-03	23.65	76.35
2008-05-30 03:15	10.7	489	5.000E-03	1.112E-03	3.888E-03	22.23	77.77

Date/Time, τ_S	T_{DF} (°C)	SC_{DF} (µS/cm)	Q_{DF} (m^3/s)	Q_{FF} (m^3/s)	Q_{SF} (m^3/s)	Q_{FF} (%)	Q_{SF} (%)
2008-05-30 03:30	10.7	494	5.000E-03	1.073E-03	3.927E-03	21.47	78.53
2008-05-30 03:45	10.7	491	5.000E-03	1.094E-03	3.906E-03	21.88	78.12
2008-05-30 04:00	10.7	489	5.000E-03	1.116E-03	3.884E-03	22.32	77.68
2008-05-30 04:15	10.8	480	5.000E-03	1.190E-03	3.810E-03	23.80	76.20
2008-05-30 04:30	10.7	488	5.000E-03	1.120E-03	3.880E-03	22.40	77.60
2008-05-30 04:45	10.7	493	5.000E-03	1.079E-03	3.921E-03	21.58	78.42
2008-05-30 05:00	10.7	495	5.000E-03	1.064E-03	3.936E-03	21.27	78.73
2008-05-30 05:15	10.6	505	5.000E-03	9.822E-04	4.018E-03	19.64	80.36
2008-05-30 05:30	10.6	511	5.000E-03	9.365E-04	4.063E-03	18.73	81.27
2008-05-30 05:45	10.6	512	5.000E-03	9.259E-04	4.074E-03	18.52	81.48
2008-05-30 06:00	10.6	513	5.000E-03	9.186E-04	4.081E-03	18.37	81.63
2008-05-30 06:15	10.6	513	5.000E-03	9.137E-04	4.086E-03	18.27	81.73
2008-05-30 06:30	10.6	515	5.000E-03	8.974E-04	4.103E-03	17.95	82.05
2008-05-30 06:45	10.6	518	5.000E-03	8.738E-04	4.126E-03	17.48	82.52
2008-05-30 07:00	10.6	521	5.000E-03	8.501E-04	4.150E-03	17.00	83.00
2008-05-30 07:15	10.6	520	5.000E-03	8.566E-04	4.143E-03	17.13	82.87
2008-05-30 07:30	10.7	522	5.000E-03	8.412E-04	4.159E-03	16.82	83.18
2008-05-30 07:45	10.7	529	5.000E-03	7.857E-04	4.214E-03	15.71	84.29
2008-05-30 08:00	10.5	568	5.000E-03	4.671E-04	4.533E-03	9.34	90.66
2008-05-30 08:15	10.4	572	5.000E-03	4.394E-04	4.561E-03	8.79	91.21
2008-05-30 08:30	10.3	574	5.000E-03	4.198E-04	4.580E-03	8.40	91.60
2008-05-30 08:45	10.3	577	5.000E-03	3.937E-04	4.606E-03	7.87	92.13
2008-05-30 09:00	10.2	579	5.000E-03	3.799E-04	4.620E-03	7.60	92.40
2008-05-30 09:15	10.2	580	5.000E-03	3.701E-04	4.630E-03	7.40	92.60
2008-05-30 09:30	10.2	581	5.000E-03	3.611E-04	4.639E-03	7.22	92.78
2008-05-30 10:00	10.2	586	5.000E-03	3.236E-04	4.676E-03	6.47	93.53
2008-05-30 10:15	10.2	588	5.000E-03	3.025E-04	4.698E-03	6.05	93.95
2008-05-30 10:30	10.2	583	5.000E-03	3.473E-04	4.653E-03	6.95	93.05
2008-05-30 10:45	10.2	578	5.000E-03	3.848E-04	4.615E-03	7.70	92.30
2008-05-30 11:00	10.3	574	5.000E-03	4.182E-04	4.582E-03	8.36	91.64
2008-05-30 11:15	10.4	570	5.000E-03	4.508E-04	4.549E-03	9.02	90.98
2008-05-30 11:30	10.4	567	5.000E-03	4.769E-04	4.523E-03	9.54	90.46

Date/Time, τ_S	T_{DF} (°C)	SC_{DF} (µS/cm)	Q_{DF} (m^3/s)	Q_{FF} (m^3/s)	Q_{SF} (m^3/s)	Q_{FF} (%)	Q_{SF} (%)
2008-05-30 11:45	10.5	563	5.000E-03	5.095E-04	4.491E-03	10.19	89.81
2008-05-30 12:00	10.5	560	5.000E-03	5.364E-04	4.464E-03	10.73	89.27
2008-05-30 12:15	10.6	558	5.000E-03	5.527E-04	4.447E-03	11.05	88.95
2008-05-30 12:30	10.7	554	5.000E-03	5.804E-04	4.420E-03	11.61	88.39
2008-05-30 12:45	10.8	553	5.000E-03	5.942E-04	4.406E-03	11.88	88.12
2008-05-30 13:00	10.9	549	5.000E-03	6.227E-04	4.377E-03	12.45	87.55
2008-05-30 13:15	11.0	547	5.000E-03	6.423E-04	4.358E-03	12.85	87.15
2008-05-30 13:30	11.1	542	5.000E-03	6.773E-04	4.323E-03	13.55	86.45
2008-05-30 13:45	11.3	538	5.000E-03	7.099E-04	4.290E-03	14.20	85.80
2008-05-30 14:00	11.4	537	5.000E-03	7.230E-04	4.277E-03	14.46	85.54
2008-05-30 14:15	11.5	534	5.000E-03	7.442E-04	4.256E-03	14.88	85.12
2008-05-30 14:30	11.6	532	5.000E-03	7.637E-04	4.236E-03	15.27	84.73
2008-05-30 14:45	11.7	529	5.000E-03	7.882E-04	4.212E-03	15.76	84.24
2008-05-30 15:00	11.9	526	5.000E-03	8.151E-04	4.185E-03	16.30	83.70
2008-05-30 15:15	12.0	524	5.000E-03	8.265E-04	4.174E-03	16.53	83.47
2008-05-30 15:30	12.1	523	5.000E-03	8.363E-04	4.164E-03	16.73	83.27
2008-05-30 15:45	12.2	519	5.000E-03	8.664E-04	4.134E-03	17.33	82.67
2008-05-30 16:00	12.3	517	5.000E-03	8.876E-04	4.112E-03	17.75	82.25

Appendix C

The following are the results of the soil specific calibration for the EC-5 (Decagon) with Campbell datalogger. A small, representative sample from the Blairsburg field site was sent to Doug Cobos, research scientist with Decagon Devices. To establish the linear regression, the soil sample was increasingly wetted, measuring the probe output of the EC-5 at different volumetric water content (VWC) values.

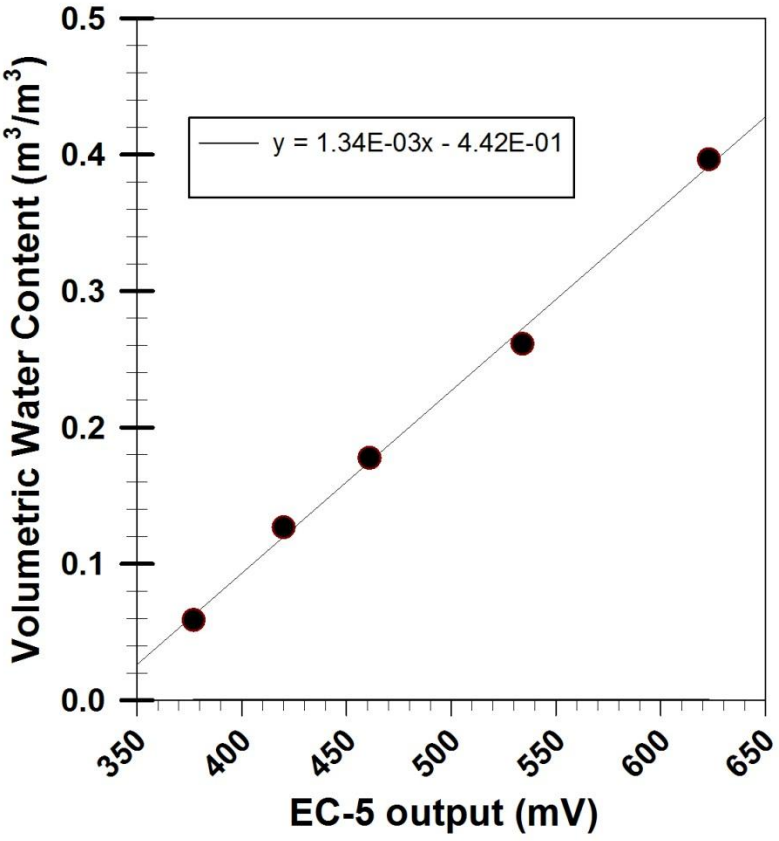

Appendix D

Summary of all the v_{max} events, including the drainable porosity (p_{dp}) with pre- and maximum event water table height.

Date/Time	Precip. (mm)	Pre-event water table height (m)	Max-event water table height (m)	p_{dp}	v_{max} (m/day)	$v_{max\text{-}1mm}$ (m/day)
0.3 m away from subsurface drain (in field array)						
2007-04-24 05:15	30.73	1.052	0.902	--	3.200	3.793
2007-04-24 17:30	13.21	0.945	0.731	0.061	9.071	11.338
2007-04-25 07:30	13.97	0.860	0.530	0.042	7.501	10.314
2007-05-23 16:00	32.77	1.009	0.905	--	1.797	1.829
2007-06-22 02:15	13.21	1.006	0.866	--	10.241	11.379
2007-08-19 17:15	44.20	1.067	0.549	--	17.069	17.069
2007-08-20 10:45	8.64	0.750	0.643	0.081	35.990	35.990
2007-08-20 21:45	18.29	0.814	0.494	0.057	39.062	39.062
2007-08-21 22:15	18.54	0.869	0.512	0.052	41.695	41.695
2007-08-22 10:15	10.16	0.616	0.564	0.157	3.477	11.821
2007-10-07 23:15	12.19	1.091	0.939	--	3.793	6.828
2007-10-13 21:45	17.53	1.088	1.048	--	0.966	1.280
2008-03-27 07:15	6.60	1.091	1.024	--	1.576	1.829
2008-04-24 19:45	58.17	1.073	0.546	--	14.630	14.630
2008-05-06 19:15	36.07	1.070	0.945	--	5.121	5.121
2008-05-29 04:15	76.96	1.073	0.942	--	2.560	2.560
2008-06-04 21:15	38.86	1.076	0.539	--	12.802	12.802
2008-06-07 19:15	11.94	1.055	0.040	--	8.534	11.379
0.9 m away from subsurface drain (in field array)						
2007-04-24 05:15	30.73	1.128	0.957	--	3.511	4.187
2007-04-24 17:30	13.21	1.006	0.792	0.061	9.656	12.070
2007-04-25 07:30	13.97	0.924	0.594	0.042	8.060	11.082
2007-05-23 16:00	32.77	1.155	0.917	--	2.016	2.054
2007-06-22 02:15	13.21	1.137	0.890	--	12.094	13.606
2007-08-19 17:15	44.20	1.119	0.600	--	27.213	27.213
2007-08-20 10:45	8.64	0.786	0.680	0.081	25.163	25.163
2007-08-20 21:45	18.29	0.844	0.543	0.061	40.525	40.525

Date/Time	Precip. (mm)	Pre-event water table height (m)	Max-event water table height (m)	SY	v_{max} (m/day)	$v_{max\text{-}1mm}$ (m/day)
0.9 m away from subsurface drain (in field array), cont.						
2007-08-21 22:15	18.54	0.896	0.552	0.054	28.675	28.675
2007-08-22 10:15	10.16	0.658	0.600	0.140	3.718	12.640
2007-10-07 23:15	12.19	1.149	0.994	--	4.031	7.257
2007-10-13 21:45	17.53	1.137	1.061	--	1.078	1.451
2008-03-27 07:15	6.60	1.146	1.079	--	1.675	1.944
2008-04-24 19:45	58.17	1.161	0.579	--	15.550	15.550
2008-05-06 19:15	36.07	1.128	0.984	--	5.443	5.443
2008-05-29 04:15	76.96	1.128	1.009	--	2.366	2.366
2008-06-04 21:15	38.86	1.137	0.628	--	15.550	15.550
2008-06-05 21:45	12.70	1.116	1.085	0.417	6.299	7.139
2008-06-07 19:15	11.94	1.134	0.098	--	9.895	13.606
2008-06-11 10:45	22.35	1.146	1.106	--	1.675	1.675
3.0 m away from subsurface drain (in field array)						
2007-03-31 02:00	23.88	1.177	1.030	--	1.804	2.157
2007-04-02 19:00	15.49	1.128	1.024	0.150	7.218	8.328
2007-04-10 17:00	6.35	1.173	1.140	0.189	0.569	0.578
2007-04-24 05:15	30.73	1.158	0.777	--	4.232	5.239
2007-04-24 17:30	13.21	0.838	0.643	0.063	6.190	7.315
2007-04-25 07:30	13.97	0.799	0.500	0.047	4.791	5.897
2007-05-06 00:45	26.01	1.170	1.036	--	3.334	6.472
2007-05-23 16:00	32.77	1.158	0.701	--	2.157	2.200
2007-06-01 08:15	7.87	1.177	1.052	0.049	8.688	12.550
2007-06-06 06:45	24.13	1.167	1.015	--	6.876	6.876
2007-06-22 02:15	13.21	1.073	0.756	--	12.225	13.753
2007-08-19 17:15	44.20	1.128	0.594	--	9.168	9.168
2007-08-20 10:45	8.64	0.735	0.634	0.086	14.104	14.104
2007-08-20 21:45	18.29	0.771	0.533	0.077	24.677	24.677
2007-08-21 22:15	18.54	0.814	0.546	0.069	19.532	19.532
2007-08-22 10:15	10.16	0.634	0.558	0.107	3.580	12.173
2007-08-28 18:15	23.11	1.103	0.957	0.158	13.241	13.241

Date/Time	Precip. (mm)	Pre-event water table height (m)	Max-event water table height (m)	SY	v_{max} (m/day)	$v_{max\text{-}1mm}$ (m/day)
3.0 m away from subsurface drain (in field array), cont.						
2007-10-07 08:45	29.21	1.061	1.030	--	11.002	11.002
2007-10-07 23:15	12.19	1.094	0.875	--	5.239	12.225
2007-10-13 21:45	17.53	1.103	0.856	--	2.500	6.112
2008-01-07 06:45	5.33	0.985	0.841	--	3.794	36.674
2008-03-27 07:15	6.60	1.152	1.061	--	1.804	2.116
2008-03-29 00:00	5.97	1.119	1.018	0.056	2.148	2.902
2008-03-31 05:15	38.86	1.116	0.994	0.229	17.849	53.547
2008-04-10 02:15	21.59	1.140	0.954	--	1.429	1.487
2008-04-17 08:15	15.24	1.134	0.963	0.089	1.361	1.414
2008-04-24 19:45	58.17	1.039	0.424	0.094	16.630	16.630
2008-05-02 08:15	11.43	1.064	0.942	0.094	4.085	12.765
2008-05-06 19:15	36.07	1.015	0.759	0.141	10.827	10.827
2008-05-10 20:15	5.33	1.009	0.975	0.159	10.762	48.427
2008-05-29 04:15	76.96	1.155	0.792	--	11.002	11.002
2008-06-04 21:15	38.86	1.030	0.616	0.093	24.725	24.725
2008-06-05 21:45	12.70	0.927	0.893	0.379	6.354	7.413
2008-06-07 19:15	11.94	0.985	0.027	0.011	15.752	31.504
2008-06-11 10:45	22.35	0.975	0.917	0.386	1.897	1.897
2008-07-17 14:15	48.26	1.128	1.067	--	5.501	5.501
2008-07-19 18:30	11.18	1.091	1.042	--	6.876	6.876
2008-07-21 01:15	12.19	1.128	1.097	--	4.232	4.584
7.6 m away from subsurface drain (in field array)						
2007-03-31 02:00	23.88	1.183	0.951	0.091	6.678	16.219
2007-04-02 19:00	15.49	0.994	0.875	0.130	10.599	13.627
2007-04-10 17:00	6.35	1.091	1.006	0.074	1.455	1.518
2007-04-22 11:45	10.57	1.152	1.036	0.091	4.254	5.027
2007-04-24 05:15	30.73	1.048	0.616	0.071	4.575	5.921
2007-04-24 17:30	13.21	0.710	0.442	0.045	7.575	9.739
2007-04-25 07:30	13.97	0.597	0.405	0.073	9.558	19.117
2007-05-06 00:45	26.01	0.997	0.826	0.152	2.990	5.980
2007-05-23 16:00	32.77	1.106	0.637	0.052	3.035	3.124

Date/Time	Precip. (mm)	Pre-event water table height (m)	Max-event water table height (m)	SY	v_{max} (m/day)	$v_{max\text{-}1mm}$ (m/day)
7.6 m away from subsurface drain (in field array), cont.						
2007-06-01 08:15	7.87	1.027	0.884	0.043	9.861	16.435
2007-06-06 06:45	24.13	1.015	0.860	0.155	6.960	6.960
2007-06-22 02:15	13.21	1.177	0.747	0.030	18.873	22.648
2007-08-19 17:15	44.20	1.119	0.765	0.125	26.846	26.846
2007-08-20 10:45	8.64	0.786	0.725	0.142	15.098	15.098
2007-08-20 21:45	18.29	0.768	0.616	0.120	24.579	24.579
2007-08-21 22:15	18.54	0.765	0.570	0.095	18.361	18.361
2007-08-22 10:15	10.16	0.640	0.539	0.081	3.614	12.289
2007-08-28 18:15	23.11	0.981	0.808	0.133	10.469	10.469
2007-10-07 08:45	29.21	1.225	1.134	--	14.370	14.370
2007-10-07 23:15	12.19	1.103	0.884	0.056	5.311	13.277
2007-10-13 21:45	17.53	1.064	0.777	0.059	3.003	12.765
2008-03-27 07:15	6.60	1.250	1.180	0.087	1.718	1.971
2008-03-31 05:15	38.86	1.250	1.067	0.176	14.996	29.992
2008-04-10 02:15	21.59	1.152	0.896	0.084	2.698	2.911
2008-04-17 08:15	15.24	1.027	0.805	0.068	1.541	1.617
2008-04-24 19:45	58.17	0.887	0.268	0.094	28.382	28.382
2008-05-02 08:15	11.43	0.869	0.732	0.081	3.791	16.678
2008-05-06 19:15	36.07	0.884	0.457	0.085	42.427	42.427
2008-05-10 20:15	5.33	0.802	0.762	0.135	8.550	38.477
2008-05-29 04:15	76.96	1.052	0.585	0.165	18.476	18.476
2008-06-04 21:15	38.86	0.863	0.619	0.157	20.702	20.702
2008-06-05 21:45	12.70	0.728	0.671	0.219	5.828	6.993
2008-06-07 19:15	11.94	0.796	0.040	0.014	15.274	38.185
2008-06-11 10:45	22.35	0.774	0.704	0.319	2.230	2.230
2008-07-17 14:15	48.26	1.308	1.189	0.400	20.921	20.921
15.2 m away from subsurface drain (in field array)						
2007-03-31 02:00	23.88	1.332	1.067	--	3.726	5.279
2007-04-02 19:00	15.49	1.076	0.963	0.137	7.378	8.608
2007-04-10 17:00	6.35	1.173	1.079	0.067	1.522	1.587
2007-04-22 11:45	10.57	1.234	1.122	0.094	4.086	4.740

Date/Time	Precip. (mm)	Pre-event water table height (m)	Max-event water table height (m)	SY	v_{max} (m/day)	$v_{max\text{-}1mm}$ (m/day)
15.2 m away from subsurface drain (in field array), cont.						
2007-04-24 05:15	30.73	1.128	0.719	0.075	4.331	5.413
2007-04-24 17:30	13.21	0.704	0.305	0.033	7.510	9.656
2007-04-25 07:30	13.97	0.415	0.195	0.064	4.974	7.959
2007-05-06 00:45	26.01	1.039	0.872	0.155	2.772	4.989
2007-05-23 16:00	32.77	1.186	0.756	0.069	2.587	2.647
2007-06-01 08:15	7.87	1.079	0.948	0.052	5.755	7.399
2007-06-06 06:45	24.13	1.067	0.936	0.184	6.401	6.401
2007-06-22 02:15	13.21	1.268	0.853	0.031	17.473	20.385
2007-10-13 21:45	17.53	1.116	0.881	0.074	2.434	5.950
2008-04-10 02:15	21.59	1.274	1.055	--	1.863	1.949
2008-04-17 08:15	15.24	1.134	0.917	0.070	1.361	1.414
2008-04-24 19:45	58.17	0.984	0.082	0.064	94.512	94.512
2008-05-02 08:15	11.43	0.927	0.771	0.074	3.558	11.119
2008-05-06 19:15	36.07	0.920	0.329	0.061	29.456	29.456
2008-05-10 20:15	5.33	0.835	0.802	0.159	8.908	40.087
2008-05-29 04:15	76.96	1.122	0.552	0.135	7.919	7.919
2008-06-04 21:15	38.86	0.887	0.649	0.163	42.574	42.574
2008-06-05 21:45	12.70	0.677	0.622	0.231	4.997	5.905
2008-06-07 19:15	11.94	0.747	0.107	0.017	23.896	23.896
2008-06-11 10:45	22.35	0.707	0.637	0.319	1.980	1.980
0.3 m away from subsurface drain (in buffer array)						
2009-03-22 23:30	21.59	1.390	0.619	0.028	4.942	5.559
2009-03-23 21:45	30.48	1.103	0.485	0.049	26.480	35.307
2009-04-04 22:30	8.38	1.396	1.369	0.306	1.176	1.197
2009-04-26 08:00	10.67	1.475	1.414	0.175	12.875	35.406
2009-04-26 16:00	38.35	1.408	0.686	0.053	22.530	67.591
2009-05-05 19:00	11.18	1.344	1.195	0.075	14.338	16.130
2009-05-25 23:00	69.85	1.448	1.192	0.273	3.232	3.309
2009-06-17 23:00	29.72	1.475	1.347	0.232	3.934	4.046
2009-07-07 16:00	20.32	1.600	1.551	0.407	3.414	3.414
2009-07-09 06:45	7.87	1.561	1.533	0.287	12.484	12.484

Date/Time	Precip. (mm)	Pre-event water table height (m)	Max-event water table height (m)	SY	v_{max} (m/day)	$v_{max\text{-}1mm}$ (m/day)
0.9 m away from subsurface drain (in buffer array)						
2009-03-22 23:30	21.59	1.426	0.564	0.025	4.891	5.478
2009-03-23 21:45	30.48	1.116	0.387	0.042	26.773	35.697
2009-04-04 22:30	8.38	1.436	1.411	0.344	1.209	1.231
2009-04-26 08:00	10.67	1.512	1.454	0.184	14.514	48.379
2009-04-26 16:00	38.35	1.451	0.625	0.044	27.856	139.280
2009-05-05 19:00	11.18	1.381	1.219	0.069	16.569	18.936
2009-05-25 23:00	69.85	1.484	1.219	0.263	3.167	3.239
2009-06-17 23:00	29.72	1.506	1.381	0.238	4.251	4.380
2009-07-07 16:00	20.32	1.640	1.588	0.382	3.498	3.498
2009-07-09 06:45	7.87	1.600	1.567	0.234	12.802	12.802
3.0 m away from subsurface drain (in buffer array)						
2009-03-22 23:30	21.59	1.323	0.783	0.040	4.233	4.703
2009-03-23 21:45	30.48	0.829	0.171	0.046	11.369	13.264
2009-04-26 08:00	10.67	1.430	1.405	0.437	6.535	9.802
2009-04-26 16:00	38.35	1.402	0.719	0.056	22.434	67.302
2009-05-05 19:00	11.18	1.283	1.146	0.081	7.246	7.699
2009-05-25 23:00	69.85	1.396	1.201	0.358	2.792	2.851
2009-06-17 23:00	29.72	1.408	1.338	0.424	3.219	3.297
2009-07-07 16:00	20.32	1.515	1.478	0.543	3.232	3.232
2009-07-09 06:45	7.87	1.478	1.454	0.323	2.580	2.580
7.6 m away from subsurface drain (in buffer array)						
2009-03-22 23:30	21.59	1.262	0.134	0.019	4.326	4.845
2009-03-23 21:45	30.48	0.738	--	0.041	35.407	70.813
2009-04-04 22:30	8.38	1.274	1.234	0.212	1.223	1.248
2009-04-25 23:30	10.92	1.375	1.335	0.276	16.496	16.496
2009-04-26 08:00	10.67	1.338	1.259	0.135	9.881	21.409
2009-04-26 16:00	38.35	1.253	0.219	0.037	20.044	60.132
2009-04-29 17:00	2.29	1.039	1.009	0.075	5.251	5.543
2009-05-05 19:00	11.18	1.237	0.930	0.036	11.879	13.199
2009-05-25 23:00	69.85	1.338	1.052	0.244	2.294	2.335
2009-06-17 23:00	29.72	1.347	1.213	0.222	3.695	3.804

Date/Time	Precip. (mm)	Pre-event water table height (m)	Max-event water table height (m)	SY	v_{max} (m/day)	$v_{max\text{-}1mm}$ (m/day)
7.6 m away from subsurface drain (in buffer array), cont.						
2009-07-07 16:00	20.32	1.457	1.411	0.434	3.108	3.108
2009-07-09 06:45	7.87	1.423	1.393	0.258	8.038	8.038
15.2 m away from subsurface drain (in buffer array)						
2009-03-22 23:30	21.590	1.106	0.122	0.022	1.562	1.609
2009-03-23 21:45	30.480	0.454	--	0.066	24.754	24.754
2009-04-04 22:30	8.382	1.106	1.024	0.102	14.264	114.115
2009-04-25 23:30	10.922	1.289	1.192	0.112	11.620	13.557
2009-04-26 08:00	10.668	1.189	0.975	0.050	10.387	11.541
2009-04-26 16:00	38.354	1.006	0.192	0.047	3.503	3.606
2009-04-29 17:00	2.286	--	0.762	0.027	3.134	3.134
2009-05-05 19:00	11.176	1.082	0.600	0.023	8.159	8.159
2009-05-25 23:00	69.850	1.253	0.905	0.190	3.934	4.426
2009-06-17 23:00	29.718	1.277	1.009	0.111	43.603	43.603
2009-07-07 16:00	20.320	1.469	1.439	0.652	7.427	10.728
2009-07-09 06:45	7.874	1.445	1.399	0.172	2.147	2.187

Appendix E

Summary of field-saturated hydraulic conductivity (K_{fs}) from 2008 and 2010, including laboratory measurements of gravimetric water content and loss on ignition (LOI).

Measurement	Cover Type	Soil Type	Grav. Water Content[1]	Loss on Ignition (LOI)	K_{fs} (m day^{-1})	K_{fs} (m s^{-1})
May 19, 2008						
05192008a	Bare ground	Canisteo	--	--	--	4.262×10^{-5}
05192008b	Bare ground	Canisteo	--	--	--	5.515×10^{-5}
05192008c	Bare ground	Canisteo	--	--	--	3.938×10^{-5}
05192008d	Bare ground	Canisteo	--	--	--	1.357×10^{-5}
June 2, 2008						
06022008a	Bare ground	Canisteo	--	--	1.529	1.770×10^{-5}
06022008b	Bare ground	Canisteo	--	--	1.558	1.803×10^{-5}
06022008c	Bare ground	Canisteo	--	--	4.406	5.099×10^{-5} x
06022008d	Bare ground	Canisteo	--	--	0.155	1.790×10^{-6}
06022008e	Bare ground	Canisteo	--	--	0.041	4.718×10^{-7}
06022008f	Bare ground	Canisteo	--	--	0.075	8.733×10^{-7}
06032008a	--	Canisteo	--	--	0.023	2.682×10^{-7}
06032008b	--	Canisteo	--	--	0.030	3.505×10^{-7}
06032008c	--	Canisteo	--	--	0.442	5.115×10^{-6}
06042008a	--	Canisteo	--	--	0.014	1.608×10^{-7}
06042008b	--	Canisteo	--	--	0.015	1.754×10^{-7}
06042008c	--	Canisteo	--	--	0.069	7.942×10^{-7}
July 28, 2008						
07282008a	--	Canisteo	--	--	2.554	2.956×10^{-5}
07282008b	--	Canisteo	--	--	7.940	9.190×10^{-5}
07282008c	--	Canisteo	--	--	2.352	2.722×10^{-5}
07282008d	--	Canisteo	--	--	0.282	3.258×10^{-6}
07282008f	--	Canisteo	--	--	0.595	6.889×10^{-6}
07302008a	Corn	--	--	--	0.050	5.741×10^{-7}
07302008b	Corn	--	--	--	0.188	2.174×10^{-6}
07302008c	Corn	--	--	--	1.170	1.355×10^{-5}
07302008d	Corn	--	--	--	1.061	1.228×10^{-5}

Measurement	Cover Type	Soil Type	Grav. Water Content[1]	Loss on Ignition (LOI)	K_{fs} (m day^{-1})	K_{fs} (m s^{-1})
July 28, 2008 (cont.)						
07302008e	Corn	--	--	--	0.806	9.333×10^{-6}
August 21, 2008						
08202008a	Corn	--	--	--	3.823	4.424×10^{-5}
08202008b	Corn	--	--	--	35.071	4.059×10^{-4}
08202008c	Corn	--	--	--	9.609	1.112×10^{-4}
08212008a	Corn	--	--	--	48.250	5.585×10^{-4}
08212008b	Corn	--	--	--	0.910	1.053×10^{-5}
08212008c	Corn	--	--	--	16.361	1.894×10^{-4}
08212008d	Corn	--	--	--	0.245	2.841×10^{-6}
08212008e	Corn	--	--	--	17.366	2.010×10^{-4}
08212008f	Corn	--	--	--	11.078	1.282×10^{-4}
08212008g	Corn	--	--	--	5.226	6.049×10^{-5}
August 23-25, 2010						
B1-0	Grass buffer	Canisteo	0.126	0.090	6.389	7.395×10^{-5}
B1-20	Grass buffer	Canisteo	0.231	0.077	7.032	8.139×10^{-5}
B1-40	Grass buffer	Canisteo	0.106	0.067	43.530	5.038×10^{-4}
B1-60	Grass buffer	Canisteo	0.110	0.063	3.715	4.300×10^{-5}
B1-80	Grass buffer	Canisteo	0.136	0.067	1.043	1.207×10^{-5}
B1-100	Grass buffer	Canisteo	0.177	0.118	2.946	3.410×10^{-5}
C1-10	Corn	Clarion	0.084	0.078	25.942	3.003×10^{-4}
C1-20	Corn	Clarion	0.138	0.036	18.065	2.091×10^{-4}
C1-30	Corn	Clarion	--	---	6.599	7.638×10^{-5}
C1-40	Corn	Clarion	0.143	0.046	12.106	1.401×10^{-4}
C1-40_rep	Corn	Clarion	0.154	0.040	4.244	4.912×10^{-5}
C1-50	Corn	Clarion	0.143	0.044	49.076	5.680×10^{-4}
F1-0	Corn	Canisteo	0.092	0.114	3.804	4.403×10^{-5}
F1-10	Corn	Canisteo	0.132	0.064	10.920	1.264×10^{-4}
F1-20	Corn	Canisteo	0.116	0.072	15.419	1.785×10^{-4}
F1-30	Corn	Canisteo	0.234	0.061	0.083	9.561×10^{-7}
F1-40	Corn	Canisteo	0.151	0.055	0.159	1.836×10^{-6}
F1-50	Corn	Canisteo	0.125	0.045	20.792	2.407×10^{-4}

Measurement	Cover Type	Soil Type	Grav. Water Content[1]	Loss on Ignition (LOI)	K_{fs} (m day^{-1})	K_{fs} (m s^{-1})
August 23-25, 2010 (cont.)						
F1-60	Corn	Canisteo	0.111	0.092	3.879	4.489×10^{-5}
F1-70	Corn	Canisteo	0.130	0.054	0.720	8.334×10^{-6}
F1-80	Corn	Canisteo	0.303	0.067	16.177	1.872×10^{-4}
F1-90	Corn	Canisteo	0.126	0.118	18.551	2.147×10^{-4}
F1-100	Corn	Canisteo	0.121	0.064	25.686	2.973×10^{-4}
F3-10	Corn	Canisteo	---	---	34.437	3.986×10^{-4}
F3-20	Corn	Canisteo	0.248	0.040	1.193	1.381×10^{-5}
H1-10	Corn	Harps	0.201	0.087	2.382	2.756×10^{-5}
H1-20	Corn	Harps	0.194	0.076	13.697	1.585×10^{-4}
H1-30	Corn	Harps	0.205	0.082	3.217	3.723×10^{-5}
H1-40	Corn	Harps	0.155	0.081	3.756	4.347×10^{-5}
H1-50	Corn	Harps	0.197	0.077	2.941	3.404×10^{-5}
N1-0	Corn	Nicollet	---	---	41.206	4.769×10^{-4}
N1-10	Corn	Nicollet	0.150	0.050	7.736	8.953×10^{-5}
N1-20	Corn	Nicollet	0.165	0.054	11.850	1.372×10^{-4}
N1-30	Corn	Nicollet	0.169	0.056	21.300	2.465×10^{-4}
N1-40	Corn	Nicollet	0.225	0.056	49.787	5.762×10^{-4}
N1-50	Corn	Nicollet	0.143	0.063	134.262	1.554×10^{-3}
OB1-10	Bare ground	Okoboji	0.243	0.085	23.483	2.718×10^{-4}
OB1-20	Bare ground	Okoboji	0.221	0.090	12.597	1.458×10^{-4}
OB1-30	Corn	Okoboji	0.262	0.108	15.775	1.826×10^{-4}
OB1-40	Corn	Okoboji	0.201	0.091	20.414	2.363×10^{-4}
OB1-50	Corn	Okoboji	0.210	0.084	3.751	4.341×10^{-5}
S1-10	Soybeans	Canisteo	0.144	0.073	0.944	1.093×10^{-5}
S1-20	Soybeans	Canisteo	0.095	0.067	4.289	4.965×10^{-5}
S1-30	Soybeans	Canisteo	0.139	0.075	6.158	7.128×10^{-5}
S1-40	Soybeans	Canisteo	0.148	0.059	11.693	1.353×10^{-4}
S1-50	Soybeans	Canisteo	0.104	0.084	34.980	4.049×10^{-4}
November 9-10, 2010						
B1-20 (2)	Grass buffer	Canisteo	---	---	9.698	1.123×10^{-4}

Measurement	Cover Type	Soil Type	Grav. Water Content[1]	Loss on Ignition (LOI)	K_{fs} (m day^{-1})	K_{fs} (m s^{-1})
November 9-10, 2010 (cont.)						
B1-40 (2)	Grass buffer	Canisteo	---	---	3.383	3.916×10^{-5}
B1-60 (2)	Grass buffer	Canisteo	---	---	2.229	2.580×10^{-5}
C1-10 (2)	Bare ground	Clarion	---	---	0.723	8.372×10^{-6}
C1-20 (2)	Bare ground	Clarion	---	---	0.372	4.311×10^{-6}
C1-30 (2)	Bare ground	Clarion	---	---	4.441	5.141×10^{-5}
C1-40 (2)	Bare ground	Clarion	---	---	1.309	1.515×10^{-5}
C1-50 (2)	Bare ground	Clarion	---	---	25.148	2.911×10^{-4}
F1-10 (2)	Bare ground	Canisteo	---	---	0.055	6.317×10^{-7}
F1-20 (2)	Bare ground	Canisteo	---	---	1.046	1.211×10^{-5}
F1-30 (2)	Bare ground	Canisteo	---	---	3.639	4.212×10^{-5}
F1-40 (2)	Bare ground	Canisteo	---	---	0.075	8.666×10^{-7}
F1-50 (2)	Bare ground	Canisteo	---	---	9.195	1.064×10^{-4}
H1-10 (2)	Bare ground	Harps	---	---	18.578	2.150×10^{-4}
H1-20 (2)	Bare ground	Harps	---	---	1.288	1.490×10^{-5}
H1-30 (2)	Bare ground	Harps	---	---	2.788	3.227×10^{-5}
H1-40 (2)	Bare ground	Harps	---	---	1.725	1.997×10^{-5}
H1-50 (2)	Bare ground	Harps	---	---	10.397	1.203×10^{-4}
N1-10 (2)	Bare ground	Nicollet	---	---	5.398	6.247×10^{-5}
N1-20 (2)	Bare ground	Nicollet	---	---	1.528	1.769×10^{-5}
N1-30 (2)	Bare ground	Nicollet	---	---	108.553	1.256×10^{-3}
N1-40 (2)	Bare ground	Nicollet	---	---	19.463	2.253×10^{-4}
N1-50 (2)	Bare ground	Nicollet	---	---	3.814	4.414×10^{-5}

Appendix F

Soil specific parameters, representing the distinct soil types, collected from the field site in 2009-2010. Measured parameters included soil bulk density, particle density, and particle size analysis (PSA) distribution (USDA size classification).

Sample	Soil type	Bulk density (dry)	Porosity (calc.)	Particle density	Clay	Silt	Very fine sand	Fine sand	Med. sand	Coarse sand	Very coarse sand	Gravel
		g cm^{-3}	m^3 m^{-3}	g cm^{-3}	<0.002 mm	0.002 – 0.05 mm	0.05 – 0.1 mm	0.1 – 0.25 mm	0.25 – 0.5 mm	0.5 – 1 mm	1 – 2 mm	>2 mm
Samples collected October 22, 2009												
Surface	Canisteo	--	--	--	3.66	34.57	20.51	16.82	13.76	7.35	0.00	3.31
Tile	Canisteo	--	--	--	5.61	45.87	11.70	15.69	4.99	0.00	0.00	16.16
4-6"	Canisteo	--	--	--	3.63	32.96	19.88	15.27	9.05	11.37	1.13	6.69
10-12"	Canisteo	--	--	--	3.74	31.21	20.06	23.73	10.71	8.63	0.32	1.61
16-18"	Canisteo	--	--	--	5.49	41.05	14.97	6.97	13.58	5.83	0.00	12.07
22-24"	Canisteo	--	--	--	3.59	25.94	10.72	9.59	11.92	15.52	2.78	19.93
28-30"	Canisteo	--	--	--	1.58	15.44	5.38	7.51	19.43	23.26	14.28	13.13
34-36"	Canisteo	--	--	--	0.85	6.84	1.86	4.01	6.33	6.97	7.01	66.13
40-42"	Canisteo	--	--	--	7.02	54.21	11.13	15.80	3.96	0.00	0.00	7.90
46-48"	Canisteo	--	--	--	8.63	58.43	9.77	11.97	0.00	0.00	0.00	11.22
52-54"	Canisteo	--	--	--	8.17	55.73	10.04	10.73	0.00	0.00	0.00	15.32
54-57"	Canisteo	--	--	--	8.43	55.31	9.82	14.09	0.10	0.00	0.00	12.22
Samples collected October 22, 2009 (pre-treated to separate aggregates)												
Surface	Canisteo	--	--	--	21.34	59.94	7.35	8.07	0.00	0.00	0.00	3.31
Tile	Canisteo	--	--	--	18.22	51.73	10.13	3.75	0.00	0.00	0.00	16.16
4-6"	Canisteo	--	--	--	17.68	58.17	6.19	11.17	0.14	0.00	0.00	6.69

Sample	Soil type	Bulk density (dry)	Porosity (calc.)	Particle density	Clay	Silt	Very fine sand	Fine sand	Med. sand	Coarse sand	Very coarse sand	Gravel
		g cm^{-3}	m^3 m^{-3}	g cm^{-3}	<0.002 mm	0.002 – 0.05 mm	0.05 – 0.1 mm	0.1 – 0.25 mm	0.25 – 0.5 mm	0.5 – 1 mm	1 – 2 mm	>2 mm
Samples collected October 22, 2009 (pre-treated to separate aggregates), cont.												
10-12"	Canisteo	--	--	--	23.37	65.73	5.88	3.41	0.00	0.00	0.00	1.61
16-18"	Canisteo	--	--	--	25.55	58.43	3.97	0.00	0.00	0.00	0.00	12.07
22-24"	Canisteo	--	--	--	13.57	29.60	2.59	9.98	16.73	7.04	0.56	19.93
28-30"	Canisteo	--	--	--	4.66	11.08	1.95	7.33	22.80	28.54	10.51	13.13
34-36"	Canisteo	--	--	--	7.57	26.05	0.25	0.00	0.00	0.00	0.00	66.13
40-42"	Canisteo	--	--	--	18.53	67.21	6.34	0.00	0.00	0.00	0.00	7.90
46-48"	Canisteo	--	--	--	20.79	66.88	1.11	0.00	0.00	0.00	0.00	11.22
52-54"	Canisteo	--	--	--	19.29	64.28	1.10	0.00	0.00	0.00	0.00	15.32
54-57"	Canisteo	--	--	--	16.44	45.06	9.01	16.48	0.81	0.00	0.00	12.22
Samples collected August 23-25, 2010												
H1_0_6_18	Harps	0.800	0.678	2.485	14.70	80.48	3.68	0.00	0.00	0.00	0.00	1.16
H1_0_18_30	Harps	1.678	0.356	2.605	11.21	79.67	7.77	0.00	0.00	0.00	0.00	1.33
H1_0_30_42	Harps	1.809	0.309	2.619	12.82	70.51	10.27	1.37	0.00	0.00	0.00	5.05
H1_0_42_54	Harps	1.926	0.260	2.602	13.92	81.18	2.12	0.00	0.00	0.00	0.00	2.75
H1_0_54_66_U	Harps	1.455	0.441	2.603	11.75	70.42	9.64	0.18	0.00	0.00	0.00	8.03
H1_0_54_66_D	Harps	1.819	0.293	2.570	12.45	70.37	6.84	0.00	0.00	0.00	0.00	10.37
F1_60_6_18	Canisteo	1.308	0.490	2.564	10.03	70.87	12.67	3.63	0.00	0.00	0.00	2.78
F1_60_18_30	Canisteo	1.453	0.438	2.585	8.62	70.47	10.53	1.13	0.00	0.00	0.00	9.28

Sample	Soil type	Bulk density (dry)	Porosity (calc.)	Particle density	Clay	Silt	Very fine sand	Fine sand	Med. sand	Coarse sand	Very coarse sand	Gravel
		g cm^{-3}	m^3 m^{-3}	g cm^{-3}	<0.002 mm	0.002 – 0.05 mm	0.05 – 0.1 mm	0.1 – 0.25 mm	0.25 – 0.5 mm	0.5 – 1 mm	1 – 2 mm	>2 mm
Samples collected August 23-25, 2010 (cont.)												
F1_60_30_42	Canisteo	1.663	0.374	2.655	11.43	66.20	10.69	6.64	0.00	0.00	0.00	5.03
F1_60_42_54	Canisteo	1.849	0.147	2.166	8.89	65.43	11.26	4.71	0.00	0.00	0.00	9.74
F1_60_54_66	Canisteo	1.527	0.421	2.639	18.67	76.47	0.00	0.00	0.00	0.00	0.00	4.85
N1_0_6_18	Nicollet	1.411	0.461	2.620	11.15	67.76	10.25	3.68	0.00	0.00	0.00	7.18
N1_0_16_28	Nicollet	1.683	0.366	2.656	7.68	49.40	8.30	11.83	9.18	6.05	1.61	5.94
N1_0_28_38	Nicollet	1.577	0.404	2.644	5.45	29.00	17.62	26.20	6.04	6.07	1.88	7.75
N1_0_38_48	Nicollet	1.931	0.264	2.624	15.04	79.23	2.15	0.00	0.00	0.00	0.00	3.58
N1_0_48_60	Nicollet	1.612	0.388	2.635	4.81	21.95	21.26	29.11	5.53	5.47	2.00	9.87
N1_0_60_66	Nicollet	1.689	0.356	2.621	5.21	26.33	19.19	27.14	6.43	6.42	2.04	7.28
C1_6_18	Clarion	1.478	0.426	2.576	8.69	69.77	11.21	3.45	0.00	0.00	0.00	6.89
C1_18_30	Clarion	1.671	0.350	2.571	9.16	73.33	10.69	4.38	0.00	0.00	0.00	2.40
C1_30_42	Clarion	1.599	0.381	2.585	13.64	80.86	0.91	0.00	0.00	0.00	0.00	4.58
C1_42_54	Clarion	1.450	0.433	2.556	12.34	76.93	2.98	0.00	0.00	0.00	0.00	7.74
C1_54_66	Clarion	1.192	0.535	2.564	14.85	78.90	0.28	0.00	0.00	0.00	0.00	5.98
OB1_0_6_18	Okoboji	1.584	0.376	2.537	13.11	83.33	3.45	0.00	0.00	0.00	0.00	0.17
OB1_0_18_28	Okoboji	1.732	0.337	2.614	17.12	78.18	1.75	0.00	0.00	0.00	0.00	2.92
OB1_0_38_48	Okoboji	1.728	0.337	2.605	18.31	80.56	0.00	0.00	0.00	0.00	0.00	1.13
OB1_0_38_50	Okoboji	1.544	0.404	2.590	11.91	80.62	1.17	0.00	0.00	0.00	0.00	6.29
OB1_0_50_58	Okoboji	1.621	0.376	2.599	14.81	82.85	0.75	0.00	0.00	0.00	0.00	1.59

Appendix G

Visual Basic Computer Code for the source-responsive (S-R) model.

Public Sub SR_model()

```
Dim wks As Worksheet
Set wks = ActiveWorkbook.Sheets("Model_Results")

'Formatting steps
wks.Columns("A").ColumnWidth = 28
wks.Columns("B").ColumnWidth = 10
wks.Columns("C").ColumnWidth = 15
wks.Columns("D:V").ColumnWidth = 10
wks.Columns("A:V").Font.FontStyle = "Arial"
wks.Columns("A:V").Font.Size = 8
wks.Range("B2:B5,B10").NumberFormat = "0.000E+00"
wks.Range("B17:B18").NumberFormat = "0.0000"
wks.Columns("E:T").NumberFormat = "0.0000"
wks.Columns("U:V").NumberFormat = "0.000000"
wks.Range("B6,B9,B11:B12").NumberFormat = "0.000"
wks.Range("B8").NumberFormat = "0.00"
wks.Columns("D").NumberFormat = "0.00"
wks.Range("B7,B13:B15").NumberFormat = "0"
wks.Columns("T").NumberFormat = "0"
wks.Columns("C").NumberFormat = "YYYY-MM-DD HH:MM"
wks.Columns("A:A").Font.Bold = True
wks.Columns("A:A").Font.Italic = True
wks.Rows("1:1").Font.Bold = True
wks.Rows("1:1").Font.Italic = True
Application.ScreenUpdating = False

'Source-responsive model parameters
Dim Vo As Double 'Maximum velocity, in units of m/s
Dim Vu As Double 'Average velocity, 2/3 of maximum velocity,
'in units of m/h
Dim Lu As Double 'Average thickness of laminar film,
'in units of m
Dim VuLu As Double 'Combined parameter of Vu and Lu,
'in units of m2/h
Dim v As Double 'Kinematic viscosity of water,
'temperature-dependent, in units of m2/s
Dim Y As Double ‘Drainable porosity, no units
Dim Mlim As Double 'Smallest value of M for z between 0
'and "new water table rise", in units of /m
Dim tao As Double 'Proportionality constant,
```

```
'affects the recession rate, in units of /h
Dim SD As Double 'Steady-diffuse depth,
'depth of confining layer, in units of m
Dim qslim As Double 'critical rainfall rate
'analogous to the infiltration capacity, in units of
Dim SD_elev As Double 'Steady-diffuse depth
'elevation, in units of m
Dim LSD As Double 'Land surface elevation at
'piezometer, dependent on piezometer, in units of m
Dim Offset As Double 'offset, in reference to
"delaying' the f parameter in order to get the best fit
Dim Mlim_inc As Double 'amount to increase Mlim
'by for each run of the model, in units of /m

'Other parameters, such as rainfall and intensity
Dim t As Range 'time from the beginning
Dim delta_t As Double 'difference between i and i+1
Dim int_rainfall_depth As Range 'rainfall depth during
'the event between i and i+1, in this case 15 minutes
Dim cum_rainfall_depth As Range 'cumulative precipitation
'since the beginning of the event
Dim int_rainfall_inty As Range 'rainfall intensity
'during the event between i and i+1, in this case 15 minutes
Dim well_level As Range 'copied to spreadsheet,
'individual piezometer's water depth measurement (in meters)
Dim Hmeas As Range 'measured head
Dim f As Range 'active area fraction, flow
'along some of the internal surface area of pores (ranges from 0 to 1)
Dim H As Range 'calculated head, eq. 28 on p. 300 of Nimmo, 2010 (VZJ)
Dim SR_hours As Double 'number of hours in the SR-model
Dim IntervalLength As Single 'increase to next interval
Dim k_length As Single 'length of k-intervals

'Nash-Sutcliffe model efficiency coefficient and residual coefficient
Dim NashFSum As Double 'Nash F parameter sum, calcuated
'by squaring the actual data value - the range's actual value average
Dim NashF0TempSum As Double 'Temporary Nash F0 parameter sum
Dim NashF0Sum As Double 'Nash F0 parameter sum, calcuated
'by squaring the actual data value - the range's actual value average
Dim NashF0Avg As Double 'Nash parameter, F0 average
Dim NashE As Range 'Nash E result
Dim MlimResult As Range 'Mlim associated with Nash E result
Dim NashStart As Single 'start of the range for calculating
'the Nash E and residual
Dim NashEnd As Single 'end of the range for calculating the
'Nash E and residual
```

```
Dim Residual As Range 'residual sum
Dim ResidualSum As Double 'calculated residual, based on the
'absolute value of the time steps (model - observed value)

Dim i As Single
Dim j As Single
Dim k As Single
Dim IntCol As Single
Dim IntRow As Single

'Height above sealevel, different piezometers
'Field 0.3 m = 358.713024
'Field 0.9 m = 358.700832
'Field 3.0 m = 358.679496
'Field 7.6 m = 358.725216
'Field 15.2 m = 358.819704
'Buffer 0.3 m = 358.365552
'Buffer 0.9 m = 358.389936
'Buffer 3.0 m = 358.33812
'Buffer 7.6 m = 358.30764
'Buffer 15.2 m = 358.298496

'Kinematic viscosity, at different temperatures
'(http://www.mhtl.uwaterloo.ca/old/onlinetools/airprop/airprop.html)
'Kinematic viscosity: 1.0°C: 1.6438E-6; 2.0°C: 1.5948E-6;
'3.0°C: 1.5477E-6; 4.0°C: 1.5025E-6; 5.0°C: 1.4592E-6;
'6.0°C: 1.4176E-6; 7.0°C: 1.3776E-6; 8.0°C: 1.3392E-6;
'9.0°C: 1.3024E-6; 10.0°C: 1.2670E-6; 11.0°C: 1.2329E-6;
'12.0°C: 1.2002E-6; 13.0°C: 1.1688E-6; 14.0°C: 1.1385E-6;
'15.0°C: 1.1094E-6; 16.0°C: 1.0814E-6; 17.0°C: 1.0544E-6;
'18.0°C: 1.0285E-6; 19.0°C: 1.0035E-6; 20.0°C: 9.7937E-7;
'21.0°C: 9.5616E-7; 22.0°C: 9.3379E-7; 23.0°C: 9.1223E-7;
'24.0°C: 8.9143E-7; 25.0°C: 8.7137E-7;

'Parameters to change every run
Mlim = 0
Mlim_inc = 25
Offset = 7
LSD = 358.725216
Vo = 2.13843809530923E-04
v = 0.000001267
NashStart = 0
NashEnd = 145
SR_hours = 36
k_length = 30
```

```
ActiveSheet.ChartObjects("Chart 1").Activate
ActiveChart.Axes(xlCategory).MaximumScale = SR_hours
ActiveChart.SeriesCollection(1).XValues = wks.Range(Cells(2, 4), _
Cells((SR_hours * 4) + 2, 4))
ActiveChart.SeriesCollection(1).Values = wks.Range(Cells(2, 11), _
Cells((SR_hours * 4) + 2, 11))
ActiveChart.SeriesCollection(2).XValues = wks.Range(Cells(2, 4), _
Cells((SR_hours * 4) + 2, 4))
ActiveChart.SeriesCollection(2).Values = wks.Range(Cells(2, 9), _
Cells((SR_hours * 4) + 2, 9))
ActiveChart.SeriesCollection(3).XValues = wks.Range(Cells(2, 4), _
Cells((SR_hours * 4) + 2, 4))
ActiveChart.SeriesCollection(3).Values = wks.Range(Cells(2, 6), _
Cells((SR_hours * 4) + 2, 6))

i = 1
j = 1
k = 1
IntRow = 2
IntCol = 2

Vu = Vo * (2 / 3) * 3600
Lu = (((Vu / 3600) * 3 * v) / 9.80665) ^ (1 / 2)
VuLu = Vu * Lu
Y = 5.19382578418675E-02
SD = 1.8
SD_elev = LSD - SD
delta_t = 0.25
tao = 504
IntervalLength = (SR_hours * 4) + 2

Set t = wks.Range("D2:D40000")
Set int_rainfall_depth = wks.Range("E2:E40000")
Set cum_rainfall_depth = wks.Range("F2:F40000")
Set int_rainfall_inty = wks.Range("G2:G40000")
Set well_level = wks.Range("H2:H40000")
Set Hmeas = wks.Range("I2:I40000")
Set f = wks.Range("J2:J40000")
Set H = wks.Range("K2:K40000")
Set MlimResult = wks.Range("T2:T1000")
Set NashE = wks.Range("U2:U1000")
Set Residual = wks.Range("V2:V1000")

For i = 1 To 1
Do
Hmeas(j) = well_level(j) - SD_elev
```

```
j = j + 1
Loop Until j = IntervalLength
Next i
i = 1
j = 1

For i = 1 To (NashEnd - NashStart)
NashF0TempSum = NashF0TempSum + Hmeas(i + NashStart)
Next i
NashF0Avg = NashF0TempSum / (NashEnd - NashStart)
i = 1
For i = 1 To (NashEnd - NashStart)
NashF0Sum = ((Hmeas(i + NashStart) - NashF0Avg) ^ 2) + NashF0Sum
Next i
i = 1

For k = 1 To k_length
Mlim = Mlim + Mlim_inc

For j = 1 To 1
t(i) = 0
cum_rainfall_depth(i) = int_rainfall_depth(i)
int_rainfall_inty(i) = int_rainfall_depth(i) / delta_t
If k > 1 Then
Hmeas(i) = well_level(i) - SD_elev
End If
qslim = VuLu * Mlim
f(i) = int_rainfall_inty(i) / (qslim * 1000)
If f(i) > 1 Then
f(i) = 1
Else: f(i) = f(i)
End If
H(i) = well_level(i) - SD_elev
Cells(IntRow, IntCol).Value = Vu
Cells(IntRow + 1, IntCol).Value = Lu
Cells(IntRow + 2, IntCol).Value = VuLu
Cells(IntRow + 3, IntCol).Value = v
Cells(IntRow + 4, IntCol).Value = Y
Cells(IntRow + 5, IntCol).Value = Mlim
Cells(IntRow + 6, IntCol).Value = tao
Cells(IntRow + 7, IntCol).Value = SD
Cells(IntRow + 8, IntCol).Value = qslim
Cells(IntRow + 9, IntCol).Value = SD_elev
Cells(IntRow + 10, IntCol).Value = LSD
Cells(IntRow + 11, IntCol).Value = NashStart
Cells(IntRow + 12, IntCol).Value = NashEnd
```

```
Cells(IntRow + 13, IntCol).Value = Offset
Cells(IntRow + 14, IntCol).Value = SR_hours
i = i + 1
Next j

For j = 2 To (IntervalLength - 1)
t(i) = t(i - 1) + delta_t
cum_rainfall_depth(i) = int_rainfall_depth(i) + _
cum_rainfall_depth(i - 1)
int_rainfall_inty(i) = int_rainfall_depth(i) / delta_t
Hmeas(i) = well_level(i) - SD_elev
qslim = VuLu * Mlim
f(i) = int_rainfall_inty(i) / (qslim * 1000)
If f(i) > 1 Then
f(i) = 1
Else: f(i) = f(i)
End If
If (j - Offset) > 0 Then
H(i) = H(i - 1) * (Exp(-delta_t / tao)) + (((f(i - Offset) _
* qslim * tao) / Y) * (1 - (Exp(-delta_t / tao))))
Else
H(i) = H(i - 1) * (Exp(-delta_t / tao)) + (((0 * qslim * tao) _
/ Y) * (1 - (Exp(-delta_t / tao))))
End If
If i > NashStart And i <= NashEnd Then
   NashFSum = (Hmeas(i) - H(i)) ^ 2 + NashFSum
   ResidualSum = Abs(H(i) - Hmeas(i)) + ResidualSum
End If
i = i + 1
Next j

i = i + 1
j = 1
IntRow = IntRow + IntervalLength
NashStart = NashStart + IntervalLength
NashEnd = NashEnd + IntervalLength

ActiveSheet.ChartObjects("Chart 1").Activate
Application.CutCopyMode = False
Selection.Copy
wks.Cells(IntRow, 12).Select
ActiveSheet.Paste
ActiveChart.SeriesCollection(1).Values = _
ActiveCell.Offset(0, -1).Range(Cells(1, 1), Cells(IntervalLength - 1, 1))
ActiveChart.SeriesCollection(2).Values = _
ActiveCell.Offset(0, -3).Range(Cells(1, 1), Cells(IntervalLength - 1, 1))
```

```
ActiveChart.SeriesCollection(3).Values = _
ActiveCell.Offset(0, -6).Range(Cells(1, 1), Cells(IntervalLength - 1, 1))
ActiveChart.Axes(xlValue).MinimumScaleIsAuto = True
ActiveChart.Axes(xlValue).MaximumScaleIsAuto = True
ActiveChart.Axes(xlCategory).MaximumScale = SR_hours
ActiveCell.Offset(0, -10).Range("A1:A4,A9").NumberFormat = "0.000E+00"
ActiveCell.Offset(0, -10).Range("A16:A17").NumberFormat = "0.0000"
ActiveCell.Offset(0, -10).Range("A5,A8,A10:A11").NumberFormat = "0.000"
ActiveCell.Offset(0, -10).Range("A7,A15").NumberFormat = "0.00"
ActiveCell.Offset(0, -10).Range("A6,A12:A14").NumberFormat = "0"

wks.Range("A2:A18").Select
Application.CutCopyMode = False
Selection.Copy
wks.Cells(IntRow, 1).Select
ActiveSheet.Paste

wks.Range("C1:L1").Select
Application.CutCopyMode = False
Selection.Copy
wks.Cells(IntRow - 1, 3).Select
ActiveSheet.Paste

wks.Range(Cells(2, 3), Cells(IntervalLength, 3)).Select
Application.CutCopyMode = False
Selection.Copy
wks.Cells(IntRow, 3).Select
ActiveSheet.Paste

wks.Range(Cells(2, 5), Cells(IntervalLength, 5)).Select
Application.CutCopyMode = False
Selection.Copy
wks.Cells(IntRow, 5).Select
ActiveSheet.Paste

wks.Range(Cells(2, 8), Cells(IntervalLength, 8)).Select
Application.CutCopyMode = False
Selection.Copy
wks.Cells(IntRow, 8).Select
ActiveSheet.Paste

MlimResult(k) = Mlim
NashE(k) = 1 - (NashFSum / NashF0Sum)
Residual(k) = ResidualSum
NashFSum = 0
ResidualSum = 0
```

```
Cells(IntRow - IntervalLength + 15, IntCol).Value = NashE(k)
Cells(IntRow - IntervalLength + 16, IntCol).Value = Residual(k)

Next k

End Sub
```